الجامعة الإسلامية بالمدينة المنورة
ISLAMIC UNIVERSITY OF MADINAH

The Islamic University Journal of Applied Sciences (JESC)

Refereed periodical scientific journal

Volume: VI Issue: II Year: 2024

Paper version

Filed at the King Fahd National Library No. 8742/1439 on 17/09/1439 AH International serial number of periodicals (ISSN) 1658-7936

Online version

Filed at the King Fahd National Library No. 8742/1439 on 17/09/1439 AH International Serial Number of Periodicals (e-ISSN) 1658-7944

The Journal's Website

https://jesc.iu.edu.sa

The papers are sent in the name of the Editor-in-Chief of the Journal to this E-mail address

jesc@iu.edu.sa

Publication Rules at the Journal (*)

General rules:

- Report original scientific research (the main results and conclusions must not have beenpublished or submitted elsewhere).
- Fit with the topics of the journal.
- Report novel results, innovative work and show a new scientific contribution.
- Not to bear similarity of more than 25% of a previously published work of the sameauthor(s).
- Follow the rules, regulation and authentic research methodologies.
- Fulfill the required items and the format of the journal provided in appendix below relatedto the guide for author.
- Opinions expressed in published articles commit the authors themselves only and notnecessarily the opinion of the journal.

For all articles:

- The exclusive right to publish and distribute and article, and to grant rights to others, including commercial purposes.
- For open access articles, IU will apply the relevant third-party user license where IUpublishes the article on its online platforms.
- The right to provide the article in all forms and media so the article can be used on the latest technology even after publication.
- The authority to enforce the rights in the article, on behalf of an author, against thirdparties, for example in the case of plagiarism or copyright infringement.

(*) These general rules are explained in details along with other rules for Author's guide in the journal's website: https://jesc.iu.edu.s

The Editorial Board

The Advisory Board

The Islamic University Journal of Applied Sciences

Issued By

Islamic University of Madinah, Madinah, Saudi Arabia

Table of Contents

Emerging Mobile Learning Technologies for Future Emergencies: Lessons Learned from COVID-19 Experience from the Perspective of Al-Baha University Faculty

Ali Saeed Alowayr
Aalowayr@bu.edu.sa
Information Technology department, Computing and Information Faculty, Al-Baha University, Saudi Arabia

Mohammed Yahya Alghamdi
myahya@bu.edu.sa
Computer Science department, Computing and Information Faculty, Al-Baha University Saudi Arabia

Abstract: The purpose of this research was to investigate the adoption of m-learning application f the faculty members' perspective at Al-Baha University not limited to the COVID-19 pandemic b rather future advancement of e-learning in higher education. This research aims to contribute t development of improvements in adoption, implementation, and barriers to ML tools to provid on how to improve training and learning in situations that are disrupted further in the future by technology and increased shift toward distance and flexible learning environments. A survey re design with analytical descriptive design was conducted to analyse the level of adoption and us smart devices in teaching learning activities. The sample comprised 100 faculty members, with collected via an online questionnaire containing 12 items divided into two key factors: the state practices of using mobile learning applications in teaching after the pandemic as well the difficu met in the process.

The results revealed that the attitudes of the faculty members toward the mobile learning appl for distance education were mostly positive. Therefore, the study showed that the participants on some challenges that are experienced when using such applications. This work is relevant si fosters understanding of mobile learning as a teaching strategy at universities with reference to crisis/emergency situation and potential didactical distance learning ideas in the future. Speaki findings made in the study, the emphasis is made upon the necessity to develop the ways to im support and training for faculty what means that an academic staff, to share their experience a students with adequate knowledge about online classes. Thus, the contributions of this study tr studying and advancing education policy and practice, helping institutions coordinate their mob learning and remove barriers that affect teaching and the learning process. They are particularl valuable as institutions plan for further disruptions such as future pandemics, technological advancements or other, to make sure that mobile learning stays viable solution in context of co changing environment of education.

keywords: Mobile learning application; Future emergencies; User experience (UX), Online learni Human mobile interaction.

تقنيات التعلم عبر الهاتف المحمول الناشئة في حالالات الط
ستقبلية: الدروس المستفادة من تجربة كوفيد-19 من وجهة
نظر أعضاء هيئة التدريس بجامعة الباحة

الملخص: كان الغرض من هذا البحث هو التحقيق في تبني تطبيق التعلم المحمول من وجهة نظر أع
التدريس في جامعة الباحة ليس فقط في ظل جائحة كوفيد-19 ولكن أيضًا التقدم المستقبلي للتع
التعليم العالي. يهدف هذا البحث إلى المساهمة في تطوير التحسينات في التبني والتنفيذ والحواجز
التعلم الآلي لتوفير رؤى حول كيفية تحسين التدريب والتعلم في المواقف التي تعطلت بشكل أكبر
بسبب التكنولوجيا والتحول المتزايد نحو بيئات التعلم عن بعد والمرنة. تم إجراء تصميم بحث مسحي
لتحليل مستوى تبني واستخدام الأجهزة الذكية في أنشطة التعلم والتعليم. ضمت العينة 100 عضو
، وتم جمع البيانات عبر استبيان عبر الإنترنت يحتوي على 12 عنصرًا مقسمة إلى عاملين رئيسيين
حالة وممارسات استخدام تطبيقات التعلم المحمول في التدريس بعد الوباء بالإضافة إلى الصعوبات
العملية. كشفت النتائج أن مواقف أعضاء هيئة التدريس تجاه تطبيقات التعلم المحمول للتعليم عن بع
في الغالب. لذلك، أظهرت الدراسة أن المشاركين اتفقوا على بعض التحديات التي يواجهونها عند اس
هذه التطبيقات. هذا العمل ذو أهمية لأنه يعزز فهم التعلم عبر الهاتف المحمول كاستراتيجية تدريس
مع الإشارة إلى حالة الأزمة / الطوارئ وأفكار التعلم عن بعد التعليمية المحتملة في المستقبل. عند
النتائج التي توصلت إليها الدراسة، يتم التركيز على ضرورة تطوير طرق لتحسين الدعم والتدريب للأعض
التدريس، أي الموظفين الأكاديميين، لمشاركة خبراتهم وتزويد الطلاب بالمعرفة الكافية حول الفص
عبر الإنترنت. وبالتالي، تنتقل مساهمات هذه الدراسة إلى دراسة وتطوير سياسة التعليم وممارساته
المؤسسات على تنسيق التعلم عبر الهاتف المحمول وإزالة الحواجز التي تؤثر على التدريس وعملية الت
ذات قيمة خاصة حيث تخطط المؤسسات لمزيد من الاضطرابات مثل الأوبئة المستقبلية أو التقد
غير ذلك، للتأكد من أن التعلم عبر الهاتف المحمول يظل حلالاً قابلاً للتطبيق في سياق
باستمرار.

1. Introduction

The acceleration of technology has dramatically transformed education, with e-learning becomi prominent feature in both routine and emergency scenarios. Part of e-learning, mobile learning learning provides convenience, availability and richer learning engagements when using handh devices like phones and tablets. Though, COVID-19 has played a good role to shift its concentra towards mobile learning as a crisis response, the current discussion has moved ahead to look a contributions of this technology in other educational issues like providing distance education in away areas or to find out how prepared we are for next such crises [1]. Al-Baha university, like m institutions worldwide, implemented mobile learning applications to ensure continuity during th pandemic. These applications enabled faculty to deliver lectures, share resources, and interact students, transcending geographical barriers. However, as learning management systems (LMS offered similar capabilities for over a decade, it is vital to identify how mobile applications contr uniquely to educational outcomes beyond conventional systems [2]. This study evaluates the effectiveness and challenges of mobile learning applications in a post-pandemic context, with a on preparing for future scenarios where flexible, technology-driven learning may be essential. M learning applications contain several types, including: educational content development applica in which educational content is created and disseminated to students [3]. To highlight the Coron pandemic, it is considered a crisis that has affected systems education in many countries of the which led to the widespread closure of schools and universities wide. In order to continue the educational process after this pandemic, it is necessary to keep up with developments and rapi technological evolutions. Perhaps resorting to the online learning strategy after the Corona pan has played an important role in the continuation of the educational process [4].Therefore, it is i to investigate the importance and role of modern technologies in continuing, improving and de the process of education after the Corona pandemic requires robust mechanisms and strategie success of the educational process. Learning through mobile applications has become a tangibl in most schools and universities across the global [5]. The world to confront the Corona pander the transmission of infection between students and their teachers, and thus learning has becor learning in general and what it includes, such as mobile learning applications, is one way out in this pandemic to continue the educational process [6]. From this standpoint, and in light of the challenges posed by the COVID-19 pandemic, which led to the closure of schools and universitie the rapid shift to distance learning, this study was conceived as an attempt to explore the realit mobile learning applications among instructors at Al-Baha University. While the pandemic provi an urgent context for the adoption of mobile learning, this research also seeks to assess how th can be effectively integrated into higher education in the long term, in preparation for future di whether from pandemics, technological advancements, or other unforeseen challenges.

2.Literature review

According to the researchers, m-learning means an ability to employ wireless devices like smar personal devices connected into the Internet to get the learning content irrespective of the tim space [7], [8]. In other word [9], they defined that m-learning is the learning whereby; use PDA access to the learning content and help them to perform other functions for instance, submitt assignments and quizzes.

M-learning is defined as the delivery of learning content through use of mobile technologies w enhancing the learner's experience and traditional face-to-face education may be supplemented w learning and m-learning [10].

Many a study in the field suggests that integration of e-learning and especially m-learning is m effective when it complements traditional pedagogy rather than when it is implemented as a contained system [11]. The use of classroom teaching and teaching through information techno with the same device is called blended learning [9]. In some definitions the successful completion course module means the use of various varieties of instructional media as well as instructional m Exact reference: or Mobile learning m-learning is education that is delivered through mobile techr and smart devices. Another advantage that mobile learning points to is greater availability and convenience [3], [12]. With the use of learners' pocket devices, students can learn at their own convenience ignoring space and time intervals [10]. Mobile learning also assists in different form learning such as the adaptive learning technologies and apps that addresses the needs of every in learner [13]. This personalized learning can improve participation as well as increase learning outc making it easier for students to learn more comfortably through materials that cover their pref learning styles at a difficulty level that matches their capability [13]. In most of the mobile learn platforms, data analytics was employed to monitor performance and adapt the learning process sequel Hence, the students experience more unique learning environments. Social integration of in m-learning enables students to easily work in a group through the use of communication tools as; Group text, social media networks, shared documents and forums [15].

This connectivity can improve conditions for cooperative learning among peers and support for g assignments where participants are dispersed in different geographical areas. The quality of lea environment plays an important role in the case of mobile learning and has significant impact acceptability of technologies used in learning [16]. Accessibility is the degree to which learners are to undertake learning tasks, also known as usability; engagement pertains to the creation of spe learning outcomes; overall satisfaction is a measure of the extent to which learners perceived lea design as helpful, easy to use, or enjoyable [17], [18].

Accessibility can be defined as the ability of users in terms of the ease at which they can access move through the mobile learning platform. The usability features, as per [18], include learnabi efficiency, memorability, error frequency, and satisfaction. In the case of mobile learning, the intu presentation of course content is the most pivotal factor in keeping learners from disengageme pointed out by [12], it is evidenced that the 'intuitiveness and clearly defined navigation paths ma contributes to usability of the application in the mobile learning system. While referring to accessi in mobile learning, media refers to integration of the learning platform, to address the aspects of ability in the learning platform for learners with disabilities and the learning platform regardles physical locations [19]. These include for instance the screen reader for visually impaired user, sub for hearing impaired user, flexible layout that can cater for different levels of lighting and other interfaces [20]. This is so the case since other studies have shown that barriers in accessibility hamper learning and the general user experience [21]. Also, the level of learners' interest and involvement is now considered as an element of UX in mobile learning, known as engagement [Among them, game incorporation, 'fun' items, and the use of content and other media product widely applied in order to increase activity level [18]. Besides this they also showed that gamificat can increase the motivation of the users by a factor of 2 in education related systems. Further, incorporation of videos, quizzes, and interactive simulations increase on the quality of learning co by adding on the value of fun and interesting [22][23]. In adopting affective mobile learning, UX i complex model that has implications on the success and adaptation of mobile learning technol [16]. The pieces that must be implemented in order to improve the overall UX include usabil accessibility, interaction, user personalization, social interaction, contextual learning, and continu feedback from the users [14]. These elements, when addressed, result in creative, full of interest effective mobile learning solutions.

There are many potential benefits of using m-learning ; however, there are numerous factors challenge the utilization and implementation of m-learning [24]. These can be further subclassifie technology and teacher related factors and also factors related to students and context [25]. m learning has also its problems in this regard also that it raises some digital divide problems in fro learners, here not all the learners are able to get mobile devices and internet connections [26]. vib and screen and there are also problems associated with distractions data privacy and security [27 Mobile devices are also not as efficient as the conventional type of computers. Reduced display s limited data storage and processing abilities have an impact on the usability and the learning acti taking place [27]. These restrictions may make it difficult to enter multi-parameter working characteristics or observe diagrams and large texts. In addition, there is the provision of reliable in access which is very essential in m-learning in view of accommodation of Web 2.0 tools, and ot resources located on cloud in addition to real time interaction. However, bandwidth, connection reliability and cost of data present major challenges, especially in rural or developing areas [30], [Likewise, the absence of calls for technical support and maintenance to mobile learning platforms devices may also hinder use [32]. This is about the provision of IT help desk for technical suppo upgrading of applications and other software and the physical framework to host enterprise m learning projects [33]. Overcoming these barriers is therefore critical to the optimization of the opportunities of mobile learning.

3. Methodology

The research method used in the present study was analytical-descriptive in the assessment of t of mobile learning applications in higher education. The participants in the study comprised 100 fa members of Al-Baha University, KSA, asked for their experiences, perception, and contingencies mobile learning tools. The questionnaire included two main dimensions:

1) the application of m-learning and/or mobile learning applications for instruction.
2) the problems faced while implementing these technologies.

Data analysis was done by use of Statistical Package for the Social Sciences (SPSS). Quantitativ analysis, coefficient, and frequency distribution in the survey results were used to analyze the re from the faculty's next survey for presence of pattern of the faculty responses. To gain impro understanding, the responses were contextualized using data from prior research in mobile learn Accordingly with the objectives and questions of the study, the researchers used the questionnair line with the objectives from the perspective of Al-Baha University faculty members. The current s in its final form, consisted of two factors: the first one is the reality of the teachers mobile learn applications usage in teaching, and this factor embraced the following seven items:

1) Each of the applications explored in this study improved the learning performance compared to that of traditional learning.
2) Incorporate mobile learning applications in teaching students after COVID-19 (Corona).
3) Mobile learning applications have engaged the student hence making it easier to track their performance and document what they've learnt.
4) With the use of mobile learning applications, it is very easy to, and positively, engage students a any given time and place.
5) Mobile learning Application is easy and understandable.
6) Using mobile learning apps, contents are provided to students in a continuous or related way w taken in sequence.

7) Learning contents in mobile learning apps contain appealing and intriguing features.

The second one is the difficulties facing teachers in using learning applications mobile after the CO
19, and this factor includes (5) items as listed below:
1) I don't have time to use mobile learning applications.
2) I prefer traditional methods of teaching students instead of teaching using applications of mobi
learning.
3) My lack of knowledge about the optimal use of mobile applications for teaching.
4) I feel that using mobile learning devices causes a waste of time.
5) I feel that there is no benefit in using mobile learning applications in the learning process.

The researchers took care in formulating the questionnaire as simple and easy as possible; theref
is understandable to the research sample which was 100 instructors. The survey is graded respon
according to a five-point Likert scale, which corresponds to each item of the questionnaire. The
questionnaire has a specific value as follows: : Typically 5 marks which include 4.21-5, regularity
marks which includes 3.41-4.20, occasionally 3 marks which includes 2.61-3.40, Rarely 2 marks wh
includes 1.81-2.60, never 1 mark ranging 1-1.80.

4. Results and discussion

To determine the objectives that were set and to analyze the data collected, it analysed via the Statistical Packages for the Social Sciences (SPSS) program. A number of statistical methods and techniques were used to determine the trends of members as a representative of the study population. All but three of the faculty also noted the effectiveness of lecturing and sharing of resources or time irrespective of the time / geographical location and this was especially significant given the current confined mobility and access to learning institutions. As for the relations with the attendees, the mobile learning applications were described enabling one to engage in interactive sessions via Multimedia tools. However, one faculty said, the students could not pay attention for a long time; there is a literature of students possibly requiring faculty-directed promptness to remain active on the mobile platforms. The researchers used the following statistical tests such as frequencies, percentage, mean (weighted), standard deviation, and correlation coefficient. The responses of the first factor which is the reality usage for mobile learning applications in teaching after COVID-19, as presented in the following Table 1, and Figure1.

Table 1.The reality usage for mobile learning applications in teaching

No	Statement	Not at all (1)	Seldom (2)	Some (3)	Regularly (4)	Often (5)	Mean	SD	Choice
1	Mobile learning applications enhanced the learning performance compared to traditional education	5	17	5	33	40	3.85	1.33	Regularly
2	Use mobile learning applications in teaching students after COVID-19 (Corona)	0	5	11	25	59	4.40	0,91	Often
3	Mobile learning applications have made it easier to monitor students' performance and record their progress in learning	3	11	12	29	45	4,1	1.2	Regularly
4	Mobile learning applications have made it easier to communicate and interact positively with students anywhere, anytime	3	23	13	28	33	3.71	1.33	Regularly
5	Using mobile learning apps is simple and clear	2	10	8	52	28	3.97	0,93	Regularly
6	Mobile learning apps deliver content in a sequential and interconnected manner for students	3	12	15	31	39	3.83	1.23	Regularly
7	Mobile learning apps have interesting and attractive elements into the learning contents	6	16	20	20	38	3.47	1.20	Regularly
The mean of the total statements							3.90	1.22	Regularly

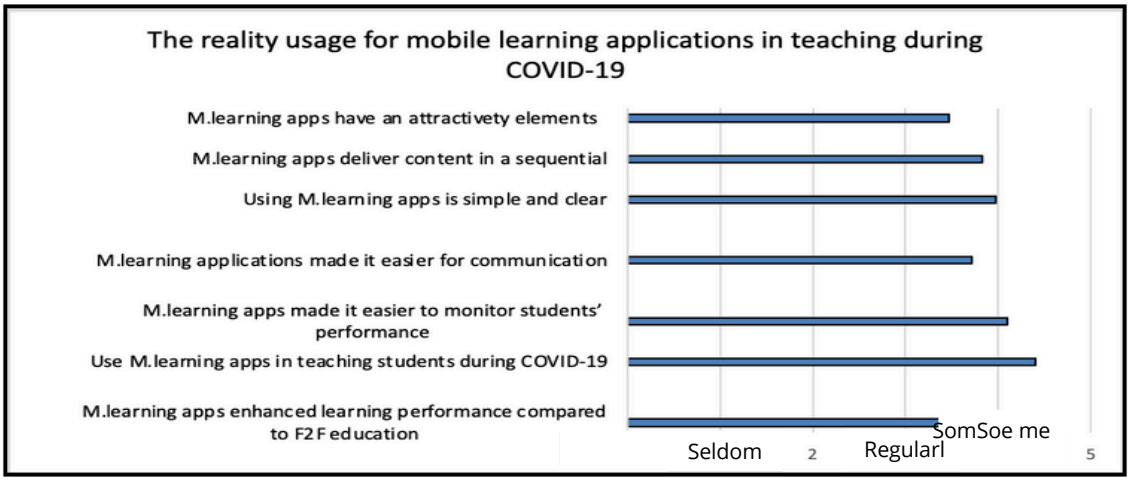

Figure 1. The reality usage for mobile learning applications in teaching

When looking into the Table 1, the result that found for statement of "Mobile learning applicati enhanced the learning performance compared to traditional education" is 3.85 which is regul Whenever designed and facilitated correctly, we can obtain choice, simplicity, interaction, and individualization that may not always be feasible in classroom instruction. Consumers can make u the content at any time and from anywhere making it easier and adaptable for learning. Also, m learning applications can include audio and video, as well as opportunities for learning through qu control simulations, and others, which can improve results of knowledge and motivation. They ca be used to create multi-media presentation that enhances learning and communication among s and instructors. Furthermore, the result that been drawn from the sample for the statement c mobile learning applications in teaching students after COVID-19 (Corona)" was 4.40 which mea often. This is might because mobile learning applications provide flexibility for students to learn a own pace and convenience. They can access educational materials anytime, anywhere, which is especially beneficial after periods of remote learning or lockdowns. This is influenced by other fac such as access to technology, engagement levels, teacher support, assessment methods, and interaction opportunities. [34] and [35] confirmed an effective mobile learning applications desig provide flexibility for students to learn at their own pace and convenience and their research outc support the use of mobile learning applications in education. When moving into the stateme "Mobile learning applications have made it easier to monitor students' performance and record progress in learning", the mean of the responses was 4.1 which is regularly.

Most mobile learning applications provide tools whereby the trainer is able to track the achieven of their students in real time through quizzes, tests and assignments. They can monitor the time s spend on resources, on tasks as well as time spent on different modules and content they use. assessments provide immediate feedback to both students and instructors, allowing for quick identification of areas where students may need additional support or intervention. This findi consistent with that [36] and [12] who investigated the effects of monitoring students' progress th mobile devices and found that mobile learning applications made the process of monitoring stud progress easy for instructors and they can get full details about their students learning progress i of what they have achieved and not achieved form the learning outcomes. Moreover, the result re that "Using mobile learning apps is simple and clear" was 3.97 which means regularly. Mobile lear apps are typically designed with consistency and intuitive user interfaces that prioritize ease of navigation and accessibility. Clear menu structures, well-labelled buttons, and simple layouts ma easy for users, including students and instructors, to find and use the app's features. This consis enhances usability by ensuring that users can easily recognize and understand common interface elements and interactions. These features ensure that the app remains clear and usable for indiv with different abilities and preferences. This is in line with the statement made by [37] who stated mobile learning apps are intuitively designed with friendly user interfaces that prioritize ease of navigation and accessibility and this will make the app remains clear and usable for users with dif capabilities. The last two statements which are "Mobile learning apps have interesting and attra elements into the learning contents" and "Mobile learning apps deliver content in a sequentia interconnected manner for students" revealed that the result is about 85% which was regularly. T could because of mobile learning apps leverage multimedia elements such as videos, animations, infographics, and interactive simulations to make learning content more engaging and dynamic. V and auditory stimuli enhance students' understanding and retention of complex concepts. Some frequently applied approaches to encourage the learners are related to the fact that many mobile applications created to aid the learning process are designed as educational games. Gamified ele bring levels of engagement from students, compel them into participation and make student accomplished.

The finding is consistent with that [38] who investigated the combination of interesting and attra elements in mobile learning apps and found it enhances students' engagement, motivation, and l outcomes by delivering content in an interactive, interconnected, and personalized manner. T results support the findings of [39] who stated that mobile learning apps combined by the eleme interest and attractiveness can increase students' engagement, motivation, and learning outcome moving to the data that been collected in order to answer the second factor which investigat difficulties that faced teachers when using mobile learning applications after the COVID-19, the findings analysed and shown in following Table 2, and Figure 2.

Table 2. The difficulties faced by teachers when using mobile learning applications.

No	Statement	Not at all (1)	Seldom (2)	Some (3)	Regularly (4)	Often (5)	Mean	SD	Choice
1	I don't have time to use mobile learning applications	1	16	19	29	35	3.7	1.07	Regularly
2	I prefer traditional methods of teaching students instead of teaching using applications of mobile learning	1	6	31	37	25	3.85	0.87	Regularly
3	My lack of knowledge about the optimal use of mobile applications for teaching	1	1	6	43	39	4.4	0.71	Often
4	I feel that using mobile learning devices causes a waste of time.	15	57	10	9	9	2.3	1.2	Seldom
5	I feel that there is no benefit in using mobile learning applications in the learning process.	21	41	7	21	10	2.63	1.4	Seldom
The mean of the total statements							3.37	1.05	Some

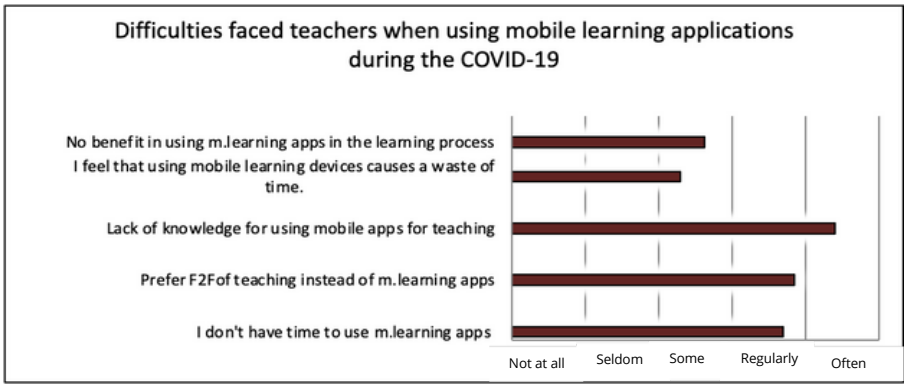

Figure 2. The difficulties faced by teachers when using mobile learning applications.

In Table 2, the findings revealed that the study sample is regular in their approval of the difficulties instructors face after the usage of mobile learning applications as the mean between 2.62 to 3.4 addition, the mean result that has been shown in the above table is between 1.05 to 3.8 that these indicate their opinion is between (some to regular) against the barriers of using mobile device learning. That way the study stresses on benefits that mobile learning applications has in a proce changing education all while putting into emphasis that much has to be done in order to maximiz use of the technological advancements. Some faculty members' feedback pointed out on one differences between potential advantages and on the other hand implementation difficulties. How in using multimedia and gamification elements in developing mobile tools, the authors have rea that these two aspects are not enough to ensure attention from the students. It was also reveal designing the mobile courses with several non-consecutive sections will improve the students; att span [2]. In order to make the desired equity possible, a lot of emphasis should be placed on infrastructure and offer trainings to the faculties severally. On the other hand, support services include technical support services like IT support round the clock are handy and minimize on the l a user is most likely to encounter with the product or tool. In addition to synthesizing the fac responses, this study found potential original sources of several of the challenges. In the same wa digital divide increases disparities in the use of mobile learning, and when there is no support fro university, faculty members will not be prepared. Solving these challenges requires a complex solu set that involves technology solutions, policy, and instructional design. Furthermore, collaboratio the tasks under implementation may have the effect of promoting peer interaction and engageme lack of knowledge about how to effectively leverage mobile applications for teaching can indeed significant barrier for instructors which is 4.4 out of 5, especially during times like the COVID-1 pandemic. This might be related to the limited training opportunities for instructors. They may no had sufficient training or exposure to use mobile apps for teaching purposes. Therefore, without p training, they may struggle to navigate these tools effectively. This supports the findings of the res study which conducted by [40] on what affect instructors' intention to use mobile apps. They foun teachers without adequate training to use mobile applications for teaching, they faced challeng navigate these apps effectively. In statement number 4 which investigates the usage of mobile technology in learning causes a waste of time, the result revealed that 2.3 out of 5 which means responds are seldom.

This feeling might be related to the interactivity or engagement that behind the educational co
design for mobile devices to hold students' attention. If the material is poorly presented, student
perceive it as a waste of time. This result reflects [41] who reported that the usage of mobile techn
in learning causes a waste of time if the material is poorly presented for the students as this will c
disengagement with learning contents. The last statement which is "I feel that there is no benefit
using mobile learning applications in the learning process" shows the mean responses of the sam
2.63 out of 5 which means seldom. This result indicates that much more of the sample does not
with this statement of no benefit when using mobile devices in learning. The rest of the sample wh
agree there is no benefit in using mobile learning might because technical challenges. Issues su
poor internet connectivity and device compatibility problems can hinder the learning experience
leave users feeling frustrated. People naturally tend to resist change, especially when it involves
adopting new technologies or learning methods. Resistance to mobile learning applications may
from a fear of the unknown or a reluctance to step outside of what they dealt with. According to s
research studies [42] [43][44] which conducted to investigate the effects of using mobile learn
applications in the learning process and studying the benefits and challenges of mobile learning
applications in education, it can be inferred that the use of mobile learning can be beneficia
instructors if they know how to use them properly whereas mobile learning apps can be useless if
those instructors do not know how to use them or no enough training provided to them.

5.Conclusions

An analysis of the impact of employing mobile learning applications in Al-Baha University with emphasis on the effectiveness of these applications in the presence of the new reality owing to COVID- 19 pandemic reveals pros and cons. It has been a time that saw a revolution in education across the world and Al-Baha University could not be left out. The authors determined that due to COVID-19, the shift towards online learning contributed to the emergence of mobile learning application among the faculty. At the same time, it became clear some of the main issues even in the spheres of staff development, information technology, and students' motivation. These are important lessons because as institutions adapt to post-Covid strategies, the lessons learned in Covid conscious and other disruptions in that line is paramount if the mobile learning needs to be a continued key player in current and future methods of delivering education. Building upon the main findings derived from the present studies, this conclusion addresses the advantages, difficulties, and consequences of employing these applications. Several advancements in mobile learning applications contributed to the improvement of access and flexibility the overall educational process. Lecturers could also teach as well as provide materials, students, and faculty, all without the restrictions of geographical location. This flexibility was important during such lock down periods because the education of the students was not interrupted. Mobile learning applications expanded the user participation using interactive instruments and multimedia. This marks the work interactivity and that they can be used to improve the performance of learning are statistically correlated. Discussion boards, quizzes, and recorded lectures kept students' attention and encouraged them because, compared to conventional classroom face-to-face teaching methods, which are mere talking and explaining, the formal distance learning tools provided adaptability and enhanced different forms of teaching–learning approaches. But major technological challenges were met there. The challenges encountered included poor internet connection, limited access to better devices and using a new set of technology altogether in some cases, by the faculty members. Among these challenges, the least developed mobile learning region experienced the most challenges due to the lack of adequate ICT infrastructures. The importance of this study therefore resides in the fact that it will bring out the faculty's practical experiences when the education system was undergoing change.

This study is helpful to report both advantages and disadvantage of integrating and impleme mobile learning since such information can help to strategize and policy educational direction to p disruptions in distance learning. The studies provide direction for institutions to improve the professional development of their faculty, to help educators become more prepared to integrate technology within their classroom and other educational settings. The technological factors mu resolved to enhance the use of mobile learning especially in areas that lack robust technological systems. By taking these implications into account, educational institutions will be more capabl create more tolerant, malleable, and adaptive learning environment that will not be as much affec further global disruptions such as pandemics, shifts in technologies and so on to the existing tradi education paradigm.

REFERENCES

[1] MASHHADI, M. A. HUSSEIN, and A. K. FAHAD, "Mobile learning for teacher professional development: An empirical assessment of an extended technology acceptance model," *Porta Linguarum Rev. Interuniv. Didáctica las Lenguas Extranj.*, no. December, pp. 349–369, 2023, doi: 10.30827/portalin.vi2023.28658.

[2] I. Alkhadi and A. M. Alzaidiyeen, "The mobile blackboard system in higher education: Discovering benefits and challenges facing students," *Int. J. Adv. Appl. Sci.*, vol. 6, no. 6, pp. 6–14, 2019, doi: 10.21833.

[3] A. Almaiah *et al.*, "A Conceptual Framework for Determining Quality Requirements for Mobile Learning Applications Using Delphi Method," *Electron.*, vol. 11, no. 5, 2022, doi: 10.3390/electronics11050788.

[4] Busuttil and R. C. Farrugia, "Teachers' response to the sudden shift to online learning during COVID-19 pandemic: Implications for policy and practice," *Malta Rev. Educ. Res.*, vol. 14, no. 2, pp. 211–241, 2020.

[5] O. Abdullah and O. Alshehri, "Examining the existing reality of using social media as e-learning tools at an Emerging University in Saudi Arabia from the viewpoint of tutors and studen *PhD thesis*, 2021.

[6] A. I. Samuel, "The Concept of E-Learning amid Coronavirus (Covid-19) Pandemic in Nigeria : Issues , Benefits , Challenges , and Way Forward," *Int. J. Educ. Eval.*, vol. 7, no. 3, pp. 23–32, 2021.

[7] S. Mohamed, L. Elgamel, and H. Aldabbas, "Mobile Learning (M-learning) and Educational Environments," *Int. J. Distrib. Parallel Syst.*, vol. 3, no. 4, pp. 31–38, 2013.

[8] S. Gure, "' M - Learning ': Implications and Challenges," vol. 5, no. 12, pp. 2087– S. Kumar Bosak, 2093, 2016.Wotto, and P. Bélanger, "E-learning, M-learning and D-learning: Conceptual

[9] definition and comparative analysis," *E-Learning Digit. Media*, vol. 15, no. 4, pp. 191–216, 2018, doi: 10.1177/2042753018785180.

[10] Marunevich, V. Kolmakova, I. Odaruyk, and D. Shalkov, "E-learning and m-learning as tools for enhancing teaching and learning in higher education: a case study of Russia," *SHS Web Conf.*, vol. 110, p. 03007, 2021, doi: 10.1051/shsconf/202111003007.

[11] A. Campbell and L. Norton, "Learning, Teaching and Assessing in Higher Education: Developing Reflective Practice," *Learn. Matters Ltd*, 2007.

[12] Criollo-C, A. Guerrero-Arias, Á. Jaramillo-Alcázar, and S. Luján-Mora, "Mobile learning technologies for education: Benefits and pending issues," *Appl. Sci.*, vol. 11, no. 9, 2021, doi: 10.3390/app11094111.

[13] R. Muñoz *et al.*, "Systematic Review of Adaptive Learning Technology for Learning in Higher Education," *Eurasian J. Educ. Res.*, vol. 2022, no. 98, pp. 221–233, 2022, doi: 10.14689/ejer.2022.98.014.
[14] Maseleno, N. Sabani, M. Huda, R. Ahmad, K. A. Jasmi, and B. Basiron, "Demystifying learning analytics in personalised learnin," *Int. J. Eng. Technol.*, vol. 7, no. 3, pp. 1124–1129, 2018, doi: 10.14419/ijet.v7i3.9789.
[15] Sippard, O. Nasser, and P. Reddy, "The next generation of technology: Mobile apps in the english language classroom," *Int. J. Emerg. Technol. Learn.*, vol. 11, no. 4, pp. 21–27, 2016, doi: 10.3991/ijet.v11i04.5293.
[16] A. Zardari, Z. Hussain, A. A. Arain, W. H. Rizvi, and M. S. Vighio, "Development and validation of user experience-based e-learning acceptance model for sustainable higher educa *Sustain.*, vol. 13, no. 11, pp. 1–17, 2021, doi: 10.3390/su13116201.
[17] A. S. Mustafa and K. Karimi, "Enhancing Gamified Online Learning User Experience (UX): A Systematic Literature Review of Recent Trends," *Human-Computer Interact. Beyond Adv. Towar. Smart Interconnected Environ. (Part I)*, no. September, pp. 74–99, 2021, doi: 10.2174/9789814998819121010007.
[18] L. Hasan, "Examining User Experience of Moodle e-Learning System," *Int. J. Adv. Comput. Sci. Appl.*, vol. 12, no. 11, pp. 358–366, 2021, doi: 10.14569/IJACSA.2021.0121141.
[19] Alam and A. Mohanty, *Learning on the Move: A Pedagogical Framework for State-of-the-Art Mobile Learning*, vol. 662 LNNS, no. June. Springer Nature Singapore, 2023. doi: 10.1007/978-981-99-1414-2_52.
[20] Miura and K. I. Yabu, "Narrative Review of Assistive Technologies and Sensory Substitution in People With Visual and Hearing Impairment," *Psychologia*, vol. 65, no. 1, pp. 70–99 2023, doi: 10.2117/psysoc.2022-B031.
[21] M. Zalat, M. S. Hamed, and S. A. Bolbol, "The experiences, challenges, and acceptance of e-learning as a tool for teaching during the COVID-19 pandemic among university medical staff," *P One*, vol. 16, no. 3 March, pp. 1–12, 2021, doi: 10.1371/journal.pone.0248758.
[22] Ramadhan, "Revolutionizing Geography Education: Developing Mobile Learning Multimedia via the Nearpod Platform," *Futur. Sp. Stud. Geo-Education*, vol. 1, no. 1, pp. 82–98, 2024, [Online]. Available: https://www.futurespace.es/data-analytics/
[23] T. A. Lashari, R. Fiayaz, S. A. Lashari, I. Khan, S. Sultana, and T. Afzal, "Kahoot: A game-based web tool to assess motivation, engagement fun, and learning outcomes among engineers," *Comput. Appl. Eng. Educ.*, vol. 32, no. 2, 2024, doi: 10.1002/cae.22684.
[24] Ghoulam, B. Bouikhalene, A. Babori, and N. Falih, "Exploring the impact of mobile devices in electronics e-learning: A case study evaluating the effectiveness of mobile learning applications in the field of electronics and sensors," *Adv. Mob. Learn. Educ. Res.*, vol. 4, no. 2, pp. 1058–1072, 2024, doi: 10.25082/amler.2024.02.001.
[25] Kulaksız and F. Karaca, "Elaboration of science teachers' technology-based lesson practices in terms of contextual factors influencing TPACK," *Res. Sci. Technol. Educ.*, vol. 42, no. 2, pp. 357–377, Apr. 2024, doi: 10.1080/02635143.2022.2083598.
[26] Mogapi, B. Kagiso, and I. Gabajesane, "Examining the Learner-Teacher Digital Divide: Implications for Learning in Basic Education Classes - Insights from Teachers in Botswana," *J. Educ Soc. Behav. Sci.*, vol. 36, no. 8, pp. 61–80, 2023, doi: 10.9734/jesbs/2023/v36i81248.
[27] Ashiq, S. U. Rehman, A. Yousaf, and M. Safdar, "Exploring the use of mobile technologies for learning: an empirical study of library and information science (LIS) students," *Digit. Libr. Perspect.*, vol. 39, no. 4, pp. 604–619, 2023, doi: 10.1108/DLP-04-2023-0032.
[28] Almekhled and H. Petrie, "Concerns of Saudi Higher Education Students About Security and Privacy of Online Digital Technologies During the Coronavirus Pandemic," *Lect. Notes Comput Sci. (including Subser. Lect. Notes Artif. Intell. Lect. Notes Bioinformatics)*, vol. 14144 LNCS, no.

September, pp. 481–490, 2023, doi: 10.1007/978-3-031-42286-7_27.
[29] S. Wang, M. C. Wu, and H. Y. Wang, “Investigating the determinants and age and gender differences in the acceptance of mobile learning,” *Br. J. Educ. Technol.*, vol. 40, no. 1, pp. 92–118, 2009, doi: 10.1111/j.1467-8535.2007.00809.x.
[30] Matli and M. Malatji, “A Review of Internet Use and Access for BRICS Sustainable Futures: Opportunities, Benefits, and Challenges,” *J. Inf. Syst. Informatics*, vol. 6, no. 1, pp. 435–452, 2024, doi: 10.51519/journalisi.v6i1.636.
[31] A. Raque *et al.*, “Disruptions caused in Pakistan by the COVID-19 Pandemic and their Wireless Technology Based Solutions,” pp. 1–17, 2022, [Online]. Available: https://doi.org/10.21203/rs.3.rs-1716250/v1
[32] Mohtar, N. Jomhari, N. A. Omar, M. B. P. Mustafa, and Z. M. Yusoff, “The usability evaluation on mobile learning apps with gamification for middle-aged women,” *Educ. Inf. Techno* vol. 28, no. 1, pp. 1189–1210, 2023, doi: 10.1007/s10639-022-11232-z.
[33] Kovacs, S. Buzura, B. Iancu, V. Dadarlat, A. Peculea, and E. Cebuc, “Practical Implementation of a Blockchain-Enabled SDN for Large-Scale Infrastructure Networks,” *Appl. Sci* vol. 14, no. 5, 2024, doi: 10.3390/app14051914.
[34] S. Saikat *et al.*, A systematic review of the benefits and challenges of mobile learning during the COVID-19 pandemic. Education Sciences, 2021, 11(9), p.459.
[35] A.L.R., "Accelerating the Move Towards Online Learning Through Cloud Platforms in Higher Education Sectors Using Smart Devices during COVID-19". *International Journal of Interactive Mobile Technologies*, 2021, 15(10).
[36] A. Qashou. "Influencing factors in M-learning adoption in higher education". *Education and information technologies*, 2021, 26(2), pp.1755-1785.
[37] L.A.Zaina, Fortes, R.P., Casadei, V., Nozaki, L.S. and Paiva, D.M.B., "Preventing accessibility barriers: Guidelines for using user interface design patterns in mobile applications". *Journal of Syst and Software*, 2022, 186, p.111213.
[38] Videnovik, Trajkovik, V., Kiønig, L.V. and Vold, T., "Increasing quality of learning experience using augmented reality educational games". *Multimedia tools and applications*, 2020, 79(33), pp.23861-23885.
[39] Nikolopoulou, Gialamas, V. and Lavidas, K., "Habit, hedonic motivation, performance expectancy and technological pedagogical knowledge affect teachers' intention to use mobile internet". *Computers and Education Open*, 2021, 2, p.100041.
[40] Al-Emran, Mezhuyev, V. and Kamaludin, A., "Towards a conceptual model for examining the impact of knowledge management factors on mobile learning acceptance". *Technology in Soci* 2020, 61, p.101247.
[41] J. Balanyà Rebollo, and De Oliveira, J.M., "Teachers' Evaluation of the Usability of a Self-Assessment Tool for Mobile Learning Integration in the Classroom". *Education Sciences*, 2024, 14(1 p.1.
[42] N.S. Adzifome, and Agyei, D.D., "Learning with mobile devices-insights from a university setting in Ghana". *Education and Information Technologies*, 2023, 28(3), pp.3381-3399.
[43] M.A. Adarkwah, “I’m not against online teaching, but what about us?”: ICT in Ghana post Covid-19. *Education and information technologies*, 2021, 26(2), pp.1665-1685.

Clean cultivation of (*Vicia faba* L) using household waste

Hala Ali Mohammad
Field Crops Department, Faculty of Agriculture, Tishreen University, Syria

Email: halamohammad445@gmail.com

Abstract: Agriculture has been practiced for thousands of years without the use of any chemicals, and the use of these agricultural chemicals not only causes degradation of arable land, but also causes soil pollution. To overcome this situation, organic agriculture is the only solution that only involves natural resources such as organic materials, plant and animal waste, and microbes. This is what helped increase the importance of research, as a pot experiment was carried out in Tartous Governorate for the 2021- 2022 season to study the effect of some household waste, such as (Rice water and ground egg shells) in the growth and development of bean plants. In addition to the evidence, water only, as natural fertilizers free of chemical compounds. The experiment was conducted in a completely randomized block design.

The results showed that there were significant differences between the studied treatments compared to the control, and the rice water treatment achieved significant superiority in morphological traits (plant height, number of leaves, number of branches), while the eggshell treatment excelled in productive traits (number of flowers, number of pods, seed weight, productivity per hectare).

Keywords: Vicia faba, eggshells, rice water, morphological characteristics, household waste.

الزراعة النظيفة لنبات الفولVicia faba باستخدام المخلفات المنزلية

الملخص.كانت الزراعة تمارس لآلاف السنين دون استخدام أي مواد كيميائية، واستخدام هذه الك
لا يسبب تدهور الأراضي الصالحة للزراعة فحسب، بل يتسبب أيضا في تلوث التربة.
وللتغلب على هذا الوضع، فإن الزراعة العضوية هي الحل الوحيد الذي لا ينطوي إلا على
الموارد الطبيعية مثل المواد العضوية والنفايات النباتية والحيوانية والميكروبات، وهذا ما
سا على زيادة أهمية البحث عن تأثير بعض المخلفات المنزلية مثل)ماء الأرز ومطحون قشو
البيض(في نمو وتطور نبات الفول إضافة للشاهد ماء فقط، كمخصبات طبيعية خالية من المركبات
. حيث تمت التجربة بتصميم القطع العشوائية الكاملة. بينت النتائج وجود فروق معنوية بين المعام
مقارنة بالشاهد وحققت معاملة ماء الأرز تفوقا معنوياً بالنسبة للصفات المورفولوجية)ارتفاع النبا
عدد الأفرع(في حين تفوقت معاملة قشر البيض بالصفات الإنتاجية)عدد الأزهار، عدد القرون ،
إنتاجية الهكتار(.

1. Introduction

Faba bean (*Vicia faba*) is a potential, versatileleguminous crop of Fabacee family which can begrown in varied climatic conditions throughout theworld (Arya *et al*., 2018 & 2022). The crop, if usedin rotation or as intercrop (Köpke and Nemecek, 2010;Arya *et al*., 2019) with other cereal crops, providesagronomic, economic and, environmental benefits tothe farmers in the form of reducing the requirementof inorganic fertilizers for next crops (Aschi *et al*.,2017; Arya et al., 2020), by increasing the plant yields(Xiao *et al*., 2018) and by breaking the vicious cycleof disease and pests (Zhang *et al.*, 2019). Faba beanalso known as many names such as Field bean, Broadbean, Windsor bean, Horse bean, Tick bean, Longpodbean and Kaka Matar (Mínguez *et al*., 2021). It hasbeen produced in Mediterranean region (Jensen et al.,2010) China, Africa, Europe, Middle East, Asia whereit is most common crop for human and animalconsumption. Faba bean (kernel as well as maturedry seed) with well-balance d aminoacid profile(Martineau *et al*., 2022) is a rich source of protein,(Multari *et al*., 2015) carbohydrates, minerals (Rahateet al., 2020), vitamins (Oomah *et al*., 2011); and otherbioactive phytochemica ls along with some anti-nutritional compounds (Mattila *et al*., 2018).

It is also a good source of protein, and works to improve soil properties and increase its

fertility due to

its ability to stabilize atmospheric nitrogen thanks to the bacterial nodules formed on its roots (Singh *et al*., 2013). Awareness of environmental and food safety issues is responsible for the The recent increasing interest in phytonutrients and the nutritional and health benefits of faba plants confirms the importance of this crop, which contains a group of biologically active phytochemicals in its mature seeds and green pods as well as leaves. These phytochemicals inc development of organic agriculture in recent years (Masiri and *et al*., 2018). phenolic compounds, flavonoids, biologically active peptides, and dietary fiber. Amino acids are m organic compounds responsible for various biological activities and increase the importance of this plant in treating diabetes, anti-inflammatory, antihypertensive, antiviral, antibacterial, antifungal, antioxidant, antimalarial, anticancer, and cholesterol lowering)Kumae *et al*., 2022).

Recently, farmers' choice has been shifted to organic farming instead of chemical fertilizers due to high cost and inefficiency to improve soil fertility (Oyedeji et al., 2014). Organic fertilization ha become an important part of environmentally sound, sustainable agriculture. Coming from org sources makes it more valuable for agriculture (Arora and Maini,2011).
The use of organic fertilizer has improved soil fertility and helps combat diseases. It is also an environmentally friendly way to reduce waste that accumulates in landfills (Khadem et al.,2010). Eggshell waste can be used as plant fertilizer because eggshells contain 95% calcium carbonate (J and Paul, 2006). It helps in changing the exponent.

Very especially for P is 0,21%, K is 0,40%, Ca is 0,47% and Mg is 0,09%.The results of a study showe

the effect of rice husk ash (75, 50, 25, 0) g/plant and ground egg shells (0, 15, 30) g/plant on the gr of pepper plants. The results showed that rice husk gave the best values for morphological traits level of 50 g/plant.

While eggshell powder achieved the best values for production characteristics at the level of (

g/plant, as eggshell powder is considered a fertilizer that supplements organic fertilization and m the plant's calcium needs. Rice husk ash has mineral binding function and helps loosen the soil, so it can help plant roots to absorb nutrients (Kurniatuti,2018).

Rice water biofertilizers depend on the chemical reaction resulting from the mixture of starch water and milk. This mixture produces lactic acid bacteria that improve soil health by decomposing organic matter and reducing unwanted pathogens associated with decomposing material. It also eliminates unpleasant odors associated with compost. The starch water allows bacteria to grow while the milk isolates the bacteria needed for the fertilizer leaving unwanted bacteria to die. These results showed that starch water biofertilizer is a good organic fertilizer for home gardens as it is easy to make and can be accessed at any time (Abba et al., 2021).

(Pervez et al., 2000) Showed in a study of the effect of organic fertilizers on the growth of

potato and

pea crops using different types of organic fertilizers (egg shells, wood ash, banana peels, used tea waste,
and soil seedlings only), where the best values were for plant height, number of branches,

leaf surface
area, and productivity. Egg shell powder from the two plants, followed by banana peels,
then used tea
waste

A study conducted in India showed the effect of fertilizing with eggshells on the growth of the fenu
plant and increasing soil fertility by using organic fertilizers (food scraps) such as egg and fruit sh
to improve the properties of the soil. The results showed an improvement in the properties of th
and its content of calcium carbonate and nitrogen, in addition to improving the growth, develop
and productivity of the fenugreek plant (Karn *et al*., 2023).

The results of a study of eggshell powder on tomato plants were achieved in two different soils, o
which eggshell powder was added and another to which the powder was not added. A difference
observed in the characteristics of the soil that contained eggshell powder and the other that d
contain it. The results also showed that eggshell powder It helped the plant to grow, as it is consid
a natural, safe and healthy fertilizer for humans (Ayyub *et al*., 2012). A study of the effect of eggshe
on the growth of pepper plants as an organic fertilizer showed an increase in the wet and dry weig
the plant, root length, and plant height (Anugrah *et al*.,2021).
This study was conducted to determine the possibility of utilizing household waste as clean and
household fertilizers

The importance of the research stems from the importance of the bean crop, the possibility of gro
it in narrow spaces, and benefiting from household waste as clean and safe household fertilizer
the organic fertilization method and reducing the costs of chemical fertilization From the above
research aims to compare the growth and development of bean plants using two types of house
waste (egg shell powder and rice soak). Determine the best values resulting from treatment with
wastes.

Materials and methods:

(Location: Syria_Tartous_Safita. A home potting experiment was conducted

Varieties: The Spanish variety was obtained from the local market

Studied treatments: two types of household waste (such as biofertilizers) in addition to the con
water only. Water (see) _ egg shells _ rice water

Irrigation was treated with the previous treatments every 15 days for two months, 4 times durin
plant growth stages.

How to prepare eggshell fertilizer: According to (Karn *et al*., 2023) grams of egg shells were ground, and we obtained cup of finely ground shells ,Then we put it in a bowl and added three times as much apple cider vinegar to it (that is, three cups of apple cider vinegar are added to every cup of egg shells). Then mixing was done until the reaction stopped and no bubbles appeared. The container was closed well and placed in a dark place for (3-4) days for the reaction to occur

Then a very thin, brown layer forms. We remove the layer and then filter the mixture to get rid of the sediment

Then we take 10 ml of the mixture of egg shells and vinegar, dissolve it in a liter of water, and then use it, the rest of the mixture is stored in a cool place in a closed plastic container and we pierce it at the top.

1- Rice water.Rice water fertilizer is a natural fertilizer that is prepared at home and is the water that results from washing or soaking rice.

It contains a number of nutrients such as carbohydrates, vitamins, sugar, fibre, iron, magnesium and phosphorus, nitrogen, phosphorus and potassium, so it is considered a natural alternative to chemical fertilizer

But of course, the proportions of the elements are light and not concentrated, and therefore there will be no fear of harm to the plants if it is used in a concentrated form or several times. Rice fertilizer is used on all plants at all their different stages.

How to prepare rice water:According to (Abbas *et al*, 2021)

Put cup of rice in a liter of warm water and leave it for (2-3) hoursWe filter the water into a suita bowl, add 3 tablespoons of natural milk and mix well

We cover the bowl well with a piece of cloth or gauze. Then put it in a dark place and leave it for (2 days.After that, we remove the gauze, examine it, and notice the formation of a thin, white layer, s remove it. We filter the rice water, then take 10 ml of the mixture, dissolve it in a liter of water, a then use it on the plants

Store the rest of the mixture in a closed plastic container with a hole punched in the top.The trea was carried out with irrigation and the previous components every 15 days for two months, 4 t during the plant growth stages.

The readings studied: plant height (cm) / number of branches / plant - number of leaves / pla number of flowers / plant - number of pods / plant - weight of pods / plant (g).

Experiment design: The experiment was designed using a randomized block method, then the was tabulated on the Excel program and a statistical analysis was performed using the Genst program to determine the least significant difference at the 5% level.

Results and discussion:

1:The effect of household waste on the height of bean plants/cm.

Table (1) shows the effect of treatment with household waste (control, rice soak, and ground eggshells) on plant height. The averages reached (90.44, 100.10, 90.88) cm, respectively. Comparin the averages, it was noted that there were no significant differences between the studied treatme but the reason for soaking rice was an increase in the height of the plant, as soaking rice can help plant roots to absorb nutrients)Kumae *et al*., 2022).

Table (1): Shows the effect of household waste on bean plant height (cm)

ground egg shells	soaked rice	water	Refined
91.00	95.33	87.33	1
97.33	101.66	89.66	2
84.33	103.33	94.33	3
90.88 a	100.10 a	90.44 a	Average
	11.78		L.S.D5%
	5.5		CV%

2:The effect of household waste on the number of branches/plant

Table (2) shows the effect of treatment with household waste (control, rice soak, and ground eggshells) on the number of branches/plant. The averages reached (3.33, 4.33, 3.33) branches/plant, respectively.

Comparing the averages, it was noted that there were no significant differences between the studied treatments, but the reason for the rice soaking was an increase in the number of branches, as the rice soaking can help the plant roots to absorb the nutrients that caused an increase in the number of branches. The height of the plant, and this in turn was reflected in the number of branches/plant)Kumae *et al*., 2022).

Table (2): shows the effect of household waste on the number of branches of bean plants

ground egg shells	soaked rice	water	Refined
4.00	4.00	3.00	1
3.00	5.00	3.00	2
3.00	4.00	4.00	3
3.33 a	4.33 a	3.33 a	Average
	1.31		l.S.D5%
	15.7		CV%

3:The effect of household waste on the number of leaves/plant

Table (3) shows the effect of treatment with household waste (control, rice soak, and ground eggshells) on the number of branches/plant. The averages reached (37.00, 46.00, 41.00), leaf/p respectively.

Comparing the averages, significant differences were found between the studied treatments, where soaked rice achieved significant superiority over the other treatment and the control, and achieved the best value (46.00) leaf/plant, and in turn, ground was superior. Eggshells on the control that gave the lowest value (37.00) leaf/plant. This may be attributed to the role of both types of fertilizers used (egg shells and rice water) and the role of organic extracts in germination and increasing the overall productivity of the plant, and this is what the rice soaking achieved(Arora and Maini,2011).

Table (3): shows the effect of household waste on the number of leaves of bean plants

ground egg shells	soaked rice	water	Refined
46.00	51.00	42.00	1
40.00	46.00	35.00	2
36.00	42.00	34.00	3
41.00 b	46.00 a	37.00 c	Average
	2.07		L.S.D.5%
	2.2		CV%

4:The effect of household waste on the number of flowers/plant

Table (4) shows the effect of treatment with household waste (control, rice soak, and ground eggshells) on the number of flowers/plant. The averages reached (15.00, 17.00, 21.00) flower/plan respectively. Comparing the averages, significant differences were found between the studied treatments, where ground eggshell achieved significant superiority over the other treatment and control and achieved the best value (21.00) leaf/plant, and in turn, ground Egg shells were the con that gave the lowest value (37.00) flower/plant, followed by soaked rice, superior to the control th gave the lowest value (15.00) flower/plant. The increase in the number of flowers is due to the eggshells containing 95% calcium carbonate. It helps in changing the pH of acidic soil and thus he in increasing the absorption of nutrients for the plant (Singh *et al*., 2013).

Table (4): shows the effect of household waste on the number of flowers/bean plant*s*

ground egg shells	soaked rice	water	Refined
23.00	21.00	17.00	1
18.00	14.00	12.00	2
21.00	16.00	16.00	3
21.00 a	17.00 b	15.00 c	Average
	2.07		L.S.D5%
	2.2		CV%

5:The effect of household waste on the number of pods/plant

Table (5) shows the effect of treatment with household waste (control, rice soak, and ground eggs on the number of pods/plant. The averages reached (6.66, 10.33, 13.66), pods/plant, respectively.

Comparing the averages, significant differences were found between the studied treatments, where the ground eggshell had a significant superiority over the other treatment and the control, and achieved the best value (13.66) pods/plant, and in turn was superior to Soaked rice was the control that gave the lowest value (6.66) pod/plant. Eggshells contain trace elements of magnesium, sodium, calcium, zinc, manganese, and copper, at a rate of 0.3%. Magnesium (Mg) plays an important role in transporting phosphate in plants, and therefore the phosphate content in plants can be increased by adding magnesium through eggshells, and this in turn is reflected in increasing the number of pods on the plant (Khadem et al, 2010).

Table (5): Shows the effect of household waste on the number of pods/bean plant

ground egg shells	soaked rice	water	Refined
14.00	12.00	8.00	1
13.00	9.00	5.00	2
14.00	10.00	7.00	3
13.66 a	10.33 b	6.66 c	Average
	1.51		L.S.D.%
	6.5		CV%

6:The effect of household waste on the weight of pods/plant

Table (6) shows that there was a significant increase in the weight of the pods between the studied treatments (water, soaked rice, ground eggshells), where the averages reached (257.46, 167.83, 85.44) g/plant, respectively, where the ground eggshells achieved significant superiority over the treatments. studied and gave the highest value (257.46) g/plant, followed by soaked rice and then water, which gave the lowest value (85.44) g/plant. The reason may be because eggshells contain up to 0.3% phosphorus and trace elements (magnesium, sodium, potassium, zinc, manganese, copper) contain 0.3%. Phosphorus plays a role in energy transfer in plant cells, such as ADP and ATP. Phosphorus (P) for plants is beneficial in stimulating root growth. In addition, phosphorus acts as a raw material for photosynthesis and respiration. It accelerates flowering, the appearance of fruits, and increases their weight (Arora and Maini, 2011).

Table (6): shows the effect of household waste on the weight of pods/bean plants

ground egg shells	soaked rice	water	Refined
272.46	191.66	102.83	1
247.53	143.83	64.83	2
252.46	168.00	88.66	3
257.46 a	167.83 b	85.44 c	Average
	15.38		L.S.D5%
	4.0		CV%

7: The effect of household waste on the weight of seeds/plant (g)

Table (7) shows that there was a significant increase in seed weight among the studied treatments (water, soaked rice, ground eggshells), where the averages reached (214.61, 133.58, 63.04) g/plant, respectively, where ground eggshells achieved significant superiority over the treatments. studied and gave the highest value (214.61) g/plant, followed by soaked rice and then water, which gave the lowest value (63.04) g/plant. The reason may be because eggshells contain up to 0.3% phosphorus, as phosphorus plays a role in energy transfer in plant cells, such as ADP and ATP. In addition, phosphorus acts as a building block for nucleic acids (DNA and RNA), lipids and proteins (John and Paul,2006).

Table (7): shows the effect of household waste on the weight of seeds/bean plants (g)

ground egg shells	soaked rice		Refined
228.00	151.90	wate	1
206.57	114.90	r	2
209.26	133.96	76.43	3
214.61 a	133.58 b	63.04 c	Average
	11.28	48.50	L.S.D5%
	3.6		CV%
		64.19	

8: The effect of household waste on the weight of seeds/plant (g)

Table (8) shows that there was a significant increase in productivity among the studied treatments (water, soaked rice, ground eggshells), where the averages reached (94.56, 200.38 (321.92 g/plant). Comparing the averages, significant differences were found between the studied treatments, and the ground eggshells achieved it was significantly superior to the second treatment and the control and gave the highest value (321.92) g/plant, followed by rice water, then water. This may be attributed to the fact that ground eggshell contains up to 0.3% of phosphorus and contains trace elements (magnesium, sodium, potassium, zinc, manganese, and copper) at a rate of 0.3. %. Phosphorus acts as a raw material that helps photosynthesis and respiration. Accelerates flowering and the appearance of fruits. Moreover, calcium has an important role in maintaining the quality of the fruit, maintaining the integrity of the cells, and the growth of the fruits and increasing their weight)Kumae *et al*., 2022).

Table (8): shows the effect of household waste on productivity per hectare, kg/ha

ground egg shells	soaked rice	water	Refined
342.00	227.85	114.65	1
309.86	172.35	72.75	2
313.89	200.94	96.29	3
321.92 a	200.38 b	94.56 c	Average
	16.85		L.S.D5%
	3.6		CV%

Conclusions:

•The treatment is superior to the rice soak in terms of the number of leaves, the number of branc and the length of the plant

•Eggshell ground treatments were superior in terms of number of pods, number of flowers, seed weight, and productivity.

Suggestions :

Use these household wastes because they are natural, inexpensive, economical, and do not stress soil. They help improve the properties of the soil and are not harmful to the environment

REFERENCES

[1] Arya, R. K., 2018 : Evaluation of faba bean genotypes for seed yield under Haryana conditio Forage Res., 44 : 60-62.

[2] Arya, R. K., R. Kumar, J. S. Hooda, J. M. Sutaliya, G. S. Dahiya, Vandana., H. L. Raiger, S. K. Yadav, R. K. Gill, J. L. Mehto, J. K. Tiwari, C. B. Yadav, M. K. Deen, R. Punia, K. Raj, R. Lal, P. Kumar, R. N. Tripathi, G. Singh, S. P. Singh, 2022 : Pre-breeding evaluation of germplasm for hybridization and screening of resulting transgressive elite genotypes faba bean for yield and its attributes for semi-arid regions of India. Ekin J., 8(1) :17- 26.

[3] Köpke, U. and T. Nemecek, 2010 : Ecological services of faba bean. Field Crops Res.,115 : 217–233.

[4] Arya, R.K., R. Kumar, J.M. Sutalia, G.S. Dahiya, and V.K. Madan, 2019 : Studies on genetic variability for seed yield and its contributing traits in faba bean. In proceeding: First national confe on 'Neglected and Under Utilized Crop Species for Food, Nutrition, Energy and Environment' held August 2, 2019 at NIPGR, New Delhi, India, pp. 123-124. www.nucsfnee2019.co.in

[5] Jeuffroy, M.H., A. Bouchi, M. Aubert, W. Riah-Anglet, S. Nélieu, C. Dubois, M. Akpa-Vinceslas, I. Trinsoutrot-Gattin, 2017 : Introduction of Faba bean in crop rotation: Impacts on soil chemical a biological characteristics. Appl. Soil Ecol.,120 : 219–228

[6] Arya, R. K., G. S. Dahiya, R. Kumar, J. M. Sutaliya, Vandana and P. Kumar, 2020 : Effect of heat stress on the elite genotypes of faba bean under semiarid conditions. Forage Res., 46 : 236-2

[7] Zhao, J., X. Yin, J. Ren, M. Zhang, L. Tang, Y. Zheng, 2018 : Complementation drives higher growth rate and yield of wheat and saves nitrogen fertilizer in wheat and faba bean intercropping Crops Res.,221 : 119–129.

[8] Zhang, C., Y. Dong, L. Tang, Y. Zheng, D. Makowski, Y. Yu, F. Zhang, W. vander Werf, 2019 : Intercropping cereals with faba bean reduces plant disease incidence regardless of fertilize a meta-analysis. Eur. J. Plant Pathol., 154 : 931–942.

[9] Vinguez, M. I., & Rubiales, D. (2021). Faba bean. In V. O. Sadras & D. F. Calderini (Eds.), Crop Physiology Case Histories for Major Crops (pp. 452–481). Academic Press. https://doi.org/10.1016/B978-0-12- 819194-1.00015-3.

[10] Jensen, E. S., M. B. Peoples, H. Hauggard-Nielsen, 2010 : Faba bean in cropping system. Fie
Crop Res.,115(3) : 203- 216.
[11] Martineau-Côté, D., A. Achouri, S. Karboune, L. L'Hocine, 2022 : Faba Bean: An untapped source of quality plant proteins and bioactives. Nutrients, 14 : 1541.
[12] Mattila, P.; J. M. Pihlava, J. Hellström, M. Nurmi, M. Eurola, S. Mäkinen, T. Jalava, A. Pihlanto, 2018 : Contents of phytochemicals and antinutritional factors in commercial protein-rich plant products. Food Qual. Saf., 2 : 213–219.
[13] Rahate, K. A., M. Madhumita, P. K. Prabhakar, 2020 : Nutritional composition, anti-nutritional factors, pre-treatments-cum-processing impact and food formulation potential of faba (Vicia faba L.): A comprehensive review. LWT - Food Sci. Technol., 138 : 110796.
[14] Jiamah, B. D., G. Luc, C. Leprelle, J. C. Drover, J. E. Harrison, M. Olson, 2011 : Phenolics, phytic acid, and phytase in Canadian-grown low-tannin faba bean (Vicia faba L.) genotypes. J. Agri. Food Chem., 59(8) : 3763-3771.
[15] Multari, S., D. Stewart, W. R. Russell, 2015 : Potential of fava bean as future protein supply to partially replace meat intake in the human diet. Compr. Rev. Food Sci. F., 14 : 511–522. https://doi.org/ 10.1111/1541-4337. 12146.
[16] Masarirambi M.T, Mduduzi, M.H , Olusegun T.O. ,Thokozile, E.S. 2010.Effects of Organic Fertilizers on Growth, Yield, Quality and Sensory Evaluation of Red Lettuce (Lactuca sativa L.) "Veneza Roxa". Agriculture and Biology Journal of North America, 1: 1319-1324.
[17] Kumae R , Duhan A, Sangwan S , Yadav N , Singh A , Kaushik D , Arya k, Dahiya S , Sutaliya J, Kumar V , Yadav V And Kumaa P. 2022.Brief Overview Of the Biological Activites Of Fababean (VICIA FABA). Forage Res., 48(2) : pp. 152-160
[18] Oyedeji S, Animasaun A , Bello A, Agboola A. 2014.Effect of NPK and Poultry Manure on Growth, Yield, and Proximate Composition of Three Ama-ranths. Journal of Botany, Article ID: 828750.
[19] Arora N, Maini P. 2011.Anaerobic Digested Slurry an Input for Sustainable Agriculture. Asia Journal of Experimental Sciences, 25: 59-62.
[20] Zadem A , Galavi M, Ramrodi M , Mousavi R, Rousta J. ; Mogha-dam P. .2010.Effect of Animal Manure and Superabsorbent Polymer on Corn Leaf Relative Water Content, Cell Memb Stability and Leaf Chlorophyll Con-tent under Dry Condition. Australian Journal of Crop Science, 4 642-647.
[21] John H. ; Paul, K. 2006.Can Ground Eggshells Be Used as a Liming Source? Integrated Crop Management Conference, Iowa State University:235-238.
[22] Kurniatuti T. 2018."Effect of Rice husk ash and Eggshell On the growth and yield OF Red Chill (Capsicum annuum L.)." JARES (Journal of Academic Research and Sciences. 3(1): 4-4.
[23] Abba N, Sung C. B., Paing T. N and Zuan K. 2021.Wastewater from Washed Rice Water as Plant Nutrient Source. Pertanika J. Sci. & Technol. 29 (3): 1347 - 1369.
[24] Perez A, Faqir M; Ehsan U. 2000.Effect Organic and Inorganic Manures on Physical and Characteristic of Potato (Solanum tuberosum L.) International Journal of Agriculture and Biology, 2: 1-2. [25]
Karn H, Harale P, Firodiya R, Gandhi S, Gore Shreya, Khalse R. 2023.Effect of Egg Shell Manure on Growth of Fenugreek Plants. Journal of Survey in Fisheries Sciences. Vol. 10 No. 1S: Special Issue 1

[35] Ayub C, Pervez M, Shaheen M, Ashraf I, Haider W, Hussain S; Mahmood N. . 2012.Assessment of Various Growth and Yield Attributes of Tomato in Response to PreHarvest Apllications of Calcium Chloride. Pakistan Journal of Life and Social Science, 10(2): 102-105.

[36] Anggraini R D, and Luthpi S. 2021."The effect of eggshell organic fertilizer on vegetative growth of cayenne pepper (Capsicum frutescens L)." In IOP Conference Series: Earth and Environmental Science, vol. 755, no. 1, p. 012001. IOP Publishing

Assessment of Airport Pavement Sustainability Using an Integrated Fuzzy ANP-TOPSIS Decision Model

Badr T. Alsulami
Civil Engineering Department, College of Engineering and Architecture, Umm Al-Qura University, Makkah, Saudi Arabia

Abstract: Sustainable design is the future of heavy construction projects such as airports. However, these structures usually require constant maintenance, which can become a major financial burden. The maintenance and rehabilitation of pavement, especially at airports, is a costly process which includes labour, equipment, and material expenses. By transitioning to a system that uses more sustainable designs and building materials, it is possible to build better structures that will not suffer serious damage. This research aims at building a new assessment framework for sustainable air-port pavements to be later applied to the case study of Taif airport in Saudi Arabia. To assess the proposed international airport in terms of sustainability, four sustainable alternatives (A1, A2, A3, and A4) are proposed, along with nine criteria. These alternatives are studied and the TOPSIS method is used to select the best alternative. Additionally, weights are calculated using the Fuzzy Analytic Network Process (FANP). According to achieved results, the best alternative is A4 (pavement made with recycled materials). This eco-friendly solution is recommended to the local Saudi authority as the optimal material to be used in the construction of the new Taif airport by including sustainability factors into the design process, allowing for informed judgements. Enhances airport pavement design processes and decrease environmental impacts connected with airport operations in a variety of contexts and locations. However, it can be concluded that the key findings of this study could provide a robust framework for optimizing sustainability in airport pavement management, enhancing decision-making efficiency and promoting long-term environmental, economic, and operational benefits.

Keywords*:* Airport, Analysis multi-criteria, Sustainability development

تقييم استدامة رصف المطارات باستخدام نموذج القرار الض
المتكامل ANP-TOPSIS

الملخص: التصميم المستدام هو مستقبل مشاريع البناء الثقيلة مثل المطارات. ومع ذلك، تتطلب هذه الهياكل عادة صيانة مستمرة، والتي يمكن أن تصبح عبئا ماليا كبيرا. إن صيانة وإعادة تأهيل الرصف، وخاصة في المطارات، هي عملية مكلفة تشمل العمالة والمعدات ونفقات المواد. من خلال الانتقال إلى نظام يستخدم تصاميم ومواد بناء أكثر استدامة، من الممكن بناء هياكل أفضل لن تعاني من أضرار جسيمة. يهدف هذا البحث إلى بناء إطار تقييم
[illegible]
[illegible]
ذلك، يتم حساب الأوزان باستخدام عملية الشبكة التحليلية ANP وفقًا للنتائج المحققة، فإن أفضل بديل هو A4)رصف مصنوع من مواد معاد تدويرها(. يُوُوصى بهذا الحل الصديق للبيئة للسلطة المحل باعتباره المادة المثلى التي يجب استخدامها في بناء مطار الطائف الجديد من خلال تضمين عوامل عملية التصميم، مما يسمح بأحكام مستنيرة. يعزز عمليات تصميم رصف المطارات ويقلل من التأثي المرتبطة بعمليات المطار في مجموعة متنوعة من السياقات والمواقع. ومع ذلك، يمكن أن نستنتج الرئيسية لهذه الدراسة يمكن أن توفر إطارًا قويًا لتحسين الاستدامة في إدارة رصف المطارات، وتعز اتخاذ القرار وتعزيز الفوائد البيئية والاقتصادية والتشغيلية طويلة الأجل.

1. Introduction

The concept of sustainability was first formulated in the Brundtland Report [1], where it was stated that the goal of sustainability is to “meet the needs of the present generation without compromising the ability of future generations to meet their own needs” [2]. The concept of sustainability is considered as a anticipated objective of development and environmental management [3]. Terminology which either directly cites or is related to sustainable development is becoming more and more common, with the number of sustainability-related terms increasing along with the rapid rise in aware-ness of the importance of sustainability [4]. According to many authors [5, 6], “sustainability” is coloured by context, that is, whether the notion of sustainability being ad-dressed concerns ecological sustainability, economic sustainability, social sustainability, or some other form [7]. The rapid expansion of the global society and economy has had a negative impact on sustainability, and the aviation industry, which is growing at an average annual rate of 5%, has contributed significantly to environmental issues while also promoting economic growth and addressing social employment challenges [8,9]. Airports play a crucial role in integrating air and ground traffic, and their sustainability is essential to meet the industry's growing objectives. To enhance airport sustainability, international initiatives have been implemented, such as the "Airports Sustainability Declaration" signed by over 20 airports in 2016 [10, 11]. However, technological innovation alone cannot address the issues posed by aviation as air travel continues to increase [12]. Effective management requires a thorough assessment of sustainability before any action can be taken [13]. The evaluation criteria and method-ologies used are critical in ensuring and enhancing airport sustainability through focused initiatives [14, 15]. Although numerous scholars have concentrated on operational aspects such as energy efficiency, water resource management, pavement materials, and the expansion of commercial facilities within airports, research specifically dedicated to the holistic assessment of airport sustainability remains relatively limited [16, 17]. Addressing this gap necessitates a comprehensive understanding of the interplay between theoretical frameworks and the practical challenges faced by airports in their current operational contexts. Such an approach is critical for ensuring effective evaluation and enhancement of sustainability practices [18, 19]. This study aims to highlight the importance of adopting environmentally sustainable pavement systems for the international airport located in Taif City, Saudi Arabia. By employing a combination of an indicator- based methodology and a comprehensive index, the research provides a dynamic assessment framework for Airport Pavement Sustainability (APS). The evaluation process explores APS alongside alternative sustainable solutions to identify strategies that minimize environmental impacts associated with intensive construction activities and prolonged industrial operations. This aligns with the broader vision of Saudi Arabian authorities to promote eco-friendly practices, thereby reducing ecological footprints and mitigating adverse effects on both the environment and public health.

To the best of our knowledge from previous literatures, the present study would be of the first of its kind to assess APS by employing a hybrid method that includes the Fuzzy Analytic Network Process (FANP) and the TOPSIS method. A variety of mathematical methodologies has been used in the suggested assessment model. First, fuzzy set theory (FST) has been utilized to cope with uncertainty in the judgements of decision makers (DMs). Second, aspects and indicator weights were calculated using the fuzzy analytic network method (FANP). Finally, the TOPSIS approach has been utilized to compute the total sustainability index and pick the optimal option. For clarity's sake, the novelty of this research lies in the development of a hybrid decision-making framework that uniquely integrates FANP and TOPSIS to assess airport pavement sustainability. This innovative combination allows for precise handling of complex interdependencies among sustainability criteria while addressing uncertainties in decision-making. By applying this framework to evaluate sustainable pavement alternatives for Taif airport, the study pioneers an advanced methodology that enhances decision-making efficiency and promotes eco-friendly solutions in airport construction projects.

2. Literature review

The construction of airport infrastructure is essential to the global transportation network, facilitating efficient travel and economic growth. Nonetheless, the environmental impact of airports is undeniable. Pavement systems are crucial for airport sustainability since they constitute a fundamental aspect of the infrastructure. Therefore, with the right methods to optimise airport pavement improvements are important. Thus, this literature review aims to introduce a summary of the state-of-the-art sustainability assessment methods applied on airports pavement. It is discussed case studies using different methods, critique and compare these approaches and reflect on trends or innovations made along the way, whilst identifying opportunities for future research efforts. Sustainability assessment procedures are structured frameworks or instruments used to assist decision-makers and policymakers in discerning acceptable and unacceptable acts to enhance societal sustainability [20]. Numerous sustainability evaluation approaches are used worldwide to evaluate airport projects, including Green Building Certification Systems (LEED and BREEAM), Life Cycle evaluation (LCA), and Multi-Criteria Decision Analysis (MCDA).

Numerous studies have developed various sustainability evaluation methodologies to evaluate airports broadly, as well as specific approaches for paving projects, each exhibiting differing levels of efficacy. For example, Fann and Rakas [21] proposed a structured methodology to evaluate the environmental sustainability of airport expansion projects. This framework is designed to be adaptable and integrates multiple criteria for assessing environmental impacts across the entire life cycle of airport projects, encompassing carbon emissions, resource utilization, and ecological consequences. The main objective of this research approach is to provide airport administrators and stakeholders with a structured framework for making sustainable decisions during the initial stages of project planning and design.

Although the framework is theoretically robust, its practical utility remains limited due to

This analysis relied on secondary data sources, including the Ecoinvent database, to model construction processes and material production in compliance with ISO 14040 standards. To address uncertainties in the life-cycle inventory data, a probabilistic LCA tool was developed using the Monte Carlo simulation method. A case study on Runway 10R-28L at Chicago O'Hare International Airport revealed that material production processes, particularly those involving asphalt binder and Portland cement, were the primary contributors to environmental impacts. In contrast, construction activities contributed less than 2% of the total TPE and GHG emissions. The findings further demonstrated that incorporating recycled materials and warm-mix asphalt during the design phase significantly reduced environmental impacts, achieving a 30% decrease in both total primary energy use and greenhouse gas emissions compared to traditional designs. This outcome was verified through probabilistic analysis, highlighting the potential for sustainable practices in airport pavement construction to mitigate environmental harm. However, the scope of this study is limited to confine to the construction phase of airport pavements and does not extend to other critical life-cycle stages, such as maintenance, rehabilitation, operational use, or end-of-life processes. Consequently, the study underscores the need for further research to address these omitted phases, providing a more comprehensive understanding of sustainability in airport infrastructure development. Besides, it is assessed sustainability measures at Polish airports, including the use of solar panels and environmentally sustainable technology [23].

This article evaluates the advancement of Polish airports in implementing sustainable practices using a survey and case study methodology, highlighting the obstacles and possibilities related to Integration of environmentally friendly infrastructure amid increasing air traffic and environmental issues.

"Focusing just on Polish airports restricts the application of the results to other locations, since va countries possess distinct regulatory frameworks, economic conditions, and environmental objec

It is also examined the sustainability performance of leading global airports on a capital basis framework based on environmental, social and economic dimensions [24]. Using Data Envelopm Analysis (DEA) to derive sustainability attributes (waste, energy, water and carbon) and favoura outcomes (passenger, revenue and employment), this study sought to perform two things: identif performing "frontier" airports from among the entire US airport network; and explore differe between them.

This benchmarking method seeks to establish performance improvement objectives and enhance transparency in sustainability reporting. Nevertheless, the system depends on continuous, high-c data to provide dependable benchmarking. However, airports globally vary in their degree of transparency and data availability, potentially affecting the reliability of the comparative findir Similarly, it is reported that another study built a physical and operating requirement-based asses framework to evaluate the environmental sustainability of airports [25]. This paper utilizes text mi methods to evaluate airport sustainable development reports as a preliminary step for recog priority environmental indicators. The final results generated an airport-specific environmental database (As a basic study, these metrics should be optimally evaluated by comparing against GB this last step is beyond the scope of the paper). Using GRI and other green certification database the report aims to identify shortcomings and align environmental categories within an aviation sustainability framework.

Certain airports disseminate environmental data; nonetheless, sustainability reporting is inconsistent and lacks commitment, especially in developing nations. A green grading system tailored for airports is introduced, which evaluates energy, water, emissions, and waste management [16]. The absence of consistent and comprehensive data in airport sustainability reports undermines the framework's reliability and applicability. This diversity, particularly in underdeveloped countries, complicates the establishment and implementation of environmental indicators for various airport operations.

In a recent study, established guidelines for the utilization of recycled materials in airport pavement design to enhance sustainability while meeting the stringent performance requirements of aircraft traffic [26]. The study does a comprehensive assessment of various recycled materials, such as industrial slag, recycled asphalt pavement (RAP) , and crumb rubber, and examines their applications in asphalt, concrete, and granular pavement layers [27]. Sustainability is assessed based on a triple bottom line framework that consists of financial, environmental and social dimensions using methods such as life cycle cost analysis and life cycle assessment (LCA). Recycled materials deliver significant environmental, (including reduced GHG emissions and lower vulnerability to supply chain disruptions because of decreased reliance on virgin materials), but their adoption is hampered by issues such as material inconsistency, difficulties in scaling up production and a natural risk aversion within industry [12]. The research emphasizes the need of performance testing, localized material sourcing, and modifications to procurement techniques and performance-based criteria to enhance acceptance. The primary weakness of this study is its dependence on a qualitative review of prior research instead of offering empirical validation or case studies to clearly evaluate the proposed principles for using recycled materials into airport pavements. In summary, assessing sustainability in airport pavement projects helps to meet the environmental, social and economic objectives desired for long-term success. The present sustainability evaluation methods (such as green building certification systems, life cycle assessment (LCA) and multi-criteria decision analysis (MCDA)) have continued to identify necessary characteristics for assessing the airport pavements sustainability performance. However, these methods have shortcomings that must be addressed. Future studies should address the shortcomings of current data collection methods based on a stakeholder analysis and a longer time horizon by including representatives of different

3. Research methodology

The research methodology, as illustrated in Figure 1, commences with an extensive review of existing literature, which involves a systematic examination of prior studies to extract pertinent findings. This step aims to identify existing gaps in the body of knowledge that necessitate further investigation. Additionally, it explores the integration of fuzzy logic and the TOPSIS as analytical tools for promoting sustainability in airport pavement manufacturing, facilitating the selection of an initial set of Sustainability Indicators (SIs). The justification of selection these SIs was based on their comprehensive representation of key sustainability dimensions in airport pavement systems. Economic factors ensure cost-effectiveness and financial feasibility, while technical aspects address performance and durability.

Environmental indicators minimize ecological impacts, such as emissions and resource use, and social criteria consider safety, community acceptance, and job creation. These indicators collectively ensure a balanced and holistic evaluation of sustainability, tailored to the unique demands of airport pavement projects.

Following this preliminary stage, the methodology incorporates a structured questionnaire survey to refine and prioritize the key SIs. The process of identifying sustainability benchmarks for airport pavements involves a comprehensive evaluation of critical environmental, social, and economic dimensions. This systematic approach ensures that the selected indicators effectively address the multifaceted nature of sustainability in airport infrastructure, providing a robust foundation for the subsequent phases of the research. Reviewing pertinent research and speaking with professionals in the field helped determine the requirements This is succeeded by conducting interviews with experts to compute chosen SI's using fuzzy logic methodology. In this stage, membership functions such as trapezoidal or triangular ones was used to transform crisp values numbers with definite values into fuzzy values, which have uncertain or im-precise values.

Fuzzification makes it possible to handle these situations which uses a FANP to ascertain the relative relevance of each criterion. Using a matrix that allocates weights depending on relevance (e.g., equally important, fairly important, and highly important), the ANP technique compares criteria pairwise. Then, TOPSIS methodology has been used to calculate the distance between each alternative (e.g., various airport pavement materials or de-signs) and the ideal solution (i.e., the best alternative) based on sustainability criteria. Based on sustainability criteria, the options that are closest to the ideal solution, deeming the most sustainable. A real-world case study was employed to demonstrate the validity of the developed model. The fifth phase was also incorporated the fuzzy TOPSIS technique into actual airport pavement design methods. This could be done in conjunction with stakeholders and industry experts to guarantee the methodology's applicability and practicality. This stage is also entailed at putting the technique to the test using case studies at certain airports to assess how well it works to improve the sustainability of airport pavement while maintaining functioning and safety.

This study presents findings from a case analysis conducted to assess the effectiveness of a newly developed fuzzy hybrid methodology for sustainability evaluations in infrastructure projects. The proposed assessment framework integrates multiple mathematical techniques to ensure comprehensive and reliable evaluations. The research framework begins by employing fuzzy set theory (FST) to address and reduce uncertainties associated with the subjective assessments provided

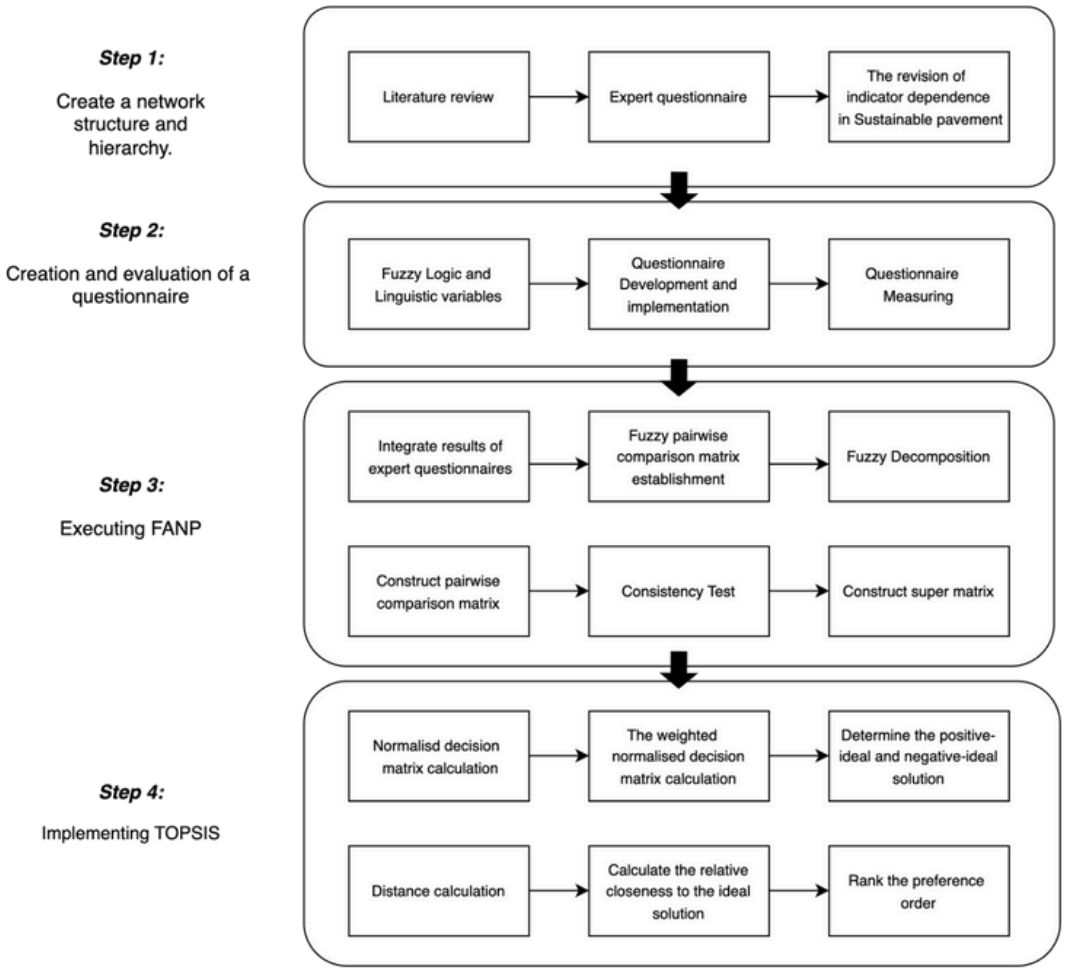

Fig. 1. The proposed Fuzzy-ANP–TOPSIS methodology for sustainable airport pavement performance

4. Materials and Methods

4.1. Fuzzy linguistic variables

As Zadeh [28] defines, a linguistic variable represents expressions in the form of word sentences, derived from either natural or artificial languages, rather than numerical va This concept proves particularly advantageous for describing complex phenomena that easily captured through conventional quantitative methods [29].

Consequently, linguistic variables are invaluable in contexts that require qualitative descriptors to convey information effectively [20, 31].

Within the realm of performance evaluation, the application of linguistic variables provides decision-makers with a flexible and intuitive mechanism to express their judgments [23]. For instance, when assigning ratings to performance criteria, decision-makers can employ linguistic scales tailored to the specific assessment context. A commonly utilized scale consists of five fundamental fuzzy subsets: Very Low (VL), Low (L), Moderate (M), High (H), and Very High (VH). This approach enhances clarity and adaptability in performance assessments.

4.2. Arithmetical operations based on support values

The mathematical foundation of arithmetic operations involving fuzzy numbers lies in the extension principle, which extends traditional arithmetic to accommodate the fuzzy domain. This principle operates by executing pointwise calculations on the discrete elements of fuzzy input numbers, ultimately deriving the membership functions of the resulting fuzzy outputs. Within the proposed framework, these arithmetic operations are implemented using the support values method, chosen for its computational efficiency and straightforward implementation. This approach ensures that the assessment model remains user-friendly and accessible for practical applications. In this framework, the arithmetic operations leverage the support values method to process two triangular fuzzy numbers (TFNs) as inputs, resulting in two output TFNs. The detailed procedure for performing these operations is mathematically expressed through Equations 1 to 5, illustrating the application of this method in deriving fuzzy results. This structured approach enhances both the precision and usability of the proposed model in handling fuzzy data. Addition of two TFNs:

$$\tilde{A} + \tilde{B} = (a_1, a_2, a_3) + (b_1, b_2, b_3) = (a_1 + b_1, a_2 + b_2, a_3 + b_3) \quad (1)$$

Subtraction of two TFNs:

$$\tilde{A} - \tilde{B} = (a_1, a_2, a_3) - (b_1, b_2, b_3) = (a_1 - b_1, a_2 - b_2, a_3 - b_3) \quad (2)$$

Multiplication of two TFNs:

$$\tilde{A} \times \tilde{B} = (a_1, a_2, a_3) \times (b_1, b_2, b_3) = (a_1 \times b_1, a_2 \times b_2, a_3 \times b_3), \quad (3)$$

Division of two TFNs:

$$\tilde{A} / \tilde{B} = (a_1, a_2, a_3) / (b_1, b_2, b_3) = \left(\frac{a_1}{b_1}, \frac{a_2}{b_2}, \frac{a_3}{b_3}\right) \text{ where } a_i \geq 0, b_i > 0, \forall i = 1,2,3 \quad (4)$$

Average of two TFNs:

$$Average = \frac{1}{n}\sum_{i=1}^{n} a_i = \frac{1}{n}(a_1 + a_2 + \cdots + a_n) \quad (5)$$

Where *a*, *b* and *c* are real numbers.

An algorithm using fuzzy numbers is called fuzzy logic. Fuzzy numbers were examined light of this [24]. Initially, a number of academics [31-33] noted that in order to make fu numbers more useful in real-world applications, their properties are typically stated mathematically. The triangular fuzzy number *A*(*a*1, *a*2, *a*3), for instance, is represented b following equation and is shown in Figure 2.

$$\mu_{??}(x) = \begin{cases} \frac{x - a_1}{a_2 - a_1} & a_1 \le x \le a_2 \\ \frac{x - a_3}{a_2 - a_3} & a_2 \le x \le a_3 \\ 0 & otherwise \end{cases} \quad (6)$$

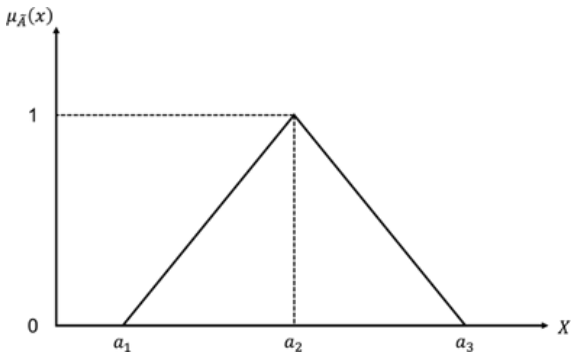

Fig. 2. Fuzzy triangular number

In the meantime, a large body of research [27] indicated that the crisp value is the most value for triangular fuzzy numbers. The following equation provides the triangular fu numbers' crisp value:

$$A\,a = [\,(a_2 - a_1)\,a - (a_3 - a_2)\,a + a_3\,] \quad (7)$$

4.3. Defuzzification Expert opinion in fuzzy set theory is usually expressed as a linguistic variable value. It is numerically transformed so that it may be used for rating, weighing, or grading purposes. The process is known as defuzzification. Most people prefer to use the centroid approach, which is also called the centre of gravity method, since it is quick, easy, and accurate. Because of these features, the centroid method is used for defuzzification in the proposed model [32] by applying following equation,

$$X = \frac{\int \mu_e(x) \cdot x \, dx}{\int \mu_e(x) \, dx} \quad (8)$$

Where, e = defuzzification (crisp value) of TFN (x1, x2, x3)

4.4. Fuzzy Analytic Network Process (FANP)

The analytic hierarchy process (AHP), which was introduced by Saaty (1980) several deca ago, deals with principles of synthesis, pairwise comparisons, decomposition, and pric vector generation. Since its introduction, AHP has been the general default approach handling feedback and dependence around decision-making strategies [31-33]. The pri benefit of AHP has been its ability to deal with multiple criteria, whether quantitative qualitative [32, 34].

Saaty and Takizawa [35] introduced an extension of AHP called ANP, which is a system th includes feedback. While this study is mainly focused on developing a hybrid decision-m framework that distinctively combines FANP and TOPSIS methodologies to evaluate t sustainability of airport pavements. In general terms, ANP is useful in instances involv interactions of system elements within a network structure. Furthermore, unlike AHP, A does not have a rigid hierarchical structure, which means it can model and frame a dec problem by employing a “system with feedback” strategy. Specifically, ANP is able to cap feedback in addition to interdependent relationships at the component level. Numerous researchers [34, 35] have highlighted various advantages of employing the Analytic Netw Process (ANP) over the Analytic Hierarchy Process (AHP). Unlike the linear structure o AHP, ANP utilizes a more flexible and non-linear network structure, allowing for a broad and more nuanced analysis. It facilitates the integration of both tangible and intangible e within the decision-making process, offering a realistic perspective on complex proble through the formation of clusters. Moreover, ANP accommodates intricate and interdep relationships among elements [36-38]. Despite these strengths, ANP is not without limita one notable drawback is its inability to adequately address the inherent subjectivity in pa comparisons. The computation process for the Fuzzy Analytic Network Process (FANP based on Chang’s [39] extent analysis method, involves four systematic steps, detailed follows.

Consider an object let X={x1, x2,..., xn}, G = {g1, g2,..., gm}. In this method, each object is evaluated by conducting an extent analysis for every goal, gig_igi. Consequently, mmm extent analysis values are generated for each object, represented with specific notations.

$$M_{g_i}^1, M_{g_i}^2, \ldots, M_{g_i}^m, \quad i = 1, 2, \ldots, n \tag{9}$$

where all $M_{g_i}^j$ values are represented as triangular fuzzy numbers (TFNs).
The steps involved in Chang's extent analysis method (1992, 1996) can be outlined as fol

Step 1: The fuzzy synthetic extent value corresponding to the i-th object is defined as:

$$S_i = \sum_{j=1}^{m} M_{g_i}^j \otimes \left[\sum_{i=1}^{n} \sum_{j=1}^{m} M_{g_i}^j \right]^{-1} \tag{10}$$

To obtain $\sum_{j=1}^{m} M_{g_i}^j$, make the fuzzy addition operation on m extent analysis values for a specific matrix, ensuring accuracy and consistency, such that

$$\sum_{j=1}^{m} M_{g_i}^j = \left(\sum_{j=1}^{m} l_j, \sum_{j=1}^{m} m_j, \sum_{j=1}^{m} u_j \right) \tag{11}$$

To obtain $\left[\sum_{i=1}^{n} \sum_{j=1}^{m} M_{g_i}^j\right]^{-1}$, perform the fuzzy addition operation of $M_{g_i}^j$ $(j = 1, 2, \ldots$ values, such that

$$\sum_{i=1}^{n} \sum_{j=1}^{m} M_{g_i}^j = \left(\sum_{j=1}^{m} l_j, \sum_{j=1}^{m} m_j, \sum_{j=1}^{m} u_j \right) \tag{12}$$

Then compute the inverse of the vector in Equation (12), such that

$$\left[\sum_{i=1}^{n} \sum_{j=1}^{m} M_{g_i}^j \right]^{-1} = \left(\frac{1}{\sum_{j=1}^{m} u_j}, \frac{1}{\sum_{j=1}^{m} m_j}, \frac{1}{\sum_{j=1}^{m} l_j} \right) \tag{13}$$

Step 2: The possibility degree $M2 = (l2, m2, u2) \geq M1 = (l1, m1, u1)$ is defined as:

$$V(M_2 \geq M_1) = \sup_{x \geq y} \left[\min \left(\mu_{M_1}(x), \mu_{M_2}(y) \right) \right] \tag{14}$$

and can be consistently stated as:

$$V(M_2 \geq M_1) = hgt(M_2 \cap M_1) = \begin{cases} 1, & if \ m_2 \geq m_1 \\ 0, & if \ l_1 \geq u_2 \\ \frac{l_1 - u_2}{(m_2 - u_2) - (m_1 - l_1)}, & otherwise \end{cases} \quad (15)$$

Where *d* represents the ordinate of the highest intersection point *D* between μ(M1) and

To compare M1 and M2, it needs the values of both V (M2 ≥ M1) and V (M1 ≥ M2)

Step 3: The degree of possibility for a convex fuzzy number M to be greater than k conv fuzzy numbers Mi (*i* = 1, 2... k) can be well-defined by:

$$V(M \geq M_1, M_2, ..., M) = V[(M \geq M_1) \text{ and } (M \geq M_2) \text{ and... } (M \geq M_k)] \quad (16)$$
$$= \min V(M \geq M_i), i = 1, 2, ..., k$$

Assume that

$$d'(A_i) = \min V(S_i \geq S_k) \quad (17)$$

For k = 1, 2, ..., n; k ≠ i. The weight vector is then given by:

$$W' = (d'(A_1), d'(A_2), ..., d'(A_n))^T \quad (18)$$

where *A*i (*i* =1, 2, ..., n) are *n* elements.

Step 4: Via normalization, the normalized weight vectors are:

$$W = (d(A_1), d(A_2), ..., d(A_n)) \quad (19)$$

where *W* is a nonfuzzy number.

4.5. TOPSIS method

The method for formulating importance weights in evaluation criteria by applying the fu ANP approach was given in preceding sections. In this section, TOPSIS is used for rankin alternatives. It should be noted that, when using criteria restricted by amount, every st the fuzzy ANP for ranking alternatives would have to be followed. In the present work order to hold the pairwise comparisons from DMs below a certain amount, only fuzzy A has been applied for calculating relative weights in the evaluation criteria. TOPSIS is th used to obtain final ranking results. More details for these methods can be acquired by applying the following equations. TOPSIS comprises the following six sequential steps:

Step 1: The normalized decision matrix is computed by calculating the normalized valu using the following formula:=

$$x_{ij} \sqrt{\sum_{i=1}^{m} x_{ij}^2} \quad , \quad i = 1, 2, \ldots, m \quad \text{and} \quad j = 1, 2, \ldots, n . \tag{20}$$

Step 2: Determine the weighted normalized decision matrix, where the weighted norma value vij is calculated as:

$$v_{ij} = r_{ij} w_j \quad , \quad i = 1, 2, \ldots, m \quad \text{and} \quad j = 1, 2, \ldots, n \tag{21}$$

where w_j is the weight of the jth criterion or attribute, and $\sum_{j=1}^{n} w_j = 1$

Step 3: Find the ideal (A^*) and negative ideal (A^-) solutions:

$$A^* = \{ (\max_i v_{ij} \mid j \in C_b), (\min_i v_{ij} \mid j \in C_c) \} = \{ v_j^* \mid j = 1, 2, \ldots, n \} \tag{22}$$

$$A^- = \{ (\min_i v_{ij} \mid j \in C_b), (\max_i v_{ij} \mid j \in C_c) \} = \{ v_j \mid j = 1, 2, \ldots, n \} \tag{23}$$

Step 4: Calculate the separation measures using the m-dimensional Euclidean distance separation measures for each alternative from both the positive ideal solution and the n ideal solution are as follows:

$$S_i^* = \sqrt{\sum_{j=1}^{n} (v_{ij}^* - v_j)^2}, i = 1, 2, \ldots, m \tag{24}$$

$$S_i^- = \sqrt{\sum_{j=1}^{n} (v_{ij}^- - v_j)^2}, i = 1, 2, \ldots, m \tag{25}$$

Step 5: Determine the relative closeness to the ideal solution. The relative closeness of alternative Ai to A^* is defined as:

$$RC_i^* = \frac{S_i^-}{S_i^* + S_i^-}, \quad i = 1, 2, \ldots, m \tag{26}$$

Step 6: Rank the preference order.

4.6. Normalize quantitative indicators

To utilize the values of sustainability indicators, the quantitative indicators need to be normalized. The normalization is computed via the below equations [40]:

when indicator is larger:

$$r_{ij} = \frac{[x_{ij} - \min\{x_{ij}\}]}{[\max\{x_{ij}\} - \min\{x_{ij}\}]} \tag{27}$$

when indicator is smaller:

$$r_{ij} = \frac{[\min\{x_{ij}\} - x_{ij}]}{[\max\{x_{ij}\} - \min\{x_{ij}\}]} \tag{28}$$

where r_{ij} = normalized value of indicator.

4.7. Sustainability Assessment

In formulating alternatives, DMs (or assessors) should first and foremost com-prehend main objectives of a project, while at the same time being cognizant of any expressed n underlying the project's proposal. Having a solid understanding of the project's objective needs to ensure the compliance of any proposed alternatives with the project overall. Fo case study, we present four alternatives, as shown in Table 1.

Table 1: Proposed project alternatives.

ative	ption	atures
		ent with natural mnag natural materials in sub-base layer, the pav ruction Strategy 1) esigned to have 20 years life.
		ent with natural mnag natural materials in sub-base layer, the pav ruction Strategy 2) esigned to have 10 years life.
		ent with recycled mnag recycled materials in sub-base layer, the pav ruction Strategy 1) s designed to have 20 years life.
		ent with recycled mnag recycled materials in sub-base layer, the pav ruction Strategy 2) esigned to have 10 years life.

In the proposed model integrating FANP and TOPSIS is designed to address complicated decision-making scenarios characterized by interdependencies across sustainability indi and alternatives, while also facilitating the effective ranking of alternatives.

this sustainable model for selecting the optimal concrete is composed of three levels (1, 3). In level 1, the problem is defined, and the alternatives (Ai) and Indicators (Ci) are identified. In level 2, the pairwise matrix is established, and weights are calculated. In lev the alternatives are evaluated and the best one selected. In the pro-posed assessment there are eight steps that lead to calculating the overall sustainability performance

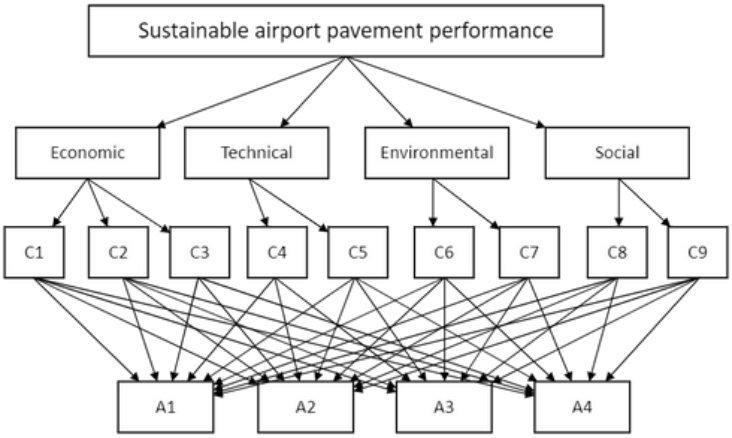

Fig. 3. The research's network structure and hierarchy.

5. Results & Discussions

Various methodologies have been developed for conducting sustainability assessments. From a decision-making standpoint, the indicator-based approach emerges as particularly advantageous due to its inherent transparency, temporal consistency, and practical applicability. This study aims to identify sustainability indicators (SIs) commonly employed within the industry by compiling a comprehensive list derived from an extensive review of existing literature, including academic publications and practitioner-oriented journals. The identified SIs are categorized into four primary dimensions of sustainability, each corresponding to specific indicators: (1) economic, (2) technical, (3) environmental, and (4) social. A detailed representation of these indicators is provided in Table 2.

Table 2. Sustainability Indicators used in the case study.

Aspect	Indicator	Measurement unit
Economic	Capital cost (C1)	Monetary unit (SAR)
	Benefits (C2)	Qualitatively Qualitatively
	Affordability (C3)	Young's Modulus
Technical	Performance (C4)	(Kgf/cm2) Qualitatively
	Flexibility (C5)	Qualitatively
	Ecological Impacts (C7)	Qualitatively
Environmental	GHG (C6)	T CO2 eq
Social	Community Engagement (C9)	Qualitatively
	Safety and Security (C8)	Qualitatively

The main aim of quantifying sustainability indicators (SI) rates for each alternative is quantifying any of the indicators that were selected during the assessment. Note that the quantitative and qualitative indicators must be subjected to different forms of calculations. For quantitative indicators, traditional engineering calculations can be applied, whereas for qualitative indicators, the fuzzy set approach is used for numerically quantifying indicator rates. The DMs utilize classic membership functions (MFs) for linguistic variables suggested in the assessment model. The fuzzy linguistic variables scale proposed in the assessment model are reported on Table 3.

Table 3. Linguistic scale for rating of project alternatives.

Linguistic set	Fuzzy number
Very well (VW)	(0.75,1.0,1.0)
Well (W)	(0.5,0.75,1.0)
Moderate (M)	(0.25,0.5,0.75)
Poor (P)	(0,0.25,0.5)
Very poor (VP)	(0,0,0.25)

Numerical rates for the qualitative indicators of each alternative are reported in Table 4.

Table 4. Quantitative values for the qualitative indicators of each alternative.

	A1	A2	A3	A4
Affordability (C3)	0.25	0.4	0.6	0.8
Flexibility (C5)	0.28	0.63	0.28	0.63
Ecological impacts (C7)	0.0	0.2	0.5	0.7
Personal safety/security (C8)	0.4	0.5	0.7	0.8
Community engagement (C9)	0.25	0.25	0.5	0.5

In order to employ the sustainability indicator values, the quantitative indicators need to be norm

The normalization is calculated using the methods of Bardossy & Duckstein [40]. The quantitat indicators have been normalized accordingly. Table 5 presents the values of the sustainability indi for each alternative.

Table 5. Normalized indicators values.

Indicator		Alternatives			
		A1	A2	A3	A4
Total Capital cost	C1	0.25	0.2	0.47	0.54	1.0
Affordability	C3	1.0	0.28	0.4	0.6	0.8
Benefits	C2	0.0	0.0	0.4	0.7	1.0
Performance	C4	0.25	0.4	1.0	0.0	0.0
Flexibility	C5			0.63	0.28	0.63
GHG	C6			0.89	0.11	1.0
Ecological Impacts	C7			0.2	0.5	0.7
Community engagement	C9			0.25	0.5	0.5
Safety and Security	C8			0.5	0.7	0.8

Also, fuzzy pair-wise comparison matrices are formed by the DMs using the scale given in Table 2. For instance, a comparison is made between the economic aspect (EA) and the technical aspect (TA) through the inquiry, “How significant is (EA) in relation to (TA)?” with the answer being “JE, MI”, as given by the two DMs. The linguistic scales are laced in the relevant cell against the TFNs (1, 1, 1) and (1, 3/2, 2), which are then aggregated. All fuzzy assessment matrices are generated using a consistent methodology. The subsequent step involves analyzing the pairwise comparison matrices through the application of Chang’s [39] extent analysis method. This process is employed to determine the local weights (LW) for the four key sustainability aspects. The calculation of these weights follows the same methodology used for deriving the local weights of individual indicators. Furthermore, advancing environmental sustainability within global aviation infrastructure can be significantly supported by incorporating recycled materials into construction and maintenance practices. As airport pavements can be considered a source of air pollution due to their production of greenhouse gases, odors, volatile organic compounds and dusts, airport DMs are interested in selecting the preferred pavement design and rehabilitation strategy that takes economic, environmental, and societal constraints into consideration, along with performance requirements. However, most of the activities belonging to airport transportation must take into account a large number of alternatives, which some-times hinders their management as a whole. Many mathematical methods and models have been used over the years to help authorities and communities model complex problems such as these. Of these, several can be used to evaluate the proposed solutions and alternatives.

The TOPSIS is a widely employed method for optimizing complex multi-criteria decision-making (MCDM) systems [40]. This approach is based on the concept that the best alternative should have the smallest distance from the positive ideal solution and the greatest distance from the negative ideal solution. In this analysis, the TOPSIS method is applied to determine the most optimal alternative from a set of choices. The process begins with determining the weights of the criteria, which are then used to scale the indicator values by multiplying them with their respective weights. This step ensures that each criterion is proportionally represented in the decision-making process. The alternatives (denoted as A1, A2, A3, and A4) are evaluated against multiple criteria functions (C1, C2, C3, C4, C5, C6, C7, C8, C9). The ranking of alternatives is then derived by assessing their relative proximity to the ideal solution, as depicted in Table 6 and Figure 4. Both the positive ideal solution and the negative ideal solution are defined within the analysis.

The negative ideal solution is calculated using the same methodology applied to the positive ideal, ensuring a consistent framework. The distances of each alternative from the ideal and negative solutions are computed using the specified mathematical formulations (Equations 11 and 12). These calculations facilitate a systematic ranking of alternatives, providing a robust mechanism for identifying the most sustainable option. This systematic approach ensures a robust comparison and ranking of alternatives.

$$A^{*} = \{ (\max_i a_{ij} \mid j \in C_b), (\min_i a_{ij} \mid j \in C_c) \mid j = 1, 2, \ldots, n \} = \{ v_j^{*} \mid j = 1, 2, \ldots, n \} \quad (29)$$

$$A^{-} = \{ (\min_i a_{ij} \mid j \in C_b), (\max_i a_{ij} \mid j \in C_c) \mid j = 1, 2, \ldots, n \} \quad (30)$$

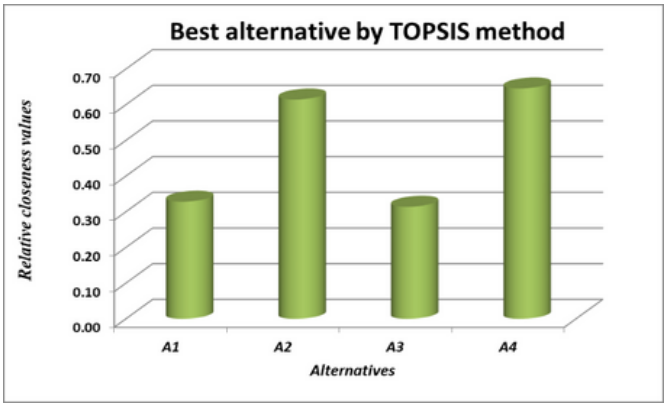

Fig. 4. TOPSIS method as tool to select the best alternatives.

Table 6. Relative closeness values.

Alternative	A1	A2	A3	A4
E+	0.51	0.27	0.45	0.28
E-	0.25	0.43	0.20	0.51
E-/(E- + E+)	0.33	0.61	0.31	0.65

The application of advanced decision-making frameworks has shown considerable potential in addressing the multifaceted challenges of sustainability within pavement and infrastructure management. It is demonstrated the practicality of combining fuzzy AHP with the VIKOR method prioritize pavement maintenance, effectively balancing technical, economic, and operational fac [41]. Similarly, it is extended the decision-making paradigm by integrating IMF D-SWARA and Roug MARCOS to optimize the selection of road construction machinery, emphasizing sustainability a efficiency in resource-intensive operations [42]. While these models excel in structured decision support, their scalability across diverse contexts remains a critical challenge. In urban transportati is showcased the utility of multi-criteria decision-making to identify and address inefficiencies, presenting a replicable framework for sustainability assessments in metropolitan areas [43].

Adding to this, it is leveraged the TOPSIS method to compare road sustainability rating syster offering insights into their adaptability in localized contexts such as Hungary, yet raising questi about their global applicability [44]. Also, it is provided a systematic review of decision-making techniques like ANP and TOPSIS in sustainable infrastructure, underscoring their versatility while a highlighting the need for further empirical validation in real-world scenarios [45]. It is also utilized TOPSIS method to evaluate aggregates for road construction, providing a structured framewor selecting materials that balance performance, cost, and sustainability. This highlights the role of m criteria decision-making in enhancing infrastructure durability [46]. Similarly, it is employed GI integrated Spatial Multi-Criteria Analysis (MCA) to optimize airport and control tower site selectio demonstrating how geospatial data and analytical tools can address complex spatial planning cha [47]. Together, these studies had revealed the promise, limitations and the transformative poten combining systematic analysis with technological tools of integrating multi-criteria decision-mak approaches in engineering and urban planning, emphasizing the importance of contextual adap and expanded validation to enhance their practical relevance and generalizability.

6. Conclusions and recommendations

In Saudi Arabia, the government and private sector are currently taking steps to reduce their cli change impact, with a major part of their strategies focusing on the concept of sustainability. Ac to the Saudi Vision 2030 plan, there is a concerted effort within both government and the privat to reduce overall environmental impacts caused by industrialization. In the present paper, we investigated a range of suitable solutions for building the new airport at Taif, Saudi Arabia. Usin different methods, we tested various sustainable solutions/alternatives, looking for the one tha best reduce the environmental impact caused by heavy construction and long-term industrial u

Mathematical tools were applied to select the best alter-native. Using the selected model, our tests revealed that alternative (A4) was the most environmentally sustainable, followed closely by alternatives (A2) and (A3), ranked second and third, respectively. The results indicate that the alternatives fully or partially aligned with construction strategy 2 are ranked highest. This ranking is based on the most significant indicators, as determined by the FANP results, which received the highest ratings reflected in the overall sustainability index. Performance (C4), recognized as the second most influential indicator based on its global weight analysis, demonstrated the highest evaluation scores when compared across all alternatives. Notably, alternatives categorized under construction strategy 1 were ranked lower in performance compared to those associated with construction strategy 2.

Moreover, the key findings revealed that the third-ranked alternative (A3), which incorporates recy materials, exhibits a greater overall sustainability compared to alternatives relying exclusively on natural materials. This outcome underscores the potential benefits of integrating recycled materia construction practices to enhance sustainability. According to the results obtained, the pavement with recycled mate-rials will be proposed as a sustainable solution. This eco-friendly solution sho be tested under real conditions in Saudi Arabia. By using this method, airport pavements may be more sustainable by using less materials, using less energy, and leaving a smaller carbon imp Potential avenues for further study might involve conducting field testing and real-world applicat to better validate the fuzzy logic model. Furthermore, investigating the incorporation of additional friendly technology like smart sensors, renewable energy sources, and recycled materials might improve the efficiency and sustainability of airport pavements. Fuzzy logic models combined w artificial intelligence would be applied to make more effective decision maker. It is also a signific to apply various optimizations techniques like Particle swarm, Whale, Penguin emperor or Jaya e combined with Artificial intelligence would produce more than one solution with optimal value each case as a reference for engineers and manufacturers.

Further, emerging technologies, such as smart pavements and artificial intelligence (AI), offer promising avenues to enhance sustainability assessments in the context of airport pavement management. Smart pavements, equipped with embedded sensors and data-gathering capabiliti provide real-time information on structural performance, traffic loads, and environmental condi allowing for dynamic and precise evaluations. By leveraging these technologies, sustainability met can be updated continuously, fostering a proactive approach to maintenance and resource alloc Similarly, AI can be integrated into decision models like the Fuzzy ANP-TOPSIS framework to enab predictive analytics, optimize resource usage, and simulate the environmental impacts of various scenarios. AI-powered algorithms can analyze large datasets from smart pavements, offering ins that refine sustainability metrics and provide actionable recommendations. Future studies incorp these technologies could advance the field by offering comprehensive, data-driven solutions, ultim contributing to the development of more resilient and environmentally sustainable airport pavem

Declaration of Competing Interest

The authors declare no conflict of interest.

Data availability

No data was used for the research described in the article.

Acknowledgment

The authors thank specially the Deanship of scientific research at Umm Al-Qura University Sau
Arabia.

REFERENCES

[1] Keeble, B. R. (1988). The Brundtland report: 'Our common future'. *Medicine and war*, *4*(1), 17-25.

[2] Arena, M., Ciceri, N. D., Terzi, S., Bengo, I., Azzone, G., & Garetti, M. (2009). A state-of-the-art of industrial sustainability: Definitions, tools and metrics. *International Journal of Product Lifecycle Management*, *4*(1-3), 207-251.

[3] Brown, B. J., Hanson, M. E., Liverman, D. M., & Merideth, R. W. (1987). Global sustainability: Toward definition. *Environmental management*, *11*, 713-719.

[4] Glavič, P., & Lukman, R. (2007). Review of sustainability terms and their definitions. *Journal of cleaner production*, *15*(18), 1875-1885.

[5] Zink, K. J., & Fischer, K. (2013). Do we need sustainability as a new approach in human factors and ergonomics?. *Ergonomics*, *56*(3), 348-356.

[6] Goodland, R., Daly, H., & El Serafu, S. (1991). Environmental Sustainable Economic Development. Building in Brundtland. Washington DC: World Bank.

[7] Baxter, G., Srisaeng, P., & Wild, G. (2018). Sustainable airport energy management: The case of kansai international airport. *International Journal for Traffic & Transport Engineering*, *8*(3).

[8] Baxter, G., Srisaeng, P., & Wild, G. (2018). *An assessment of airport sustainability, Part 1—Waste management at Copenhagen Airport. Resources, 7 (1), 21*.

[9] Sustainable Airport Solutions (2012) Continuous Descent Approach Groningen Airport Eelde, T Netherlands.

[10] Sarkar, A. (2012). Evolving green aviation transport system: A holistic approach to sustainable green market development. American Journal of Climate Change, 1(3), 164-180.

[11] McManners, P. (2016). The action research case study approach: A methodology for complex challenges such as sustainability in aviation. *Action Research*, *14*(2), 201-216.

[12] Payán-Sánchez, B., Plaza-Úbeda, J. A., Pérez-Valls, M., & Carmona-Moreno, E. (2018). Social embeddedness for sustainability in the aviation sector. *Corporate Social Responsibility and Environmental Management*, *25*(4), 537-553.

[13] Monsalud, A., Ho, D., & Rakas, J. (2015). Greenhouse gas emissions mitigation strategies withi the airport sustainability evaluation process. *Sustainable Cities and Society*, *14*, 414-424.

[14] Mahmoudi, R., Shetab-Boushehri, S. N., Hejazi, S. R., & Emrouznejad, A. (2019). Determining the relative importance of sustainability evaluation criteria of urban transportation network. *Sustainable Cities and Society*, *47*, 101493.

[15] Oysal, M. F., & Soğut, M. Z. (2017). An integrated research for architecture-based energy management in sustainable airports. *Energy*, *140*, 1387-1397.

[16] Somerville, A., Baxter, G. S., Richardson, S., & Wild, G. (2015). Sustainable water management at major Australian regional airports: The case of Mildura Airport. *Aviation*, *19*(2), 83-89.

[17] Greg White, G., Fairweather, H., & Jamshidi, A. (2018). Sustainable runway pavement rehabilitation: A case study of an Australian airport. *Journal of cleaner production*, *204*, 380-389.

[18] Setiawan, M.I., Surjokusumo, S., Ma'Soem, D.M., Johan, J., Hasyim, C., Kurniasih, N., Sukoco, N., Dhaniarti, I., Suyono, J., Sudapet, I.N., Nasihien, R.D., Mudjanarko, S.W., Wulandari, A., Ahmar, A.S., Wajdi, M.B.N. (2018). Business centre development model of airport area in supporting airport sustainability in Indonesia. Journal of Physics: Conference Series, 954(1): 012024.

[19] Sala, S., Ciuffo, B., & Nijkamp, P. (2015). A systemic framework for sustainability assessment. Ecological economics, 119, 314-325.

[20] Fann, J. C., & Rakas, J. (2013). Methodology for Environmental Sustainability Evaluation Of Airport Development Alternatives. International Journal of Applied Logistics (IJAL), 4(4), 8-31.

[21] Yang, R., & Al-Qadi, I. L. (2017). Development of a life-cycle assessment tool to quantify the environmental impacts of airport pavement construction. Transportation Research Record, 2603(1), 89-97.

[22] Tłoczyński, D., Wach-Kloskowska, M., & Martin-Rojas, R. (2020). An assessment of airport sustainability measures: A case study of polish airports. Transport Problems, 15(4, cz. 2), 287-300.

[23] Karagiannis, I., Vouros, P., Skouloudis, A., & Evangelinos, K. (2019). Sustainability reporting, materiality, and accountability assessment in the airport industry. Business Strategy and the Environment, 28(7), 1370-1405.

[24] Kucukvar, M., Alawi, K. A., Abdella, G. M., Bulak, M. E., Onat, N. C., Bulu, M., & Yalçıntaş, M. (2021). A frontier-based managerial approach for relative sustainability performance assessment of the world's airports. Sustainable Development, 29(1), 89-107.

[25] Ramakrishnan, J., Liu, T., Yu, R., Seshadri, K., & Gou, Z. (2022). Towards greener airports: Development of an assessment framework by leveraging sustainability reports and rating tools. Environmental Impact Assessment Review, 93, 106740.

[26] Jamieson, S., White, G., & Verstraten, L. (2024). Principles for Incorporating Recycled Materials into Airport Pavement Construction for More Sustainable Airport Pavements. Sustainability, 16(17), 7586.

[27] Zadeh, L. A. (1975). The concept of a linguistic variable and its application to approximate reasoning-III. *Information sciences*, *9*(1), 43-80.

[28] Delgado, M., Herrera, F., Herrera-Viedma, E., Verdegay, J. L., & Vila, M. A. (1999). Aggregation of linguistic information based on a symbolic approach. *Computing with Words*, 428-440.

[29] Delgado, M., Herrera, F., Herrera-Viedma, E., Martin-Bautista, M. J., & Vila, M. A. (2001). Combining linguistic information in a distributed intelligent agent model for information gathering on the Internet. *Computing with words*, 251-276.

[30] Triantaphyllou, E.(2000). *Multi-criteria decision making methods* (pp. 5-21). Springer.

[31] Kaufmann, A., & Gupta, M. M. (1991). Introduction to fuzzy arithmetic: Theory and application 1991. *VanNostrand Reinhold, New York*.

[32] Wind, Y., & Saaty, T. L. (1980). Marketing applications of the analytic hierarchy process. *Management science*, *26*(7), 641-658.

[33] Vargas, L. G. (1990). An overview of the analytic hierarchy process and its applications. *Europe journal of operational research*, *48*(1), 2-8.

[34] Saaty, T. L., & Takizawa, M. (1986). Dependence and independence: From linear hierarchies t nonlinear networks. *European journal of operational research*, *26*(2), 229-237.

[35] Percin, S. (2008). Using the ANP approach in selecting and benchmarking ERP systems. *Benchmarking: An International Journal*, *15*(5), 630-649.

[36] Wijnmalen, D. J. (2007). Analysis of benefits, opportunities, costs, and risks (BOCR) with the AHP–ANP: A critical validation. *Mathematical and computer modelling*, *46*(7-8), 892-905.

[37] Devuyst, D., Hens, L., & De Lannoy, W. (Eds.). (2001). *How green is the city? Sustainability assessment and the management of urban environments*. Columbia University Press.

[38] Chang, D.-Y., Extent analysis and synthetic decision, optimization techniques and applications Vol. 1. 1992, World Scientific, Singapore.

[39]Babashamsi, P., Golzadfar, A., Yusoff, N. I. M., Ceylan, H., & Nor, N. G. M. (2016). Integrated fuzzy analytic hierarchy process and VIKOR method in the prioritization of pavement maintenance activities. *International Journal of Pavement Research and Technology*, *9*(2), 112-120.

[40] Bárdossy, András, and Lucien Duckstein (1992). Analysis of a karstic aquifer management problem by fuzzy composite programming 1. JAWRA Journal of the American Water Resources Association 28(1) 63-73.

[41] Babashamsi, P., Golzadfar, A., Yusoff, N. I. M., Ceylan, H., & Nor, N. G. M. (2016). Integrated fuzzy analytic hierarchy process and VIKOR method in the prioritization of pavement maintenance activities. International Journal of Pavement Research and Technology, 9(2), 112-120.

[42] Mahdi, S., Marinković, M., Jovanović, S., Sremac, S., & Stević, Ž. (2022). Intelligent novel IMF D-SWARA—rough MARCOS algorithm for selection construction machinery for sustainable construction of road infrastructure. Buildings, 12(7), 1059.

[43] Oses, U., Rojí, E., Cuadrado, J., & Larrauri, M. (2018). Multiple-criteria decision-making tool for local governments to evaluate the global and local sustainability of transportation systems in urban areas: case study. Journal of Urban Planning and Development, 144(1), 04017019.

[44] Szpotowicz, R., & Tóth, C. (2020). Revision of sustainable road rating systems: selection of the best suited system for Hungarian road construction using TOPSIS method. Sustainability, 12(21), 8884.

[45] Mardani, A., Jusoh, A., Zavadskas, E. K., Cavallaro, F., & Khalifah, Z. (2015). Sustainable and renewable energy: An overview of the application of multiple criteria decision-making techniques and approaches. Sustainability, 7(10), 13947-13984.

[46] Bilim, N., & GüNeş, H. A. M. Z. A. (2023). Selection of the best aggregates to be used in road construction with TOPSIS method. Gospodarka Surowcami Mineralnymi, 39(2).

[47] Muodum, E. N. (2022). Spatial Multi-Criteria Analysis (MCA) for airport with air traffic control tower site selection based on GIS platform (Master's thesis). Universidade NOVA de Lisboa, Portugal.

Review on the implementation of rotation/curvature correction function in the RANS model in predicting highly swirling flows

Yaser H. Alahmadi,

Faculty of Engineering, Islamic University of Madinah, Saudi Arabia

yhalahmadi@iu.edi.sa

Abstract: The implementation of rotation and curvature correction functions in Reynolds-Averaged Navier-Stokes (RANS) models has significantly enhanced the accuracy of turbulence predictions in complex flows, which contains strong curvature or system rotation. The conventional turbulence models, i.e. $k-\epsilon$, $k-\omega$, Spalart-Allmaras and $k-\omega$ SST, have limitations in accurately capturing the flow phenomena influenced by system rotation and streamline curvature. To overcome these deficiencies, various modifications have been proposed, including the Spalart-Shur and Smirnov- Menter corrections, which have been applied to eddy-viscosity models (EVMs). This review paper provides a comprehensive overview of the development, implementation, and performance of rotation/curvature corrections in RANS models, with a focus on their application to swirling flow such as cyclone separators and curved channels. By comparing results of the modified EVMs and conventional models against experimental and direct numerical simulation (DNS) data, this study highlights the impact of these corrections on improving the model accuracy while maintaining convenient computational cost. The results showed that modified provide a practical balance between numerical accuracy and computational cost, particularly in industrial applications that involve highly swirling flow or strong curvatures.

Keywords: turbulence model, swirling flow, rotation and curvature, eddy viscosity models.

مراجعة حول تنفيذ دالة تصحيح الدوران الالانحناء في نمو
RANSفي التنبؤ بالتدفقات شديدة الدوام ة

الملخص: أدى تنفيذ دالة تصحيح الدوران والالانحناء في نماذج رينولدز-نافير-ستوكس المتوسطة
لتنبؤات بالالاضطرابات في التدفقات المعقدة، والتي تحتوي على انحناء قوي أو دوران النظام. تعاني
فيود في التقاط ظواهر ،*k-ω SST* و*Spalart-Allmaras* و*k-ω* و*k-ϵ* نماذج الالاضطرابات التقليدية، أي
رة بدوران النظام وانحناء التيار بدقة. للتغلب على هذه العيوب، تم اقتراح تعديلات مختلفة، بما في
والتي تم تطبيقها على نماذج اللزوجة الدوامية ،*Smirnov-Menter* و*Spalart-Shur* ذلك تصحيحات
ورقة المراجعة هذه نظرة عامة شاملة على تطوير وتنفيذ وأداء تصحيحات الدوران / الالانحناء .(*EVMs*
على تطبيقها على التدفق الدوامي مثل فواصل الأعاصير والقنوات المنحنية. من ،*RANS* في نماذج
ارنة نتائج *EVMs* المعدلة والنماذج التقليدية مع بيانات المحاكاة العددية التجريبية والمباشرة (*DNS*)،
الدراسة الضوء على تأثير هذه التصحيحات على تحسين دقة النموذج مع الحفاظ على تكلفة حسابية
ملالائمة. أظهرت النتائج أن التعديل يوفر توازنًا عمليًا بين الدقة العددية والتكلفة
الحسابية، خاصة في التطبيقات الصناعية التي تنطوي على تدفق شديد الدوامة أو انحناءات قوية.

1. Introduction

Vortex and swirling flows are widespread in a variety of mechanical systems, including dust collect spray dryers, vortex tubes, and combustion chambers. Furthermore, these flow phenomena are frequently observed in nature, such as tornadoes, oceanic eddies and dust devils. Consequently, t numerical simulation of such flows is of critical importance for advancing both industrial applicati and scientific research to understand and analyze these flow phenomena. Swirling flows, particula those influenced by system rotation and streamline curvature, presents a significant challenge to conventional eddy viscosity turbulence (EVMs) models to solve and close the Rynolds Averaged Navier-Stokes Equations (RANS). The full-Reynolds-stress turbulence models (RSM), detached eddy simulation (DES) and the large eddy simulation explicitly account for rotation and curvature effect their equations. This is seen as a significant advantage compared to simpler eddy-viscosity models which doesn't handle these effects as. Despite advances in turbulence-resolving methods like LES, DES, and RSM, the RANS models remain the most widely used in industrial computational fluid dynamics (CFD). RANS are preferred due to their balance between efficiency and accuracy, even though Reynolds Stress Models (RSMs) could theoretically be more accurate than simpler Eddy-Viscosity Models (EVMs), the robustness and the computational cost are in the favor of RANS mod Conventional Reynolds-Averaged Navier-Stokes (RANS) models, including the widely used $\boldsymbol{k-\varepsilon}$ and $\boldsymbol{k-\omega}$ models, are incapable in predicting swirling flows accurately, and hence they cannot capture t effects resulting from strong streamline curvature and rotating systems [1, 2]. The limitations of th models are due to the implementation of the Boussinesq hypothesis, which deal with the eddy vis term appear in the RANS model as an isotropic scalar [3]. To overcome these weaknesses, several attempts have been proposed over the years, focusing on modifying the production term in the turbulence model.

The implementation of rotation and curvature corrections in turbulence models has significantly improved the ability of RANS models to predict swirling flows. The evolution of the RANS models from its original formulation to the modified alternatives, reflects the efforts of the RANS model balance between the model accuracy and the computational efficiency.

This research paper aims to critically review the implementation of rotation and curvature corre functions within the Reynolds-Averaged Navier-Stokes (RANS) model. It further highlights the mathematical formulations of these modifications and compare their performance towards sw flow phenomenon by assessing the effectiveness and accuracy of these corrections in improving turbulence modeling. It also explores their application to highly swirling flow conditions. The m objective is to identify potential enhancements and offer practical insights for better numerical predictions in engineering applications.

2. RANS models modifications to account for rotation/curvature effects.

2.1 Spalart and Shur modifications SARC (1997)

One of the earliest modifications was proposed by Menter in the formulation of the Shear Stress Transport (SST) model, which combined the capabilities of the k-ω model near the walls and the k-ε model in the far field [4]. Despite its success, the SST model still has a limitation in handling the effects of rotation and streamline curvature. In 1997, Spalart and Shur proposed a correction term to sensitize turbulence models to rotation and curvature effects [5].

This correction term was applied to the Spalart-Allmaras (SA) model, the results demonstrated efficacy in flows involving curved channels and rotating systems. The model was tested on a b facing step, the results demonstrated the superiority to some degree of the modified version conventional models when compare to experimental data.

They concluded that the proposed rotation function did not reflect a clear and strong relationshi the curvature of the streamlines. Their proposed rotation function aimed to unify rotation and cu effects and further testing are necessary to fully understand and validate this modification in co flows.

2.2 Hellsten modifications RCSST (1998)

Based on the Spalart-Shur correction, Hellsten [6] introduced modifications to the SST model, all it to be rotationally invariant and more suitable for flows in rotating systems. This modification w particularly important for applications involving strong streamline curvature. The empirical funct developed by Hellsten was calibrated for rotating channel flow with spanwise rotation, and furth validated on a range of complex aerodynamic flows. They investigated their modification on a ch flow with spanwise rotation and on a boundary layer over convex-curved surface. The results sh improvement in predicting the pressure distribution and skin friction when the RCSST is used. It showed that for the rotating channel flow the RCSST model gives accurate results for flows with rotation numbers below 0.1. For the convex-curved, the RCSST model predicts flow behavior mo accurately than the conventional SST model.

2.3 Smirnov and Menter modifications SSTCC (2009)

In 2009, Smirnov and Menter implemented the Spalart-Shur correction function to the SST mo resulting in the SST with Curvature Correction (SSTCC) model [7]. Thess modifications improve ability to predict swirling flows by applying the correction function to the production terms of turbulent kinetic energy (k) and specific dissipation rate (ω) equations. The results of their wor showed that the SSTCC model significantly enhance the accuracy of swirling flow predictions w maintaining the computational cost compared to more computationally expensive approaches Large Eddy Simulation (LES) and Reynolds Stress Models (RSMs). The model was tested on hyd cyclone and centrifugal compressor. The results as shown in figure 3 demonstrate that the sta model fails in capturing the correct tangent velocity profile, which represent the near wall regi loss vortex" part of the Rankine vortex profile, while the modified version was in good agreem the experimental data.

2.4 Arolla and Durbin modifications (2013)

Other researchers have also explored alternative approaches to account for rotation and cur effects. Arolla and Durbin [9] proposed two approaches namely, the bifurcation approach an coefficients approach. The bifurcation approach adjusted to parameterize the eddy viscosity While the modified coefficients approach parameterizes the model coefficients such that the rate of turbulent kinetic energy is enhanced. They validated the model on several benchmark the results were encouraging in capturing the incorporate the effects of rotation and curvatu

2.5 Alahmadi and Nowakowski modifications SSTCCM (2016)

In proposed modified, Alahmadi and Nowakowski [10] proposed a modified SSTCC model to simulate swirling flows in a cyclone separator. They introduced the Richardson number (Ri) as a simplification to avoid the use of Lagrangian derivatives, and hence a reduction in the computational cost of the model. Their findings showed that the SSTCCM model, is superior to teddy- viscosity models (EVMs) in capturing the swirling motion and vortex breakdown in cyclone flows. The modified model tested against conventional EVMs and experimental data.

The results showed that the conventional EVMs failed to capture the flow separation due to strong curvature. On the contrary, all the modified versions with the rotation function successfully capture the flow separation and reattachment.
To further examine the ability of the SSTCCM model Alahmadi and Nowakowski performed a simulation of a flow in cyclone separator. Their findings demonstrated that the only modified versions are capable of capturing the Rankine vortex profile in accordance with the experimental measurements.

In addition to that, Alahmadi et al. [11] performed a numerical simulation on 3D sudden expansion pipe. They examined different numerical schemes. It is found that the linear upwind scheme (LU) provides the most accurate predictions compared to experimental measurements. It has been shown that both the axial and the tangential velocity profiles predictions are in good agreements with experimental measurements. It showed that Rankine profile of the tangential velocity cannot be captured using EVMs because of the implementation of the Boussinesq hypothesis, while the SSTCCM model accurately predicts the Rankine profile of the tangential velocity, and this attributed to the use of the rotation function.

3. Mathematical Model

The fundamental physics of the fluid flow is governed mathematically by Navier-Stokes Equation, namely, the continuity equation and the mass conservation equation [13]. For transient incompressible flow, these equations can be expressed as follows;

$$\frac{\partial u_i}{\partial x_i} = 0 \qquad (1)$$

$$\frac{\partial u_i}{\partial t} + \frac{\partial u_i u_j}{\partial x_j} = -\frac{1}{\rho}\frac{\partial p}{\partial x_i} + \frac{\mu}{\rho}\frac{\partial^2 u_i}{\partial x_j \partial x_j} \qquad (2)$$

The Reynolds-Averaged Navier-Stokes (RANS) equations represent the time-averaged formulation equations (1) and (2). The averaging formulation was proposed by O. Reynolds [14], these equat now serve as a fundamental framework for numerous turbulence models. The RANS equations expressed as follows:

$$\rho\left[\frac{\partial \bar{u}_i}{\partial t} + \frac{\partial \bar{u}_i \bar{u}_j}{\partial x_j}\right] = \frac{\partial \bar{p}}{\partial x_i} + \frac{\partial}{\partial x_j}(2\mu S_{ij} + \tau_{ij}) \qquad (3)$$

where S_{ij} is the time averaged strain rate tensor, and τ_{ij} is the Renolds stress tensor, and they are given by:

$$S_{ij} = \frac{1}{2}\left(\frac{\partial \bar{u}_i}{\partial x_j} + \frac{\partial \bar{u}_j}{\partial x_i}\right) \qquad (4)$$

$$\tau_{ij} = -\rho \overline{u} \overline{u} \quad (5)$$

The commonly models sensitized to rotation/curvature are the Spallart-Allmaras and the Shear S Transport $k-\omega$ (SST $k-\omega$), for turbulence in swirling flows is often the Shear Stress Transport (SST) model, which combines the advantages of both the $k-\varepsilon$ and $k-\omega$ models. The governing equations for the SST model consist of the transport equations for the turbulent kinetic energy (k the specific dissipation rate (ω):

$$\frac{\partial k}{\partial t} + U_j \frac{\partial k}{\partial x_j} = P_k - \beta k^* \omega + \frac{\partial}{\partial x_j}\left[(\nu + \frac{\nu_t}{\sigma k}) \frac{\partial k}{\partial x_j}\right] \quad (6)$$

$$\frac{\partial \omega}{\partial t} + U_j \frac{\partial \omega}{\partial x_j} = \alpha \frac{P_k}{\nu_t} - \beta \omega^2 + \frac{\partial}{\partial x_j}\left[(\nu + \frac{\nu_t}{\sigma \omega}) \frac{\partial \omega}{\partial x_j}\right] \quad (7)$$

Here, P_k represents the production term, ν_t is the eddy viscosity, and α, β, and σ_k are model constants.

To account for the effects of rotation and curvature, Spalart and Shur [5] proposed a correction function that modifies the production term in the k equation:

$$P_k^{modified} = P_k \cdot [1 + c_{rc} \cdot f(\Omega, S)] \quad (8)$$

where c_{rc} is a calibration constant and $f(\Omega, S)$ is a function of the rotation rate (Ω) and strain rate (

This correction is applied to both the production term and the dissipation rate in the transport eq for (k) and (ω), which leads to accurate predictions for swirling flows [7].

Hellsten [6] further refined this approach by introducing a modification to the specific dissipation equation, making the model more robust for rotating systems. The Richardson number (Ri) was introduced as a measure of the rotational effects, leading to a more efficient formulation of the correction function [10]. This modification has been particularly successful in applications involving cyclone separators and other systems with strong curvature or rotational motion [11].

3.1 Spalart-Allmars with rotation and curvature model (SARC)

The standard one equation Spalart-Allmars model without rotation/curvature correction can be found in [15]. In the standard model, the Reynolds stress tensors are related to the shear strain rate by employing the Boussinesq hypothesis as in the following formula:

$$\tau_{ij} = -\rho \overline{u}_i \overline{u}_j = 2\mu_t S_{ij} = \rho \nu_t \left(\frac{\partial \overline{u}_i}{\partial x_j} + \frac{\partial \overline{u}_j}{\partial x_i}\right) \quad (9)$$

The transport equation of the viscos (turbulent) is given by:

$$\frac{\partial}{\partial t}(\rho \tilde{\nu}) + \frac{\partial}{\partial x_i}(\rho \tilde{\nu} u_i) = C_{b1}\rho \tilde{S}\tilde{\nu} + \frac{1}{\sigma_\nu}\frac{\partial}{\partial x_j}\left[\left(\mu + \rho\tilde{\nu}\right)\frac{\partial \tilde{\nu}}{\partial x_j}\right] + C_{b2}\rho\left(\frac{\partial \tilde{\nu}}{\partial x_j}\right)^2 - Y_\nu \quad (10)$$

The implementation of the rotation/curvature effects in the SA model can be achieved by multiplying the production term ($C_{b1}\rho\tilde{S}\tilde{\nu}$) appear in equation (10) by the rotation function (f_{r1}), which is given by:

$$f_{r1}(r^*, \tilde{S}) = (1 + c_{r1})\frac{2r^*}{1 + r^*}\left[1 - c\tan\left(c_{r2}\tilde{r}\right)\right] - c_{r1} \quad (11)$$

The dimensionless variables r^* and $\tilde{r}$ are given by:

$$r^* = \frac{S}{\Omega} \quad (12)$$

$$\tilde{r} = \frac{2\omega_{ij}S_{ij}}{D^4}\left(\frac{DS_{ij}}{Dt} + \varepsilon_{imn}S_{jn}\Omega_m + \varepsilon_{jmn}S_{in}\Omega_m\right) \quad (13)$$

where S_{ij}, ω_{ik}, D, and the empirical constants c_{r1}, c_{r2}, and c_{r3} are summarized in table 1.

Table 1. Strain tensors, system rotation rate and the empirical constants.

Term	Expression/value
S_{ij}	$\frac{1}{2}\left(\frac{\partial u_i}{\partial x_j} + \frac{\partial u_j}{\partial x_i}\right)$
ω_{ij}	$\frac{1}{2}\left(\frac{\partial u_i}{\partial x_j} - \frac{\partial u_j}{\partial x_i}\right) + 2\varepsilon_{mji}\Omega_m$
ε_{imn}	Levi-Cvita symbol
$\frac{DS_{ij}}{Dt}$	The Lagrangian derivative
D^4	$\left(\frac{1}{2}\left(S^2 + \Omega^2\right)\right)^2$
S^2	$2S_{ij}S_{ij}$

$\Omega 2$	$2\omega_{ij}\omega_{jk}$
c_{r1}	1.0
c_{r2}	2.0
c_{r3}	1.0

3.2 Simpler version of Spalart-Allmars rotation and curvature model (SARCM)

In 2013, Zhang and Yang proposed a simpler version of the SARC model by avoiding the calculation of the Lagrangian derivative term by implementing the Richardson number Ri defined by Hellsten [16]. The modified model is identical to the SARC model except for the nondimensional quantity $\tilde{r}$, which redefined as follows:

$$\tilde{r} = \frac{\Omega}{S}\left(\frac{\Omega}{S} - 1\right) \quad (14)$$

3.3 Smirnov- Menter rotation and curvature model (SSTCC)

The SSTCC model is built on the SST $k-\omega$ turbulence model. Smirnov and Menter implemented Spalart-Shur correction function to the production term in the transport equations of both the turbulent
kinetic energy (k) and the specific dissipation rate (ω). Therefore, the production term (P_k) appears in
equations (6) and (7) is multiply by the rotation function $f_{rotation}$, which is given by:

$$f_{rotation} = \max\{\min(fr1 \cdot (1+c_{r1}), 1.25), 0\} \quad (15)$$

where $fr1$is given by equation (11). Equations (12) and (13) were used to calculate the dimensionless quantities r_* and $\tilde{r}$.

3.3 Alahmadi-Nowakowski rotation and curvature model (SSTCCM)

The SSTCCM model is a simpler version of the SSTCC model. Both models built on the SST $k-\omega$ turbulence model. The limiter function (equation (15)) proposed by Smirnov and Menter was implemented in the SSTCCM. The dimensionless quantity $\tilde{r}$ in equation (14) was used to avoid the calculation of the complex Lagrangian derivative term, while equation (12) used to calculate the term r_*.

Table 2 listed a summary of various numerical research where the swirling flows were simulated
using EVMs with rotation and curvature modifications.

Table 2. List of literatures that implements modified EVMs to numerically predicts swirling flow phenomenon in different applications.

Literature	Application	Modified EVMs	Findings	Computational cost
Chaderjian et al. [17]	NACA 0012 airfoil and a flexible UH-60A rotor	SARC	SARC model improves the boundary layer profiles for highly curved flows and helps reduce the TEV in the tip vortex cores.	5.6 hr for 210 million grid points 17.6 hr for 360 million grid points
Chaderjian [18]	V22 rotor in hover	SARC	the SARC-DES turbulence model is highly recommended over the SARC-RANS turbulence model for hover simulations	computational cost is reduced significantly by using the quick-start procedure
Shur et al. [19]	Duct with U-Turn, 3D curved channel	SARC	SARC model has demonstrated superiority over a wide range of EVMs in terms of accuracy and superior over RSM in terms of computational cost	The CPU time is 20% larger than the original SA model
Huang et al. [20]	Turbulent impinging jet heat transfer	SSTCC	In the downstream region of turbulent impinging jet, the performance of the SSTCC and original SST is similar	Not available
Ferreira et al. [21]	biradial turbine with movable guide-vanes	SARC	The SARC model is more robust and allows the application of implicit residual smoothing, which leads to faster calculation of the operating curves	Not available
Li et al. [22]	Swirling Supersonic Jets Generated Through a Nozzle-Twisted Lance	SSTCC	The numerical predictions are validated against theoretical values, and the maximum errors of the simulated Mach number and	Not available

			mass flow rate are 2.98% and 0.33%, respectively.	
Alahmadi et al. [11]	Sudden expansion pipe	SSTCCM	Conventional EVMs i.e. standard k−ϵ, RNG k−ϵ, and the SST k−ω models failed to capture the vortex breakdown phenomenon. The SSTCCM showed better performance and predicted the location of the central recirculation zone in the swirling flow	23 hours
Khaleed et al. [23]	Pressure distribution on new designed propeller	SSTCCM	The SSTCCM was implemented to numerically calculate the pressure distribution on the propeller for the upstream region.	Not available
Viken et al. [24]	Numerical simulations of airfoild and flap for DEP X 57 airplane	SARC	Wide range of RANS models were implemented to investigate the aerodynamic performance of different airfoils. For high angle attack, only the SARC and the SST models captures the recirculation region behind the upper surface of the flap.	Not available
Rogovyi et al [25]	Swirling Submerged Flow Through a Confuser	SSTCC	The SSTCC model predict the flow shape, the magnitude of the attenuation of rotation, and the velocity values in different sections in were in a good agreement with the stereo-PIV measurements.	The modified SST turbulence model predicts the main characteristics of the swirl flow using medium-power computers.
Zhang et al. [26]	Centrifugal impeller in the rotating frame of reference	SSTCC	The original SST model failed to capture the unsteady feature of the swirling flow, while the SSTCC showed better performance by predicting the flow in the centrifugal	Not available

			pump impeller, the unsteady stall and turbulence fluctuation.	
Xiaoyu et al. [27]	60 degree circularly bent channel	SSTCC & SARC	The RSM and modified models showed better performance when compared with DNS. The EVMs without modification flailed to predict the flow at the separation zone	Not available
Hreiz et al. [28]	Numerical investigation of swirling flow in cylindrical cyclones	SARC	For single tangential inlet LES and Re realizable $k-\varepsilon$ model that give the best results. For more than one inlet, only LES capture the shape of the velocity profile	Not available

3. Conclusion

The most popular model to numerically simulate highly swilling flows is the Reynolds Stress Model (RSM). Although RSM is computationally heavy compared to the modified RANS models, its use is more common due to its availability in many commercial software like ANSYS. All the sensitized RANS model to rotation/curvature corrections are not available in any commercial software, therefore it is not popular among researchers. The sensitized RANS models feature favorably classified as robust numerical tool for simulating complex swirling flows. It seems that these models could be further extended by saying that they could be successfully applied to other case studies such as industrial axi-centrifugal compressors or other gas turbines of comparable characteristics.

- SARC and SARCM perform well for external aerodynamic flows but still underestimate the effect of curvature at high Reynolds numbers.
- SSTCC and SSTCCM showed good performance for internal flows subjected to highly swirling flow and strong streamline curvature.
- Neither the SSTCC nor SSTCCM were examined or tested for external aerodynamic flows.

4. Acknowledgments

The author would like to express his appreciation for the support provided by the Scient
Research Deanship, Islamic University of Madinah, Kingdom of Saudi Arabia.

REFRENCES

1] F. R. Menter, M. Kuntz, R. Langtry and others, "Ten years of industrial experience with the SST turbulence model," Turbulence, heat and mass transfer, vol. 4, p. 625–632, 2003.

[2]G. Gronald and J. J. Derksen, "Simulating turbulent swirling flow in a gas cyclone: A comparison of various modeling approaches," Powder technology, vol. 205, p. 160–171, 2011.

[3] J. Gimbun, T. G. Chuah, T. S. Y. Choong and A. Fakhru'l-Razi, "A CFD study on the prediction of cyclone collection efficiency," International Journal for Computational Methods in Engineering Science and Mechanics, vol. 6, p. 161–168, 2005.

[4] F. Menter, "Zonal two equation k-ω turbulence models for aerodynamic flows," in 23rd flu dynamics, plasmadynamics, and lasers conference, 1993.

[5] P. R. Spalart and M. Shur, "On the sensitization of turbulence models to rotation and curvature," Aerospace Science and Technology, vol. 1, p. 297–302, 1997.

[6] A. Hellsten, "Some improvements in Menter's k-omega SST turbulence model," in 29th AIAA, Fluid Dynamics Conference, 1998.

[7] P. E. Smirnov and F. R. Menter, "Sensitization of the SST turbulence model to rotation and curvature by applying the Spalart-Shur correction term," in Turbo Expo: Power for Land, Sea, and Air, 2008.

[8] C. D. Hartley, "'Measurement of flow velocities within a hydrocyclone using laser doppler anemometry'," AEA, Power Fluidics, BNFL, Technical Report No. FTN/X/82, 1994.

[9] K. Arolla and P. A. Durbin, "Modeling rotation and curvature effects within scalar eddy viscosity model framework," International Journal of Heat and Fluid Flow, vol. 39, p. 78–89, 2013.

[10] Y. H. Alahmadi and A. F. Nowakowski, "Modified shear stress transport model with curvature correction for the prediction of swirling flow in a cyclone separator," Chemical Engineer Science, vol. 147, p. 150–165, 2016.

[11] Y. H. Alahmadi, S. A. Awadh and A. F. Nowakowski, "Simulation of swirling flow with a vortex breakdown using modified shear stress transport model," Industrial & Engineering Chemis Research, vol. 60, p. 6016–6026, 2021.

[12] P. A. Dellenback, D. E. Metzger and G. Neitzel, "Measurements in turbulent swirling flow through an abrupt axisymmetric expansion," AIAA journal, vol. 26, p. 669–681, 1988.

[13] S. N. A. Yusuf, Y. Asako, N. A. C. Sidik, S. B. Mohamed and W. M. A. A. Japar, "A short review on rans turbulence models," CFD Letters, vol. 12, p. 83–96, 2020.

[14] O. Reynolds, "IV. On the dynamical theory of incompressible viscous fluids and the determination of the criterion," Philosophical transactions of the royal society of london.(a.), p. 12 164, 1895.

[15] P. Spalart and S. Allmaras, "A one-equation turbulence model for aerodynamic flows," in 30th aerospace sciences meeting and exhibit, 1992.

[16] Q. Zhang and Y. Yang, "A new simpler rotation/curvature correction method for Spalart–Allmaras turbulence model," Chinese Journal of Aeronautics, vol. 26, p. 326–333, 2013.

[17] N. M. Chaderjian, "Numerical Simulation of Dynamic Stall Using Near-Body Adaptive Mesh Refinement," in International Conference on Computational Fluid Dynamics (ICCFD), 2018.

[18] N. M. Chaderjian, "A quantitative approach for the accurate CFD simulation of hover in turbulent flow," Journal of the American Helicopter Society, vol. 68, p. 42009–42028, 2023.

[19] M. L. Shur, M. K. Strelets, A. K. Travin and P. R. Spalart, "Turbulence modeling in rotating and curved channels: assessing the Spalart-Shur correction," AIAA journal, vol. 38, p. 784–792, 2000.

[20] H. Huang, T. Sun, N. Li and G. Zhang, "Sensitization of the modified SST model to the swirling and curvature for turbulent impinging jet heat transfer," International Journal of Heat and Mass Transfer, vol. 182, p. 121980, 2022.

[21] D. N. Ferreira, L. M. C. Gato, L. Eça and J. C. C. Henriques, "Aerodynamic analysis of a biradial turbine with movable guide-vanes: Incidence and slip effects on efficiency," Energy, vol. 200, p. 117502, 2020.

[22] M. Li, Q. Li, Z. Zou and X. An, "Computational investigation of swirling supersonic jets generated through a nozzle-twisted lance," metallurgical and Materials transactions B, vol. 48, p. 713–725, 2017.

[23] H. M. T. Khaleed, I. A. Badruddin, Y. H. Alahmadi, A. A. G. Haider, V. Tirth, A. A. Rajhi, A. Algahtani, A. E. Anqi, S. Alamri, S. Kamangar and others, "Comparison of 3D Printed Underwate Propeller Using Polymers and Conventionally Developed AA6061," Journal of Materials Engineerin and Performance, vol. 31, p. 5149–5158, 2022.

[24] J. K. Viken, S. Viken, K. A. Deere and M. Carter, "Design of the Cruise and Flap Airfoil for the X-57 Maxwell Distributed Electric Propulsion Aircraft," in 35th AIAA Applied Aerodynamics Conference, 2017.

[25] A. Rogovyi, S. Khovanskyi, I. Hrechka and A. Gaydamaka, "Studies of the swirling submerged flow through a confuser," in Design, Simulation, Manufacturing: The Innovation Exchange, Springer, 2020, p. 85–94.

[26] W. Zhang, Z. Ma, Y.-C. Yu and H.-X. Chen, "Applied new rotation correction κ–ω SST model for turbulence simulation of centrifugal impeller in the rotating frame of reference," Journa Hydrodynamics, Ser. B, vol. 22, p. 404–407, 2010.

[27] X. Yang and P. G. Tucker, "Assessment of turbulence model performance: Large streamlin curvature and integral length scales," Computers & Fluids, vol. 126, p. 91–101, 2016.

[28] R. Hreiz, C. Gentric and N. Midoux, "Numerical investigation of swirling flow in cylindrical cyclones," Chemical engineering research and design, vol. 89, p. 2521–2539, 2011.

Advances in Bioinformatics Techniques to Predict Neoantigen: Exploring Tumor Immune Microenvironment and Transforming Data into Therapeutic Insights

Abdulwahed Alrehaily
Biology Department, Faculty of Science, Islamic University of Madinah, Madinah

42351, Saudi Arabia

Email: alrehaily.abdulwahed@gmail.com
ORCID: https://orcid.org/0000-0002-3509-7565

Abstract: The incorporation of bioinformatics into the prediction of neoantigens has greatly enhanced cancer immunotherapy by improving the understanding of tumor-specific antigens that can trigger targeted immune responses. This review emphasizes the vital role of bioinformatics in identifying neoantigens, which are unique antigens arising from somatic mutations, and their significance in customizing cancer treatments like therapeutic vaccines and T-cell therapies. It critically examines advanced sequencing technologies, such as whole-genome (WGS) and whole-exome sequencing (WES), for their role in assessing mutations that lead to neoantigen production. The review also discusses innovative computational methods, including artificial intelligence (AI), machine learning (ML), and deep learning (DL), for their effectiveness in predicting immunogenic neoantigens and tailoring personalized therapies. Case studies illustrate the successes achieved through these bioinformatics advancements, showcasing their potential in developing personalized vaccines that address the specific genetic makeup of tumors. Despite challenges like tumor heterogeneity and the complexities of data analysis, ongoing advancements.

Keywords: Bioinformatics, Machine Learning (ML), Artificial Intelligence (AI), Immuno-oncology, Immunotherapy, Computational Pipelines.

التطورات في تقنيات المعلوماتية الحيوية للتنبؤ بالمستضد
الجديدة: استكشاف البيئة المناعية للورم وتحويل البيانات إل
رؤى علاجية

الملخص أدى دمج المعلوماتية الحيوية في التنبؤ بالمستضدات الجديدة إلى تعزيز العلاج المناعي للس
كبير من خلال تحسين فهم المستضدات الخاصة بالأورام والتي يمكن أن تؤدي إلى استجابات مناع
تؤكد هذه المراجعة على الدور الحيوي للمعلوماتية الحيوية في تحديد المستضدات الجديدة، وهي مس
تنشأ عن الطفرات الجسدية، وأهميتها في تخصيص علاجات السرطان مثل اللقاحات العلاجية وع
التائية. يتناول هذا البحث بشكل نقدي تقنيات التسلسل المتقدمة، مثل تسل (WGS) وتسلسل الإكسوم الكامل (WES)، لدورها في تقييم الطفرات التي تؤدي إلى إنتاج المستضدات الجديدة. كما يناق
الأساليب الحسابية المبتكرة، بما في ذلك الذكاء الاصطناعي (AI)، والتعلم الآلي (ML)، والتعلم العميق (DL)،
لفعاليتها في التنبؤ بالمستضدات الجديدة المناعية وتصميم العلاجات الشخصية. توضح دراسات الح
التي تحققت من خلال هذه التطورات في المعلوماتية الحيوية، حيث تعرض إمكاناتها في تطوير لقاح
تعالج التركيبة الجينية المحددة للأورام. وعلى الرغم من التحديات مثل تباين الورم وتعقيدات تحليل ا
التطورات الجارية .

1. Introduction

Cancer is primarily a genetic illness, during its course, it is accompanied by genomic instability leading to point mutations and structural changes [1]. Cancers can be classified into metastatic and nonmetastatic forms, with metastasis arising during the development of tumors. Metastatic dissemination enables cancer cells to evade main tumors and establish colonies in other organs [2]. Tumors are intricate systems consisting of neoplastic cells, extracellular matrix (ECM), and "accessory" nonneoplastic cells, such as resident mesenchymal support cells, endothelial cells, and infiltrated inflammatory immune cells. Tumor growth is influenced by interactions between accessory cells and cancer cells. During tumor growth, the structure of the tissue changes and becomes a specialized microenvironment that is defined by a damaged extracellular matrix (ECM) and long-lasting inflammation [3]. Cancer-related inflammation plays a role in causing genetic instability, modifying epigenetic patterns, promoting the growth of cancer cells, enhancing pathways that prevent cell death, stimulating the formation of new blood vessels, and facilitating the spread of cancer [4]. The role of inflammatory immune cells in cancer-related inflammation is crucial, and several studies have demonstrated how immune cells affect tumor fate at various stages of the disease, such as early neoplastic transformation, clinically detected tumors, metastatic dissemination, and therapeutic intervention [5].

Cells of the innate immune system, such as natural killer (NK) cells, eosinophils, basophils, a

phagocytic cells, have a role in suppressing tumors by either directly killing them or by trigger
adaptive immunological responses. The adaptive immune system, which comprises lymphocytes,
a crucial role in both humoral and cell-mediated immune responses. Unfortunately, cancer cells
developed defense mechanisms against immune surveillance, which impairs immune cells' abili
act as effectors thereby rendering immunotherapy less successful [6]. Gaining insight into these ir
interactions inside the tumor microenvironment (TME) is essential for the advancement of more p
cancer treatments. Immunotherapy has made significant improvements in the treatment of a var
cancer types by utilizing the immune system's capacity to recognize and destroy cancer cells. Re
advancements in single-cell technologies and spatial transcriptomics have yielded valuable inform
about the diversity and spatial arrangement of immune cells within tumors. This has allowed f
thorough understanding of the tumor microenvironment (TME) and the discovery of new target
therapeutic intervention [7].

These genetic changes can result in the production of neoantigens, or tumor-specific antigens

immune system interprets these neoantigens as alien, which sets off cellular immunological resp
[8]. One major problem that contributes to treatment failure and disease progression in human p
and metastatic cancers is cancer heterogeneity. The immune system's selective pressure, hierar
architecture from the start of cancer stem cells, and genetic instability are a few of the factors tha
account for this variability [5]. Tumor clonal growth and heterogeneity reduction are facilitated
cancer immune editing, which eradicates immunogenic cancer cells. Nevertheless, the absence of
immune selection leads to a greater diversity of neoantigens. Neoantigen heterogeneity in lung
melanoma patients increases their vulnerability to T-cell attacks and responsiveness to tumor
checkpoint inhibition [9]. This heterogeneity is heightened due to the inactivation of DNA repair
machinery in colorectal, breast, and pancreatic cell lines. As genetic variation within a tumor increa
certain subpopulations of cells may evade the immune system's defenses. Metastatic developme
therapeutic resistance often originate from a few clones inside the original tumors. In ovarian ca
shrinking metastatic tumors were linked to an immune infiltrate characterized by CD4+ and CD8
cells, with higher tumor mutation and neoepitope load compared to advancing lesions [9].

Understanding the intricate connections between cancer cells and immune responses is crucial developing effective cancer treatments.

1.1. Scope and Objectives of the Review

This review specifically examines the critical role of bioinformatics techniques in the prediction of neoantigens, which are essential for advancing personalized cancer immunotherapy. The primary focus is on how computational tools and sequencing technologies enable the identification of tumor-specific neoantigens that can be targeted for tailored cancer treatments, including therapeutic vaccines and T- cell-based therapies. The first domain explores the application of bioinformatics tools in the prediction of neoantigens, which play a vital role in tailored cancer immunotherapies such as vaccinations and T- cell treatments [10]. In addition, the second domain explores, data integration techniques for researching tumor-immune interactions covered in the review, with a focus on the significance of combining various data types from transcriptomics, proteomics, and genomes [11]. The third domain discusses various tools and platforms, such as single-cell RNA sequencing, spatial transcriptomics, CIBERSORT, and TIDE, which are being investigated to gain a thorough comprehension of the interactions between tumors and the immune system [12-14]. These methods aim to uncover possible targets for therapeutic interventions. The review also emphasizes the clinical benefit and ongoing progress in the field of bioinformatics-driven immunotherapy development, including immune checkpoint inhibitors, personalized cancer vaccines, and CAR-T cell therapy.

This review offers an extensive analysis of the transformative impact of bioinformatics on the fiel immuno-oncology. The review emphasizes the most recent progress in bioinformatics tools and techniques, providing a clear explanation of cutting-edge methodologies. It also demonstrates the practical significance of bioinformatics in the development of efficient immunotherapies, as evide by case studies and success stories. In addition, it addresses potential future research avenues to cancer treatment and tackles persistent problems like data integration and complexity. The review to be a beneficial resource for researchers and clinicians by summarizing important discoveries, t and methodologies. It aims to assist in the development and implementation of innovative investi and therapeutic applications.

2. Bioinformatics Tools for Predicting Neoantigens

The study of neoantigens has greatly expedited the progress and regulatory approval of tumor immunotherapies. These include cancer vaccines, adoptive cell therapy, and antibody-based therapies [15]. Neoantigens are newly formed antigens created by tumor cells. They arise due to tumor-specific alterations, such as genomic mutations, dysregulated RNA splicing, and viral open reading frames. These antigens can trigger an immune response that bypasses central and peripheral tolerance mechanisms. Neoantigens are crucial for personalized cancer immunotherapies and have the potential to induce strong immune responses and reduce the likelihood of targeting normal tissues [16]. Their unique characteristics make them potential candidates for immunotherapeutic techniques including customized cancer vaccines and adoptive T-cell treatments. Synthetic peptides that imitate neoantigens are used in personalized cancer vaccines to train the immune system to recognize and destroy cancer cells. Adoptive T-cell therapies design T cells to target neoantigens, thereby improving cancer control [17]. The prediction of neoantigens proves challenging due to tumor heterogeneity, as each tumor has unique mutations and neoantigens can differ greatly between patients. As a result, it is necessary to implement highly personalized strategies to effectively identify and target neoantigens [18].

One of the challenges experienced by researchers in the field of immunology is accurately recognizing immunogenic neoantigens. These are mutations that can trigger an immune response. However, not all mutations result in neoantigens that can effectively elicit this response. To predict which mutations will produce neoantigens that bind to major histocompatibility complex (MHC) molecules and are recognized by T cells, computational tools are used. The stability and affinity with which neoantigen peptides bind to MHC molecules are the main characteristics that computational methods need to consider. Additionally, computational methods must account for how these complexes are recognized by T-cell receptors [19, 20]. The tumor microenvironment plays a crucial role in the presentation of neoantigens and the recognition of these antigens by the immune system.

Tumors can manipulate the immune response by downregulating antigen presentation machine creating an immunosuppressive microenvironment. These mechanisms make it challenging to accurately predict neoantigens and develop effective immunotherapies [21, 22]. Additionally, the of somatic mutation identification is not without its challenges. Significant challenges are pose technological restrictions, such as the inability to identify low-frequency mutations and differen genuine somatic changes from sequencing artifacts. Furthermore, modern bioinformatics too skills are required for the technically challenging integration of multi-omics data to provide a thor understanding of the neoantigen landscape [23]. However, despite these obstacles, significant pr has been made in developing bioinformatics tools for neoantigen prediction. These tools are continuously improving in accuracy and efficiency, and they play a crucial role in advancing personalized cancer immunotherapy. Since somatic mutations lead to neoantigen formation, th step in neoantigen prediction is the identification of somatic mutation. Some of the sequencing technologies and bioinformatics tools for predicting somatic mutations are discussed below.

To understand the complex mechanism of human diseases, researchers rely on integrating data multiple omics techniques, including genomics, transcriptomics, epigenomics, and proteomics to u next-generation sequencing (NGS) in analyzing DNA. NGS enables the analysis of DNA throug various approaches such as whole-genome sequencing (WGS), whole-exome sequencing [24], targeted sequencing. This powerful tool allows for the sequencing of millions of DNA fragme simultaneously, providing detailed information about the structure of genomes, genetic variation activity, and alterations in gene behavior [25].

2.1 Whole-genome sequencing (WGS)

Whole-genome sequencing (WGS) is demonstrated to be a powerful technique for determinin individual's DNA sequence. It lists all genes, regulatory areas, and non-coding elements in an individual's genome. It can be applied in plant and animal studies, cancer research, rare gene population genetics, and genome assembly. This technique is highly useful in identifying geno variations from single-nucleotide polymorphisms (SNPs) to structural changes by sequencing genome [26]. There are two methods of WGS: Large and small, which are used to interpret eu and prokaryotic genomes, respectively. Short-read sequencing is best for mutation calling, an read for genome assembly. These two can be applied to accurate genome assembly without a sequence [27].

2.2 Whole-Exome Sequencing (WES)

The whole-exome sequencing (WES) technique is centered on sequencing the exome, or the par the genome that code for proteins. Though it is a minor portion of the whole genome, the majo variations that cause disease are found in the exome. WES is applied to identify genetic variatio protein-coding genes, including single-nucleotide variants, insertions, deletions, and copy numb changes. Additionally, it can be applied to population and cancer genetics as well as rare clinical illnesses, where it is a more affordable option than WGS. Whole-exome sequencing enriches ex regions through hybrid capture or target-specific amplification techniques followed by high-thro sequencing. The Illumina NGS platform can be used with a variety of exome capture assays [28] WES is a component of WGS, the bioinformatic analysis method utilized for WES data is the sam that used for WGS. Therefore, WGS is a valuable technique for identifying genetic variations in p coding regions of the genome, making it particularly useful in disease research and clinical appl

2.3 Targeted sequencing

Targeted sequencing is a successful approach that focuses on particular sections of the gene, enabling the identification of different types of genetic variants linked to disease phenotypes. Although targeted sequencing may have lower exploratory capabilities than WGS or WES, it offers benefits such as cost- effectiveness and manageable data for medical professionals.

This allows for more precise and well-informed clinical decisions based on disease-specific inform

[29]. In addition, targeted sequencing can offer enhanced coverage for rare alleles in genetic diso and low-frequency evolving mutant clones in cancer, enabling a more thorough comprehensi tumor heterogeneity and disease progression. In general, targeted sequencing has the potenti advance genomics research significantly, enhance personalized healthcare, and improve our understanding of diseases. The candidate gene approach and commercially available targeted p come from large-scale WGS/WES projects. These panels can test both inherited (germline) and acquired (somatic) variants. Some examples are listed in Table 1. Targeted panels use region-spe primers to amplify selected DNA regions. The resulting libraries are then sequenced and analyzed bioinformatics tools. Overall, targeted sequencing is a valuable method for identifying genetic vari linked to diseases, offering cost-effective and focused insights for clinical applications.

Table 1: Some Examples of Targeted Panels in Research and Diagnostics

Disease Condition	Panel Name	Inheritance Type	Sample Type
Cardiovascular defects	Cardiovascular Panel	Germline	Blood
Arrhythmias and cardiomyopathies	Arrhythmia and Cardiomyopathy Panel	Germline	Blood
Drug sensitivity	Pharmacogenomics Panel	Germline	Blood
Antimicrobial treatment efficacy	Antimicrobial Resistance Panel	Microbial Gene	Bacterial Culture
Infertility	Infertility Panel	Germline	Blood
Homologous recombination defects	HRR Gene Panel	Somatic	Tumor Tissue
Myeloid cancers	Myeloid Cancer Panel	Somatic	Tissue
HIV drug resistance	HIV-X Gene Panel	Pathogen	Blood Plasma
Antimicrobial resistance in TB	TB Resistance Panel	Pathogen	TB Specimen
Metabolic disorders	Metabolism Error Panel	Germline	DBS/Blood
Hereditary cancers	BRCA and Hereditary Cancer Panel	Germline	Blood

3. Bioinformatics Pipelines

The rapid advancements in next-generation sequencing (NGS) technologies have significantly aided in the identification of mutations within the exomes of individual tumors. These mutations lead to neoantigens, which can be presented by the patient's Human Leukocyte Antigen [30] molecules to the immune system, which triggers an immune response against the tumor. The identification and selection of these neoantigens have become crucial in developing personalized cancer immunotherapies, particularly in the design of cancer vaccines and adoptive cell therapies. The prediction of neoantigens begins with the identification of somatic mutations, which is the critical first step in neoantigen prediction, as these mutations lead to the formation of neoantigens. The advancement in sequencing technologies and bioinformatics tools have greatly added to the identification of genetic differences and differentiate between somatic mutations, which occur in specific cells, and germline variations, which are inherited and present in all cells of an individual [31].

The process of neoantigen identification involves multiple computational steps, each contributin

the accurate prediction of neoantigens. Initially, HLA typing is performed using RNA-seq, WGS, o
WES data to determine the specific HLA alleles of the patient, followed by the prediction of muta
peptides resulting from somatic mutations identified in the tumor. The next step involves the
identification of neoantigens that are likely to be presented on the surface of tumor cells, whi
achieved by predicting the binding affinity of the peptides to the HLA molecules.

Finally, candidate neoantigens are prioritized based on their predicted binding affinities and c factors, such as proteasomal processing and peptide transport [32].

In recent years, there has been significant growth and improvement of bioinformatics pipelin improve the process of identifying and selecting neoantigens in a more precise and effective way. pipelines encompass advanced machine learning algorithms and merge various kinds of omics like mass spectrometry and RNA-seq, to enhance the predictive power of neoantigen exploration existing bioinformatics pipelines are characterized by the incorporation of four principal computa components: HLA typing, mutation-driven peptide deduction, MHC binding and forecast of antig presentation, and prioritization of neoantigens. The integration of these distinct modules withi bioinformatics pipelines plays a crucial role in advancing the field of neoantigen prediction, th facilitating the identification of potential targets for immunotherapy [33].

In this section, we discuss bioinformatics tools and pipelines, developed to address neoantigen identification. These tools not only support the identification of potential neoantigens but also fac their selection for therapeutic applications, paving the way for personalized cancer treatments. A summary of these pipelines, including their strengths, limitations, and key references, is provide Table 1.

The Sequence Alignment/Map (SAM)-SAMtools is a suite of utilities for manipulating alignments i the SAM (Sequence Alignment/Map) format, including sorting, merging, indexing, and generati variant calls. It is used for processing next-generation sequencing data. The 'mpileup' function SAMtools is used to call variants, including somatic mutations, by generating a pileup format fr BAM files. It is widely adopted, simple to use, and highly efficient for basic operations on sequenc data. However, it has limitations in handling complex variant calling scenarios and lacks advan algorithms for distinguishing somatic from germline mutations [34]. Another highly effective to VarScan2 that detects single nucleotide variants (SNVs) using SAMtools 'mpileup' data. It compare tumor and normal sample data to identify germline and somatic mutations. Additionally, it detects number analysis and structural variants. One of the main strengths of VarScan2 is its ability to accurately call low-frequency variants. Nevertheless, this tool is constrained by accurate pileup generation and may be less effective for highly heterogeneous samples [35]. Another robust to developed by the Broad Institute for identifying genetic variations in large-scale sequencing da GATK (Genome Analysis software). It offers a variety of tools for data pre-processing, variant callin and variant filtering. The HaplotypeCaller tool from GATK is widely recognized for its ability to cal germline variants, while MuTect2 accurately recognizes somatic variants. GATK is extensively documented and is supported by the community. Moreover, it is adept at managing intricate ge regions. Nevertheless, big datasets, need a substantial resource [36]. MuTect is a tool within the G suite specifically designed for identifying somatic point mutations in tumor samples. The tool emp a Bayesian classifier to effectively distinguish between somatic mutations and sequencing artifac germline variants by using matched normal samples. MuTect possesses high sensitivity and specif rendering it highly proficient in the detection of infrequent somatic mutations. However, the to focused on point mutations, and minor insertions/deletions, and is less efficient for major struct variations [37]. Strelka is a specialized tool used for identifying single nucleotide variations (SNV and small insertions or deletions (indels) in tumor-normal pairs. It utilizes a Bayesian framewor precisely identify genetic variations and is capable of analyzing data from both WGS and WES. Stre is highly sensitive and accurately identifies low-frequency somatic mutations and small indels. Moreover, it has high computational efficiency.

However, it only emphasizes detecting minor genetic differences and not on larger structural changes [38]. FreeBayes is a variant detector that can identify SNPs, indels, MNVs, and complex events in both diploid and polyploid genomes. It is suitable for both germline and somatic variant calling. One of its strengths is its ability to handle complex variants and mixed ploidy populations. However, it can be computationally intensive and requires high-quality input data [39]. Platypus is a variant caller that detects SNVs and indels from NGS data using local realignment and assembly. It is faster than other tools and generates calls from raw aligned read data without preprocessing. It offers high accuracy and is effective in identifying complex variants. However, it is computationally intensive and requires significant memory resources [40]. Lancet is another pipeline for the somatic variant caller that employs localized micro-assembly to identify SNVs and indels in tumor-normal pairs. It is particularly effective in challenging genomic regions due to its high sensitivity and specificity; however, it is computationally intensive and requires high-quality input data [41].

Another pipeline developed by Google Health is DeepVariant, which is a deep learning-based var

caller. It uses a convolutional neural network (CNN) to call variants from NGS data, treating the va
calling process as an image classification problem. It offers high accuracy and robustness and is ca
of handling complex variants and various sequencing technologies. However, requires significant
computational resources, particularly GPU power for training and inference [42]. SomaticSniper
variant caller that detects somatic mutations by comparing tumor and normal samples. It differen
somatic mutations from germline variants by identifying differences in base calls. It is simple to
and offers effective analyses for paired tumor-normal samples, however, it lacks sensitivity for l
frequency variants [43]. LoFreq is a variant caller that uses a Poisson-based model to detect l
frequency variants in high-throughput sequencing data. It is highly sensitive and suitable for analy
heterogeneous samples, but may require significant computational resources for large dataset
JBrowse is a genome browser that allows one to visualize and explore genomic data by integrating
multiple variant calling methods. It displays somatic mutations and other genomic variations. Its
advantages include a user-friendly interface and compatibility with other bioinformatics tools. As
essentially a visualization tool, it must be integrated with other pipelines to do variant calling [4
Germline is a software application that uses a probabilistic model to detect both somatic and ger
mutations in whole-genome sequencing data. It is well-suited for in-depth genomic investigati
while conducting whole-genome analyses may necessitate substantial computational resources
HaplotypeCaller is a GATK suite tool for calling variants by building haplotypes in specific genomi
regions. It is effective for both germline and somatic variations and provides high precision via lo
haplotype assembling. However, it is computationally demanding and may necessitate substantia
resources for huge datasets [47].

Another robust pipeline is Pisces, which is a precise somatic variant caller optimized for Illumi

sequencing data. It offers high specificity and sensitivity for low-frequency mutations. Its streng
include high accuracy and sensitivity; however, it may require significant computational resources
A pipeline, Sentieon TNscope, is a high-performance variant caller that offers accurate and fast
identification of somatic mutations. Its performance is better with faster runtimes and supports
scale genomic studies. However, it requires licensing as commercial software [49]. A micro-assem
based variant caller for indels, developed in C/C++, is the Scalpel pipeline. It is high in accuracy in
calling indels from NGS data. And also offers a pipeline integration, simplifying workflows for
researchers working with NGS data. However, it may require more computational resources, pote
slowing down analysis, especially for large datasets [50].

For identifying somatic variants, a deep convolutional neural network-based pipeline, NeuSomatic, was developed to accurately identify somatic mutations from high-throughput sequencing data. It offers high accuracy and robustness; however, it requires significant computational resources, particularly GPU power for training and inference [51].

Another variant caller that uses local haplotype assembly and Bayesian statistical models is Octop

is highly accurate in germline and somatic variant calling. However, it is computationally exhaust and may necessitate substantial resources for large datasets [52]. Strelka2 is an updated version Strelka variant caller, offering somatic and germline variant calling in both WGS and WES. It provid high sensitivity and specificity and improves computational efficiency but may not capture lar structural variations [53]. SomaticSignatures is an R package that offers tools for analyzing and visualizing mutational signatures in somatic mutations. It is not a variant caller but can integrate r from other variant callers for comprehensive analysis. The package is user-friendly and designe data exploration and hypothesis testing within the R environment. However, it requires input from variant calling tools and is R dependent, which may be a limitation for users not accustomed to programming language [54]. Maftools is an R package designed for analyzing and visualizing som variants in cancer studies. It offers comprehensive visualization, user-friendly interface, and integr capabilities for data from various sources. However, it is not a variant caller and requires variant from other pipelines. Additionally, it is R dependent, requiring familiarity with R, which may be limitation for some researchers. Overall, Maftools provides a comprehensive view of cancer genom [55]. DeconstructSigs is a R package that quantifies the contribution of known mutational process cancer genomes. It is user-friendly, offering comprehensive documentation and examples. DeconstructSigs can integrate output from various variant callers, making it versatile for different data types.

However, it does not perform variant calling and relies on variant data generated by other tools.

Additionally, users need to be familiar with R to effectively use DeconstructSigs, which may be barrier for those not accustomed to working with R [56]. Finally, understanding cancer genomes personalized treatment relies heavily on identifying somatic mutations. The wide array of bioinformatics pipelines examined, each possessing distinct advantages and drawbacks, unders the intricate and meticulous nature necessary for the precise identification of mutations. Based o characteristics of their datasets and their specific requirements, researchers can choose the most tools. The comprehensive explanations and relative advantages and disadvantages of various pipelines are summarized in Table 2, offering a great reference for choosing the most approp pipeline for somatic mutation analysis.

Table 2: Bioinformatics Pipelines for Somatic Mutation Identification

Pipeline	Year	Language	Description	Strengths	Limitations	Class CA	Reference
SAMtools	2009	C	Utilities for manipulating alignments and calling variants.	Simple, widely adopted, efficient for basic operations.	Limited handling of complex variants, less effective for highly		[34]
VarScan2	2009	Java	Detects SNVs and indels, suitable for tumor-normal comparisons.	Effective for low-frequency variants, includes copy number analysis.	heterogeneous samples.	CA	[35]
GATK	2010	Java	Comprehensive toolkit for variant discovery and genotyping.	High accuracy, robust, extensive documentation.	Computationally intensive.	CA	[36]
MuTect	2013	Java	Identifies somatic point mutations in tumor samples. Detects SNVs and indels in tumor-normal pairs.	High sensitivity and specificity for low-frequency mutations.	Focused on point mutations, less effective for structural variants.	CA	[37]
Strelka	2012	C++	and in	Highly sensitive to low-frequency variants and small indels.	Limited to small variants.	CA	[38]

FreeBayes	2012	C++	Haplotype-based variant detection for complex and diploid polyploid genomes.	Handles complex variants, flexible.	Computationally intensive.	CA	[39]
VarDict	2014	Java, Perl	Detects SNVs, indels, and structural variants in both germline and somatic.	High sensitivity and specificity, effective for complex indels.	Requires parameter tuning.	CA	Lai et al. (2016)
Platypus	2014	Python, C	Detects SNVs and indels using local realignment and assembly.	High accuracy for complex variants.	Computationally intensive.	CA	[40]
Lancet	2017	C++	Somatic variant caller using localized micro-assembly to identify SNVs and indels in tumor-normal pairs.	High sensitivity and specificity, effective in challenging genomic regions.	Computationally intensive, requires high-quality input data.	CA	[41]
DeepVariant	2018	Python, C++	Deep learning-based variant caller using a convolutional neural network to call variants	High accuracy and robustness, effective for complex variants across various sequencing technologies.	Requires significant computational resources, particularly GPU power for training	DL	[42]

			from NGS data.		and inference.		
SomaticSniper	2011	C	Detects somatic mutations by comparing tumor and normal samples.	Effective for paired samples.	Limited to SNV calling.	CA	[43]
LoFreq	2012	C	Uses a Poisson-based model to call low-frequency variants.	High sensitivity for low-frequency variants.	Requires significant computational resources.	SM	[44]
JBrowse	2009	Java Script, Perl	Genome browser for visualizing and exploring genomic data, integrates with various variant calling tools. Tool	User-friendly interface, integrates with other bioinformatics tools for comprehensive visualization.	Primarily a visualization tool, requires integration with variant calling pipelines for analysis.	CA	[45]
Germline	2013	Python	identifying both somatic mutations, germline mutations in WGS data.	Capable of identifying both somatic and germline suitable for comprehensive genomic studies.	May require significant computational resources for WGS data.	CA	[46]
HaplotypeCaller	2013	Java	Part of GATK suite, builds haplotypes and calls variants.	High accuracy due to haplotype assembly, effective for complex	Computationally intensive, requires significant resources	CA	[47]

				genomic regions.	for large datasets.		
Pisces	2015	C#	Detects somatic variants with high specificity and sensitivity.	Optimized for Illumina data.	Limited to Illumina data.	CA	[48]
Sentieon TNscope	2018	C/C++	High-performance variant caller with fast runtimes. Detects indels using micro-assembly.	High accuracy, faster than GATK.	Commercial software.	CA	[49]
Scalpel	2014	C/C++, Python		High accuracy for indels.	Computationally intensive.	CA	[50]
NeuSomatic	2019	Python	Deep learning-based somatic variant caller. Uses	High accuracy due to deep learning.	Requires significant computational resources.	DL	[51]
Octopus	2019	C++	local haplotype assembly and Bayesian models for variant calling. Improved version	High accuracy for both germline and somatic variants.	Computationally intensive.	BM	[52]
Strelka2	2019	C++	Strelka more accurate and efficient for variant calling. Analyzes	High sensitivity and specificity, and computationally efficient.	Focused on SNVs and small indels.	CA	[53]
SomaticSignatures	2015	R		Effective for mutational	Not a variant	SM	[54]

			visualizes mutational signatures in somatic mutations.	signature analysis.	caller, requires input from other tools.		
Maftools	2018	R	Analyzes and visualizes somatic variants in cancer studies. Quantifies the contribution of known mutational processes in cancer genomes.	Comprehensive visualization and analysis tools.	Not a variant caller, requires input from other tools.	SM	[55]
DeconstructSigs	2016	R		Effective for identifying mutational processes.	Not a variant caller, requires input from other tools.	SM	[56]

Abbreviations: Classical Algorithms: CA; Deep Learning: DL; Bayesian Methods: BM; Statistical Methods: SM

4. Neoantigen Prediction and Bioinformatics Methods and Tools

Neoantigen prediction includes several steps: identifying somatic mutations, predicting peptide sequences, evaluating binding affinities to MHC molecules, and assessing the immunogenicity of t neoantigens. Certain notable case studies of successful neoantigen predictions in cancer treatme as follows:

A case study by Sahin et al. demonstrated the development of personalized neoantigen vaccines f melanoma patients. The study applied an RNA-based poly-neo-epitope approach that included wh exome sequencing and RNA sequencing to identify tumor-specific mutations by predicting the bin of the resulting peptides to MHC molecules using the NetMHCpan tool to mobilize immunity agai a spectrum of cancer mutations. All patients presented T-cell responses against multiple new epit from the vaccine. The personalized vaccines thus developed when administered to the patients le significant reduction in the rate of metastatic events, resulting in sustained progression-free survi [57]. This case is a pioneering example of how *in silico* neoantigen prediction can be directly transl into a therapeutic vaccine.

In another study, neoantigens were predicted as personalized immunotherapy for glioblastoma p The neoantigens were identified by sequencing the tumor's genome and conducting *in silico* predi such as Broad Picard Pipeline and NetMHCpan tool [58].

In another study, the team of researchers addressed the shortcomings and constraints associated with non-chemotherapy treatment modalities for non-small cell lung cancer (NSCLC) by introducing a novel approach involving neoantigen vaccines. These vaccines were engineered based on unique and individualized tumor DNA mutations, thereby modulating immune response mechanisms to effectively and precisely target the malignant cells responsible for the disease. Potential neoantigens from lung cancer tumors were predicted and the binding affinity between these mutations and MHC class I molecules (specifically the H-2 Kb allele in LLC cells and C57BL/6 mice) was predicted using NetMHCpan, NetMHC, NetMHCcons, Pick Pocket, MHCflurry, SMM, SMMPBMC and MHCnug getsI [59]. The comprehensive analysis of some of these case studies serves to effectively illustrate the successful implementation of *in silico* techniques to successfully identify neoantigens that can be employed in personalized therapeutic regimens to treat a diverse array of cancer types, Figure 1. Neoantigen prediction and bioinformatics tools have shown promising results in developing personalized cancer therapies through successful case studies.

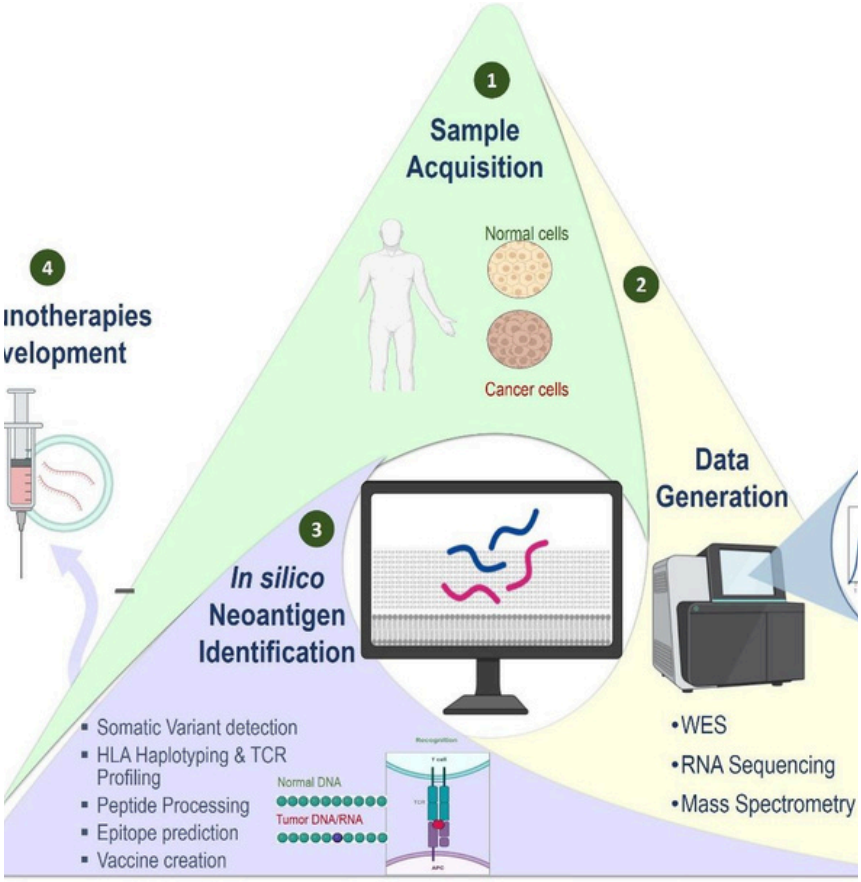

1: Representation of application of bioinformatics methods in neoantigen predic
p immunotherapies.

5. The Impact of Artificial Intelligence and Machine Learning on Immuno-Oncology

The introduction of innovative technological developments, notably those related to artificial intelligence (AI), machine learning (ML), and quantum computing, creates a powerful opportunity f the progressive refinement of immuno-oncology, a sector dedicated to using the immune system fight against cancer. The methodologies driven by AI can analyze extensive datasets with a level of efficiency that far surpasses traditional analytical techniques, thereby unveiling new and transforn insights into the complex biology of tumors and the multifaceted immune responses they elicit. In following section, the role of different types of technologies in neoantigen prediction and vaccine development is discussed:

5.1 Application of Artificial Intelligence (AI) in Neoantigen Prediction

Recent advancements in technology have significantly improved the prediction of neoantigens by enabling the analysis of large genomic and proteomic datasets. Specifically, deep learning algorith have shown promise in predicting which mutated peptides are likely to bind to a patient's MHC molecules, which is essential for assessing the immunogenic potential of neoantigens.. Machine learning techniques, as a branch of artificial intelligence, excel at estimating the binding affinities between peptides and Major Histocompatibility Complex molecules, which is essential for determ the potential for an immune response from a neoantigen. Traditional methodologies may lack the feasibility to accurately predict immunogenic peptides as effectively as AI and ML; for instance, AI-enhanced instruments like NetMHCpan leverage deep learning methodologies to refine peptide-M binding predictions by integrating data from a broad spectrum of HLA alleles, including those with minimal experimental binding evidence.

This skill is essential for crafting personalized cancer vaccines since it facilitates the choice of the n

viable neoantigens to hone in on the individual tumor makeup of the patient. Additionally, AI frameworks are capable of modeling and optimizing the immune reaction, potentially discoverin ideal set of neoantigens to be included in a vaccine, thereby improving its overall efficacy [60, 61]. significantly enhances the development of personalized cancer vaccines by improving neoantigen prediction and optimizing immune responses.

5.2 Application of Quantum Computing in Neoantigen Prediction

Quantum computing adds to the advancement in computational capabilities, by potential to tran neoantigen prediction and vaccine formulation. In contrast to classical computing systems, which bits for information processing, quantum computing uses quantum bits, or qubits, enabling mult execution of intricate calculations [62]. This capability is especially valuable in analyzing the va multi-dimensional datasets required for accurate neoantigen prediction.. Quantum algorithms im the efficacy of bioinformatics workflows by accelerating the detection of candidate neoantigens enhancing the precision of predicting MHC-binding. This advancement not only expedites the formulation of personalized cancer vaccines but also permits more advanced modeling of the im response. Additionally, combining quantum computing with artificial intelligence enables the crea of superior predictive models, which can provide detailed dynamics between neoplastic cells and immune system. This integration ultimately forges a path for more potent immunotherapies [63]. Quantum computing significantly enhances neoantigen prediction and vaccine formulation in immunotherapy, paving the way for more effective treatments.

5.3 Application of Deep Learning in Neoantigen Prediction

Deep learning (DL), a subset of AI, has become a transformative tool in neoantigen prediction and cancer vaccine development. DL models, such as convolutional neural networks (CNNs) and recurrent neural networks (RNNs), are designed to automatically learn patterns from large datasets. These models can also learn representations from data. These models are implemented in image recognition, natural language processing, and bioinformatics [64]. Since deep learning models have the capability to analyze complex biological patterns, therefore, in healthcare, it is applied to make algorithms for disease diagnosis and personalized treatment [65]. Furthermore, deep learning is revolutionizing immunotherapy by enhancing neoantigen prediction and facilitating the development of cancer vaccines through advanced pattern recognition in biological data.

5.4 Application of Natural Language Processing (NLP) in Neoantigen Prediction Natural Language Processing (NLP) plays a crucial role in managing and analyzing the extensive unstructured biomedical text data present in immuno-oncology research. It is particularly effective in extracting and processing information pertinent to neoantigen prediction from various sources, including scientific literature, clinical trial reports, and genomic databases.These core processes include: Information Retrieval (IR), which identify and retrieve relevant documents from large datasets or databases in response to specific queries; Semantics and Information Extraction, which accurately interprets the text. NLP systems are designed to perform semantic analysis, which involves recognizing the relationships between words, their definitions, and their syntactic roles within a sentence. This semantic understanding is crucial for tasks such as information extraction, where the goal is to identify specific entities (e.g., genes, proteins, mutations) and their interactions within a text; Information Extraction, which involves identifying and categorizing specific pieces of information from unstructured text. In the context of immuno-oncology, IE is used to automatically extract data about potential neoantigens, patient-specific mutations, and immune response markers from clinical reports and research articles. This process is essential for building comprehensive databases of neoantigens, which can be integrated into bioinformatics pipelines for personalized vaccine development [66]. NLP techniques are used to extract relevant information from scientific literature, clinical trial reports, and patient records, which can then be integrated into bioinformatics pipelines for neoantigen prediction [67]. For instance, NLP can be used to mine databases of scientific publications to search studies that report on neoantigen discovery and validation, thus accelerating the research process by quickly bringing relevant findings to the researchers [68]. Additionally, NLP algorithms can assist in the annotation of genetic sequences by identifying and categorizing mutations that may produce neoantigens. This automated processing of text data not only speeds up the research process but also ensures that no critical information is overlooked, thereby enhancing the accuracy of neoantigen predictions and the subsequent development of personalized cancer vaccines. Also, NLP significantly enhances immunotherapy research by efficiently processing unstructured text data to extract vital information for neoantigen development and personalized vaccine creation.

6. Applications of Neoantigen Prediction in Personalized Cancer Immunotherapy

In silico neoantigen prediction plays a crucial role in the development of personalized cancer vaccines, such as NeoVax for melanoma. By employing advanced bioinformatics tools, researchers can analyze whole-exome sequencing data to identify somatic mutations unique to an individual's tumor. These mutations generate neoantigens—tumor-specific peptides that the immune system recognizes as foreign. Utilizing algorithms like NetMHCpan, scientists predict which neoantigens are most likely to bind to the patient's MHC molecules, thereby facilitating a targeted immune response. The synthesized neoantigens are then formulated into a personalized peptide-based vaccine, which has shown promising results in clinical trials, demonstrating safety and the ability to elicit strong T-cell responses. The success of NeoVax underscores the transformative potential of *in silico* neoantigen prediction in tailoring vaccines that effectively target the distinct mutational profiles of individual tumors, particularly in cases with high mutational burdens [69, 70]. Another personalized vaccine based on in silico neoantigen is exemplified by platforms like iNeST (Individualized Neoantigen-Specific Immunotherapy) developed by BioNTech and Genentech [71]. This innovative approach utilizes whole-exome sequencing and RNA sequencing to identify somatic mutations in a patient's tumor, followed by bioinformatics tools that predict immunogenic neoantigens based on their binding potential to the patient's MHC molecules. Unlike traditional peptide-based vaccines, iNeST employs an mRNA delivery system that encodes these predicted neoantigens, allowing for the direct translation into neoantigenic proteins that elicit a robust immune response. Clinical trials, such as the Phase I study on advanced melanoma patients, have demonstrated the efficacy of this method, showing significant T- cell responses and tumor shrinkage. The advantages of mRNA technology, including the ability to encode multiple neoantigens and rapid production, underscore the transformative potential of in silico neoantigen prediction in advancing personalized cancer immunotherapy [72]. Another example is, TG4050, created by Transgene. This innovative vaccine leverages whole-exome sequencing and RNA sequencing to identify somatic mutations in tumors, followed by a bioinformatics pipeline that predicts the most immunogenic neoantigens. By utilizing these predicted neoantigens, TG4050 employs a viral vector-based approach to enhance the immune response, effectively presenting these neoantigens to the immune system. Early clinical trials have demonstrated TG4050's ability to elicit strong T-cell responses, indicating its potential effectiveness in treating various solid tumors, particularly those with lower mutational burdens. This highlights the significance of in silico prediction in tailoring vaccines to individual patients, ultimately advancing personalized cancer immunotherapy [73]. Additionally, In silico neoantigen prediction plays a crucial role in the development of neoantigen-based therapies, particularly in the engineering of chimeric antigen receptor (CAR)-T cells. By utilizing WES and advanced computational algorithms, researchers can identify patient-specific neoantigens that are unique to individual tumors. This personalized approach allows for the precise engineering of CARs that specifically target these neoantigens, leading to the expansion of T cells *ex vivo* before re-infusion into the patient. The effectiveness of this strategy has been demonstrated in clinical studies, such as the work by Tran et al. (2016), which showcased significant tumor reduction in patients with epithelial cancer. Ultimately, in silico neoantigen prediction enhances the specificity and efficacy of CAR-T therapies, minimizing off-target effects and providing a promising avenue for treating solid tumors with tailored immunotherapeutic options [74]. Therefore, neoantigen predictions have transformed immuno- oncology with personalized cancer vaccines and therapies like NeoVax and iNeST.

These bioinformatics-driven therapies have enabled precision medicine, where tumors are treated according to their genetics. As bioinformatics tools improve and new technologies like AI and quantum computing are integrated into research, neoantigen prediction will improve, leading to more effective and personalized cancer treatments.

7. Challenges and Future Perspectives

Bioinformatics in immuno-oncology encounters various technical obstacles due to the intricate n and volume of the data involved. A primary challenge is the precise identification and prediction neoantigens. Regardless of the advancements in sequencing technology and computational tech the precision of predictions remains limited, particularly regarding MHC class II-restricted epitope which demonstrate increased variability and longer peptide lengths. Additionally, there are techn constraints concerning the sensitivity and specificity of algorithms utilized for HLA typing, mutatio detection, and neoantigen prediction. These tools frequently yield inconsistent results depending quality of input data and the specific algorithms applied, resulting in discrepancies across differe studies. Another hurdle faced is the tremendous data output resulting from next-generation sequ (NGS) techniques. The processing and examination of these extensive datasets necessitate consid computational power, including high-performance computing (HPC) systems. Therefore, there is pressing need for more accessible tools that researchers can utilize without requiring specialized bioinformatics expertise, as current tools often demand substantial knowledge in computational biology. The future of bioinformatics in immuno-oncology is dependent on the ongoing improvem of computational approaches. ML and DL algorithms can be implemented with further advancem boost the precision of neoantigen prediction and HLA typing, since these algorithms are capable learning from extensive datasets, allowing them to analyze intricate patterns that cannot be iden by the conventional methods. When spatial transcriptomics is combined with single-cell RNA sequencing (scRNA-seq), it enhances the ability to point to the location of neoantigens in the tum microenvironment. Such an analysis offers valuable insights into the spatial dynamics governing immune responses. Further, the construction of hybrid models can involve the synthesis of data-informed techniques alongside mechanistic models related to immune responses. These hybrid frameworks will synthesize multi-omics data to simulate the interactions occurring between tumo the immune system. This methodology will enable researchers to predict the outcomes associate various immunotherapeutic strategies. Personalized immunotherapy denotes the significant advancement in cancer treatment, wherein therapies are customized to the unique genetic and immunological characteristics of each individual. The comprehension of tumor immunology and growth and advancement in bioinformatics tools for neoantigen prediction is aligned with the de personalized vaccines and adoptive cell therapies. Moreover, the amalgamation of multi-omics da real-time monitoring technologies will significantly improve the identification of biomarkers and therapeutic adjustments, thereby optimizing treatment efficacy.

8. Conclusion

In conclusion, bioinformatics approaches have gained paramount importance in the field of imm oncology, driving significant advancements in personalized cancer treatment. AI, ML, and quantu computing have enabled the development of more effective immunotherapies, such as persona vaccines and adoptive T-cell therapies.

These technologies have not only improved the development of bioinformatics pipelines to accurately predict the neoantigen prediction but also facilitated the analysis of complex biological data, leading to a deeper understanding of the tumor microenvironment. Neoantigen prediction plays a crucial role in personalized immunotherapy, as demonstrated by therapies like NeoVax and neoantigen-targeted CAR- T cells. These advancements showcase the effectiveness of tailored treatments that target individual tumor mutations, leading to better clinical outcomes and extended survival for patients. However, the field still faces challenges, including the need for more sensitive and specific algorithms and the computational power required to process plethora of heterogenous datasets. Future research will likely focus on overcoming these challenges by refining computational approaches, integrating multi-omics data, and developing more accessible tools for researchers. The ongoing evolution of bioinformatics in immuno-oncology holds great potential for enhancing the efficacy of cancer treatments, ultimately leading to better patient outcomes.

Statements and Declarations

Conflict of Interests

The author shares no conflict of interests

Funding sources

Not available

Acknowledgment

The author acknowledges the support of the Department of Biology, Islamic University of Madin KSA.

REFERENCES

[1] Podlaha, O.; M. Riester; S. De, and F. Michor, Evolution of the cancer genome. Trends Genet, 2012. 28(4): p. 155-63.

[2] Hosseini, H.; M.M.S. Obradovic; M. Hoffmann; K.L. Harper; M.S. Sosa; M. Werner-Klein; L.K. Nanduri; C. Werno; C. Ehrl; M. Maneck; N. Patwary; G. Haunschild; M. Guzvic; C. Reimelt; M. Grauvogl; N. Eichner; F. Weber; A.D. Hartkopf; F.A. Taran; S.Y. Brucker; T. Fehm; B. Rack; S. Buchholz; R. Spang; G. Meister; J.A. Aguirre-Ghiso, and C.A. Klein, Early dissemination seeds metastasis in breast cancer. Nature, 2016. 540(7634): p. 552-558.

[3] Coussens, L.M. and Z. Werb, Inflammation and cancer. Nature, 2002. 420(6917): p. 860-7.

[4] Hanahan, D. and R.A. Weinberg, Hallmarks of cancer: the next generation. Cell, 2011. 144(5): p. 646 74.

[5] Gonzalez, H.; C. Hagerling, and Z. Werb, Roles of the immune system in cancer: from tumor initiatio to metastatic progression. Genes Dev, 2018. 32(19-20): p. 1267-1284.

[6] Wei, S.C.; C.R. Duffy, and J.P. Allison, Fundamental Mechanisms of Immune Checkpoint Blockade Therapy. Cancer Discov, 2018. 8(9): p. 1069-1086.

[7] Zhang, Y. and Z. Zhang, The history and advances in cancer immunotherapy: understanding the characteristics of tumor-infiltrating immune cells and their therapeutic implications. Cellular & Molecular Immunology, 2020. 17(8): p. 807-821.

[8] Matsushita, H.; M.D. Vesely; D.C. Koboldt; C.G. Rickert; R. Uppaluri; V.J. Magrini; C.D. Arthur; J.M. White; Y.S. Chen; L.K. Shea; J. Hundal; M.C. Wendl; R. Demeter; T. Wylie; J.P. Allison; M.J. Smyth; L.J. Old; E.R. Mardis, and R.D. Schreiber, Cancer exome analysis reveals a T-cell-dependent mechanism of cancer immunoediting. Nature, 2012. 482(7385): p. 400-4.

[9] McGranahan, N.; A.J. Furness; R. Rosenthal; S. Ramskov; R. Lyngaa; S.K. Saini; M. Jamal-Hanjani; G.A. Wilson; N.J. Birkbak; C.T. Hiley; T.B. Watkins; S. Shafi; N. Murugaesu; R. Mitter; A.U. Akarca; J. Linares; T. Marafioti; J.Y. Henry; E.M. Van Allen; D. Miao; B. Schilling; D. Schadendorf; L.A. Garraway; V. Makarov; N.A. Rizvi; A. Snyder; M.D. Hellmann; T. Merghoub; J.D. Wolchok; S.A. Shukla; C.J. Wu; K.S. Peggs; T.A. Chan; S.R. Hadrup; S.A. Quezada, and C. Swanton, Clonal neoantigens elicit T cell immunoreactivity and sensitivity to immune checkpoint blockade. Science, 2016. 351(6280): p. 1463-9.

[10] Richters, M.M.; H. Xia; K.M. Campbell; W.E. Gillanders; O.L. Griffith, and M. Griffith, Best practices for bioinformatic characterization of neoantigens for clinical utility. Genome Med, 2019. 11(1): p. 5

[11] Athieniti, E. and G.M. Spyrou, A guide to multi-omics data collection and integration for translatio medicine. Computational and Structural Biotechnology Journal, 2023. 21: p. 134-149.

[12] Jovic, D.; X. Liang; H. Zeng; L. Lin; F. Xu, and Y. Luo, Single-cell RNA sequencing technologies and applications: A brief overview. Clin Transl Med, 2022. 12(3): p. e694.

[13] Wang, Y.; B. Liu; G. Zhao; Y. Lee; A. Buzdin; X. Mu; J. Zhao; H. Chen, and X. Li, Spatial transcriptomics: Technologies, applications and experimental considerations. Genomics, 2023. 115(5): p. 110671.

[14] Chen, B.; M.S. Khodadoust; C.L. Liu; A.M. Newman, and A.A. Alizadeh, Profiling Tumor Infiltrating Immune Cells with CIBERSORT. Methods Mol Biol, 2018. 1711: p. 243-259.

[15] Xie, N.; G. Shen; W. Gao; Z. Huang; C. Huang, and L. Fu, Neoantigens: promising targets for cance therapy. Signal Transduction and Targeted Therapy, 2023. 8(1): p. 9.

[16] Zhang, T.; E. Kurban, and Z. Wang, Neoantigens: The Novel Precision Cancer Immunotherapy. Biologics, 2023. 3(4): p. 321-334.

[17] Pearlman, A.H.; M.S. Hwang; M.F. Konig; E.H.-C. Hsiue; J. Douglass; S.R. DiNapoli; B.J. Mog; C. Bettegowda; D.M. Pardoll; S.B. Gabelli; N. Papadopoulos; K.W. Kinzler; B. Vogelstein, and S. Zhou, Targeting public neoantigens for cancer immunotherapy. Nature Cancer, 2021. 2(5): p. 487-497.

[18] Alexandrov, L.B.; S. Nik-Zainal; D.C. Wedge; S.A. Aparicio; S. Behjati; A.V. Biankin; G.R. Bignell; N. Bolli; A. Borg, and A.-L. Børresen-Dale, Signatures of mutational processes in human cancer. nature, 2013. 500(7463): p. 415-421.

[19] Yadav, M.; S. Jhunjhunwala; Q.T. Phung; P. Lupardus; J. Tanguay; S. Bumbaca; C. Franci; T.K. Cheung; J. Fritsche; T. Weinschenk; Z. Modrusan; I. Mellman; J.R. Lill, and L. Delamarre, Predicting immunogenic tumour mutations by combining mass spectrometry and exome sequencing. Nature, 2014. 515(7528): p. 572-576.

[20] Hundal, J.; S. Kiwala; J. McMichael; C.A. Miller; H. Xia; A.T. Wollam; C.J. Liu; S. Zhao; Y.Y. Feng; A.P. Graubert; A.Z. Wollam; J. Neichin; M. Neveau; J. Walker; W.E. Gillanders; E.R. Mardis; O.L. Griffith, and M. Griffith, pVACtools: A Computational Toolkit to Identify and Visualize Cancer Neoantigens. Cancer Immunol Res, 2020. 8(3): p. 409-420.

[21] Spranger, S.; D. Dai; B. Horton, and T.F. Gajewski, Tumor-Residing Batf3 Dendritic Cells Are Required for Effector T Cell Trafficking and Adoptive T Cell Therapy. Cancer Cell, 2017. 31(5): p. 711-723 e4.

[22] Jardim, D.L.; A. Goodman; D. de Melo Gagliato, and R. Kurzrock, The Challenges of Tumor Mutational Burden as an Immunotherapy Biomarker. Cancer Cell, 2021. 39(2): p. 154-173.

[23] Pereira, R.; J. Oliveira, and M. Sousa, Bioinformatics and Computational Tools for Next-Generation Sequencing Analysis in Clinical Genetics. J Clin Med, 2020. 9(1).

[24] Burley, S.K.; C. Bhikadiya; C. Bi; S. Bittrich; L. Chen; G.V. Crichlow; C.H. Christie; K. Dalenberg; L. Di Costanzo; J.M. Duarte; S. Dutta; Z. Feng; S. Ganesan; D.S. Goodsell; S. Ghosh; R.K. Green; V. Guranović; D. Guzenko; B.P. Hudson; Catherine L. Lawson; Y. Liang; R. Lowe; H. Namkoong; E. Peisach; I. Persikova; C. Randle; A. Rose; Y. Rose; A. Sali; J. Segura; M. Sekharan; C. Shao; Y.-P. Tao; M. Voigt; John D. Westbrook; J.Y. Young; C. Zardecki, and M. Zhuravleva, RCSB Protein Data Bank: powerful new tools for exploring 3D structures of biological macromolecules for basic and applied research and education in fundamental biology, biomedicine, biotechnology, bioengineering and energy sciences. Nucleic Acids Research, 2020. 49(D1): p. D437-D451.

[25] Satam, H.; K. Joshi; U. Mangrolia; S. Waghoo; G. Zaidi; S. Rawool; R.P. Thakare; S. Banday; A.K. Mishra; G. Das, and S.K. Malonia, Next-Generation Sequencing Technology: Current Trends and Advancements. Biology (Basel), 2023. 12(7).

[26] Costain, G.; R.D. Cohn; S.W. Scherer, and C.R. Marshall, Genome sequencing as a diagnostic test. CMAJ, 2021. 193(42): p. E1626-E1629.

[27] Logsdon, G.A.; M.R. Vollger, and E.E. Eichler, Long-read human genome sequencing and its applications. Nat Rev Genet, 2020. 21(10): p. 597-614.

[28] Warr, A.; C. Robert; D. Hume; A. Archibald; N. Deeb, and M. Watson, Exome Sequencing: Current and Future Perspectives. G3 (Bethesda), 2015. 5(8): p. 1543-50.

[29] Williams, M.J.; A. Sottoriva, and T.A. Graham, Measuring Clonal Evolution in Cancer with Genomics Annu Rev Genomics Hum Genet, 2019. 20: p. 309-329.

[30] Li, H.; A. Coghlan; J. Ruan; L.J. Coin; J.-K. Heriche; L. Osmotherly; R. Li; T. Liu; Z. Zhang, and L. Bolund, TreeFam: a curated database of phylogenetic trees of animal gene families. Nucleic acids research, 2006. 34(suppl_1): p. D572-D580.

[31] Robbins, P.F.; Y.-C. Lu; M. El-Gamil; Y.F. Li; C. Gross; J. Gartner; J.C. Lin; J.K. Teer; P. Cliften; E. Tycksen; Y. Samuels, and S.A. Rosenberg, Mining exomic sequencing data to identify mutated antigen recognized by adoptively transferred tumor-reactive T cells. Nature Medicine, 2013. 19(6): p. 747-752.

[32] De Mattos-Arruda, L.; M. Vazquez; F. Finotello; R. Lepore; E. Porta; J. Hundal; P. Amengual-Rigo; C.K.Y. Ng; A. Valencia; J. Carrillo; T.A. Chan; V. Guallar; N. McGranahan; J. Blanco, and M. Griffith, Neoantigen prediction and computational perspectives towards clinical benefit: recommendations fro the ESMO Precision Medicine Working Group. Annals of Oncology, 2020. 31(8): p. 978-990.

[33] Hackl, H.; P. Charoentong; F. Finotello, and Z. Trajanoski, Computational genomics tools for dissec tumour–immune cell interactions. Nature Reviews Genetics, 2016. 17(8): p. 441-458.

[34] Li, H.; B. Handsaker; A. Wysoker; T. Fennell; J. Ruan; N. Homer; G. Marth; G. Abecasis; R. Durbin, and S. Genome Project Data Processing, The Sequence Alignment/Map format and SAMtools. Bioinformatics, 2009. 25(16): p. 2078-9.

[35] Koboldt, D.C.; Q. Zhang; D.E. Larson; D. Shen; M.D. McLellan; L. Lin; C.A. Miller; E.R. Mardis; L. Ding, and R.K. Wilson, VarScan 2: somatic mutation and copy number alteration discovery in cancer by exome sequencing. Genome Res, 2012. 22(3): p. 568-76.

[36] McKenna, A.; M. Hanna; E. Banks; A. Sivachenko; K. Cibulskis; A. Kernytsky; K. Garimella; D. Altshuler; S. Gabriel; M. Daly, and M.A. DePristo, The Genome Analysis Toolkit: a MapReduce framework for analyzing next-generation DNA sequencing data. Genome Res, 2010. 20(9): p. 1297- 303.

[37] Cibulskis, K.; M.S. Lawrence; S.L. Carter; A. Sivachenko; D. Jaffe; C. Sougnez; S. Gabriel; M. Meyerson; E.S. Lander, and G. Getz, Sensitive detection of somatic point mutations in impure and heterogeneous cancer samples. Nat Biotechnol, 2013. 31(3): p. 213-9.

[38] Saunders, C.T.; W.S. Wong; S. Swamy; J. Becq; L.J. Murray, and R.K. Cheetham, Strelka: accurate somatic small-variant calling from sequenced tumor-normal sample pairs. Bioinformatics, 2012. 28(14): p. 1811-7.

[39] Garrison, E. and G. Marth, Haplotype-based variant detection from short-read sequencing. arXiv, 1207.

[40] Rimmer, A.; H. Phan; I. Mathieson; Z. Iqbal; S.R.F. Twigg; W.G.S. Consortium; A.O.M. Wilkie; G. McVean, and G. Lunter, Integrating mapping-, assembly- and haplotype-based approaches for calling variants in clinical sequencing applications. Nat Genet, 2014. 46(8): p. 912-918.

[41] Narzisi, G.; A. Corvelo; K. Arora; E.A. Bergmann; M. Shah; R. Musunuri; A.-K. Emde; N. Robine; V. Vacic, and M.C. Zody, Genome-wide somatic variant calling using localized colored de Bruijn graphs. Communications Biology, 2018. 1(1): p. 20.

[42] Poplin, R.; P.-C. Chang; D. Alexander; S. Schwartz; T. Colthurst; A. Ku; D. Newburger; J. Dijamco; N. Nguyen; P.T. Afshar; S.S. Gross; L. Dorfman; C.Y. McLean, and M.A. DePristo, A universal SNP and small-indel variant caller using deep neural networks. Nature Biotechnology, 2018. 36(10): p. 983- 987.

[43] Larson, D.E.; C.C. Harris; K. Chen; D.C. Koboldt; T.E. Abbott; D.J. Dooling; T.J. Ley; E.R. Mardis; R.K. Wilson, and L. Ding, SomaticSniper: identification of somatic point mutations in whole genome sequencing data. Bioinformatics, 2012. 28(3): p. 311-7.

[44] Wilm, A.; P.P. Aw; D. Bertrand; G.H. Yeo; S.H. Ong; C.H. Wong; C.C. Khor; R. Petric; M.L. Hibberd, and N. Nagarajan, LoFreq: a sequence-quality aware, ultra-sensitive variant caller for uncovering c population heterogeneity from high-throughput sequencing datasets. Nucleic Acids Res, 2012. 40 p. 11189-201.

[45] Skinner, M.E.; A.V. Uzilov; L.D. Stein; C.J. Mungall, and I.H. Holmes, JBrowse: a next-generation genome browser. Genome Res, 2009. 19(9): p. 1630-8.

[46] Gusev, A.; J.K. Lowe; M. Stoffel; M.J. Daly; D. Altshuler; J.L. Breslow; J.M. Friedman, and I. Pe'er, Whole population, genome-wide mapping of hidden relatedness. Genome research, 2009. 19(2): p 326.

[47] Lin, Y.-L.; P.-C. Chang; C. Hsu; M.-Z. Hung; Y.-H. Chien; W.-L. Hwu; F. Lai, and N.-C. Lee, Comparison of GATK and DeepVariant by trio sequencing. Scientific Reports, 2022. 12(1): p. 1809.

[48] Obradovic, A.; L. Vlahos; P. Laise; J. Worley; X. Tan; A. Wang, and A. Califano, PISCES: A pipeline for the systematic, protein activity-based analysis of single cell RNA sequencing data. Biorxiv, 2021. 6: p. 22.

[49] Freed, D.; R. Pan, and R. Aldana, TNscope: accurate detection of somatic mutations with haploty based variant candidate detection and machine learning filtering. biorxiv, 2018: p. 250647.

[50] Fang, H.; E.A. Bergmann; K. Arora; V. Vacic; M.C. Zody; I. Iossifov; J.A. O'Rawe; Y. Wu; L.T. Jimenez Barron; J. Rosenbaum; M. Ronemus; Y.-h. Lee; Z. Wang; E. Dikoglu; V. Jobanputra; G.J. Lyon; M. Wigler; M.C. Schatz, and G. Narzisi, Indel variant analysis of short-read sequencing data with Scalpel. Nature Protocols, 2016. 11(12): p. 2529-2548.

[51] Sahraeian, S.M.E.; R. Liu; B. Lau; K. Podesta; M. Mohiyuddin, and H.Y. Lam, Deep convolutional neural networks for accurate somatic mutation detection. Nature communications, 2019. 10(1): p. 104

[52] Cooke, D.; G. Lunter, and D. Wedge, Accurate genotyping of single cells with Octopus. 2021.

[53] Kim, S.; K. Scheffler; A.L. Halpern; M.A. Bekritsky; E. Noh; M. Källberg; X. Chen; Y. Kim; D. Beyter, and P. Krusche, Strelka2: fast and accurate calling of germline and somatic variants. Nature methods, 2018. 15(8): p. 591-594.

[54] Gehring, J.S.; B. Fischer; M. Lawrence, and W. Huber, SomaticSignatures: inferring mutational signatures from single-nucleotide variants. Bioinformatics, 2015. 31(22): p. 3673-3675.

[55] Mayakonda, A.; D.-C. Lin; Y. Assenov; C. Plass, and H.P. Koeffler, Maftools: efficient and comprehensive analysis of somatic variants in cancer. Genome research, 2018. 28(11): p. 1747-17

[56] Rosenthal, R.; N. McGranahan; J. Herrero; B.S. Taylor, and C. Swanton, DeconstructSigs: delineating mutational processes in single tumors distinguishes DNA repair deficiencies and patterns of carcinoma evolution. Genome biology, 2016. 17: p. 1-11.

[57] Sahin, U.; E. Derhovanessian; M. Miller; B.-P. Kloke; P. Simon; M. Löwer; V. Bukur; A.D. Tadmor; U. Luxemburger; B. Schrörs; T. Omokoko; M. Vormehr; C. Albrecht; A. Paruzynski; A.N. Kuhn; J. Buck; S. Heesch; K.H. Schreeb; F. Müller; I. Ortseifer; I. Vogler; E. Godehardt; S. Attig; R. Rae; A. Breitkreuz; C. Tolliver; M. Suchan; G. Martic; A. Hohberger; P. Sorn; J. Diekmann; J. Ciesla; O. Waksmann; A.-K. Brück; M. Witt; M. Zillgen; A. Rothermel; B. Kasemann; D. Langer; S. Bolte; M. Diken; S. Kreiter; R. Nemecek; C. Gebhardt; S. Grabbe; C. Höller; J. Utikal; C. Huber; C. Loquai, and Ö. Türeci, Personalized RNA mutanome vaccines mobilize poly-specific therapeutic immunity against cancer. Nature, 2017. 547(7662): p. 222-226.

[58] Keskin, D.B.; A.J. Anandappa; J. Sun; I. Tirosh; N.D. Mathewson; S. Li; G. Oliveira; A. Giobbie-Hurder; K. Felt; E. Gjini; S.A. Shukla; Z. Hu; L. Li; P.M. Le; R.L. Allesoe; A.R. Richman; M.S. Kowalczyk; S. Abdelrahman; J.E. Geduldig; S. Charbonneau; K. Pelton; J.B. Iorgulescu; L. Elagina; W. Zhang; O. Olive; C. McCluskey; L.R. Olsen; J. Stevens; W.J. Lane; A.M. Salazar; H. Daley; P.Y. Wen; E.A. Chiocca; M. Harden; N.J. Lennon; S. Gabriel; G. Getz; E.S. Lander; A. Regev; J. Ritz; D. Neuberg; S.J. Rodig; K.L. Ligon; M.L. Suva; K.W. Wucherpfennig; N. Hacohen; E.F. Fritsch; K.J. Livak; P.A. Ott; C.J. Wu, and D.A. Reardon, Neoantigen vaccine generates intratumoral T cell responses in phase Ib glioblastoma trial. Nature, 2019. 565(7738): p. 234-239.

[59] Lin, X.; S. Tang; T. Guo; R. Tang; Z. Li; X. Pan; G. Chen; L. Qiu; X. Dong; L. Zhang; X. Liu; Z. Cai, and B. Xie, Personalized neoantigen vaccine enhances the therapeutic efficacy of bevacizumab and anti-PD-1 antibody in advanced non-small cell lung cancer. Cancer Immunol Immunother, 2024. 73(2): p. 26.

[60] Gevaert, C.M.; M. Carman; B. Rosman; Y. Georgiadou, and R. Soden, Fairness and accountability o AI in disaster risk management: Opportunities and challenges. Patterns, 2021. 2(11).

[61] Ahmadi, A., Quantum Computing and Artificial Intelligence: The Synergy of Two Revolutionary Technologies. Asian Journal of Electrical Sciences, 2023. 12(2): p. 15-27.

[62] Martonosi, M. and M. Roetteler, Next steps in quantum computing: Computer science's role. arXiv preprint arXiv:1903.10541, 2019.

[63] Niraula, D.; J. Jamaluddin; M.M. Matuszak; R.K.T. Haken, and I.E. Naqa, Quantum deep reinforcement learning for clinical decision support in oncology: application to adaptive radiotherapy. Scientific reports, 2021. 11(1): p. 23545.

[64] Mustapha, M.T.; I. Ozsahin, and D.U. Ozsahin, Chapter 2 - Convolution neural network and deep learning, in Artificial Intelligence and Image Processing in Medical Imaging, W.A. Zgallai and D.U. Ozsahin, Editors. 2024, Academic Press. p. 21-50.

[65] Johnson, K.B.; W.Q. Wei; D. Weeraratne; M.E. Frisse; K. Misulis; K. Rhee; J. Zhao, and J.L. Snowdon, Precision Medicine, AI, and the Future of Personalized Health Care. Clin Transl Sci, 2021. 14(1): p. 86-93.

[66] Yandell, M.D. and W.H. Majoros, Genomics and natural language processing. Nature Reviews Genetics, 2002. 3(8): p. 601-610.

[67] Rayhan, A.; R. Kinzler, and R. Rayhan, NATURAL LANGUAGE PROCESSING: TRANSFORMING HOW MACHINES UNDERSTAND HUMAN LANGUAGE. 2023.

[68] Velupillai, S.; H. Suominen; M. Liakata; A. Roberts; A.D. Shah; K. Morley; D. Osborn; J. Hayes; R. Stewart; J. Downs; W. Chapman, and R. Dutta, Using clinical Natural Language Processing for health

outcomes research: Overview and actionable suggestions for future advances. Journal of Biome Informatics, 2018. 88: p. 11-19.

[69] Linette, G.P. and B.M. Carreno, Neoantigen Vaccines Pass the Immunogenicity Test. Trends Mol M 2017. 23(10): p. 869-871.

[70] Ott, P.A.; Z. Hu; D.B. Keskin; S.A. Shukla; J. Sun; D.J. Bozym; W. Zhang; A. Luoma; A. Giobbie-Hurder; L. Peter; C. Chen; O. Olive; T.A. Carter; S. Li; D.J. Lieb; T. Eisenhaure; E. Gjini; J. Stevens; W.J. Lane; I. Javeri; K. Nellaiappan; A.M. Salazar; H. Daley; M. Seaman; E.I. Buchbinder; C.H. Yoon; M. Harden; N. Lennon; S. Gabriel; S.J. Rodig; D.H. Barouch; J.C. Aster; G. Getz; K. Wucherpfennig; D. Neuberg; J. Ritz; E.S. Lander; E.F. Fritsch; N. Hacohen, and C.J. Wu, An immunogenic personal neoantigen vaccine for patients with melanoma. Nature, 2017. 547(7662): p. 217-221.

[71] Braiteh, F.; P. LoRusso; A. Balmanoukian; S. Klempner; D.R. Camidge; M. Hellmann; M. Gordon; J. Bendell; L. Mueller, and R. Sabado, Abstract CT169: A phase Ia study to evaluate RO7198457, an individualized Neoantigen Specific immunoTherapy (iNeST), in patients with locally advanced or metastatic solid tumors. Cancer Research, 2020. 80(16_Supplement): p. CT169-CT169.

[72] Sahin, U.; P. Oehm; E. Derhovanessian; R.A. Jabulowsky; M. Vormehr; M. Gold; D. Maurus; D. Schwarck-Kokarakis; A.N. Kuhn; T. Omokoko; L.M. Kranz; M. Diken; S. Kreiter; H. Haas; S. Attig; R. Rae; K. Cuk; A. Kemmer-Brück; A. Breitkreuz; C. Tolliver; J. Caspar; J. Quinkhardt; L. Hebich; M. Stein; A. Hohberger; I. Vogler; I. Liebig; S. Renken; J. Sikorski; M. Leierer; V. Müller; H. Mitzel-Rink; M. Miederer; C. Huber; S. Grabbe; J. Utikal; A. Pinter; R. Kaufmann; J.C. Hassel; C. Loquai, and Ö. Türeci, An RNA vaccine drives immunity in checkpoint-inhibitor-treated melanoma. Nature, 2020. 585(7823): p. 107-112.

[73] Delord, J.-P.; M.S. Block; C. Ottensmeier; G. Colon-Otero; C. Le Tourneau; A. Lalanne; C. Jamet; O. Lantz; K.L. Knutson, and G. Lacoste, Phase 1 studies of personalized neoantigen vaccine TG4050 in ovarian carcinoma (OC) and head and neck squamous cell carcinoma (HNSCC). 2022, American Society of Clinical Oncology.

[74] Tran, E.; P.F. Robbins, and S.A. Rosenberg, 'Final common pathway' of human cancer immunothe targeting random somatic mutations. Nature Immunology, 2017. 18(3): p. 255-262.

Potentiometric and thermodynamic studies of N, N'-bis(4-hydroxyacetophenone) ethylenediamine and its Cu2+, Ni2+, Co2+, Fe3+, and Mn2+ complexes

Aly A. A. Soliman1, Marguerite A. Wassef 2, Hoda A. Bayoumi 2
[1] Department of Physical Sciences, Chemistry Division, College of Science, Jazan University, Jazan, Kingdom of Saudi Arabia.

[2] Department of Chemistry, Faculty of Women for Arts, Science and Education, Ain Shams University, Cairo, Egypt.

Abstract: Studying the stability constants of metal complexes offers significant insights into their applications in analytical chemistry, pharmaceuticals, catalysis, environmental science, and material science. The protonation constants of N, N'-bis(4-hydroxyacetophenone) ethylenediamine (BHAEN) and the stability constants of a number of transition metal complexes have been studied potentiometrically at 20, 25, 30 and 40oC, in water solution at 0.1 M ionic strength (KNO3), using the mole ratios (1:1) and (2:1), (L:M), where M = Cu2+, Ni2+, Co2+ , Fe3+, and Mn2+. The calculations are performed by operating the computer program SUPERQUAD. From the values of the stability constants of the complexes at the different four temperatures, the thermodynamic functions G, H and S were evaluated. The order of stability of the complexes agrees the Irving - Williams order. The positive values of H for the BHAEN complexes, especially for the most stable complexes species, (ML) in the case with Cu(II) and Fe(III), (MHL) in the case of Ni(II) & Co(II) and (ML2) in the case of Mn(II), reveal that the stability of these species is mainly due to the S values which are highly positive.

Key words: Potentiometric Titrations – Stability Constants – Complexes – Schiff bases.

دراسات الجهدية والحرارية الديناميكية لـ N'-bis(4-hydroxyacetophenone) ethylenediamine ومجمعاته + Cu2+ وNi2+ وCo2+ وFe3+ وMn2 +

ن دراسة ثوابت استقرار المركبات المعدنية تقدم رؤى مهمة في تطبيقاتها في الكيمياء التحليلية ت الصيدلانية والحفز والعلوم البيئية وعلوم المواد. تمت دراسة ثوابت بروتونات N و-N'-bis(4 ب استقرار عدد من مركبات المعادن hydroxyacetophenone) ethylenediamine (BHAEN) ريقة جهدية عند 20 و 25 و 30 و 40 درجة مئوية، في محلول مائي بقوة أيونية 0.1(KNO3) M ، دام النسب المولية)1:1(و(2:1) ، (L:M)، حيث M = Cu2+ و Ni2+ و Co2+ و Fe3+ و Mn2+. وابت استقرار المركبات SUPERQUAD. يتم إجراء الحسابات عن طريق تشغيل برنامج الكمبيوتر ترتيب استقرار S. و H و G عند أربع درجات حرارة مختلفة، تم تقييم الدوال الديناميكية الحرارية سبة لأكثر ، BHAENلمجمعات H المركبات مع ترتيب إيرفينج - ويليامز. إن القيم الإيجابية لـ

أنواع المجمعات استقرارًّرًّا، (ML)في حالة Cu(II) وFe(III)، و (MHL)في حالة Ni(II) و Co(II) بر إيجابية S تكشف أن استقرار هذه الأنواع يرجع بشكل أساسي إلى قيم ، Mn(II)في حالة(ML2) و للغاية.

1. Introduction

Schiff-base ligands have performed a significant role in the evolution of contemporary coordination chemistry, Because of their importance in a variety of interdisciplinary study domains,1

particularly as corrosion inhibitors,2 catalysts for activation of small molecules3-4 and in

biological

systems.5-12 These wide applications of Schiff bases have generated a great deal of interest in metal

complexes, kinetics of formation and hydrolysis as well as electronic spectra and acidity

constants.

Tetradentate Schiff bases, especially those with a N2O2 donor set, resulting from the condensation of

aliphatic diamines such as ethylenediamine or derivatives with Acetylacetone or salicylaldehyde, have

been extensively studied.13 In view of recent interest in the energetics of metal ligand binding in metal

chelates involving N, O donor ligands14 we started to study Schiff base complexes derived from

bidentate ligands showing a N2O2 donor atoms. Martell et al. also carried out studies of

Co(salen) which can reversibly bind molecular oxygen.16

Equilibrium studies for salicylaldimines are in general scarce due mainly to their

insolubility in water, which is the most common solvent for potentiometric determination of stability constants.15 The

majority of the thermodynamic data reported on stability constants and/or protonation constants of

Schiff bases are related to bidentate bases with a NO donor set mainly derived from salicylaldehydes

or benzaldehydes or their derivatives, anilines or substituted anilines. Tetradentate Schiff bases have

been less studied. The stability constants for the Cu(II), Ni(II) and Fe(III) complexes of the tetradentate

The present work reports the results of potentiometric investigation on BHAEN and its complexes with UO_2^{2+}, Ni^{2+}, Cu^{2+}, Fe^{3+} and Mn^{2+}. The potentiometric method is used to determine the proto constants of the free ligand as well as the stoichiometries and the stability of its complexes in appropriate solutions and with the two mole ratios, (1:1) and (2:1), (L:M). The computer progra SUPERQUAD is used to evaluate these constants. To study the effect of temperature on the stabili these complexes, the determination of the stability constants of these complexes is carried out a different temperatures, 20, 25, 30 and 40oC and from the data obtained, the thermodynamic fun G, H and S are evaluated.

2. Experimental

Materials and Solutions. Ethylenediamine (B.P.=118°C) and 4-hydroxyacetophenone (M.P. = 95- 97°C) were Prolabo and Fluka products. All other reagents used were of analytical grade (Merck, Darmstadt, Germany). Carbonate free KOH was prepared in double-distilled water, and standardized potentiometrically with potassium hydrogen phthalate solution. 1M KNO_3 solution was prepared in

double-distilled water. Stock solutions of the metal salts, were prepared in double-distilled water and

standardized by complexometric EDTA titration.17 Stock solutions of the studied ligands (0.01 M) were

prepared by dissolving an appropriate amount of a given ligand in double-distilled water.

Preparation of N, N'-bis(4-hydroxyacetophenone) ethylenediamine (BHAEN). BHAEN was prepared as already described in [18].

Instruments. The potentiometric measurements were performed with Metrohm 702 SM Titrino, Metrohm Ltd. CH-9101 Herisou, Switzerland. The titrino was supplied by 727-titration stand, with built-in magnetic stirrer.

The electrode, combined pH glass electrode, was calibrated using aqueous standard buffers of pH 4.0 and 7.0 at 20, 25, 30 and 40oC. The titrations were performed in a double-wall glass cell through the outer jacket of which water circulated from a controlled temperature bath. The temperature was controlled with the thermostat Digiterm100, J. P. Selecta, S. A., Barcelona, Spain, with a temperature uncertainty of (0.1 °C).

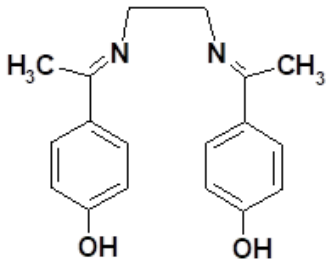

BHAEN

Validation, Verification. VESUVIUS, Support for Validation, is PC software for Metrohm titrators allowing the optimal cooperation between the titrino and PC. SUPERQUAD 91, the calculations on the pH-metric data were performed with the aid of the SUPERQUAD19 computer program.

Potentiometric measurements. The following mixtures were prepared for the determination of the protonation constants of BHAEN and titrated against standard CO2-free potassium hydroxide (0.0 M) solution. (i) (6 × 10-3 M) HNO_3 + (3 × 10-3 M) L, (ii) (4 × 10^{-3}M) HNO3 + (2 × 10^{-3}M) L and (iii) (2 × 10-3 M) HNO_3 + (1× 10^{-3}M) L. The total volume was kept at 50 ml in each case and the temperatu was adjusted at the desired temperature. For the determination of the stability constants of the complexes of BHAEN, the following mixtures were prepared and titrated against standard CO2-potassium hydroxide (0.094 M) solution. For the mole ratio (1:1) ligand-metal (L-M*). (a) (4 ×10-3 M HNO_3 (b) (4 × 10-3 M) HNO_3 + (2 × 10-3 M) L and (c) (4 × 10^{-3}M) HNO3 + (2 × 10^{-3}M) L + (2 × 10^{-3} M) M*. For the mole ratio (2:1), ligand-metal. (d) (8 × 10-3 M) HNO_3 (e) (8 × 10^{-3}M) HNO3 + (4 × 10-3 M) L and (f) (8 × 10-3 M) HNO_3 + (4× 10-3 M) L + (2 × 10^{-3}M) M*. The total volume was adjusted to 50 ml by adding double-distilled water in each case. The titration curve obtained from (a) or (d) calibration curve for the electrode system; it provides data used to calculate the standard elec potential, Eo, and the dissociation constant for water. These values were used to calculate the hyd ion concentration from potential readings.20

3. Results and discussion

Proton – Ligand (BHAEN) equilibria. Protonation constants of BHAEN, which may be considered as a triprotic acid H_3L^{+}, were determined. The potentiometric titration curves of BHAEN using the different concentrations at 25oC are presented in the Figures 1. The titration curves showed two inflections. The first inflection indicates the neutralization of the excess hydrogen ions, whereas second inflection indicates the formation of different deprotonated species. Since there are four protonation sites (two phenolic groups and two tertiary amine groups) for BHAEN, models with L^{n-} (n = 1 – 4) were tried for refinement process. But the best-fit model gave only for three proton species (H_3L^{+}, H_2L and HL^{-}) in the experimental pH region.
The equilibrium reactions for protonation constants are proposed by the following equation (ch are omitted for simplicity):

$$L + nH = HnL, \qquad \beta n = (HnL) / (L)(H)n \qquad (1)$$

Differences between the various log β values give the stepwise protonation constants KHn defined equations (2 - 4)

$$H^{+} + L^{2-} \rightleftharpoons HL^{-1} \qquad KH_1 = (HL^{-1})/(H^{+})(L^{2-}) \qquad (2)$$

$$H^{+} + HL^{-1} \rightleftharpoons H_2L \qquad KH_2 = (H_2L)/(H^{+})(HL^{-1}) \qquad (3)$$

$$H^{+} + H_2L \rightleftharpoons H_3L^{+} \qquad K3^{H} = (H3L)^{+}/(H)(^{+}H2L) \qquad (4)$$

The first two protonation constants obtained in the experimental region may be assigned to the p protons as their values, and the pH range (5 - <10) in which they exist, are in agreement with protonation constants of other phenols. 21-22 And the third protonation constant may be assigne of the imine groups.

	(21)	(22)	Present work
Log KH1	8.20	8.62	8.57
Log KH2	7.45	7.36	7.74

The protonation constants are reported in Table 1, where the highest values were found to be at indicating that the protonation reactions are favorable at high temperature.

Table 1. Protonation constants (logβ's) of BHAEN

	H: L	*20°C*	*25°C*	*30°C*	*40°C*
The mean values of log β's	HL		8.571 (0.028)	8.536 (0.023)	
	H2L	8.343 (0.029)	16.318(0.023)	16.291(0.020)	8.619 (0.025)
	H3L	16.007(0.023)	23.457(0.033)	23.359(0.028)	16.528(0.023)
		23.111(0.033)			23.581(0.031)

*(Standard deviations are given in parentheses)

The concentration distribution of various species formed in solution (formation %) as a function of pH was obtained by the use of the SUPERQUAD 91 program throughout the present work. The species distribution diagrams for BHAEN based on the fitted equilibrium constants, Figures 2-5, indicate that

at lower pH values, the only existing species is HL+3 at all the temperatures studied, whereas in the pH

range ≈ 5 – 9.7 the species HL, HL- and L2- 2coexist. The species H2L starts at pH ≈ 5.5, 5.9, 6 and 4.9

at 20, 25, 30, and 40oC, respectively, and then increases rapidly attains a maximum value (≈ 50%) at pH ≈ 7.4 at all the temperatures studied and then decreases gradually with the increasing of the species HL- which started at pH ≈ 6.5. The concentration of the species HL- increases with the increasing of the pH reaches a maximum (≈ 60%) at pH ≈ 8.2 and then decreases with the increasing of L2- species.

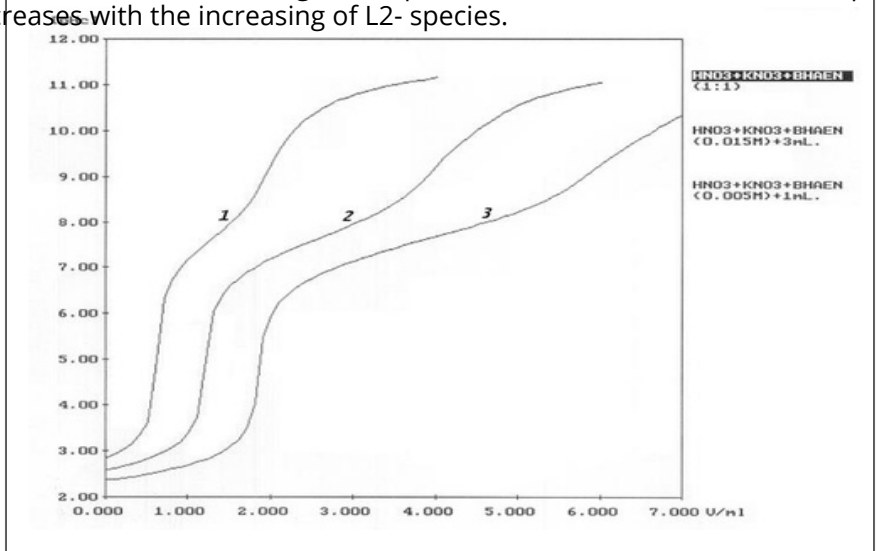

etric titration curve of H+/ BHAEN system at 25oC: (1) BHAEN (0.005M), (2
N (0.01M), (3) BHAEN (0.015M).

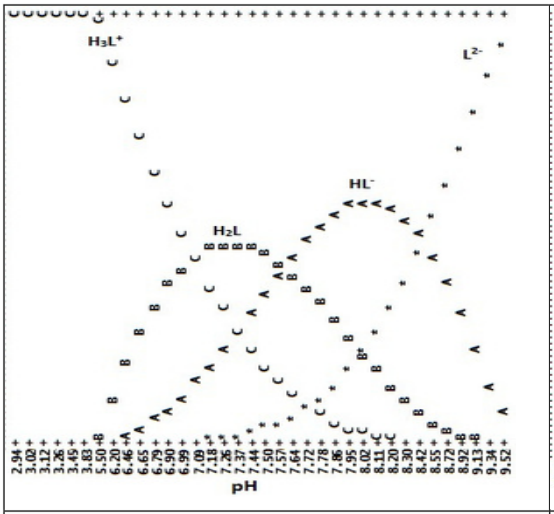

n diagram for the system H+-L-2 at 20º C

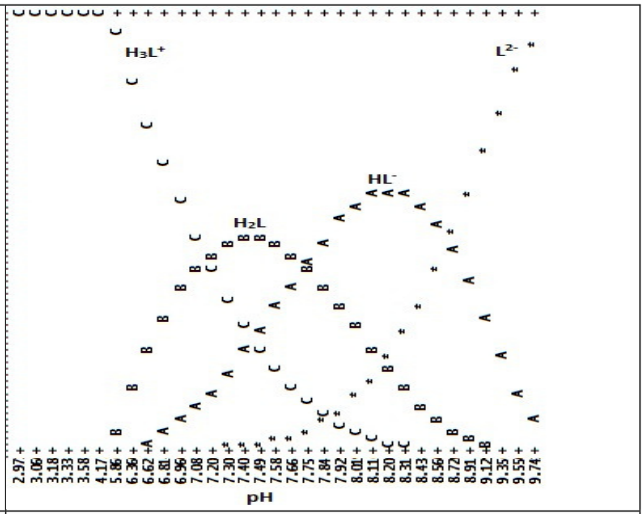

n diagram for the system H+- L-2 at 25ºC

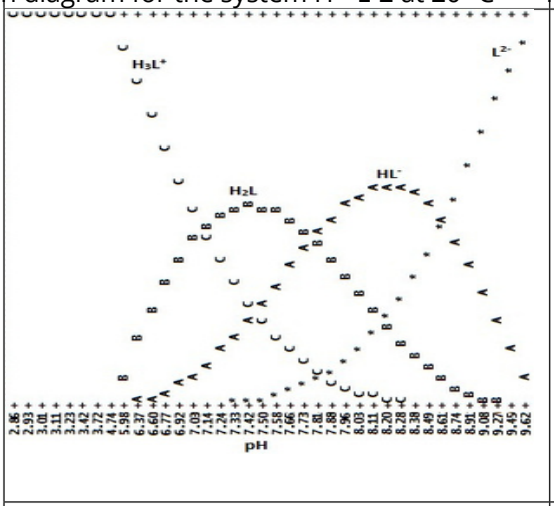

n diagram for the system H-L-2 at 30ºC

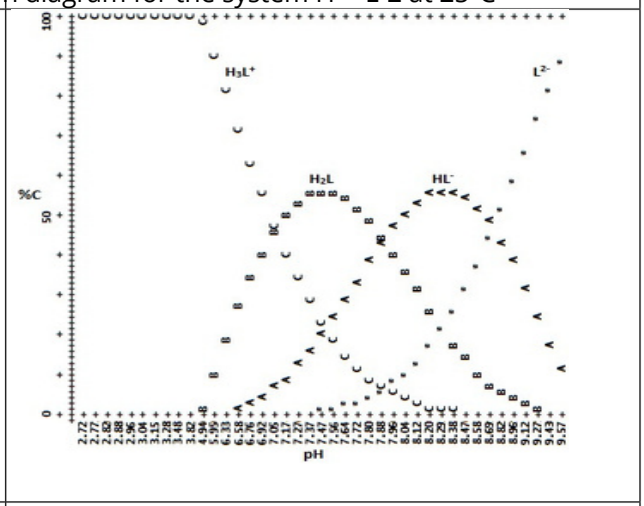

n diagram for the system H+- L-2 at 40ºC

Stability constants of the complexes.

The stoichiometry and stability constants of M – BHAEN complexes, using the molar ratios 1:1 and 2:1, (L:M), at the four different temperatures 20, 25, 30, and 40oC and under the conditions described in the experimental part are reported in Table 2. A number of models were examined in sequence using the SUPERQUAD 91 program and the reported stability constants are for the best models examined. A displacement was noticed in each curve of the titration curves for M– ligand mixtures, Figures 6-10, compared with that for the free ligand. This indicates the release of protons, which in turn depends on the reaction between the ligand and M ion.

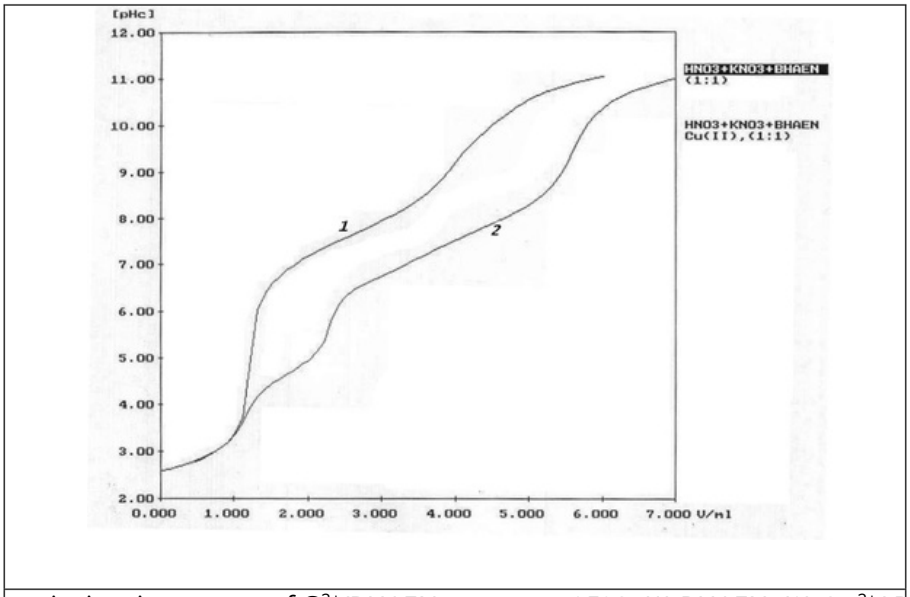

metric titration curves of Cu^{2+}/BHAEN system at 25°C: (1) BHAEN, (2) Cu^{2+}/ B
x

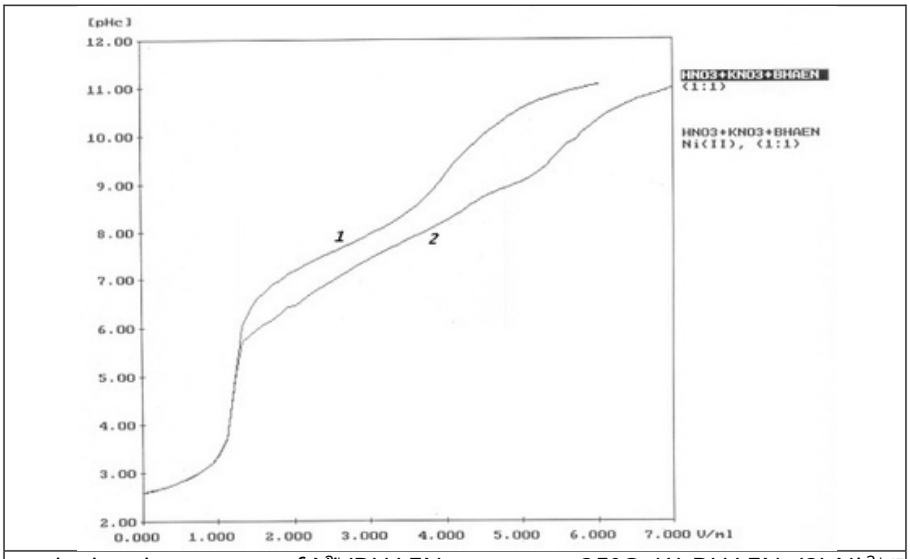

metric titration curves of Ni^{2+}/BHAEN system at 25°C: (1) BHAEN, (2) Ni^{2+}/B
x

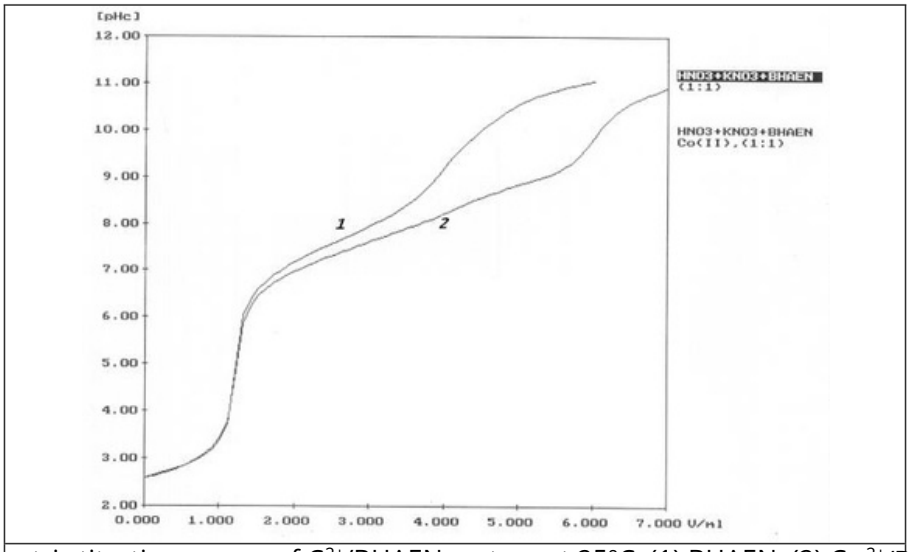

metric titration curves of Co^{2+}/BHAEN system at 25°C: (1) BHAEN, (2) Co^{2+}/BHAEN x

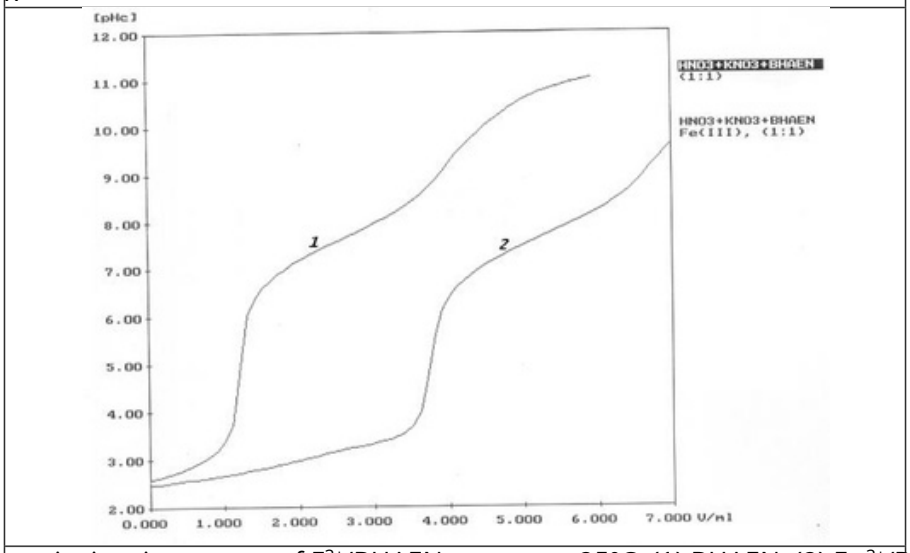

metric titration curves of Fe^{3+}/BHAEN system at 25°C: (1) BHAEN, (2) Fe^{3+}/BHAEN x

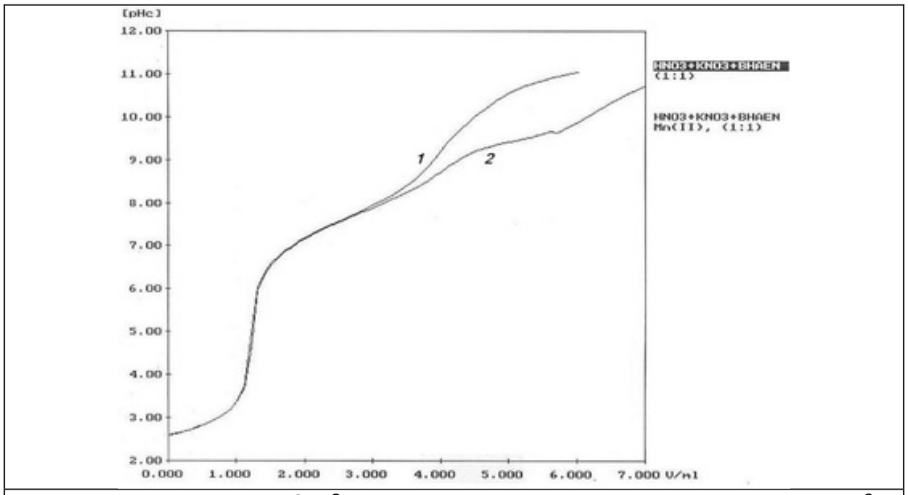

metric titration curves of Mn^{2+}/BHAEN system at 25°C: (1) BHAEN, (2) Mn^{2+}/B
x

Table 2. The stoichiometries and stability constants (logs) for the metal complexes.

Stoichiometry (L:M:H)	*Stability Constants (log's)*			
	20 oC	*25 oC*	*30 oC*	*40 oC*
Copper(II) complexes				
1:1:1	16.757(0.039)	16.792(0.032)	16.956(0.025)	17.247(0.026)
1:1:0	9.961(0.088)	10.062(0.092)	10.286(0.077)	10.758(0.072)
1:1:-1	2.877(0.072)	2.917(0.098)	3.286(0.079)	3.887(0.088)
1:1:-2	-5.005(0.109)	-5.206(0.149)	-4.683(0.128)	-4.179(0.141)
2:1:2	31.974(0.053)	32.412(0.019)	32.622(0.021)	33.091(0.033)
2:1:1	-----	24.459(0.061)	24.664(0.062)	25.364(0.090)
2:1:0	17.150(0.083)	16.935(0.028)	17.172(0.029)	17.614(0.051)
2:1:-2	0.899(0.107)	-----	-----	-----
Nickel(II) complexes				
1:1:1	13.104(0.153)	13.584(0.033)	13.867(0.027)	14.186(0.031)
1:1:0	6.807(0.076)	5.539(0.071)	6.104(0.051)	6.119(0.048)
1:1:-2	-11.385(0.079)	-12.741(0.101)	-11.710(0.065)	-11.441(0.049)
2:1:2	------	25.994(0.038)	26.744(0.051)	27.292(0.035)
2:1:1	18.989(0.107)	18.099(0.081)	19.099(0.086)	19.359(0.041)
2:1:0	10.659(0.134)	9.921(0.037)	10.135(0.054)	10.007(0.089)

Cobalt(II) complexes				
1:1:2	------	18.548(0.159)	18.945(0.066)	19.226(0.034)
1:1:1	11.457(0.081)	------	11.466(0.033)	11.517(0.048)
1:1:0	------	3.300(0.101)	3.752(0.066)	3.557(0.083)
1:1:-2	-14.917(0.059)	-14.559(0.092)	-13.990(0.072)	-14.086(0.079)
2:1:2	------	23.032(0.019)	23.775(0.028)	22.990(0.054)
2:1:1	------	------	------	14.937(0.062)
2:1:0	7.597(0.0344)	7.378(0.0230)	7.905(0.036)	6.915(0.026)
2:1:-1	-0.833(0.0279)	-1.941(0.041_	-1.008(0.098)	------
2:1:-2	-9.452(0.0581)	------	------	------
Iron(III) complexes				
1:1:1	19.310(0.105)	19.631(0.080)	19.607(0.118)	19.904(0.148)
1:1:0	16.028(0.034)	16.295(0.035)	16.740(0.023)	17.383(0.019)
2:1:4	45.514(0.084)	-----	------	-----
2:1:2	-----	36.009(0.099)	36.708(0.077)	37.530(0.092)
2:1:0	20.761(0.121)	22.115(0.099)	22.934(0.097)	22.931(0.107)
Manganese(II) complexes				
1:1:-1	-----	-4.682(0.04)	-4.913(0.043)	-4.891(0.150)
2:1:2	-----	-----	-----	22.506(0.022)
2:1:0	5.172(0.153)	5.364(0.113)	5.545(0.117)	6.478(0.044)
2:1:-2	-12.322(0.150)	-----	-----	-----

The concentration distribution of various complex species formed in solution (formation %) as a function of pH was obtained by means of the SUPERQUAD 91 program. The distribution diagrams for the systems M / BHAEN and M / 2BHAEN based on fitted stability constants at the four different temperatures are depicted in Figures 11- 19.

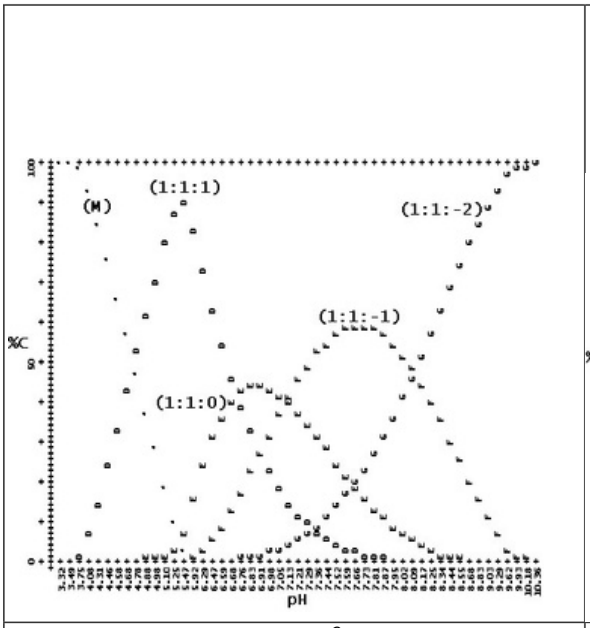

on diagram for the system Cu^{2+}/BHAEN at 25ºC

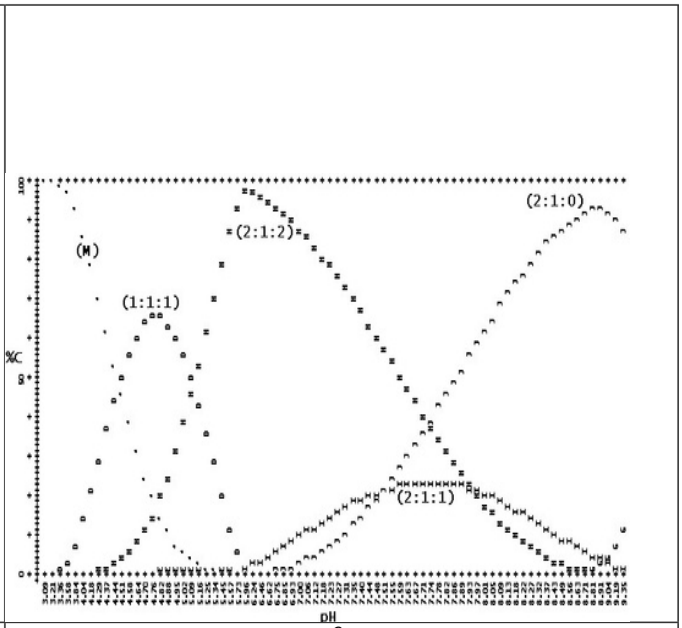

on diagram for the system Cu^{2+}/2BHAEN at 25ºC

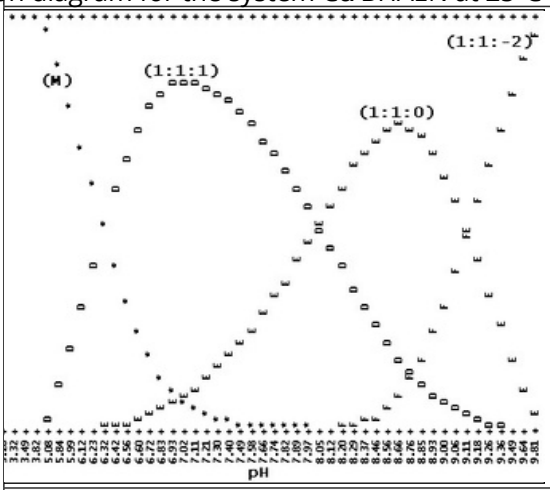

on diagram for the system Ni^{2+}/BHAEN at 25ºC

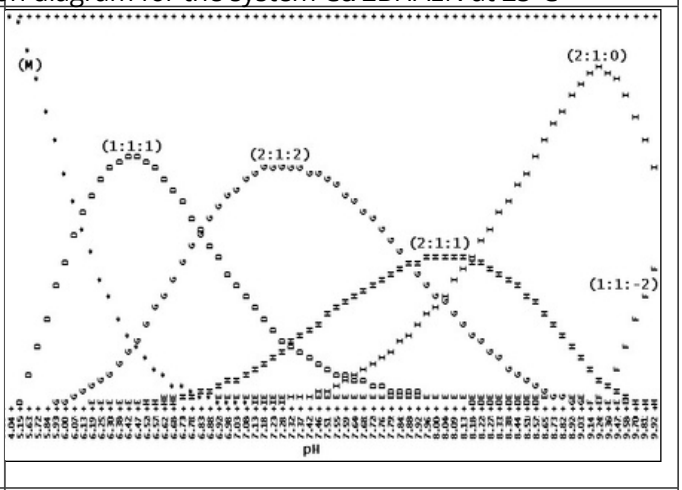

on diagram for the system Ni^{2+}/2BHAEN at 25ºC

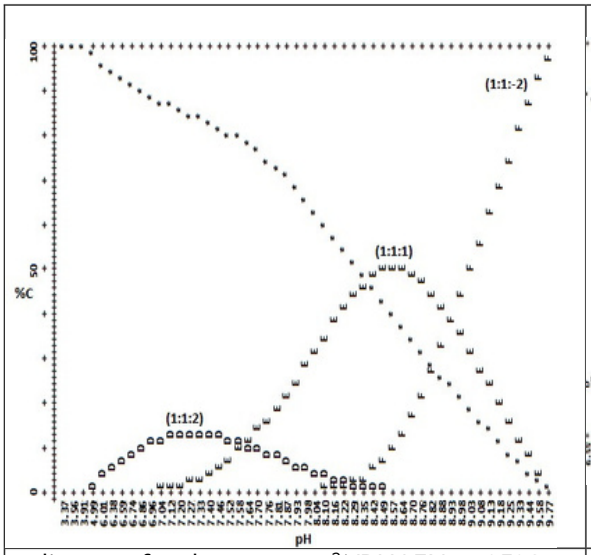

on diagram for the system Co^{2+}/BHAEN at 25ºC

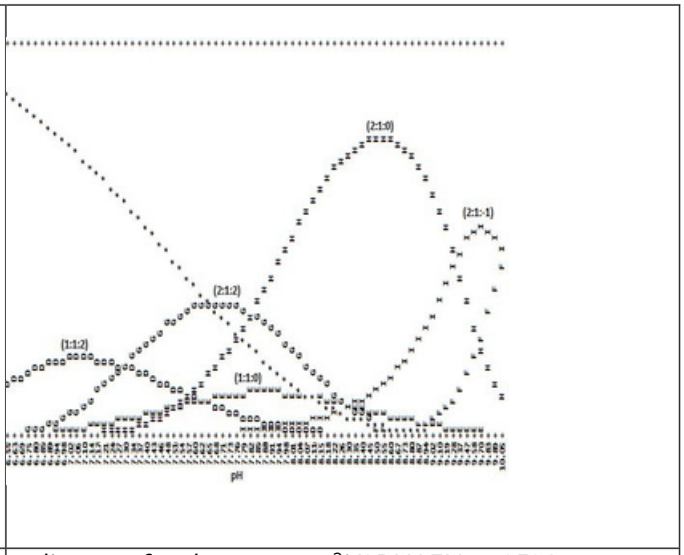

on diagram for the system Co^{2+}/2BHAEN at 25ºC

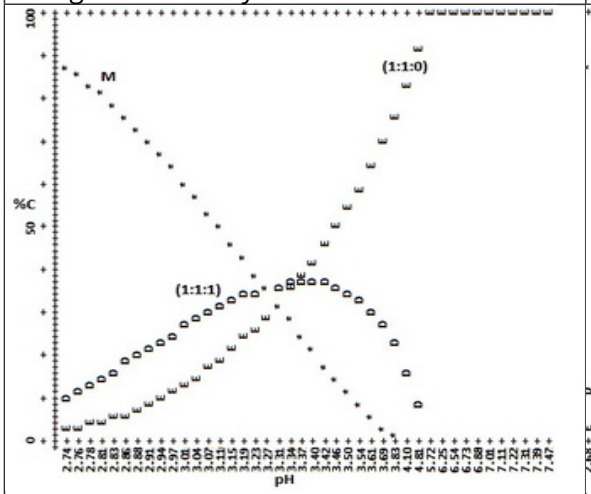

on diagram for the system Fe^{2+}/BHAEN at 25ºC

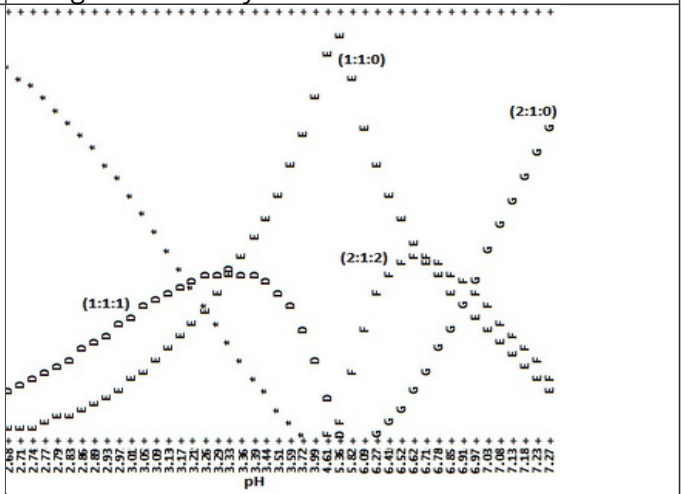

on diagram for the system Fe^{2+}/2BHAEN at 25ºC

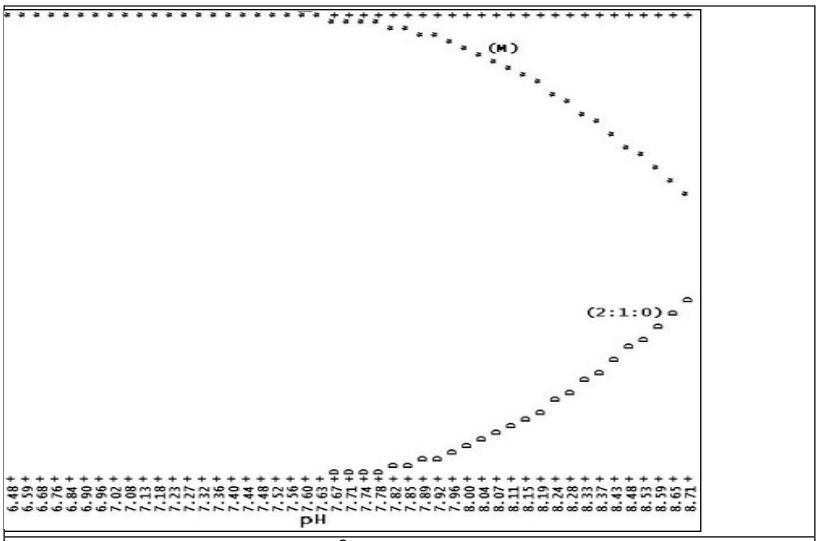

on diagram for the system Mn^{2+}/2BHAEN at 25°C

Enthalpies and entropies of protonation of BHAEN

From Arrhenius plots of logK1, logK2, and logK3, Table 3, vs. 10^3/T (K), Figure 20, the stepwise enthalpy changes □H'S were deduced, and these are given in Table 3. The free energy changes □ were also evaluated at 25oC using the expression,

$$-\square G = 2.303RT \log K \quad (1)$$

Similarly, the entropy changes □S'S were evaluated using the following relationships,

$$\square S = (\square\square - \square G)/ T \quad (2)$$

$$-RT \ln K = \square\square - \square\square S \quad (3)$$

Table 3. The stepwise enthalpy changes □H'S, the free energy changes G'S and the stepwise entropy changes S(C) & S(g).

	20 °C	*25 °C*	*30 °C*	*40 °C*	*H (kcal/mole)*	*G (kcal/mole)*	*S(g) (cal/mole. deg)*	*S(C) (cal/mole. deg)*
log K1	8.343	8.571	8.536	8.619	*4.870*	*-11.452*	*55.066*	*54.772*
log K2	7.664	7.747	7.755	7.909	*4.944*	*-10.519*	*52.238*	*51.890*
log K3	*7.104*	*7.139*	*7.068*	*7.053*	*-1.446*	*-9.751*	*27.829*	*27.869*

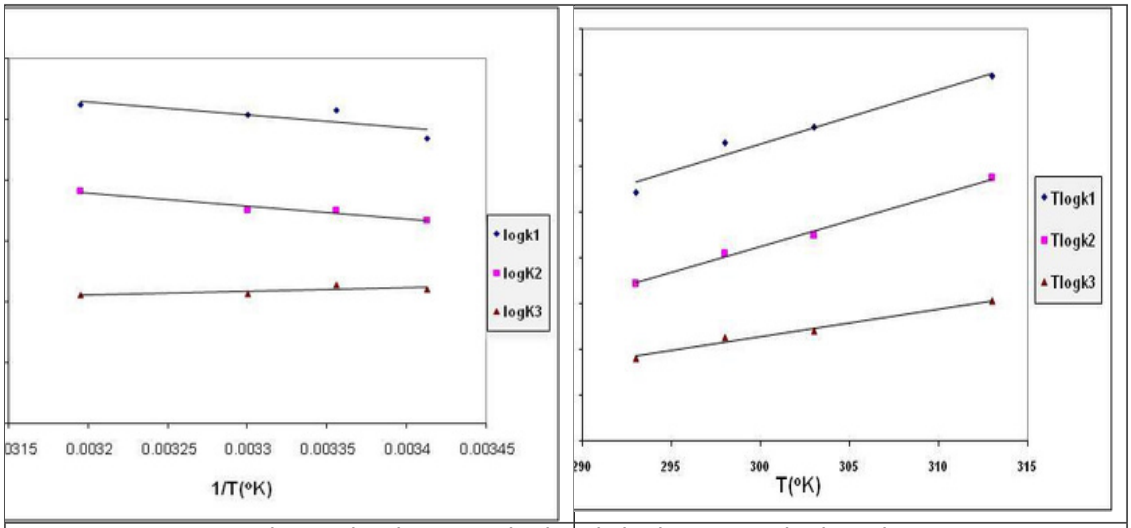

Figure 20. Relationship between logk anhdip between Tlogk and T

The stepwise entropy changes for BHAEN were evaluated from equation (2), S(C), and from the slope of TlogK vs. T plots, S(g), Figure 21. The values of S calculated by the two methods are in good agreement, Table 3.

The positive values of H's for the first and the second protonation reactions indicate that these reactions are endothermic, i.e., the reaction is enhanced with increasing temperature, and The ne value of H for the third protonation reaction indicates that this reaction is exothermic, i.e., the rea

G'S for the three protonation

is enhanced with decreasing temperature. The large negative values of G for the third reaction is reactions indicate that these reactions proceed spontaneously, the value of S's. This latter value is less less than that for the first two reactions as supported by the values of positive for the third reaction than the first two reactions.

Enthalpies and entropies of chelation of BHAEN with metal cations

The stepwise thermodynamic functions G, H, and S for the M/BHAEN complexes were calculated from the stepwise stability constants obtained at the four different temperatures used 4. The values of these thermodynamic functions of the complexes are summarized in Table 4. Arr plots of the data presented in Figures 22-24-26-28-30. to obtain H's values presented in Figures 22-24-26-28-30. to obtain

stepwise entropy changes for the formation of M/BHAEN complexes were evaluated from equa (2), S(C), and from the slope of TlogK vs. T plots, S(g), Figures 23-25-27-29-31. The values of S calculated by the two methods agree, Table 4.

Copper(II) complexes

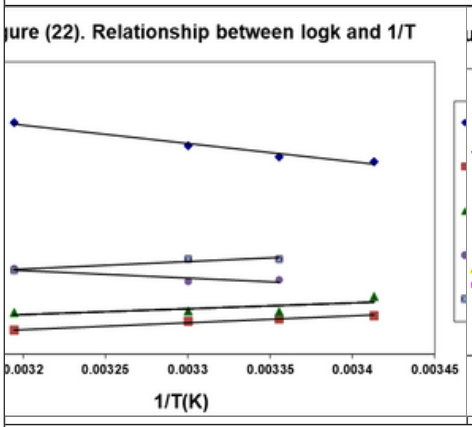

ure (22). Relationship between logk and 1/T

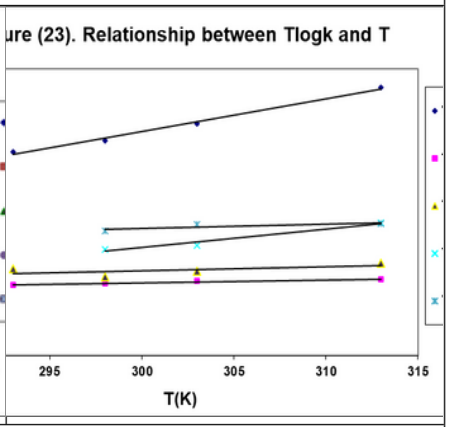

ure (23). Relationship between Tlogk and T

Nickel (II) Complexes

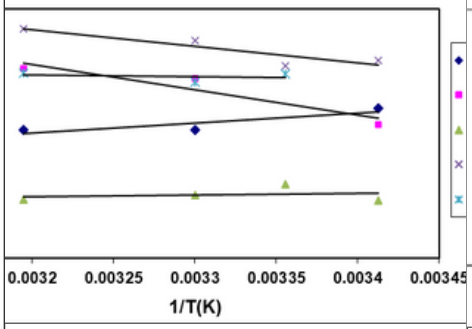

(24). Relationship between logk and 1/T

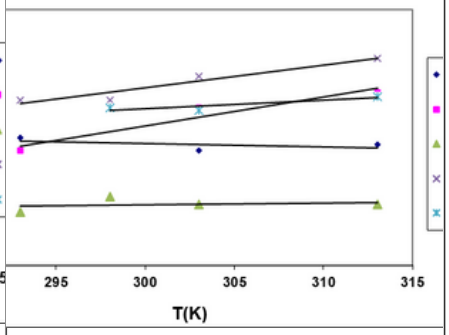

e (25). Relationship between Tlogk and T

Cobalt (II) Complexes

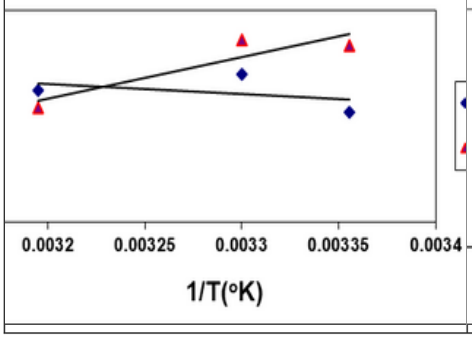

igure (26). Relation between logk and 1/T.

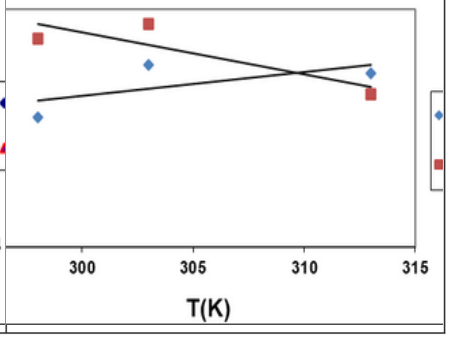

igure (27). Relationship between Tlogk and

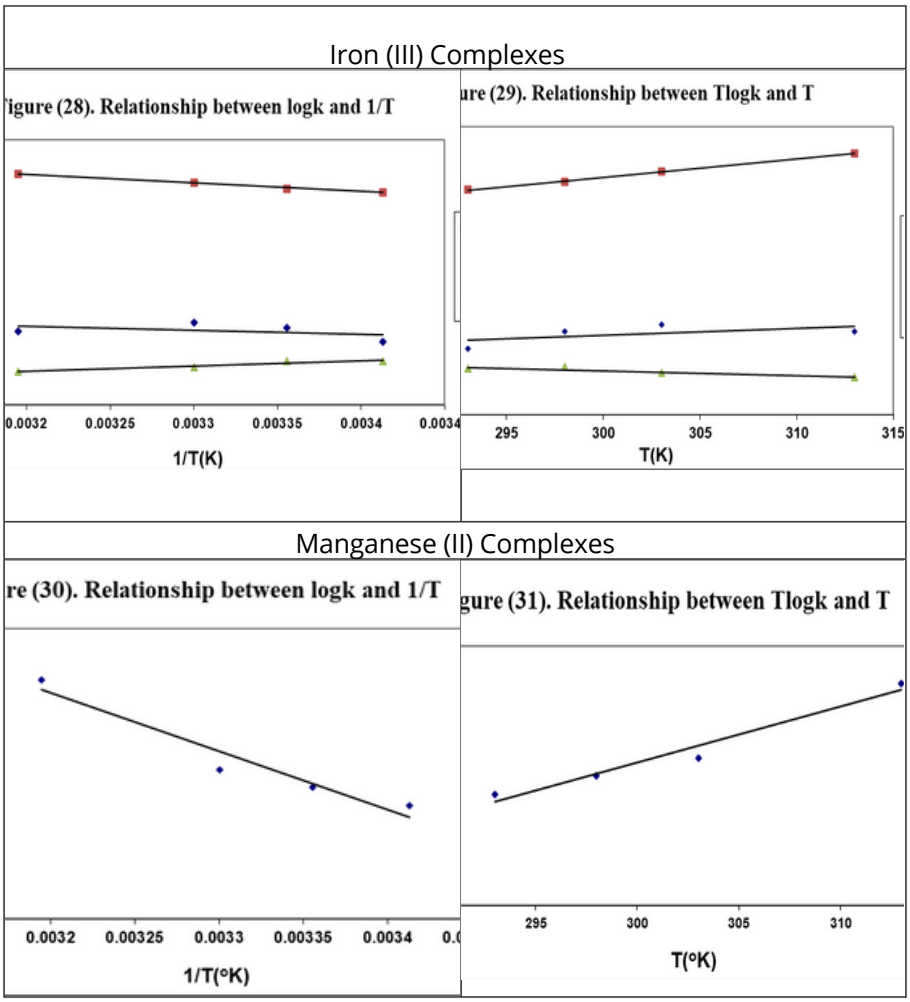

Figures 22-31. Plots of log K vs. 1/T and T log K vs. T

For the Cu(II) complexes the large negative values of G obtained for all the species indicate that

formation reaction of these species proceed spontaneously. The species (ML) has the highest neg
value of G, although it has a positive enthalpy change, but this was outweighed by the large positi
value, which is favorable to chelation. The S value obtained for the species (ML2) indicates that
formation of 1:2 complex is not entropy favorable compared with 1:1 complex, which has a la
positive S value.

For the Ni(II) complexes The high negative value of H for the formation of the species (ML) indicat

that this chelating reaction is exothermic, i.e., the reaction is enhanced with decreasing tempera
Also, it is obvious from the concentration distribution diagrams that the concentration of this sp
decreases with the temperature increasing.

The formation of the species (ML2) has a small negative value of H, this may be explained by the enhancement of the reaction from 20oC to 25oC, then decreases after that with the increasing of
temperature. The positive value of H'S for the formation of the other species indicates that these
reactions are endothermic, i.e., the reaction is enhanced with the increasing of temperature. The negative
values of G'S obtained for all the species indicate that the formation reaction of these species proceed
spontaneously. The species (MHL), (MHL2) an (MH2L2) have the highest negative values of G'S.
Moreover, these species are entropy favorable.

The species (MHL) has the highest positive entropy value, indicates the stability of this species. This
can also be observed from the concentration distribution curves for the systems of the mole ratio (1:1), and, it is also present in the systems of the mole ratio (2:1) with a relatively high concentration.

In the case of Co(II) complexes the positive value of H'S for the formation of the species with the m
ratio (1:1) indicate that these reactions are endothermic, i.e., the reaction is enhanced with the
increasing of temperature. The negative value of H for the formation of the species (ML2) indicate
this reaction is exothermic, i.e., the reaction is enhanced with the decreasing of temperature
negative values of G'S obtained for all the species indicate that the formation reaction of these sp
proceed spontaneously. The species (MHL), (MH2L) have the highest negative values of G'S, althou
they have positive enthalpy changes, but these were outweighed by the large positive S'S values, w
is favorable to chelation.

The negative S value obtained for the species (ML2) indicates that the formation of 1:2 complex is
entropy favorable compared with 1:1 complex, which has a large positive S value. This may expl
the appearance of species with the mole ratio 1:1 in the concentration distribution curves of the s
with the mole ratio 1:2, M:L.

For the Fe(III) complexes The positive values of H'S for the formation of the species (ML) and (ML2
indicate that these reactions are endothermic, i.e., the reaction is enhanced with the increasi
temperature. The negative value of H for the formation of the species (MHL) indicates that this rea
is exothermic, i.e., the reaction is enhanced with the decreasing of temperature. The negative valu
G'S obtained for all the species indicate that the formation reaction of these species proceed
spontaneously. The species (ML) has the highest negative value of G , although it has positive enth
changes, but this was outweighed by the large positive S value, which is favorable to chelation.

The S value obtained for the species (ML2) indicates that the formation of 1:2 complex is not entr
favorable compared with 1:1 complex, which has a large positive S value. The low stability of t
species (ML2) compared with that of (ML), logK = (logKML – logKML2) = 10.475, Table (14), may
be attributed to steric hindrance effect. This may explain the appearance of the species (ML) in
concentration distribution curves in all systems and at all temperatures with a large concentration
(≈ 100%).

For the Mn(II) complexes The positive value of H for the formation of the species (ML2), indicates t
this reaction is endothermic, i.e., the reaction is enhanced with the increasing of temperature
negative values of G obtained for the species (ML2) indicate that the formation reaction of this sp
proceeds spontaneously. The species (ML2) has a negative value of G, although it has positive enth
changes, but this was outweighed by the large positive S value, which is favorable for chelation.

4. Conclusion

From the obtained results, it can be concluded that the order of stability of the complexes formed between BHAEN and transition ions, Cu2+, Ni2+, Co2+ and Mn2+ investigated in this study is in the expected Irving - Williams order 23: Cu2+ > Ni2+ > Co2+ > Mn2+. A large value of charge/radius ratio for a central ion means that the central ion will form more stable complexes.24 The correlation between charge/radius ratio for the central metal ions and the stability of their complexes with BHAEN is shown in Table 5 and Figure 32.

Table 5.

The ion	*Radius (Ao)*	*Charge/radius (Z/r*	*Stability constant at 20oC (L:M)*	
			(1:1)	*(2:1)*
Cu2+	0.57	3.509	10.062	16.935
Ni2+	0.69	2.899	5.539	9.921
Co2+	0.72	2.778	3.3	7.378
Mn2+	0.91	2.198	---	5.364

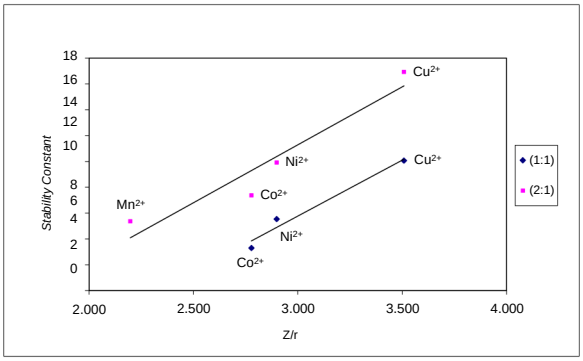

Figure (32). Relation between stability constant and charge/radius ratio

REFERENCES [1] Soroceanu, A.; Bargan, A. Advanced and Biomedical Applications of Schiff-Base Ligands and Their Metal Complexes: A Review. Crystals 2022, 12, 1436.
[2] Majumdar, D.; Chatterjee A.; Feizi-Dehnayebi M.; Kiran N. S.; Tuzun B.; Mishra D., 8-Aminoquinoline derived two Schiff base platforms: Synthesis, characterization, DFT insights, corrosion inhibitor, molecular docking, and pH-dependent antibacterial study, Heliyon, 2024, 10[
[3] Juyal, V. K.; Pathak, A.; Panwar, M.; Thakuri, S. C.; Prakash, O.; Agrwal, A.; & Nand, V., Schiff base metal complexes as a versatile catalyst: A review. Journal of Organometallic Chemistry, 20
122825.
[4] Al Zoubi, W., & Ko, Y. G. Schiff base complexes and their versatile applications as catalysts in oxidation of organic compounds: part I. Applied Organometallic Chemistry, 2017, 31[3], e3574.
[5] Kumar, M.; Singh, A. K.; Singh, V. K.; Yadav, R. K.; Singh, A. P.; Singh, S., Recent developments in the biological activities of 3d-metal complexes with salicylaldehyde-based N, O-donor Schiff ba ligands. Coordination Chemistry Reviews, 2024, 505, 215663.
[6] Brown, L.S.; Gat, Y.; Sheves, M.; Yamazaki, Y.; Maeda, A.; Needleman, R.; Lanyi, J. K. The Retinal Schiff Base-Counterion Complex of Bacteriorhodopsin: Changed Geometry during the Photocycle Is a Cause of Proton Transfer to Aspartate 85, Biochemistry, 1994, 33, 12001-1201
[7] Fishkin, N. E.; Sparrow, J. R.; Allikmets, R.; Nakanishi, K. Isolation and characterization of a retina pigment epithelial cell fluorophore: An all-trans-retinal dimer conjugate, Proc. Natl. Acad. Sci. US 2005, 102, 7091-7096.
[8] Bieschke, J.; Zhang, Q.; Powers, E. T.; Lerner, R. A.; Kelly, J. W. Oxidative Metabolites Accelerate Alzheimer's Amyloidogenesis by a Two-Step Mechanism, Eliminating the Requirement for Nucleat Biochemistry, 2005, 44, 4977-4983.
[9] Mure, M.; Brown, D. E.; Saysell, C.; Rogers, M. S.; Wilmot, C. M.; Kurtis, C. R.; McPherson. M. J.; Phillips, S. E. V.; Knowles, P. F.; Dooley, D. M. Role of the Interactions between the Active Site Base and the Substrate Schiff Base in Amine Oxidase Catalysis. Evidence from Structural and Spectroscopic Studies of the 2-Hydrazinopyridine Adduct of Escherichia coli Amine Oxidase, Biochemistry, 2005, 44, 1568-1582.
[10] Toyota, E.; Sekizaki, H.; Takahashi, Y.; Itoh, K.; Tanizawa, K. Amidino-Containing Schiff Base Copper [II] and Iron [III] Chelates as a Thrombin Inhibitor, Chem. Pharm. Bull. 2005, 53, 22-26
[11] Ahmed, Z.; Ravandi, A.; Maguire, G. F.; Kuksis, A.; Connelly, P. W. Formation of apolipoprotein AI–phosphatidylcholine core aldehyde Schiff base adducts promotes uptake by THP-1 macropha Cardiovasc. Res. 2003, 58, 712-720.
[12] Ul-Hassan, M.; Scozzafava, A.; Chohan, Z. H.; Supuran, C. T. Carbonic Anhydrase Inhibitors: Metal Complexes of a Sulfanilamide Derived Schiff base and their Interaction with Isozymes I, II a IV, J Enzyme Inhib. 2001, 16, 499-505.
[13] Mederos, A.; Domi´nguez, S.; Molina, R. H.; Sanchiz, J.; Brito, F. Coordinating ability of ligands 857-911.
[14] Garg, B. S.; Kumar, D. N. Spectral Studies of Chem. Rev. 1989, 103-195.
[15] Lloret, F.; Mollar, M.; Faus, J.; Julve, M.; Dı´az, W. Solution chemistry of N,N'-ethylenebis(salicylideneimine) and its copper[II], nickel[II] and iron[III] complexes, Inorg. Chim. Act 1991, 189, 195-206.
[16] Motekaitis, R. J.; Martell, A. E. Potentiometric determination of the stabilities of cobalt[II] complexes of polyamine Schiff bases and their dioxygen adducts, Inorg. Chem. 1988, 27, 2718-27
[17] Welcher, F. J. "The Analytical Uses of EDTA", Van. Nostrand, New York, 1957.
[18] Arida, H.A.; El-Saied, A.M.; El-Reefy S.A. Cadmium [II]-selective membrane coated graphite electrode based on recently synthesized bis-(4-hydroxyacetophenone)-ethylenediamine, Sensors, 4, 43.
[de Vargas, F. S.; Kuhnert, N. Spectral Studies of nickel[II] complexes with tetradentate schiff bas 229-234.
having N2O2 donor groups, Spectrochimica Acta, 2003, Part A 59,

[19] Gans, P.; Sabatini, A.; Vacca, A. A. SUPERQUAD: An Improved General Program for Computation of Formation Constants from Potentiometric Data. J. Chem. Soc. Dalton Trans. 1985, 1195-1200.[20] Anderegg, G.; Kholief, K. Extrapolation of molar equilibrium constants to zero ionic strength and parameters dependent on it. Copper[II], nickel[II], hydrogen[I] complexes with glycinate ion and calcium[II], hydrogen[I] complexes with nitrilotriacetate ion, Talanta, 1995, 42, 1067-79. [21] Sahoo, S. K.; Muthu, S. E.; Baral, M.; Kanungo, B. K. Potentiometric and spectrophotometric study of a new dipodal ligand N,N_-bis{2-[(2-hydroxybenzylidine)amino]ethyl}malonamide with Co[II], Ni[II], Cu[II] and Zn[II], Spectrochimica Acta, 2006, Part A: Molecular and Biomolecular Spectroscopy, Vol 63, 3, 574-586. [22] Motekaitis, R. J.; Martell, A. E.; Nelson, D. A. Formation and stabilities of cobalt[II] chelates of N-benzyl triamine Schiff bases and their dioxygen complexes, Inorg. Chem. 1984, 23, 275-283. [23] Irving, H.; Williams, R. J. P. Order of Stability of Metal Complexes, Nature, 1948, 162, 746. [24] Wahid U. M.; Tuli, G. D.; Madam, R. D. “Selected Topics in Inorganic chemistry”, S. Chand and Company LTD Ram Nagar, New Delhi, 1997.

Table 4. The stepwise stability constants (logKs) and the values of the thermodynamic functions ΔH, ΔG, and ΔS of the complexes of Cu(II), Ni(II),Co(II), Fe(III), Mn(II).

	Cu(II)			
	20°C	*25°C*	*30°C*	*40°C*
logKML	9.961	10.062	10.286	10.758
logKMHL	6.796	6.730	6.670	6.489
logKMH2L	---	---	---	---
logKML2	7.189	6.873	6.886	6.856
logKMHL2	---	7.524	7.492	7.750
logKMH2L2	---	7.953	7.958	7.727
	ΔH (kcal/mole)	*ΔG (kcal/mole)*	*ΔS(g) (cal/mole.deg*	*ΔS(C) (cal/mole.deg)*
logKML	17.357	-13.810	105.190	104.590
logKMHL	-6.497	-9.238	9.089	9.197
logKMH2L	---	---	---	---
logKML2	-5.782	-9.434	13.442	12.253
logKMHL2	7.105	-10.330	58.566	58.499
logKMH2L2	-6.950	-10.920	13.259	13.310

	Ni(II)			
	20°C	*25°C*	*30°C*	*40°C*
logKML	6.807	5.539	6.104	6.119
logKMHL	6.297	8.045	7.763	8.067
logKMH2L	---	---	---	---
logKML2	3.852	4.382	4.031	3.888
logKMHL2	8.330	8.178	8.964	9.352
logKMH2L2	---	7.895	7.645	7.933
logKML	*ΔH (kcal/mole)*	*ΔG (kcal/mole)*	*ΔS(g) (cal/mole.deg*	*ΔS(C) (cal/mole.deg)*
logKMHL	-14.692	-8.822	-18.241	-18.757
logKMH2L	37.640	-11.630	156.592	157.411
logKML2	---	---	---	---
logKMHL2	-2.472	-5.605	9.368	10.009
logKMH2L2	24.852	-13.483	122.775	122.473
	2.603	-11.437	45.262	44.857

	Co(II)			
	20°C	25°C	30°C	40°C
logKML	---	3.300	3.752	3.557
logKMHL	---	---	7.714	7.960
logKMH2L	---	---	7.479	7.709
logKML2	---	4.078	4.153	3.358
logKMHL2				
logKMH2L2				
	□H (kcal/mole)	H (kcal/mole)	□H (kcal/mole)	□H (kcal/mole)
logKML	5.268	5.268	5.268	5.268
logKMHL	10.746	10.746	10.746	10.746
logKMH2L	10.047	10.047	10.047	10.047
logKML2	-22.481	-22.481	-22.481	-22.481
logKMHL2	5.268	5.268	5.268	5.268
logKMH2L2	Co(II)	Co(II)	Co(II)	Co(II)

	Fe(III)			
	20oC	25oC	30°C	40oC
logKML	16.028	16.295	16.74	17.383
logKMHL	3.282	3.336	2.867	2.521
logKML2	4.733	5.820	6.194	5.548
	□H (kcal/mole)	□G (kcal/mole)	□S(g) (cal/mole.deg)	□S(C) (cal/mole.deg)
logKML	29.280	-22.366	173.685	173.309
logKMHL	-17.928	-4.579	-45.886	-44.795
logKML2	13.937	-7.988	68.301	73.577

	Mn(II)			
	20oC	20oC	20oC	20oC
logKML	---	---	---	---
logKMHL	---	---	---	---
logKML2	5.172	5.172	5.172	5.172
	□H (kcal/mole)	□H (kcal/mole)	□H (kcal/mole)	□H (kcal/mole)
logKML	---	---	---	---
logKMHL	---	---	---	---
logKML2	27.811	27.811	27.811	27.811

Enhancing Photovoltaic Efficiency through Engine Oil Coatings: A Comparative Analysis of New, Partially Used, and Degraded Oils

Habib Muhammad Usman1,*, Nirma Kumari Sharma, Sani Saminu and Abdulbasit Bashir Yero3, Abdurrahman Salisu Yahya4 and Farouk Isah Muhammad5

[1]Department of Electrical Engineering, Mewar University, Chittorgarh, Rajathan, India
[2]Department of Biomedical Engineering, University of Ilorin, Ilorin, Nigeria
[3]Department of Electrical and Electronics Engineering, Nile University, Nigeria
[4]Department of Electrical and Electronics Engineering, Federal University Dutsin-Ma, Nigeria
[5]Department of Electrical and Electronics Engineering, Nigerian Depense Academy Kadu Nigeria

Corresponding Author's Email: habibusman015@gmail.com

Abstract: The efficiency of photovoltaic (PV) systems is significantly influenced by surface conditions, including contamination, which impairs light absorption and reduces overall power output. This study investigates the effects of coating a PV panel with Mobil engine oil in various states and compares the results with those of a clean reference panel. The experiments utilized a 300 mm x 200 mm PV panel with a nominal power rating of 10 W, coated with 0.2 liters of oil to ensure uniform coverage. The oil samples included new oil (O1), halfway-used oil (O2), and fully degraded oil (O3). Measurements of power output, temperature, and solar irradiance were recorded hourly from 8:00 AM to 6:00 PM. The clean panel exhibited power outputs ranging from 9.02 W to 9.56 W. Coating with O1 resulted in the most significant enhancement, with power output increasing by up to 4.29% at peak irradiance (9.97 W at 2:00 PM). The O2 coating provided moderate improvements, with a maximum increase of 1.56% (9.68 W at 2:00 PM). Conversely, the degraded oil (O3) generally reduced power output, with a maximum decrease of 1.91% (9.23 W at 5:00 PM). The findings indicates that a uniform application of fresh Mobil oil can reduce light reflection and improve light absorption, enhancing PV panel performance. However, the benefits diminish as the oil degrades, underlining the importance of oil quality for sustained performance gains.

Keywords: Light Absorption, Degraded Oil, Engine Oil Coatings, Photovoltaic (PV) Efficiency, and Solar Panel Performance

تعزيز كفاءة الخلايا الكهروضوئية من خلال طلاءٍ زيت الم
تحليل مقارن للزيوت الجديدة والمستعملة جزئيًاا والمتدهـ

أثر كفاءة الألأنظمة الكهروضوئية بشكل كبير بـ الظروف السطحية، بما في ذلك التلوث، الذي يضعف
ك PV امتصاص الضوء ويقلل من إجمالي الناتج من الطاقة. تبحث هذه الدراسة في آثار طلاء لوحة
PV في حالات مختلفة وتقارن النتائج بنتائج لوحة مرجعية نظيفة. استخدمت التجارب لوحةMobil
200 مم مع تصنيف طاقة اسمي يبلغ 10 وات، مطلية بـ 0.2 لتر من الزيت لضمان التغطية الموحدة
(O3). وزيتًاا متدهورًًّا بالكامل (O2) وزيتًاا نصف مستعمل (O1) تضمنت عينات الزيت زيتًاا جديدًاا
خرج الطاقة ودرجة الحرارة والإشعاع الشمسي كل ساعة من الساعة 8:00 صباحًًّا إلى 6:00 مساءًً
سين O1 أظهرت اللوحة النظيفة مخرجات طاقة تتراوح من 9.02 وات إلى 9.56 وات. أدى الطلاء بـ
همية، مع زيادة خرج الطاقة بنسبة تصل إلى 4.29٪ عند ذروة الإشعاع)9.97 وات في الساعة 2:00
ي الساعة 2:00(%إلى تحسينات معتدلة، مع زيادة قصوى قدرها 1.56 O2 وقد أدى طلاء .)مساءًً
ى تقليل خرج الطاقة، مع انخفاض أقصى (O3) مساءًً(. وعلى العكس من ذلك، أدى الزيت المتدهور
1.9%)9.23 واط في الساعة 5:00 مساءًً(. تشير النتائج إلى أن التطبيق الموحد لزيت موبيل الطازج
يمكن أن يقلل من انعكاس الضوء ويحسن امتصاصه، مما يعزز أداء الألألواح الكهروضوئية. ومع ذلك،
الفوائد مع تدهور الزيت، مما يؤكد أهمية جودة الزيت لتحقيق مكاسب أداء مستدامة.

1. Introduction

Photovoltaic (PV) systems, a cornerstone of renewable energy technologies, have become an important component in the transition toward sustainable energy solutions. However, the efficiency of these systems is highly sensitive to external environmental factors, including surface contaminants and dust accumulation, which can significantly degrade their performance. Surface contamination impedes light absorption by the PV panels, leading to reduced power output and efficiency [1-2]. PV system performance can still be hampered by a number of operational and environmental issues even with major developments in technology [3]. The accumulation of oil on photovoltaic surfaces is one of such issue, and it can happen in areas where there is a lot of oil production, transportation, or use [4]. However, limited research has been conducted on the effect of engine oils, in various stages of degradation, as potential coatings for PV surfaces. Engine oils are known to possess unique physical properties, including viscosity and film formation capabilities, which could offer protection against dust accumulation, moisture ingress, and other surface contaminants.

Previous studies have explored various coatings, such as hydrophobic films and anti-soiling agents, to reduce the accumulation of dust and other environmental particles [5-7]. The distribution and size of dust particles play a crucial role in shading and reducing PV efficiency. The distribution and deposition of dust are influenced by factors such as composition, size, shape, weight, and external environmental conditions, including temperature, wind speed, humidity, and dirtiness. Additionally, human activities, vehicle emissions, and natural events like volcanic eruptions contribute to increased dust accumulation on PV panels [8-9]. Smaller particles cover a larger surface area compared to coarser particles, diminishing radiation absorption and negatively affecting PV performance [10-11]. Fine particles exhibit greater stability and concentration on surfaces than coarse ones [12-13], resulting in increased light diffusion, particularly at shorter wavelengths, and higher radiation loss [14]. This degradation is exacerbated in high-humidity conditions, where microscopic dust particles adhere to surfaces, forming sticky films that are resistant to removal by natural forces such as wind [15].

Several studies have investigated the factors that result to lower solar PV energy production, while some examined the effect of oil coating in enhancing the PV output, among them are, Khatib et al. investigated the effects of five air pollutants—red soil, ash, sand, calcium carbonate, and silica—on the performance degradation of multicrystalline PV modules. Their findings revealed that reductions in PV voltage and power are directly linked to the type and quantity of deposited pollutants. Among these, ash caused the most significant voltage reduction, reaching 25%, followed by red soil, calcium

In Saudi Arabia, PV panels tilted at 26° accumulated 5 g/m² of dust in 45 days, leading to a conduc reduction of approximately 20% [21]. Similarly, in Kathmandu, accumulated dust on PV panels ov five months reached 9.67 g/m², resulting in a productivity decline of about 29.76% [22].

The coating of fresh oil to photovoltaic (PV) surfaces forms a thin layer that minimizes solar radiat reflection, potentially enhancing PV efficiency by capturing more radiation and improving energy conversion [23]. However, the physical and chemical properties of oil change as it is used. Partiall used oil, containing particles, combustion byproducts, and impurities, can increase opacity, furthe reducing light transmission. This diminishes the PV system's efficiency while altering the interacti between the oil and the PV surface [24].

Because oil coating has a major effect on the efficiency of solar energy conversion, it has been extensively researched in relation to photovoltaic (PV) systems. Mustapha et al. [25] addresses general ideas behind how light transmission obstruction and localized heating caused by surface impurities, such as oil, might lower PV performance. Surface contamination, especially with fresh can drastically reduce photovoltaic performance because of its high refractive index, which enha solar reflection and scattering [26]. The methods by which oil pollution, even in trace levels, c obstruct light absorption and raise surface temperatures, resulting in rapid material degradatio studied in [27]. Research conducted by Adinoyi et al. [28] emphasizes the unique difficulties cause oil residues from industrial pollutants, pointing out that even a thin layer of new oil can cause a reduction in PV cells' energy production. In a similar vein, Cristaldi et al. [29] found that oil polluti in cities can significantly reduce photovoltaic panel efficiency, requiring frequent cleaning to pres performance. As Mani et al. [26] highlight, partially used oil further lowers light transmission and r the danger of thermal stress on PV cells due to its mixture of combustion byproducts and particle impacts of used oil on photovoltaic performance were studied by Sanjeev et al. [30], who discov that the presence of carbonaceous particles can cause significant efficiency losses as well as the degradation. Pareek et al. [31] investigated how completely degraded oil, which has a high leve impurities, significantly lowers optical clarity and creates stains that are difficult to remove. The lo term impacts of such oil as highlighted in [32] present film which require more thorough clean techniques and raise maintenance costs. Lastly, Al-Housani et al. [33] proposed that improving durability of PV materials and creating efficient cleaning methods are critical to reducing the nega impacts of oil contamination on PV systems.

While many of the existing studies consider the effects of various soil, dust, and shading on PV ou few have examined the impact of oil coating, and none have considered the effect of oil in respe its state of degradation. This study contributes to the feasibility of using engine oil coatings to enh PV efficiency, focusing on a comparative analysis of three distinct types of oils: new (O1), halfwa used (O2), and completely degraded (O3). Experimenting and analysing the impact of coating the engine oil in these three states to the surface of PV panels make this study novel. The study comp the power output of PV panels with engine oil coatings to that of uncoated, reference panels to determine whether these oils can provide a viable solution for improving PV system efficiency.

2. Material and methods

A.Materials Employed

A 10W, 22.05V, 0.63A photovoltaic (PV) panel is one of the materials used in this study to assess how dirt and oil coatings affect solar PV performance. To guarantee an accurate estimation of sun exposure, solar irradiance is measured by a solar power meter. A digital multimeter is used to measure electrical properties like voltage, current, and power output. While a fine and uniform oil coating is produced using a bottle sprayer.

Furthermore, in order to comprehend the effects of heat on PV performance, non-contact temperature measurements of the PV panels and the surrounding environment are provided using a Model GP-200 infrared thermometer. Among other things, Table 1 summarised the equipment employed in this study and Figure 1 shows the items utilized in this experiment.

Table 1. List and Specification of the equipment used

ment	cations	onal Information
oltaic Panel	mum Power (P_max): 10W	Type: Polycrystalline/Monocrystalline
	Circuit Voltage (V_oc): 22.05V	perature Coefficient (Voltage): -0.36%
	Circuit Current (I_sc): 0.63A	nsions: (300mm x 200mm)
	r Tolerance: ±5%	ht: Approx. 1.2kg
	ency: Around 15%-18%	me: Aluminum alloy for durabili ight
ed Thermometer	l: GP-200	urement Range: -50°C to 550°C (-5)
	racy: ±1.5% or ±1.5°C	ution: 0.1°C
	sivity: Adjustable (0.1–1.0) onse Time: <500ms	nce-to-Spot Ratio (D:S): 12:1 (for a s from a distance)
	urement Range: 0–1999 W/m²	ry Type: Typically uses 9V battery
Power Meter	ution: 1 W/m²	racy: ±5%
		ay Type: Digital LCD
	r Type: Silicon photodiode	r Supply: 9V battery
Multimeter	age Measurement Range: 0–1000V (DC AC)	Cent Measurement Range: 0–10A (D
	er Measurement Range: Calculated and current ranges	baracy: Typically ±0.5% for voltage, ±
	ay Type: Digital LCD	ry Type: 9V
	ional Features: Continuity buzzer, diode ce measurement	gory Rating: CAT III/CAT IV ds for measuring high-energy circuits)
Sprayer	Manual trigger sprayer	e Type: Adjustable (mist, stream)
	rial: Plastic (HDPE or PET)	city: 500mL–1L
	y Uniformity: Produces fine and consisten	cations: Used to apply uniform coati led experimental conditions

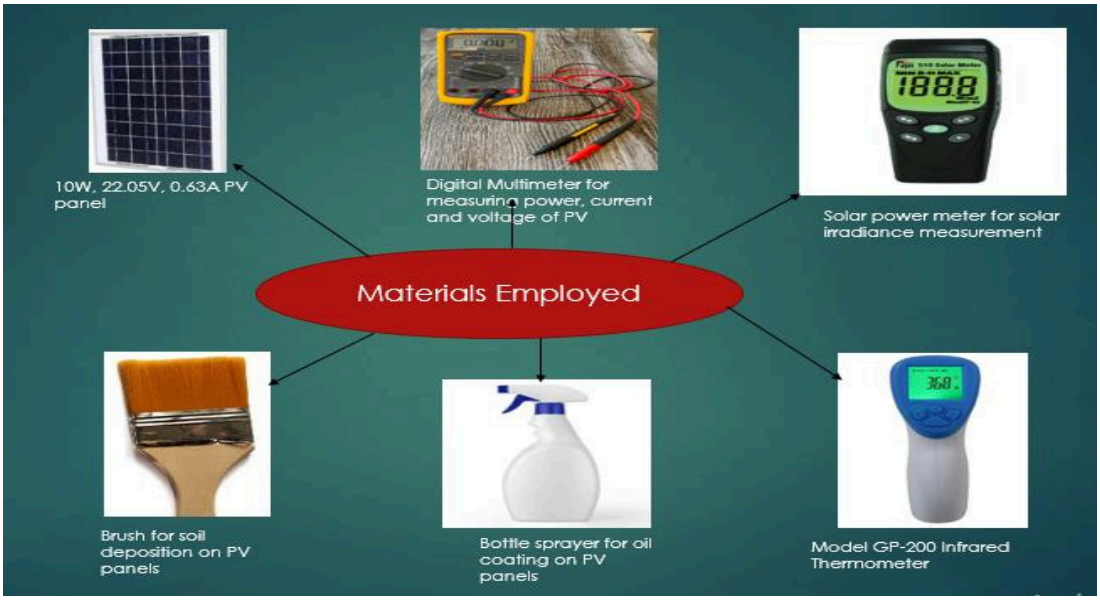

Figure 1: Materials used

B. Experimental Setup

1) *Photovoltaic panel:* In this study, we utilized photovoltaic (PV) panels with specific characteristics designed to provide consistent and reliable performance. Each panel has a maximum power output of 10W, a short circuit current (I_sc) of 0.63A, and an open circuit voltage (V_oc) of 22.05V. The power tolerance is ±5%, indicating that the actual power output can vary by up to 5% from the specified maximum power. A total of four PV panels were used in the experiment, divided into two groups to assess the impact of different oil coating on their performance. The installation of the PV panels was conducted at Mewar University, located at coordinates 25.0328° N latitude and 74.6366° E longitude. This location offers a conducive environment for solar energy experiments due to its ample sunlight exposure throughout the year. To optimize the solar energy capture, the panels were installed at a tilt angle of approximately 25 degrees, corresponding to the latitude of the location which is ideal for maximizing sunlight exposure during peak hours [34].

The effective solar irradiance that reaches the PV cells is decreased when oil contamination occurs on PV surfaces. Reduction factor (R o) can be used to model the effect of oil pollution by taking into account the transmissivity loss caused by oil. The kind and degree of oil deterioration determine this component.

$$G_{eff} = G \times (1 - R_o) \quad (1)$$

Where G_{eff} is the effective solar irradiance; Ro is the oil contamination reduction factor, which vari depending on the kind and degree of degradation of the oil. Empirical evidence from [26] demons how effective solar irradiation decreases as oil content and deterioration rise.

The incident solar radiation can also be impacted by the reflectance of the PV surface, which is alt
by oil pollution. Given reflectance, the effective solar radiation is determined by:

$$G_{eff,ref} = G \times (1 - R_0)(1 - R_f) \quad (2)$$

Where R_f is the reflectance factor due to oil, which varies based on the oil's optical properties.

When these variables are combined, the oil-contaminated PV module's output power can be writt
follows:

$$P_{out} = G_{eff,ref} \times (1 - R_0) \times A \times \eta(T) \quad (3)$$

Where P_{out} is the output power of PV, $G_{eff,ref}$ is the effective reflectance solar radiation, A is the ar
of PV, $\eta(T)$ is the efficiency of the PV module at temperature T.

2) *Oil Samples:* Three types of Mobil engine oil were selected to study their varying impacts on PV pa
performance: A New Mobil Engine Oil sample (O1) was obtained by purchasing a new container
Mobil engine oil, representing oil in its pristine, unused state. Moreover Half-used Mobil Engine C
sample (O2) was taken as the second sample after the oil had been used in a generator for four
with each day 12 hours of operation. At this halfway point, the oil had started to accumulate impu
making it a representative sample of oil in mid-usage. Finally completely Used Mobil Engine Oi
sample (O3) was the final sample which was collected after the oil had been used for eight days w
each day 12 hours of operation, aligning with its typical lifespan in the generator. This sample rep
oil that is heavily contaminated and turns dark at the end of its usable life. The oil samples are sh
in figure 2 and their properties are summarised in Table 2.

Figure 2: Various Mobil oil samples used for PV coating

Table 2: Summary of the Mobil oil samples properties with respect to degradation [35]

Property	New Mobil Engine Oil (O1)	Half-used Mobil Engine Oil (O2)	Completely Used Mobil Engine Oil (O3)
Source	Purchased new	Collected after 4 days of generator use	Collected after 8 days of generator use
Appearance	Clear, amber	Slightly darker, with impurities	Dark, with visible impurities and sludge
Viscosity	Pristine,		Low
Oil Condition	no	Moderate level of contaminants	High level of
Oxidation	contaminants		contaminants High
Level	Low	Moderate	
Wear Metals	None	Low to moderate	High
Content			
Additive	None	Moderate	Significant
Depletion			
pH Level	Neutral	Slightly acidic	More acidic
Water	None	Low	Moderate
Content			
Acid Number	Low	Moderate	High
Lubricity	Excellent	Reduced	Poor
Smell	Mild petroleum	Slightly burnt smell	Strong burnt smell
Usage Impact	smell		
	Fresh and clean	Shows signs of usage and degradation	Heavily degraded, nearing end of life

C. Experimental Procedure

After setting up the materials, the procedure of this work starts by isolating a reference panel that was left uncontaminated. In order to correctly evaluate the impact on solar PV performance, an even and controlled layer of oil coating was applied to the PV panels in this investigation using a brush. Applying paint precisely while preserving uniform thickness and dispersion throughout the panel surface is made possible by the brushing technique. This control is essential because uneven application could result in inconsistent shading effects, making it more difficult to isolate the performance impact of the oil layer [36]. Using a brush, oil samples O1, O2, and O3 were carefully applied to the PV panels. Lastly, the combined effects of oil pollutants on solar PV performance were examined using an oil-coated PV panel; the brush ensured a consistent base layer and a uniform application.

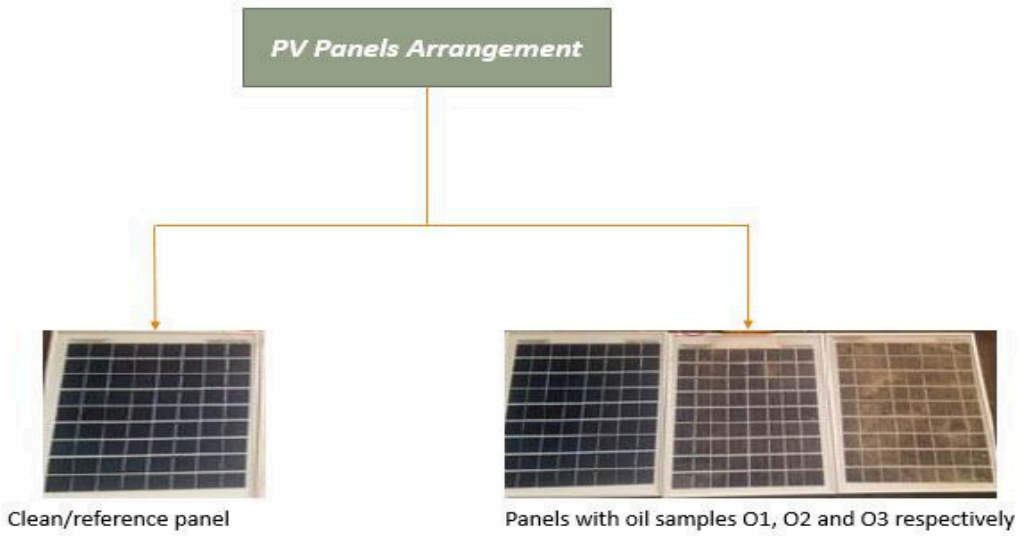

Figure 3: Experimental procedures

For the experimental grouping, the 4 PV panels were categorized as follows: one panel was kept c
and uncontaminated to serve as the control. Another three panels were coated with Mobil oil
various degradation levels and their impacts were assessed. This arrangement allowed for a
comprehensive analysis of how Mobil oil with different degradation levels affects PV panel
performance. The performance of the contaminated panels was compared against the control pa
quantify the efficiency losses attributable to each type of contaminant. Furthermore, the quantity
samples used was precisely measured to ensure consistency and reliability in the experimental re
For the oil coating, 0.2 liters of oil were applied uniformly to three separate panels. Oil samples (
O2, and O3) each with 0.2 liters were distributed across three panels respectively.

D. Performance Measurement

The performance of the PV panels was monitored hourly from 8:00 AM to 6:00 PM daily. During each hour, the power output was measured and recorded using a multimeter, solar irradiance was measured using a solar power meter, and temperature was measured with a Model GP-200 Infrared Thermometer. This experiment was conducted over a period of 30 days, and the average values of the measured variables were determined and presented in this work.

The percentage change in the power output of the PV was calculated using the following equation the results are presented in this study:

$$\%\Delta PO = \frac{P_{with\ oil} - P_{clean}}{P_{clean}} \times 100\% \quad (4)$$

Equations 1, 2 and 3 represent the percentage change in power of PV when the samples are ap

where $\%\Delta PO$ is the percentage change in power of PV with soil samples, with oil samples and with soil samples respectively. And also P_{clean} and $P_{with\ oil}$ are the power output of the reference PV a that with oil respectively.

3. Result and discussion

A. Result of the PV Clean/reference Output Power

As shown in Table 3, the 10W PV panel experiment demonstrated a strong correlation between temperature, solar irradiation, and the panel's performance. Both temperature and irradiance climbed between 8:00 and 18:00, reaching their maximums at 14:00 with values of 1250 W/m2 and 42°C, respectively. In accordance with this, at 14:00 the power production peaked at 9.56 W, little less than the 10 W specified, most likely as a result of inefficiencies due to manufactures and real world uncertainties. It is evident that the PV panel exhibited good efficiency and dependability in a range of daytime situations, as it maintained a consistent power production near its peak capacity despite the fluctuations.

Table 3: Operating conditions of the PV system and its power output

Operating conditions			Clean PV	
Time (Hrs)	Temp. (0C)	Irrad. W/m2	ISC (A)	PO (W)
8	31	225	0.38	9.02
9	32	307	0.39	9.12
10	34	477	0.42	9.26
11	35	510	0.45	9.34
12	36	783	0.49	9.43
13	39	1081	0.51	9.49
14	42	1250	0.54	9.56
15	40	1129	0.52	9.52
16	37	974	0.50	9.47
17	35	622	0.48	9.41
18	33	349	0.40	9.22

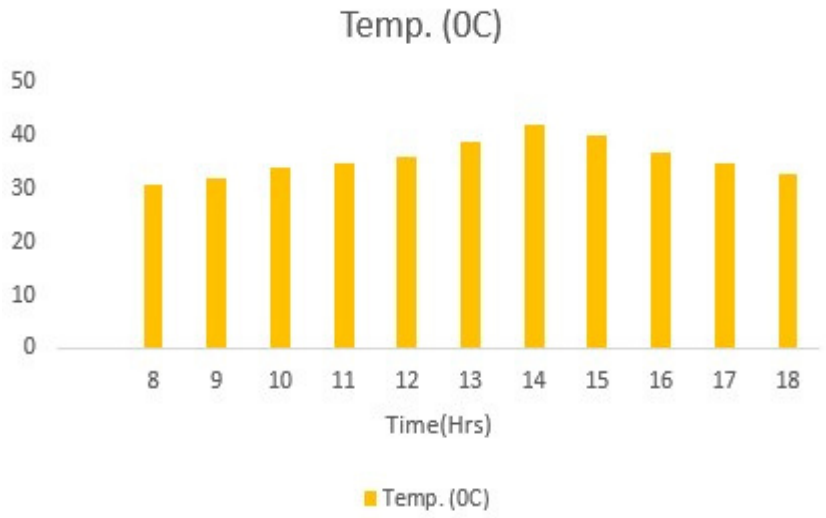

Figure 4: Average temperature variation per hours in a day

Figure 5: Average solar irradiance variation per hours in a day

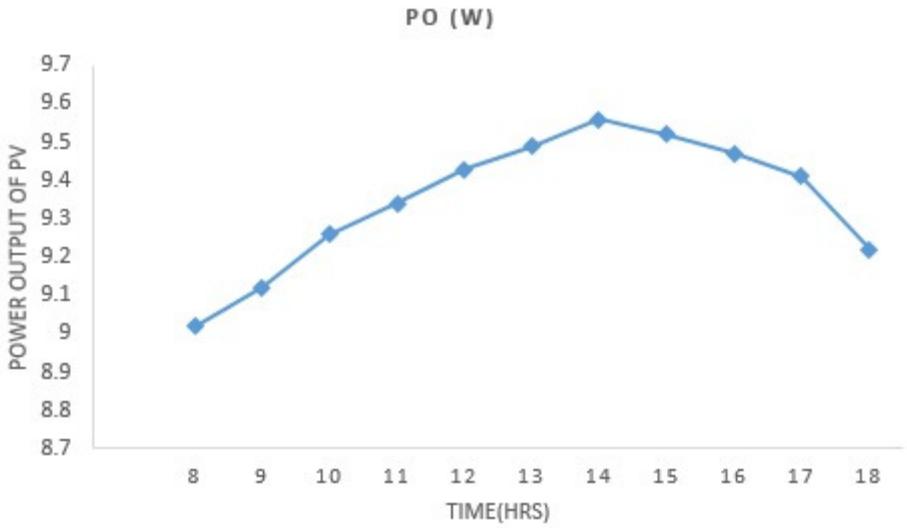

Figure 6: Average power output of clean PV per hour

The clean PV system's operational parameters and accompanying power output are shown in Ta

By 8 AM, the temperature is 31°C; by 2 PM, it reaches its highest point of 42°C; by 6 PM, it ha dropped down to 33°C. In a similar vein, solar irradiance peaks at 1250 W/m² at 2 PM, falls to 3 W/m² by 6 PM, and begins at 225 W/m² at 8 AM. With a range of 9.02 W from 8 AM to 9.56 W at 2 PM. The average hourly temperature fluctuation is shown in Figure 4, which also shows the nor daily temperature profile with a peak in the early afternoon and a decrease in the evening.
Understanding this temperature profile is crucial to comprehending the PV system's thermal prop and how they affect efficiency. The average hourly variation in solar irradiance is depicted in Figur where a bell-shaped curve peaks at midday. This variance has a direct impact on the PV system's e input, which in turn determines the power output. The clean PV's average power output per ho shown in Figure 6, which shows that even in the face of temperature and irradiance variations power output is largely constant. This demonstrates how well the PV system performs in transfor solar energy that is readily available into electrical power. The data in Table 1 indicate that b temperature and solar irradiance significantly influence the power output of PV panels. The hig power output corresponds to the periods with the highest temperature and irradiance, confirmi optimal PV performance is closely linked to these environmental conditions.

B. Pearson Correlation Analysis of the effect of Temperature and Irradiance on PV output

To calculate the Pearson correlation coefficient (r) between variables, we use the following formula:

$$r = \frac{\sum (x_i - \bar{x})(y_i - \bar{y})}{\sqrt{\sum (x_i - \bar{x})^2 \sum (y_i - \bar{y})^2}} \quad (5)$$

Where: x_i and y_i are individual data points of variables X and Y.

$\bar{x}$ and $\bar{y}$ are the means of X and Y, respectively.

Now the Pearson correlation coefficients for the relationships between the following were calcu and the results are summarized in T:

1. Temperature (°C) and Power Output (PO):
2. Irradiance (W/m²) and Power Output (PO):
3. Temperature (°C) and Irradiance (W/m²):

Table 4: Summary of the Pearson correlation coefficients

Parameter Pair	Pearson Correlation Coefficient (r) 0.931	Interpretation
Temperature (°C) and Power Output (W)	0.938	Strong positive
Irradiance (W/m²) and Power Output (W)	0.979	correlation Strong positive correlation
Temperature (°C) and Irradiance (W/m²)		very strong positive correlation

stronger as shown in Table 4. This make irradiance as the dominant factor influencing PV performance, as it directly determines the energy available for conversion into electricity. The near-linear relationship confirms that within the tested range, power output scales proportionally with irradiance. From a comparative standpoint, the relationship between irradiance and power output is more direct and predictable than the relationship between temperature and power output. Irradiance is the dominant parameter, as indicated by its slightly higher correlation coefficient, suggesting that efforts to optimize PV system performance should prioritize maximizing irradiance exposure.

Conversely, the very strong correlation between temperature and irradiance reflects the challeng

disentangling these effects in performance analysis, as their combined influence can complicat assessment of each factor's independent impact.

While both temperature and irradiance positively correlate with power output, irradiance demons

a slightly stronger and more consistent influence. The very strong correlation between temperatu irradiance further confirms their interdependence in natural operating conditions. These emphas importance of addressing both irradiance optimization and thermal management to achieve max PV efficiency. The coefficient of 0.979 between temperature and irradiance demonstrates a very s positive correlation. This reflects the inherent link between these two environmental paramete higher irradiance typically leads to increased ambient temperatures. This strong association unde the role of irradiance as the primary driver of thermal effects observed in the PV system. Such ins are critical for accurately modeling environmental influences on PV performance.

C. Result and Discussion of PV Output Power with Oil Samples

Table 5: power output of PV for various oil samples

Operating conditions			Clean PV	Oil samples (10g) each					
				O1	O2	O3	O1	O2	O3
Time (Hrs)	Temp. (0C)	Irrad. W/m	PO (W)	PO1 (W)	PO2 (W)	PO3 (W)	PO1 (%)	PO2 (%)	PO3 (%)
8 9 10 11 12 13 14 15 16 17 18	31 32 34 35 36 39 42 40 37 35 33	2 225 307 477 510 783 1081 1250 1129 974 622 349	9.02 9.12 9.26 9.34 9.43 9.49 9.56 9.52 9.47 9.41 9.22	9.35 9.43 9.48 9.52 9.61 9.86 9.97 9.90 9.74 9.58 9.50	9.15 9.21 9.27 9.35 9.46 9.53 9.68 9.57 9.49 9.43 9.30	8.96 9.00 9.11 9.16 9.26 9.37 9.50 9.41 9.31 9.23 9.14	3.66 3.40 2.38 1.93 1.91 0.45 4.29 3.99 2.85 1.81 3.04	1.44 0.99 0.11 0.11 0.32 0.41 1.56 0.53 0.21 0.21 0.87	-0.67 -1.32 -1.62 -1.93 -0.02 -1.26 -0.63 -1.16 -1.69 -1.91 -0.87

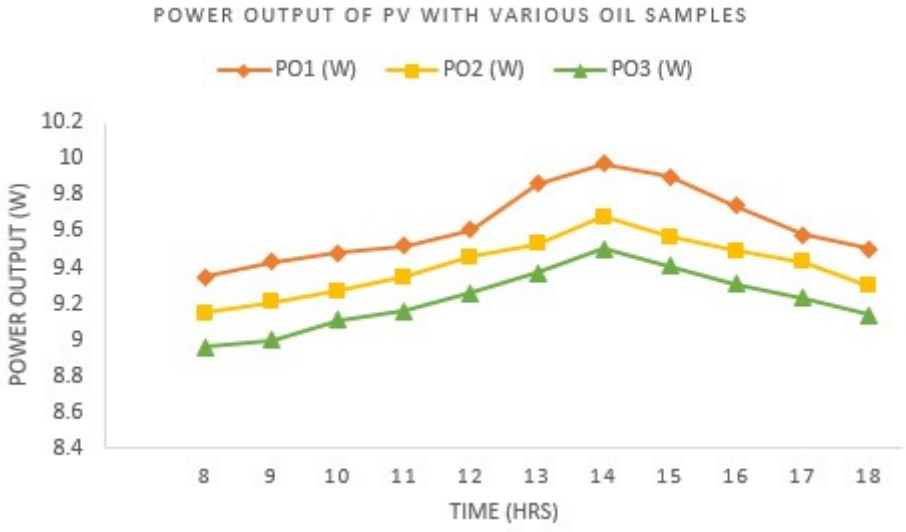

Figure 7: Power output of PV with various oil samples

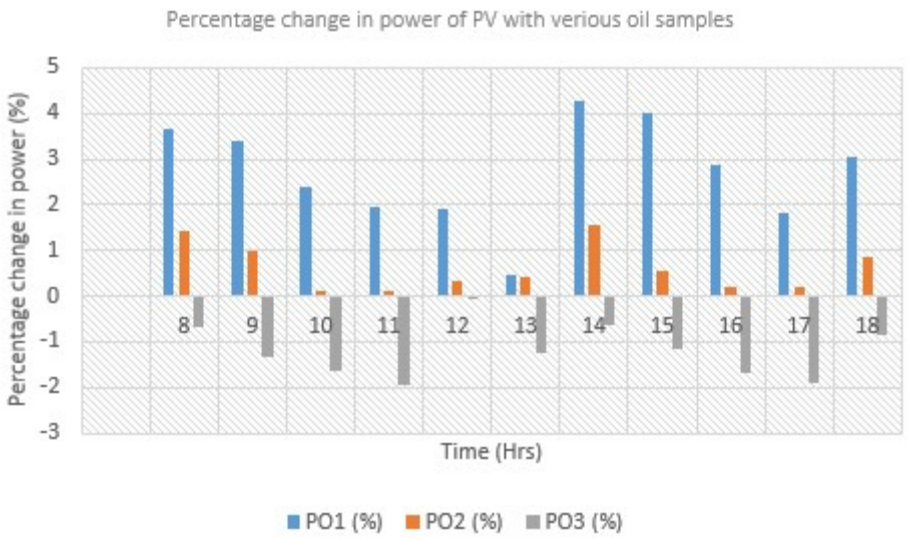

Figure 8: Percentage change in power output of PV with various oil samples

The results, presented in Table 5 and visually detailed in Figures 7 and 8, illustrate the nuanced ef of these oils on the energy conversion efficiency of PV panels. At 8:00 AM, under relatively lo irradiance (225 W/m²) and moderate temperature (31°C), the clean PV panel generated 9.02 W. Applying new oil (O1) increased the output by 3.66% to 9.35 W, attributable to its ability to form thin, uniform layer that enhances light absorption by reducing surface reflection. The halfway-use (O2) increased power output by 1.44% (9.15 W), indicating the retention of some beneficial opti properties. However, degraded oil (O3) slightly decreased the output by 0.67% (8.96 W), likely due impurities and reduced transparency. At midday (12:00 PM), under heightened irradiance (783 W and temperature (36°C), the clean panel produced 9.43 W. New oil (O1) further improved outpu 1.91% to 9.61 W, while halfway-used oil (O2) yielded a marginal increase of 0.32% (9.46 W). The degraded oil (O3) produced a negligible change (-0.02%) at 9.26 W. These results suggest that hig irradiance amplifies the impact of oil properties, with new oil maintaining its advantage while degr oil demonstrates minimal benefit.

At peak irradiance (2:00 PM), under extreme conditions (1250 W/m², 42°C), the clean panel output 9.56 W. New oil (O1) exhibited its maximum effectiveness, enhancing power output by 4.29% to 9. W, underscoring its ability to optimize light absorption during peak sunlight hours. The halfway-u oil (O2) increased output by 1.56% to 9.68 W, while degraded oil (O3) led to a slight decrease of 0.6 (9.50 W), reflecting its diminished efficacy under intense conditions. By 6:00 PM, as irradiance drop to 349 W/m² and temperature decreased to 33°C, the clean panel produced 9.22 W. The new oil maintained a positive impact, increasing output by 3.04% (9.50 W). The halfway-used oil (O2) provi a modest boost of 0.87% (9.30 W), whereas degraded oil (O3) caused a slight reduction of 0.87% (9 W).

New Mobil oil (O1) consistently improved power output across all conditions, with a maximum increase of 4.29% during peak irradiance. This improvement is attributed to its optical properties, as reduced surface reflection and enhanced transmission of sunlight to the PV cells.

The halfway-used oil (O2) exhibited moderate improvements, retaining some of the properties of new oil but with reduced efficacy due to impurities. Degraded oil (O3), characterized by opacity and uneven coverage, generally reduced power output, especially under high irradiance, highlighting its counterproductive impact on PV efficiency.

The observed power changes due to oil coatings (4.29%, 1.56%, and -1.91%) fall within the ±5% po tolerance of the PV panels; however, the consistency and reproducibility of these changes across varying irradiance levels and temperatures strongly suggest that the effects are attributable to t coatings rather than measurement inaccuracies. The instrumentation used, including calibrated power meters and multimeters, ensured high measurement precision, while repeated tests under controlled conditions confirmed the trends. Additionally, while used oil (O2 and O3) may conta contaminants such as metal particles from engine wear, which could affect the optical properties coating, these represent realistic environmental conditions for areas exposed to oil residues.

D. Real-Time Applications

This study has significant implications for real-world scenarios. The findings suggest that applying new or moderately used engine oil to PV panels could serve as an inexpensive, temporary method to enhance performance in areas with less dust or dirt accumulation. For instance, in arid or industrial regions, where frequent cleaning is impractical, such coatings could improve energy yield without requiring advanced maintenance solutions. However, the diminished effectiveness of degraded oil underlines the importance of using clean, high-quality materials to avoid counterproductive results. Furthermore, these insights are valuable for optimizing PV systems in hybrid configurations, such as microgrids, where maintaining high efficiency is critical for balancing energy supply and demand. Policymakers and renewable energy developers can use these findings to develop cost-effective strategies for improving PV performance in challenging environments, ultimately contributing to greater energy security and sustainability.

4. Conclusion

In conclusion, this study demonstrates that applying Mobil engine oil as a coating on photovoltaic (PV) panels can influence power output, with new oil (O1) enhancing performance by up to 4.29%, partially used oil (O2) showing moderate improvements, and degraded oil (O3) leading to slight reductions. These effects are attributed to the optical properties of the coatings, which impact light absorption and reflection. While the observed changes fall within the PV panel's ±5% power tolerance, the consistent trends confirm the coatings' role in modulating performance. This research confirms the potential of thin-film coatings to enhance PV efficiency and underscores the importance of mitigating environmental contaminants like oil and dust that can degrade performance. Future research should investigate the combined effects of oil and particulate matter on PV efficiency under realistic field conditions, explore advanced coatings with self-cleaning or anti-reflective properties, and develop automated maintenance systems to ensure optimal panel performance in diverse environments.

ACKNOWLEDGEMENT

The authors would like to thank the management of Mewar University for providing us with required materials for the conduction of this work.

REFERENCES

[1] H. M. Usman, N. K. Sharma, D. K. Joshi, B. I. Sani, M. Mahmud, S. Saminu, and R. S. Auwal, "Optimization of grid-connected PV systems: Balancing economics and environmental sustainab in Nigeria," Buletin Ilmiah Sarjana Teknik Elektro, vol. 6, no. 3, pp. 237–253, 2024.

[2] H. M. Usman, S. Saminu, and S. Ibrahim, "Harmonic Mitigation in Inverter Circuits Through Innovative LC Filter Design Using PSIM," J. Ilm. Teknol. Elektro Komput. Inf., vol. 10, 2024, Art. no. 28398. doi: 10.26555/jiteki.v10i1.28398.

[3] H. M. Usman, M. Mahmud, M. S. Yahaya, and S. Saminu, "Wind-Powered Agriculture: Enhancing Crop Production and Economic Prosperity in Arid Regions," Elektrika, vol. 16, no. 1, pp. 10-19, 2024

[4] M. Dida, S. Boughali, D. Bechki, and H. Bouguettaia, "Output power loss of crystalline silicon photovoltaic modules due to dust accumulation in Saharan environment," Renew. Sustain. Energy vol. 124, p. 109787, 2020. doi: 10.1016/j.rser.2020.109787.

[5] I. Nayshevsky, Q. Xu, G. Barahman, and A. Lyons, "Fluoropolymer coatings for solar cover glass Anti-soiling mechanisms in the presence of dew," Solar Energy Materials and Solar Cells, vol. 206, 110281, 2020. doi: 10.1016/j.solmat.2019.110281.

[6] M. Rudnicka and E. Klugmann-Radziemska, "Soiling effect mitigation obtained by applying transparent thin-films on solar panels: Comparison of different types of coatings," Materials, vol. 2021. doi: 10.3390/ma14040964.

[7] L. Jones, A. Law, G. Critchlow, and J. Walls, "Comparing fluorinated and non-fluorinated anti-soiling coatings for solar panel cover glass," in 2022 IEEE 49th Photovoltaics Specialists Conferen (PVSC), 2022, pp. 683–683. doi: 10.1109/pvsc48317.2022.9938738.

[8] A. H. Al-Waeli, M. T. Chaichan, H. A. Kazem, K. Sopian, A. Ibrahim, S. Mat, and M. H. Ruslan, "Comparison study of indoor/outdoor experiments of a photovoltaic thermal PV/T system conta SiC nanofluid as a coolant," Energy, vol. 151, pp. 33–44, 2018.

[9] Z. Song, J. Liu, and H. Yang, "Air pollution and soiling implications for solar photovoltaic power generation: A comprehensive review," Appl. Energy, vol. 298, p. 117247, 2021.

[10] Q. Gu, S. Li, W. Gong, B. Ning, C. Hu, and Z. Liao, "L-SHADE with parameter decomposition for photovoltaic modules parameter identification under different temperature and irradiance," Soft Comput., vol. 143, p. 110386, 2023.

[11] M. R. Gomaa, M. Ahmed, and H. Rezk, "Temperature distribution modeling of PV and coolin water PV/T collectors through thin and thick cooling cross-fined channel box," Energy Rep., vol. 8, 1144–1153, 2022.

[12] C. O. Rusănescu, M. Rusănescu, I. A. Istrate, G. A. Constantin, and M. Begea, "The effect of dus deposition on the performance of photovoltaic panels," Energies, vol. 16, p. 6794, 2023.

[13] Q. Gu, S. Li, W. Gong, B. Ning, C. Hu, and Z. Liao, "L-SHADE with parameter decomposition for photovoltaic modules parameter identification under different temperature and irradiance," Soft Comput., vol. 143, p. 110386, 2023.

[14] M. R. Gomaa, M. Ahmed, and H. Rezk, "Temperature distribution modeling of PV and coolin water PV/T collectors through thin and thick cooling cross-fined channel box," Energy Rep., vol. 8, 1144–1153, 2022.

[15] C. O. Rusănescu, M. Rusănescu, I. A. Istrate, G. A. Constantin, and M. Begea, "The effect of dus deposition on the performance of photovoltaic panels," Energies, vol. 16, p. 6794, 2023.

[16] T. Khatib, H. Kazem, K. Sopian, F. Buttinger, W. Elmenreich, and A. S. Albusaidi, "Effect of dust deposition on the performance of multi-crystalline photovoltaic modules based on experimental measurements," Int. J. Renew. Energy Res., vol. 3, pp. 850–853, 2013.

[17] S. A. Kalogirou, R. Agathokleous, and G. Panayiotou, "On-site PV characterization and the effe of soiling on their performance," Energy, vol. 51, pp. 439–446, 2013.

[18] L. Boyle, H. Flinchpaugh, and M. P. Hannigan, "Natural soiling of photovoltaic cover plates an the impact on transmission," Renew. Energy, vol. 77, pp. 166–173, 2015.

[19] B. Laarabi, Y. El Baqqal, A. Dahrouch, and A. Barhdadi, "Deep analysis of soiling effect on glass transmittance of PV modules in seven sites in Morocco," Energy, vol. 213, p. 118811, 2020.

[20] H. A. Kazem, T. Khatib, K. Sopian, and W. Elmenreich, "Performance and feasibility assessmer of a 1.4 kW roof top grid-connected photovoltaic power system under desertic weather conditio Energy Build., vol. 82, pp. 123–129, 2014.

[21] S. A. Said and H. M. Walwil, "Fundamental studies on dust fouling effects on PV module performance," Sol. Energy, vol. 107, pp. 328–337, 2014.

[22] B. R. Paudyal and S. R. Shakya, "Dust accumulation effects on efficiency of solar PV modules fo off-grid purpose: A case study of Kathmandu," Sol. Energy, vol. 135, pp. 103–110, 2016.

[23] M. Senger, A. Kefayati, A. Bertoni, V. Perebeinos, and E. Minot, "Dielectric Engineering Boosts the Efficiency of Carbon Nanotube Photodiodes," ACS Nano, 2021. doi: 10.1021/acsnano.1c02940

[24] M. Pan et al., "Modulating surface interactions for regenerable separation of oil-in-water emulsions," J. Membr. Sci., vol. 625, p. 119140, 2021. doi: 10.1016/J.MEMSCI.2021.119140.

[25] R. Mustafa, M. Gomaa, M. Al-Dhaifallah, and H. Rezk, "Environmental Impacts on the Performance of Solar Photovoltaic Systems," Sustainability, vol. 12, no. 6, p. 608, 2020. doi: 10.3390/su12020608.

[26] M. Mani and R. Pillai, "Impact of dust on solar photovoltaic (PV) performance: research statu challenges and recommendations," Renew. Sustain. Energy Rev., vol. 14, no. 9, pp. 3124-3131, 201

[27] H. Bacosa et al., "From Surface Water to the Deep Sea: A Review on Factors Affecting the Biodegradation of Spilled Oil in Marine Environment," J. Mar. Sci. Eng., 2022. doi: 10.3390/jmse10030426.

[28] M. J. Adinoyi and S. A. Said, "Effect of dust accumulation on the power outputs of solar photovoltaic modules," Renew. Energy, vol. 60, pp. 633-636, 2013.

[29] L. Cristaldi et al., "Economical evaluation of PV system losses due to the dust and pollution," doi:
2012 IEEE Int. Instrum. Meas. Technol. Conf. Proc., 2012, pp. 614-618. 10.1109/I2MTC.2012.6229521.

[30] S. Sanjeev and J. Jayaraman, "Impact of partial shading on the performance of solar PV syster Int. J. Adv. Res. Electr. Electron. Instrum. Eng., vol. 4, no. 1, pp. 374-380, 2015.

[31] R. Pareek, M. Kumbhare, C. Mukherjee, A. Joshi, and P. Gupta, "Effect of oil vapor contamination on the performance of porous silica sol-gel antireflection-coated optics in vacuum spatial filters of high- power neodymium glass laser," Opt. Eng., vol. 47, 2008, Art. no. 023801. doi: 10.1117/1.2844551.

[32] N. Dörr et al., "Correlation Between Engine Oil Degradation, Tribochemistry, and Tribological Behavior with Focus on ZDDP Deterioration," Tribol. Lett., vol. 67, pp. 1-17, 2019. doi: 10.1007/s11249-019-1176-5.

[33] M. Al-Housani, Y. Bicer, and M. Koç, "Assessment of various dry photovoltaic cleaning techniques and frequencies on the power output of CdTe-type modules in dusty environments," Sustainability, vol. 11, no. 10, p. 2850, 2019.

[34] R. Abdallah, E. Natsheh, A. Juaidi, S. Samara, and F. Manzano-Agugliaro, "A Multi-Level Comprehensive Neural Network Model for Maximum Annual Solar Irradiation on a Flat Surface," World Energies, 2020. doi: 10.3390/en13236422.

[35] "Mobil 1™ 5W-30," Mobil, Available: https://www.mobil.co.in/en-in/our-products/oil-lubricants/mobil-1-5w-30

[36] T. Sarver, A. Al-Qaraghuli, and L. L. Kazmerski, "A comprehensive review of the impact of dust on the use of solar energy: History, investigations, results, literature, and mitigation approaches," Renew. Sustain. Energy Rev., vol. 22, pp. 698-733.

Essential Mineral Content Evaluation in Fish Species Consumed in Jazan City, Saudi Arabia

Zeinhom H. Mohamed1*, Mustafa S. Elhassan2, Mukul sharma3, Medhat Mohamed4, Ayyob M. Bakry5, Zeyad M. Ahmed6, Emad M. Masoud7, and Yasser M. Riyad8

[1,2,4,5,6]*Department of Physical Sciences, Chemistry Division, College of Science, Jazan University, P.O. Box. 114, Jazan 45142, Kingdom of Saudi Arabia.*

[3.] *Environment and Nature Research Centre,Jazan University,Jazan 45142,P.O.Box 114, Saudi Arabia.*

[7,8]*Department of Chemistry, Faculty of Science, Islamic University of Madinah, Madinah 42351, Saudi Arabia*

[*]*Correspondence: zmohamed@jazanu.edu.sa*

Abstract: Fish has a high nutritional value since it contains a range of vital metals, making it an important dietary ingredient. Recognizing the levels of essential metals in fish is crucial for preserving consumer health. This study aimed to examine the levels of four essential metals; Sodium (Na), Magnesium (Mg), Potassium (K), and Calcium (Ca), in fish species collected from a fish market in Jazan, Saudi Arabia using Flame Atomic Absorption Spectrophotometer (FAAS). Epinephelus coioides had the highest levels of Mg (1140.0 ± 7.20 mg/kg) and Ca (1842.8± 3.30 mg/kg), while Sphyraena flavicauda and Scomberoides lysan species had the highest levels of K (7729.3±141.66 mg/kg) and Na (1990.8±5.24 mg/kg), respectively. The results showed that the average levels of the minerals studied in fish species were 1402.6±9.05, 706.2±2.86, 5018.9±90.47, and 672.2±4.93 mg/kg for Na, Mg, K, and Ca respectively. Minerals concentrations in fish species declined in the following order: K > Na > Mg > Ca. The obtained results revealed that the average levels of Ca and Mg in all examined fish species were within the FAO's acceptable limits, however, K and Na levels were slightly higher in three species for each element. Additionally, The Na/K ratio was found to be less than one (< 1) in all fish species under investigation. Our results demonstrated that ingesting the selected fish species can support a balanced, healthful diet and may be used to treat hypertension and cardiovascular disease in humans.

Keywords: Essential Minerals Macroelements, Fish species, FAAS, Jazan, Saudi Arabia

تقييم محتوى المعادن الأساسية في أنواع الأسماك المس
مدينة جازان، المملكة العربية السعودية

الملخص: تتمتع الأسماك بقيمة غذائية عالية لأنها تحتوي على مجموعة من المعادن الحيوية، مما ي
غذائيًا مهمًّمًا. يعد التعرف على مستويات المعادن الأساسية في الأسماك أمرًّرًا بالغ الأهمية للحف
دفت هذه الدراسة إلى فحص مستويات أربعة معادن أساسية؛ الصوديوم (*Na*)، والمغنيسيوم (*Mg*)،
ماك التي تم جمعها من سوق الأسماك في مدينة جازان، المملكة (*Ca*) والكالسيوم ،(*K*) والبوتاسيوم
العربية السعودية باستخدام مطياف الامتصاص الذري باللهب (*FAAS*). كان لدى *Plectropomus*
توىات من المغنيسيوم (1140.0 ± 7.20 مجم / كجم) والكالسيوم (1842.8 ± 3.30 مجم *leopardus*
ى مستويات من *Scomberoides lysan* و *Sphyraena flavicauda* كجم)، بينما كان لدى نوعي /
وم (7729.3 ± 141.66 مجم / كجم) والصوديوم (1990.8 ± 5.24 مجم / كجم)، على التوالي. أظهرت
متوسط مستويات المعادن المدروسة في أنواع الأسماك كانت 9.05±1402.6، 2.86±706.2
4.93 ملغ/كغ لكل من الصوديوم والمغنيسيوم والبوتاسيوم والكالسيوم على التوالي، 90.47±5018.9
وانخفضت تركيزات المعادن في أنواع الأسماك بالترتيب التالي: البوتاسيوم < الصوديوم < المغ
الكالسيوم. وكشفت النتائج التي تم الحصول عليها أن متوسط مستويات الكالسيوم والمغنيسيوم ف
الأسماك المدروسة كانت ضمن الحدود المقبولة لمنظمة الأغذية والزراعة، ومع ذلك، كانت مستوي
والصوديوم أعلى قليلاً في ثلاثة أنواع لكل عنصر. بالإضافة إلى ذلك، وجد أن نسبة الصوديوم/
1) في جميع أنواع الأسماك قيد الدراسة. وأظهرت نتائجنا أن تناول أنواع الأسماك المختارة يمكن
أن يدعم نظامًّمًا غذائيًا متوازنًا وصحيًا ويمكن استخدامه لعلاج ارتفاع ضغط الدم وأمراض القلب والأ
لدى البشر .

1. Introduction

The quality of food is becoming increasingly important due to the growing consideration of the health benefits and risks of food consumption [1, 2]. Among the foods consumed in numerous countries is fish [3]. Global fish production increased to 179 million tons in 2018, and each person is thought to consume 20.5 kilograms of fish annually [4]. Recently, fish have received much interest as a food source due to their essential nutrient content that can fulfill a considerable portion of the daily requirements of humans [5].

Fish contains high-quality proteins, carbs, vitamins, micro and macro elements, low fat and cholesterol, and essential fatty acids, including omega 3, constituting a crucial component of a healthy diet [6-9]. Important components of fish muscle include heavy metals, microminerals, and macro minerals. The human body benefits greatly from consuming them through meals. While some macro and microminerals are beneficial to humans and required, others are harmful [10]. Therefore, fish consumption has beneficial health effects, such as a reduction in the incidence of diabetes and cardiovascular diseases, normal neurodevelopment, adequate enzyme reactions in metabolism, and an increase in antioxidant activity [11, 12].As a result, global consumption of fish has been rapidly increasing [13]. The content of essential minerals, especially calcium, phosphorus, magnesium, and potassium is in large quantities in the fish [14]. Many aspects, including age, the organism's nature and production, its relationship to other foods, its mineral consumption, and its growth and nutrition adaption, affect fish's mineral intake [15, 16]. Studies on the mineral elements in living organisms have biological significance since most of these elements are involved in the metabolic processes of the body and are essential for all living beings [17]. The most important mineral elements are calcium, magnesium, potassium, sodium, and phosphorus [18]. The macroelements magnesium, calcium, potassium, and sodium are essential and have a vital role in human health [19], but all elements are harmful at excessive levels [20]. The Na/K ratio is an excellent indicator for preventing or treating hypertension and cardiovascular disease [29]. For example, based on a Chinese cohort study, Du et al. [21] discovered statistically significant associations between the probability of hypertension and sodium intake as well as between the occurrence of hypertension and the sodium to potassium (Na:K) ratio. Kim et al. [22], revealed that the Na:K ratio and urine salt showed a significant correlation with blood pressure. Therefore, it is crucial to determine the level of macroelements in fish species to evaluate the potential advantages and possible negative consequences for consumers' health. The primary goals of the current study were to determine the level of Na, Mg, K, and Ca in six fish species that were collected from fish markets in Jazan City, Saudi Arabia

Ultrapure deionized water produced by a Milli-Q purification system was employed to prepare both standard solutions and the investigated samples. HPLC-grade nitric acid, which was acquired from Sigma-Aldrich, was utilized to prepare the fish sample for analysis. The following standard solutions were acquired from Merck, Germany: 1000 mg/L of Na, Mg, K, and Ca in 0.5% (v/v) HNO_3. All glassware was thoroughly cleaned with MilliQ water, allowed to air dry, and then immersed in 10% HNO_3 for the duration of the night.

2.2. Sample collection, preparation, and digestion

The fish species: Plectropomus leopardus; Atule mate; Sphyraena flavicauda; Scomberoides lysan; Scombridae, and Carangoides bajad used in this study were collected in polystyrene icebo a fish market in Jazan City, Saudi Arabia. After that, the samples were cleaned with deionized wa put in polyethylene bags, and kept at -20 °C until the tests were completed.

The methods outlined in Periago et al. were used to extract the minerals under investigation fro species for analysis from the dorsal muscle tissues[23]. For fish sample digestion, 5g of dry weight carefully weighed into a crucible and then put in a cool muffle furnace for digestion. The tempera of the muffle is progressively increased to 450–500°C and kept there all night. 5 mL of HNO3 w carefully added and mixed after the samples were removed and allowed to cool to room temper Gently evaporate until it's totally dry. To dissolve the ash, carefully boil the liquid after adding 10 m of 1N HCl. The digested samples were then diluted to a final amount of 50 mL using deionized wa After that, the diluted solution was filtered and introduced to FAAS to detect the metals under investigation [24].

2.3. Essential macrominerals analysis

Metal levels were determined using FAAS (nov AA 350, Analytik Jena, Germany) in which acetylene gas and air were used as fuel and oxidizer, respectively. Metals concentrations were determined with the support of calibration curves. Calibrations were done by using standard solutions following the manufacturer's protocol. A hollow cathode lamp of Na, Mg, K, and Ca was employed as a light source at wavelengths 589, 285.2, 766.5, and 422.7 nm and a slit width of 0.8, 1.4, 0.8, and 1.4 nm respectively for analyzing the corresponding metals. A Particular volume of standard stock solution (1000 mg L-1) for each metal was dissolved in acidified MilliQ water to produce new working standard solutions within the appropriate concentration range to generate metal calibration curves.

2.4. Analytical method validation

This study examined validation parameters for analytical procedures based on recommendations from prior studies [25-28]. Validation parameters, such as linearity, accuracy, precision, limit of detection (LOD), and limit of quantification (LOQ), were evaluated. To assess the method's linearity, calibration curves for Na, Mg, K, and Ca were created. The correlation coefficient (R2), slope (S), and intercept (b) were calculated. The method's accuracy was tested using samples spiked with known Na, Mg, K, and Ca standards. Limits of detections (LODs) and limits of quantifications (LOQs) were calculated based on the standard deviation of the response (SD) of the calibration curve and the slope of the curve (S) using Eq. 1 and 2 [29]:

$$LOD = \frac{3 * SD}{S} \quad (1)$$

$$LOD = \frac{10 * SD}{S} \quad (2)$$

3. Results and discussion

3.1. Analytical method validation

The method's applicability for determining the selected metals in fish species was verified using important parameters such as FAAS calibration, linearity, Accuracy (recovery), Limits of detections (LODs), and limits of quantifications (LOQs). Calibrations were done by using standard solutions and shown in Fig. 1. The concentrations of each metal were determined with the support of its calibration curve. Linearity was examined for each element using the correlation coefficient of the corresponding calibration curve. The correlation coefficient (R2) determination was calculated using the least-square analysis and summarized as shown in Table 1. Accuracy was examined for each element studied by computing the Recovery (R%) and summarized in Table 1. The correlation coefficient (R2) values clearly show a good result ranging from 0.997 to 0.999. Recovery values show good results ranging from 97.58 % to 100.25 % falling within the recommended 80 –120% [30].

The accuracy results demonstrated that the analytical method was accurate for the quantification of the investigated minerals in the investigated samples. The samples were examined in triplicate and the relative standard deviation was computed as shown in Table 1. The method's RSD ranged between 0.8 % and 7.1 % as Table 1 indicates. Therefore, it can be stated that the analytical method exhibited good precision based on the obtained RSD values.

These results were also confirmed by the limits of detection (LODs) and limits of quantification (LOQs) as shown in Table 1. The LODs and LOQs values range from 0.035 to 0.899 mg/kg and 0.11 to 2.99 mg/kg, respectively.

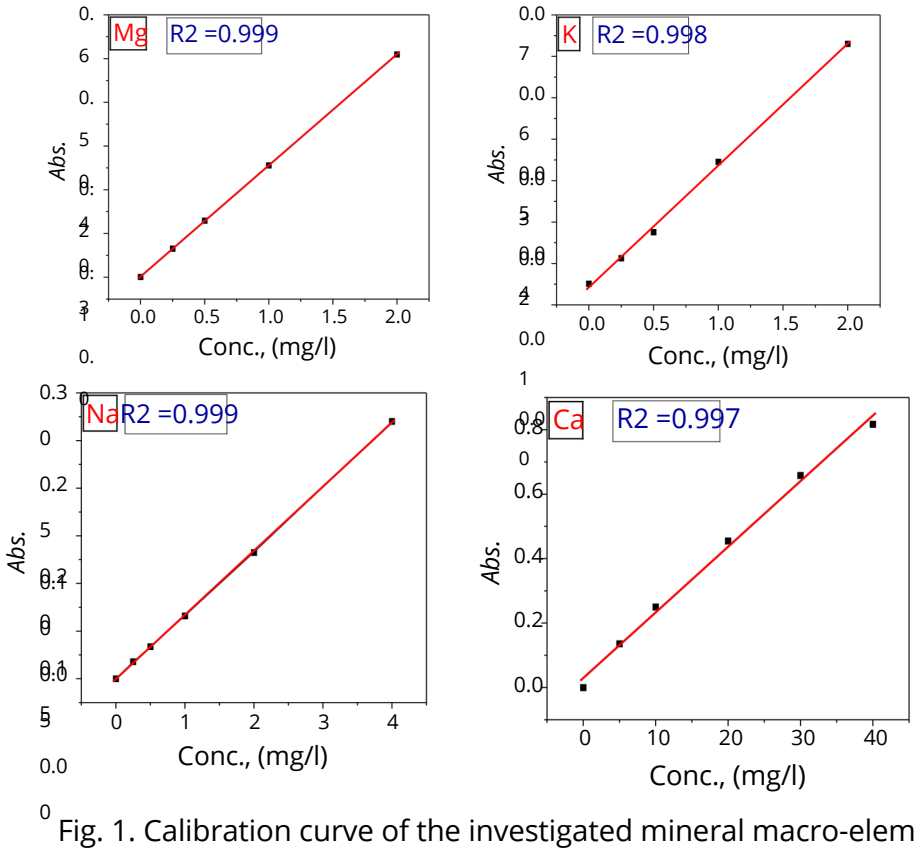

Fig. 1. Calibration curve of the investigated mineral macro-elements

Table 1: Summary of validation parameters; correlation coefficient (R2), Mean recovery (R%), Mean precision, and limits of detection (LODs) and quantification (LOQs) for each studied metal.

Metal	relation coefficientu racy (Recovery)	(Precision (RSD%)	LODs (mg/L)	LOQs (mg/L)
Na 0.999	101.2	0.8	0.899	2.99
Mg 0.999	100.25	1.46	0.035	0.11
K 0.998	97.58	7.1	0.38	1.17
Ca 0.997	98.14	4.01	0.330	1.10

3.2. Essential minerals analysis

The concentration of essential minerals under investigation in fish species (mg/kg dry wt.) is shown in Figure 2. As noted in Figure 2, the current investigation provides information on the level of four metals; Na, Mg, K, and Ca —found in six distinct fish species. In this investigation, The level of the minerals analyzed increased in an ordered sequence: K > Na > Mg > Ca. Potassium had the highest concentration (7729.3 mg/kg) in the Sphyraena flavicauda, whereas Ca had the lowest concentration (259.4 mg/kg) in the Carangoides bajad.

Calcium

Calcium is involved in the strengthening of bones and teeth, blood clotting, and muscle contraction. It is also involved as a cofactor in metabolic and enzymatic processes [31]. Fish is a rich source of this microelement [9]. Calcium levels in the investigated fish species ranged between 259.44 ±3.06 and 1842.81±3.31mg/kg with a mean value of 672.2 mg/kg. Carangoides bajad muscle had the lowest calcium content (259.44 ±3.06 mg/kg) while Plectropomus leopardus species had the highest calcium content 1842.81±3.31mg/kg. All fish species under investigation had calcium content within the permissible limits set by FAO (8810 mg/kg). The Ca values observed in the current study are similar to previous investigations that showed comparable Ca concentrations in fish consumed in Douala, Cameroon (710 mg/kg), and fish from the Northeastern Mediterranean Sea (728.55 mg/kg) [32]. On the other hand, other studies found higher Ca levels in Ethmalosa fimbriata fish (4680.05 mg/kg)[33], fish from marmara sea (8483.78 mg/l)[34]. Conversely, previous investigations found lower Ca levels in Ilisha africana fish from the Cameroon coast (462.78 mg/l) [33], and fish from Manipur, India (93.5-242.5 mg/l) [18].

Magnesium

Magnesium activates more than 300 enzymes in the body and plays a role in energy metabolism, tiredness reduction, nervous system function, and cognitive abilities like focus, reasoning, and memory [27]. Magnesium in large levels can increase the risk of heart disease and stroke [35]. Inadequate magnesium intake can disturb physiological activities, leading to weariness, tension, and muscular diseases. It can also cause dizziness, nausea, and light- headedness, creating a sense of fainting, slowing blood clotting, and causing several diseases, such as osteoporosis, and anemia [9, 28]. Magnesium levels in the investigated fish species ranged between 327.98 ± 0.6 and 1140.97± 7.19 mg/kg with a mean value of 706.23 mg/kg. Atule mate muscle had the lowest magnesium content (327.98 ± 0.6mg/kg) while Plectropomus leopardus species had the highest Mg content (1140.97± 7.19 mg/kg). All fish species under investigation had magnesium content within the permissible limits set by FAO (4520 mg/kg). On the other hand, a previous study found higher Mg levels in fish from the Northeastern Mediterranean Sea (1658.9 mg/l) [32]. Conversely, another one found lower Mg levels in the fish from eastern Poland (97.6-226 mg/l)[36].

Sodium

Sodium is an essential nutrient that regulates blood pressure, balances acids and bases, and supports muscle and nerve function. It plays a vital role in transporting molecules and retaining water [23].

Sodium is involved in the maintenance of normal cellular homeostasis and in the regulation of fluid and electrolyte balance and blood pressure (BP). Its role is crucial for osmotic action and is equally important for the excitability of muscle and nerve cells and the transport of nutrients and substrates through plasma membranes [24].

The excess of sodium causes hypertension, heart failure, decompensated liver cirrhosis, renal failure diseases, chronic kidney disease, and gastric cancer [25]. Sodium deficiency can cause water retention issues, heart, kidney, liver, and hormone diseases, as well as severe neurological issues, including coma [37]. Sodium levels in the investigated fish species ranged between 855.95 ± 5.1 and 1990.75 ± 5.2 mg/kg with a mean value of 1402.61mg/kg. Atule mate muscle had the lowest Sodium content (855.951± 5.1 mg/kg) while Scomberoides lysan species had the highest Sodium content (1990.756 ± 5.2 mg/kg). As shown in Fig. 2 the sodium content in Plectropomus leopardus, Atule mate, and Sphyraena flavicauda fish species was within the permissible limits set by FAO (4520 mg/kg). Conversely, Scomberoides lysan, Scombridae, and Carangoides bajad fish species had sodium content higher than the permissible limits set by FAO. The Na values observed in the current study are similar to a previous study that showed comparable Na concentrations in fish from the Cienfuegos Bay (1301 mg/kg) [38].Other studies found higher Na levels in fish from the Mazurian Great Lakes, Poland (1483-3285 mg/l) [39], and in fish from Red Sea (1800 mg/kg)[5]. Conversely, a previous study found lower Na levels in fish species marketed in Varna (625.24 mg/l)[9].

Potassium

Potassium plays a role in enzyme activation, muscular contraction, osmotic regulation, membrane transfer, maintaining osmotic pressure and acid-base balance, and regulating osmotic pressure within the cell [23]. Excess potassium levels in the blood can lead to life- threatening cardiac rhythm abnormalities. Insufficient potassium intake can cause muscle weakness, paralysis, and respiratory failure [23].

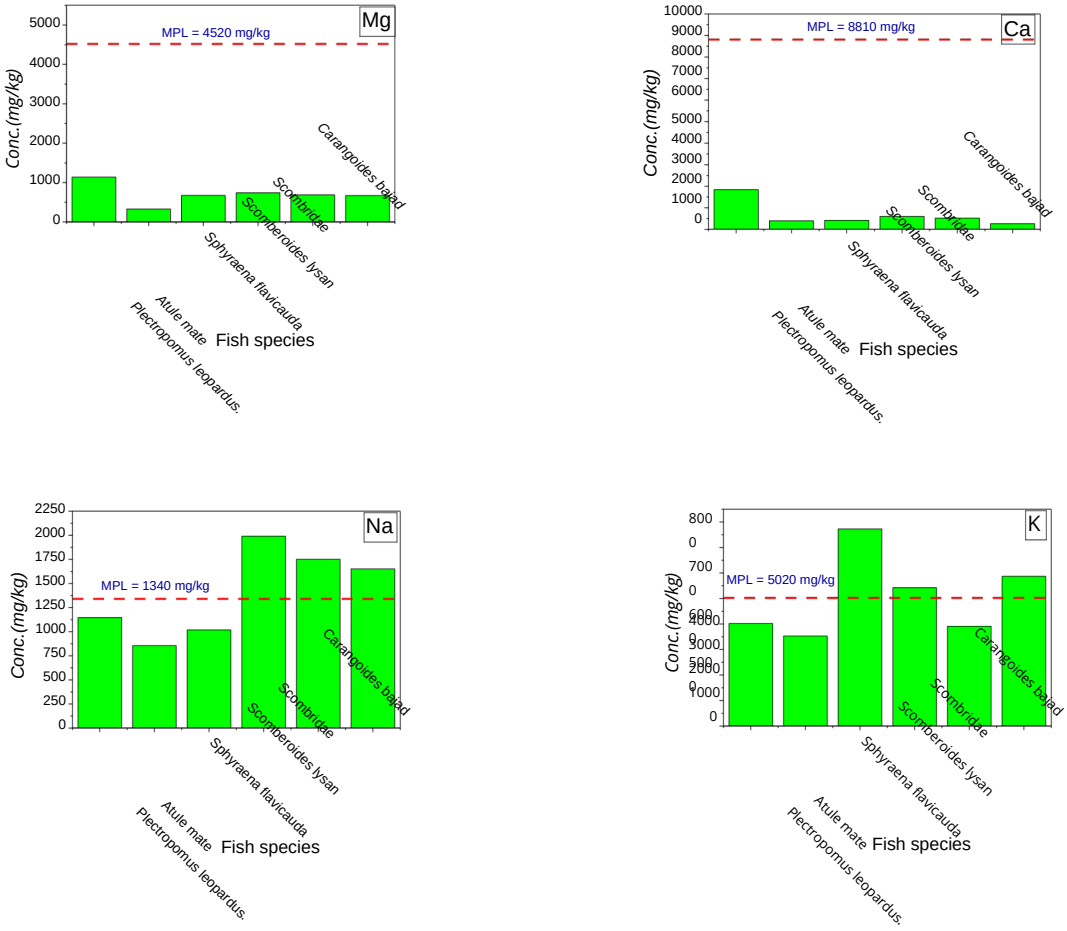

Figure 2. Concentration of essential macro elements under investigation in the selected fish species

Potassium levels in the investigated fish species ranged between 3532.083± 108.67 and 7729.331± 141.66 mg/kg with a mean value of 5081.82 mg/kg. Atule mate muscle had the lowest potassium content (3532.083± 108.67 mg/kg) while Sphyraena flavicauda species the highest potassium content (7729.331± 141.66 mg/kg). Fig.2 indicated that the potass content in Plectropomus leopardus, Atule mate, and Scombridaefish species was within permissible limits set by FAO (4520 mg/kg). Conversely, Sphyraena flavicauda, Scomberoides lysan, and Carangoides bajad fish species had potassium content higher the permissible limits set by FAO. The K values observed in the current study are similar previous study that showed comparable K concentrations in fish species sold in Erzur Turkey (4576 mg/kg) [15]. Another study found higher K levels in fish from the Cienfueg Bay (13246 mg/l) [38]. Conversely, a previous study found lower K levels in Fish from Ma in Okada, Nigeria (91.51-102.86 mg/l)[40], fish species consumed in Douala, Cameroon [4 and fishes from Bangladesh [42].

3.3. Sodium to potassium ratio (Na/K)

Low sodium and high potassium intakes together may have greater effects on blood pressure, hypertension, and associated variables than either nutrient alone [43, 44]. It w reported that any food component that has a Na/K ratio higher than one could provide risks while a ratio less than one suggests that the food item poses no health risks [45]. I 3 shows the calculated Na/K ratio for the fish species under study.

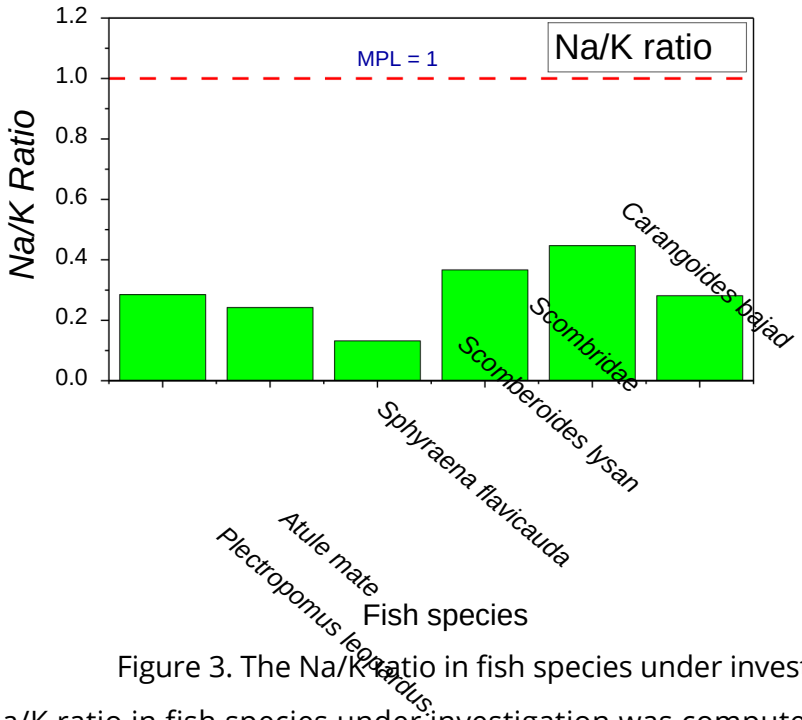

Figure 3. The Na/K ratio in fish species under investigation

The Na/K ratio in fish species under investigation was computed and depicted in Fig.3. As Fig. 3 shows, the Na/K ratio was less than one for all fish species examined in th study. The Na/K ratio observed in the current study is similar to previous investigations showed Na/K ratio was less than one fish species from the Cameroon coast [33], fish consumed in Douala, Cameroon [41], and fishes from Bangladesh [42]. These findings suggest that ingesting fish species is a healthful diet and not harmful to human health.

Conclusion

The current investigation provided information about the level of Na, Mg, K, and Ca in the selected fish species Plectropomus leopardus; Atule mate; Sphyraena flavicauda; Scomberoides lysan; Scombridae, and Carangoides bajad. The level of studied minerals increased in an ordered sequence: K > Na > Mg > Ca. K. Potassium had the highest concentration (7729.3 mg/kg) in the Sphyraena flavicauda, whereas Ca had the lowest concentration (259.4 mg/kg) in the Carangoides bajad. The obtained results revealed that the average levels of Ca and Mg in all examined fish species were within the FAO's acceptable limits, however, K and Na levels were slightly higher in 50% of fish species. Additionally, The Na/K ratio was less than one (< 1) in all fish species under investigation. The study findings demonstrated that ingesting the selected fish species can support a balanced, healthful diet and may be used to treat hypertension and cardiovascular disease in humans.

References

[1] D. R. V. Abadi et al., "Comparative investigation of heavy metal, trace, and macro element contents in commercially valuable fish species harvested off from the Persian G Environmental Science and Pollution Research, vol. 22, pp. 6670-6678, 2015.

[2] Micheline, C. Rachida, M. Céline, K. Gaby, A. Rachid, and J. Petru, "Levels of Pb, Cd, Hg and As in fishery products from the Eastern Mediterranean and human healt assessment due to their consumption," International Journal of Environmental Research 13, pp. 443-455, 2019.

[3] Ozyilmaz, A. Demirci, D. B. Konuskan, and S. Demirci, "Macro minerals, micro minerals, heavy metal, fat, and fatty acid profiles of European hake (Merluccius merluc Linnaeus, 1758) caught by gillnet," J Entomol Zool Stud, vol. 5, no. 6, pp. 272-5, 2017.

[4] C. À. LA, S. A. ET, and À. L. N. DE TOUS, "La Situation Mondiale des Pêches et de L'aquaculture," 2016.

[5] Al Solami and M. Korish, "Proximate composition, fatty acid characteristics, amino acid profile and mineral content of fish Acanthurus sohal," Heliyon, vol. 10, no. 2024.

[6] A. Kandyliari, S. Karavoltsos, A. Sakellari, P. Anastasiadis, M. Asderis, N. Papandroulakis and M. Kapsofefalou, "Trace metals in six fish by-products of two farm fishes, the gilthead sea bream (Sparus aurata) and the meager (Argyrosomus regius): Interactions with the environment and feed," Human and Ecological Risk Assessment: International Journal, vol. 27, no. 4, pp. 1126-1146, 2021.

[7] S. Barroso, F. R. Pinto, A. Silva, F. G. Silva, A. M. Duarte, and M. M. Gil, "The circular economy solution to ocean sustainability: Innovative approaches for the blue

economy," in Research Anthology on Ecosystem Conservation and Preserving Biodiversi IGI Global, 2022, pp. 875-901.

[8] Ravanbakhsh, A. Z. Javid, M. Hadi, and N. J. H. Fard, "Heavy metals risk assessment in fish species (Johnius belangerii (C) and Cynoglossus arel) in Musa Estua Persian Gulf," Environmental Research, vol. 188, p. 109560, 2020.

[9] Stoyanova, "Investigation of macroelements in the muscle of four marine fish species," International Journal of Fisheries and Aquatic Studies, vol. 6, no. 2, pp. 219-22 2018.

[10] E. Whithney and S. Rolfes, "Understanding Nutrition (11th Edn. For international student adition)," ed: USA, 2008.

[11] Merciai, C. Rodríguez-Prieto, J. Torres, and M. Casadevall, "Bioaccumulation of mercury and other trace elements in bottom-dwelling omnivorous fishes: the case of Di sargus (L.)(Osteichthyes: Sparidae)," Marine pollution bulletin, vol. 136, pp. 10-21, 2018.

[12] Lounas, H. Kasmi, S. Chernai, N. Amarni, L. Ghebriout, and B. Hamdi, "Heavy metal concentrations in wild and farmed gilthead sea bream from southern Mediterra Sea—human health risk assessment," Environmental science and pollution research, vo pp. 30732-30742, 2021.

[13] Fisheries, "The state of world fisheries and aquaculture. 2006," 2007.

[14] Fawole, M. Ogundiran, T. Ayandiran, and O. Olagunju, "Proximate and mineral composition in some selected fresh water fishes in Nigeria," Internet Journal of Food Sa vol. 9, pp. 52-55, 2007.

[15] Karataş, "Comparison of micro and macro element contents of commercial fish species sold in the Erzurum province," Eastern Anatolian Journal of Science, vol. 7, no. 2, 16-22, 2021.

[16] E. Tchounwou, C. G. Yedjou, A. K. Patlolla, and D. J. Sutton, "Heavy metal toxicity and the environment," Molecular, clinical and environmental toxicology: volume environmental toxicology, pp. 133-164, 2012.

[17] Kawarazuka and C. Béné, "The potential role of small fish species in improving micronutrient deficiencies in developing countries: building evidence," Public health nutrition, vol. 14, no. 11, pp. 1927-1938, 2011.

[18] Jhei and C. Sarojnalini, "Proximate composition, macro and micro mineral elements of some smoke-dried hill stream fishes from Manipur, India," Nature and Scie vol. 10, no. 1, pp. 59-65, 2012.

[19] Ersoy and M. Çelik, "Essential elements and contaminants in tissues of commercial pelagic fish from the Eastern Mediterranean Sea," Journal of the Science of Food and Agriculture, vol. 89, no. 9, pp. 1615-1621, 2009.

[20] C. H. Walker, R. Sibly, and D. B. Peakall, Principles of ecotoxicology. CRC press, 2005.

[21] S. Liu, A. Neiman, C. Batis, H. Wang, B. Zhang, J. Zhang and B. M. Popkin, "Understanding the patterns and trends of sodium intake, potassium intake, and sodi potassium ratio and their effect on hypertension in China," The American journal of clin nutrition, vol. 99, no. 2, pp. 334-343, 2014.

[22] K. Kim, K. Kim, M.-H. Shin, D. H. Shin, Y.-H. Lee, B.-Y. Chun and B. Y. Choi, "The relationship of dietary sodium, potassium, fruits, and vegetables intake with bl pressure among Korean adults aged 40 and older," Nutrition research and practice, vol. 4, pp. 453-462, 2014.

[23] J Periago, MD Ayala, O López-Albors, I Abdel, C Martínez, A García-Alcázar, G Ros, F Gil, "Muscle cellularity and flesh quality of wild and farmed sea bass, Dicentrarchu labrax L," Aquaculture, vol. 249, no. 1-4, pp. 175-188, 2005.

[24] A. International, Official methods of analysis of the Association of Official Analytic Chemists. Association of official analytical chemists, 1970.

[25] J. Olmedo, A. Pla, A. Hernández, O. López-Guarnido, L. Rodrigo, and F. Gil, "Validation of a method to quantify chromium, cadmium, manganese, nickel and lea human whole blood, urine, saliva and hair samples by electrothermal atomic absorpt spectrometry," Analytica Chimica Acta, vol. 659, no. 1-2, pp. 60-67, 2010.

[26] M. Thompson, S. L. Ellison, and R. Wood, "Harmonized guidelines for single-laboratory validation of methods of analysis (IUPAC Technical Report)," Pure and applie chemistry, vol. 74, no. 5, pp. 835-855, 2002.

[27] I. H. T. Guideline, "Validation of analytical procedures: text and methodology," Q2 (R1), vol. 1, no. 20, p. 05, 2005.

[28] R. S. Perelonia, K. C. D. Benitez, R. J. S. Banicod, G. C. Tadifa, F. D. Cambia, and U. M. Montojo, "Validation of an analytical method for the determination of cadmiu lead and mercury in fish and fishery resources by graphite furnace and Cold Vapor Ato Absorption Spectrometry," Food Control, vol. 130, p. 108363, 2021.

[29] A. Shrivastava and V. B. Gupta, "Methods for the determination of limit of detecti and limit of quantitation of the analytical methods," Chron. Young Sci, vol. 2, no. 1, pp. 2 25, 2011.

[30] D. Harvey, Modern analytical chemistry. McGraw Hill, 2000.

[31] R. Djama et al., "Effect of smoking, boiling and freezing on the nutritional value of three species of genus Pseudotolithus commonly consumed in Cameroon," Food Chem vol. 363, p. 130229, 2021.

[32] A. Gülcü, D. Ayas, A. Köşker, and K. Yatkin, "The Investigation of metal and mineral levels of some marine species from the Northeastern Mediterranean Sea," Journal of Marine Biology and Oceanography, vol. 3, no. 2, p. 2, 2014.

[33] M. Manz, J. Nsoga, J. Diazenza, S. Sita, G. Bakana, A. Francois, R.A. Dama, M. Ndomou, C.S.M. Milong, M.N. Nchoutpouen, M.T. Youogo, R.P.N. Ndômbôl, F.V.J. Nsoga, C. Ngo Tang, and I. Gouado, "Nutritional composition, heavy metal contents and lipid qu of five marine fish species from Cameroon coast," Heliyon, vol. 9, no. 3, 2023.

[34] A. Dökmeci, "Concentrations of different macro and trace elements in sediment and fish samples from the coast of tekirdag marmara sea," Fresenius Environmental Bul vol. 30, no. 02A, pp. 1902-15, 2021.

[35] S. Rosique-Esteban, M. Guasch-Ferré, P. Hernández-Alonso, and J. Salas-Salvadó, "Dietary magnesium and cardiovascular disease: a review with emphasis in epidemiolog studies," Nutrients, vol. 10, no. 2, p. 168, 2018.

[36] E. Flyz-Lukasik and A. Chalabis-Mazurek, "Content of macro-and microelements in the muscles of grass carp, bighead carp, Siberian sturgeon and wels catfish from eas Poland," Journal of Elementology, vol. 24, no. 1, 2019.

[37] R. M. Reynolds, P. L. Padfield, and J. R. Seckl, "Disorders of sodium balance," Bmj, vol. 332, no. 7543, pp. 702-705, 2006.

[38] M. Peña-Icart & E. Rodrigues Pereira-Filho & L. Lopes Fialho & J. A. Nóbrega & C. Alonso-Hernández & Y. Bolaños-Alvarez & A. Muñoz-Caravaca & M. S. Pomares-Alfonso, "Study of macro and microelements in fish from the Cienfuegos Bay. Relationship with content in sediments," Environmental monitoring and assessment, vol. 189, pp. 1-15, 20

[39] J. Łuczyńska, E. Tońska, and M. Łuczyński, "Essential mineral components in the muscles of six freshwater fish from the Mazurian Great Lakes (northeastern Poland)," Fisheries & Aquatic Life, vol. 17, no. 4, pp. 171-178, 2009.

[40] S. Adeniyi, C. L. Orjiekwe, J. Ehiagbonare, and S. Josiah, "Nutritional composition of three different fishes (Clarias gariepinus, Malapterurus electricus and Tilapia guineens Pakistan Journal of Nutrition, vol. 11, no. 9, p. 793, 2012.

[41] K. J. Christophe, Y. T. Marlène, N. V. J. François, N. N. Merlin, G. Inocent, and N. Mathieu, "Assessment of cooking methods and freezing on the nutritional value and h risks of heavy metals in four fish species consumed in Douala, Cameroon," Heliyon, vol. no. 7, 2024.

[42] Selim Reza , S.M. Rashadul Islam , Md. Rakibul Hasan , Debabrata Karmakar , Farzana Mim , Md. Aftab Ali Shaikh , Md. Rezaul Karim, "Unlocking critical nutritional potential: A comprehensive analysis of small indigenous fishes in Bangladesh and the development of ready-to-use fish products as balanced food," Future Foods, vol. 9, p. 10 2024.

[43] L. Sacks, "Effects on blood pressure of reduced dietary sodium and the Dietary Approaches to Stop Hypertension (DASH) diet," New England journal of medicine, vol. 344, no. 1, pp. 3-10, 2001.

[44] R. Group, "Intersalt: an international study of electrolyte excretion and blood pressure. Results for 24 hour urinary sodium and potassium excretion," BMJ: British Me Journal, pp. 319-328, 1988.

[45] S.-Y. Bu, M.-H. Kang, E.-J. Kim, and M.-K. Choi, "Dietary intake ratios of calcium-to-phosphorus and sodium-to-potassium are associated with serum lipid levels in he Korean adults," Preventive nutrition and food science, vol. 17, no. 2, p. 93, 2012.

Numerical Study of Blast-Induced Primary Injury in Mosques: Identifying High-Risk Zones and Structural Implications

Ahmed M. Bagabir

Faculty of Engineering, Jazan University, Jazan, KSA

abagabir@yahoo.com

Abstract: The present study employed numerical simulations to investigate the impact of blast waves on people praying inside a mosque. The study also investigated the influence of the location and intensity of the explosion. The inviscid Euler equations were solved numerically using a finite volume method. Dynamic mesh adaptation to coarse initial cells has proven suitable for predicting qualitative and quantitative flow features. It was assumed that explosives of different TNT equivalent weights (1.5kg, 2.5kg, and 5kg) would be detonated deliberately in two locations in the mosque: at the front and in the center. This is the weight of a typical pipe bomb or suicide explosive belt that can be carried maliciously. The flow visualizations are analyzed using a schlieren image. The time history of overpressure is monitored at several locations inside the mosque. The results reveal that the impact of explosions on the eyes, lungs, and brain varies depending on the location of the mosque. Blast waves from confined-space explosions are intensified by reflective surfaces. Individuals praying at the front and center of the mosque are assumed to be the primary targets and are more susceptible to inevitable death. However, those praying close to the reflective walls, particularly near the corners of the mosque, are at risk of primary injury due to the repeated reflections of the blast waves. The current findings will prove invaluable in the design of effective safety measures to mitigate the impact of explosions on people.

Keywords: Blast-structure interaction, CFD, compressible flow, injury prediction, numerical analys

دراسة عددية للإصابات الألأولية الناجمة عن الانفجارات المساجد: تحديد المناطق عالية الخطورة والآثار البنيوية

الملخص: استخدمت الدراسة الحالية محاكاة عددية للتحقيق في تأثير موجات الانفجار على المص المسجد. كما بحثت الدراسة في تأثير موقع وشدة الانفجار. تم حل معادلات أويلر غير اللزجة عد طريقة الحجم المحدود. أثبت التكيف الشبكي الديناميكي للخلايا الألأولية الخشنة أنه مناسب للت النوعية والكمية. افترض أن المتفجرات ذات الألأوزان المكافئة المختلفة لمادة تي إن تي)1.5 كج و5 كجم(سيتم تفجيرها عمدًا في موقعين في المسجد: في المقدمة وفي المنتصف. هذا هو وزن نموذجية أو حزام ناسف انتحاري يمكن حمله بخبث. يتم تحليل تصورات التدفق باستخدام صورة مراقبة التاريخ الزمني للضغط الزائد في عدة مواقع داخل المسجد. تكشف النتائج أن تأثير الانفج والرئتين والدماغ يختلف حسب موقع المسجد. يتم تكثيف موجات الانفجار من الانفجارات في بواسطة الألأسطح العاكسة. يُفُفُترض أن الألأفراد الذين يصلون في مقدمة ووسط المسجد هم الأ أكثر عرضة للموت الحتمي. ومع ذلك، فإن أولئك الذين يصلون بالقرب من الجدران العاكسة، وخا من زوايا المسجد، معرضون لخطر الإصابة الألأولية بسبب الانعكاسات المتكررة لموجات الانف الحالية قيمتها في تصميم تدابير السلامة الفعالة للتخفيف من تأثير الانفجارات على الناس.

1. Introduction

When high-level explosions occur, a significant amount of energy is released and this triggers the propagation of a blast wave that spreads outward. The resulting overpressure, which is characterized by a positive pressure rise, is linked to the initial blast wave created by the explosion. As this blast wave continues to expand, the positive phase is eventually followed by a decrease in pressure and the emergence of a negative wave. The duration of the positive phase is dependent on the amount of energy released and the distance from the center of the explosion [1]. The global prevalence of terrorist attacks has increased from five thousand in 2007 to more than sixteen thousand in 2020 [2]. Mosques are the most vulnerable to suicide attacks by terrorist groups that pose a serious threat to human life, security, property, and buildings [3, 4].

When a blast wave interacts with surrounding structures, it creates a reflected wave that amplifie the overpressures [5, 6, 7]. This interaction between the blast and structure can significantly comp the evolution of the blast wave [5, 6, 7, 8]. The confined explosion is a phenomenon that trigge series of shock-focusing events. These events, known as regular and Mach reflections, occur du interactions between two or more waves [5, 9]. As a result of these interactions, high-pressure z are created, which can have significant implications for the surrounding environment [5]. These pressure zones can cause damage to structures and other objects in the vicinity and can be a concern. Therefore, understanding the mechanics of shock-focusing events is crucial for predictin impact of confined explosions and mitigating any potential risks. It has been found that explosion occur in proximity to structures can have devastating effects. The shock waves from the blast can and increase the pressure near the structures by two to nine times [10]. Research has prove explosions that are confined in a specific area cause greater loss of human lives and destruction compared to explosions that are out in the open [10-13].

In the unfortunate event of an explosion, the blast overpressure is felt by the human body. As th pressure wave reaches the body, it encounters resistance and some of it is reflected, whereas the transmitted through the body. This causes a sudden and violent physical movement that can lead displacement, distortion, or even tearing of the medium, such as organs, and tissues. It is worth n that these injuries occur without any visible blunt force injury or penetrating injury, making them more dangerous and difficult to detect [14, 15]. Blast injury is a unique condition that has a h mortality and morbidity rate. There are different types of blast injuries, including primary, terti secondary, and quaternary injuries [14, 15]. Primary blast injuries (PBIs) happen when the energy a blast wave passes through the body and causes damage to the tissues. This damage can occur i that have a significant density change, such as the lungs, brain, and ear canals, even if there ar external signs of injury [14-16]. PBIs can be caused by spallation, implosion, and shearing inju mechanisms [17]. PBIs can cause immediate or delayed effects, ranging from mild to life-threate [17]. However, the severity of PBIs depends on factors such as the size of the explosive, duratio overpressure, and proximity to solid structures [14]. It is possible to sustain single or multiple b injuries at once, depending on the intensity and duration of the explosion [17, 18]. For instance closer one is to the center of the explosion, the higher the chances of severe injuries. The distance the center of the explosion also plays a role in the severity of injuries. A probe located three me away from the explosion experiences nine times greater overpressure than a probe located six m away [10].

It was found that terrorism-related explosions result in unique injuries and increased mortality compared to those caused by non-terrorism-related explosions [19]. It is essential to seek medical attention immediately after experiencing a blast injury, regardless of its severity. Delayed symptoms may manifest, such as respiratory distress, chest pain, and abdominal discomfort [17]. Timely medical intervention can improve the chances of recovery and minimize long-term complications.

When it comes to preventing primary blast injuries (PBIs), it is important to have accurate predicto of the minimum effective overpressures (thresholds) that can cause them. During the analysis significant to observe limits to ensure that loading conditions are clinically relevant, realistic, a practical even though many experimental loading conditions are achievable [20]. Whereas mul injury criteria have been used for this purpose, it is worth noting that the occurrence of PBIs ca influenced by other factors as well. Human orientation and proximity to solid structures, for exar can significantly impact PBI risk, resulting in injuries occurring at overpressures that are either be or above the expected threshold [20]. This information comes from a recent study by Denny *et al*. which provides valuable insights into the complex nature of PBI risk. By considering these factors assessing PBI risk and developing appropriate safety measures, one can better protect individuals harm and reduce the risk of PBIs occurring in explosive events. It is imperative to consider the devastating impact of blast overpressure on the human body, particularly on the auditory sys Because the ear is the most sensitive organ, the most common injuries following exposure to overpressure are those affecting the ear [21]. Even a blast wave with a relatively low overpressure of 35 kPa can rupture the eardrum and cause damage to the middle ear [21, 22]. This is a ser concern, as the eardrum is an essential component of the human ear, responsible for transmittin waves to the brain. Furthermore, it has been shown that exposure to overpressure levels of 103 k 202 kPa respectively can increase the risk of eardrum rupture by up to 50% and 100% [21, 22].

When high explosives are detonated, primary blast lung injury is the most common cause of deat particularly, in confined spaces [16, 17]. When an explosion occurs, the overpressure can cause hemorrhage in the alveoli of the lungs, leading to a lack of oxygen and suffocation, which can ultir result in acute respiratory distress syndrome [16, 23, 24]. Even a small 100-gram hand grenade cause fatal lung injury [25]. A peak overpressure of 689 kPa-1,379 kPa is considered potentially let [11]. Practicing doctors have proposed a lung injury score to classify the severity of acute respira distress syndrome based on medical diagnosis [16]. The brain, being the most important organ i human body, is particularly vulnerable to injury from exposure to excessive pressure. Such injurie cause significant damage and lead to long-term cognitive and behavioral impairments, even resu in death in some cases [18, 26] Therefore, it is crucial to ensure that the brain is adequately prot and not exposed to extreme pressure to avoid such severe consequences. Additionally, it is impo to consider that the effects of blast overpressure are not solely physical. On the other hand, the of the gastrointestinal tract can suffer damage in the face of such an event [27]. Contusions and ru may harm the eyeball and lead to poor visual outcomes [28]. Furthermore, concussion can mar even in the absence of obvious physical signs of head injury [29].

The task of determining the effect of strong blast waves on humans is a challenging one that requ laboratory experiments [7]. It is more feasible to achieve blast waves with positive phase duratio 2-10 ms experimentally; However, conducting such experiments is not always possible due to sa and ethical concerns that need to be addressed [20].

As a result, computational fluid mechanics (CFD) has emerged as a useful tool for evaluating the risk of blast injuries and mitigating their effects. This approach involves simulating the complex behavior of fluids and gases in response to explosive events. By analyzing these simulations, one can gain a better understanding of the physics underlying confined explosions, which are known to be particularly hazardous. By using CFD, one can make accurate predictions about the pressure and blast waves generated by explosive events, as well as their effects on the human body. This knowledge can pave the way for the development of more effective safety measures that can protect people from blast injuries and prevent catastrophic outcomes [23].

The present research addresses a critical research gap by focusing on the dynamics of confine explosions within mosque structures, which has received limited attention despite its relevance to safety and counterterrorism efforts. Existing studies on blast effects primarily focus on open spac general urban environments, often neglecting the unique architectural and spatial characterist mosques. These structures, with their high levels of occupancy and reflective surfaces, pose dis challenges in blast propagation and injury prediction. By employing CFD to simulate explosions a assess PBIs, this study provides essential insights into the heightened risks in confined spaces. results of the study are of immense significance because they provide valuable insights into the in mechanisms that govern blast wave propagation and their impact on human bodies. Expanding th emphasis on these distinctive contributions could enhance its significance to a broader audience, including architects, urban planners, public safety officials, and policymakers. Bridging this knowle gap is crucial for informing targeted safety measures, architectural improvements, and emerg response strategies in vulnerable community spaces.

The following four main sections offer an in-depth analysis and detailed insights into the researc process. The section on test case definition lays the foundation for the subsequent research, whe research methodology section provides a thorough overview of the methods used. The simul results section presents data-driven insights and analysis, and the final section on conclusions recommendations offers valuable suggestions for future research.

2.Problem definition

In the present study, a mosque building that covers an area of 600 m2 (30 m2 □ 20 m2) is considered.

The confined building is shown in Fig. 1. It is important to note that there is only one entrance gate

located in the middle of the back wall. Additionally, there are two emergency exit doors situated on the side walls. The gate and exit doors are treated as solid walls, as they remain closed at all times. The mosque is capable of accommodating up to 720 prayers that are distributed in 12 rows. The mosque has four columns with a diameter of 60 cm that are crucial to the structural integrity of the building. These columns provide necessary support to the mosque. However, in the model, these columns were not taken into account as their impact on the overall design was considered insignificant. As the building is symmetric around the y-axis, the simulation can be performed for half of the domain. Thus, the centerline is set as a symmetrical boundary whereas the other sides are set as wall conditions, as depicted in Fig. 1.

As mentioned previously, it is expected that the location and amount of explosions will cause varying damage. Explosives of different TNT equivalent weights, 1.5 kg, 2.5 kg, and 5 kg, are deliberately detonated in two locations in the mosque, in the front row of prayers, and in the mid the mosque. The two explosion locations, indicated by a large circle in Fig. 1, are chosen based previous suicide terrorist incidents that occurred in mosques [3].

The weight of 1.0 kg - 3.0 kg resembles to pipe bomb that can be carried maliciously in a carrying case [12, 30]. A TNT package weighing 5.0 kg is the typical weight of a suicide belt [30, 31]. It is worth mentioning that the energy released from one kilogram of TNT equivalent could demolish a small vehicle [30]. The blast wave parameters are estimated at a 0.5m stand-off distance using empirical formulas [1, 32]. The ambient conditions are 1.225 kg/m3,1atm, and 20 oC, for density, pressure, and temperature, respectively. Blast overpressure histories are monitored to estimate the PBIs at six probe locations (A, B, C, D, E, and F) around the mosque as presented in Fig. 1.

3.Computational methodology

The present study employs computational fluid dynamics (CFD) to simulate the explosion and the consequent transient blast wave propagation. The finite volume method using Ansys Fluent is used to
solve Euler's equations, which can be written in matrix form and the two curvilinear co-ordinates,
and , as:

$$\frac{\partial U}{\partial t}+\frac{\partial F}{\partial \quad}+\frac{\partial \quad}{\partial \quad}=0 \qquad (1)$$

where F represents the inviscid fluxes, t is time, and U is the conservative variables:

$$U \quad = \quad u, v, e)^T, \qquad (2)$$

where is the density, u and v are the velocity components, and e is the total energy per unit

The pressure, p, is calculated by the ideal gas equation of state based on internal energy, i:

$$p \quad = \quad (\quad - \quad 1 \quad) \quad i \qquad (3)$$

The explosion flow is simulated as an ideal gas, which has a specific heat ratio, , of 1.4 and a constant of 287 J/kg.K.

The rationale for using the two-dimensional (2D) model is that this approach captures the essenti interactions of blast waves with reflective surfaces and structural boundaries, which are critica understanding injury risks and overpressure patterns. The 2D model exploits the symmetry o mosque layout, ensuring accurate results while reducing computational complexity. By using simplified model, the study efficiently explores multiple blast scenarios and intensities, providing insights into high-risk zones and structural vulnerabilities. Ultimately, while 3D models provide additional detail, the 2D approach is sufficient to identify broad patterns in blast dynamics and implications [5, 6].

A second-order scheme is adopted to estimate the compressible spatial flow. An explicit first-orde scheme is used to estimate the transient terms. A structured quadrilateral mesh with an initial s 45,600 cells is used to solve the half-domain. Dynamic mesh adaptation is used to refine the mes to three times wherever the density gradients exceed 5% of the local normalized value.
On the other hand, the mesh becomes coarse where the density gradient is below 2%. By refining in regions with significant density gradients, the approach captures critical phenomena such as s focusing and wave interactions without overburdening computational resources.

Higher mesh refinements were also considered, but the triple mesh refinement ensures a precise balance between accuracy and computational efficiency. The results, which are not shown in the manuscript, clearly show that the resolution is independent of the mesh. Limiting the refinement to three levels avoids diminishing returns in accuracy while maintaining reliable results.

4. Results and discussion

A. *BLASTVISUALIZATION*

This section presents numerical schlieren snapshots that showcase the propagation of explosions inside a confined mosque building. These snapshots are based on the density gradient magnitude and depict the salient features of blast wave interactions and reflections. The intentional explosions took place in two locations, the front row of prayers and the center of the mosque. The explosives of varying weights of TNT equivalent (1.5 kg, 2.5 kg, and 5 kg) are detonated, which results in identical explosion patterns. However, there are differences in the time scale and intensity of the explosion. Therefore, only one numerical schlieren snapshot of each explosion location will be demonstrated. The numerical schlieren of a blast in the front row of prayers and the center of the mosque are illustrated in Figs. 2 and 3, respectively. These snapshots illustrate the evolution of explosion propagation, reflection, implosion, interaction, and diffraction.

The first snapshot of Fig. 2 reveals a striking phenomenon in the aftermath of the front explosion. As the primary incident wave, I, reaches the center of the mosque (probe B), followed by a series of pressure waves that explode in all directions. It is interesting highlight the shock-focusing phenomenon. Of particular interest is the Mach reflection causes the creation of a new Mach stem, M [5, 9]. This stem connects the triple intersec point, TP, of the incident wave segment, I, and the reflected wave segment, R, as displaye Fig.2. The TP also connects with the contact surface, CS. What's noteworthy about the M stem wave, M, is that it has a higher pressure than the incident wave, I. As the blast prog it becomes evident that the front cavity of the mosque, where the leader of prayers (in usually stands, is filled with blast waves, as depicted in Fig.2. In the second snapshot, Mach stem, M, grows and reaches probe D located next to the front corner of the mosq

When the Mach stem, M, reflects off the sidewall, it creates shock focusing, a phenomen that involves two-wave interactions known as regular reflection [5, 9]. The point where M stem, M, and reflected wave, R, converge moves along the sidewall towards the back w whereas keeping the two waves together, as shown in the third frame of Fig. 2. The area the regular reflection intersects is also a high-pressure zone [5].

It is important to note that when the explosion charge is larger, the regular reflection transforms into Mach reflection as it progresses along the solid structure [5, 9]. In this scenario, waves are being reflected and moving towards the center of a mosque. These reflected waves, R, are interacting with secondary waves, S, that are heading in the oppo direction.

This is shown in the third and fourth frames. In the fourth snapshot of Fig. 2, the crest of the incident blast wave reaches probe C at the closed main gate on the back wall. A compression wave, which accumulates secondary waves and reflected waves from the front wall or the cavity, moves behind the main incident wave. The last two snapshots of Fig. 2 depict the incident wave reflecting from the back wall and heading toward the frontal side of the mosque. Additionally, two waves reflected from the side wall head toward the center of the mosque. It can be observed that the reflected wave moves faster within the core of the explosion because of the higher sound speed in this region. It is worth noting that the last snapshot of Fig. 2 shows the creation of a new triple point, TP, for the two waves reflected from the back wall and the Mach stem, M, moving forward along the sidewalls.

Fig. 3 illustrates the development of the flow field resulting from the central explosion. Two cylindrical waves, caused by the incident and compression, exploded in a roughly symmetrical manner. These waves interacted with each other and with the low-density of the explosion after reflecting from the solid walls of the mosque. The first snapshot o 3 shows the incident blast wave arriving at the location of probes A and C, which are positioned on the front and back walls, respectively.

The second snapshot depicts the arrival of the incident wave sidewalls followed by the explosive pressure waves. It can also be observed that the explosion almost filled the im place in the front cavity of the mosque. The second snapshot of Fig. 3 also shows the ref incident waves from the front and back walls. These waves nearly approach the center o explosion in the third and fourth snapshots. Regarding the sidewalls, the incident wave segments reflected from them creep toward the center of the mosque, and the seconda head toward them as shown in Fig. 3. It is noteworthy that for a blast wave initiated at center of the mosque, the shock focusing type is regular reflection. Therefore, the typ reflection of the shock-focusing events is dependent on the distance of the explosion ch from the solid structure [5, 9]. The closer the explosive charge is to the solid surface, the the Mach stem dominates the entire incident wave [5].

Mosque-confined explosion configurations for structure-to-wave and wave-to-wave interactions are well-defined in the illustrated evolution of explosions. As expected, the f field inside the mosque becomes increasingly complex over time. The cavity produces m wave interactions and reflections. There is a phenomenon that researchers have been in in, which is the development of a complex flow structure around the sharp corners of th cavity due to the diffraction of blast waves [33].

This phenomenon occurs for both blast locations. Moreover, bubbles of light-density air can be observed around the core of the explosions. The onset of Richtmyer-Meshkov instability is caused by the sudden acceleration of gases with varying densities, resulting in the continuous deformation that occurs in the core of the explosion [6].

In conclusion, this subsection highlights the complex dynamics of the propagation and reflection of the blast waves in the confined environment of the mosque. Both frontal central explosions revealed shock-focusing phenomena, particularly at reflective surface corners. In frontal explosions, Mach reflection led to the formation of high-pressure zon corners, while central explosions displayed widespread regular reflections due to symm wave interactions. These findings emphasize the need for structural designs that mini sharp corners and reduce reflective surfaces to mitigate amplified pressure zones caus these interactions.

B. DATA OF PROBES (OVERPRESSURES)

Table 1 provides a clear and concise overview of the recorded peak overpressure, P, and positive phase duration, D, at probes for varying blast intensities for the frontal and central explosions. The table serves as an informative reference for the given blast intensities. They are essential in understanding the nature and impact of the detonations on the risk of primary blast injuries (PBIs). It is noted that the peak overpressure increases with the increase in the intensity of the explosion, but the duration of the positive phase does not adhere to this rule, see Table 1. According to the data collected by the probes, the peak overpressures are ranked from most to least for both the frontal and central explosions. This information is indicated in Fig. 4, which provide a visual representation of the recorded data. For the front explosion, the highest peak overpressure is observed in the probes A, D, F, E, B, and C, whereas for the center explosion, it is observed in the probes B, D, F, C, E, and A, as presented in Fig. 4. Additionally, the data show that after the center of the explosion, the highest overpressure is recorded in the corners of the mosque for both frontal and central explosions.

The central explosion generates a significantly higher peak overpressure on the mosqu corner probe D, as displayed in Fig. 4. Surprisingly, this effect remains true even though explosion is farther away than the frontal one. This can be attributed to regular reflec which can have a significant impact on overpressure levels [5]. This indicates that the interaction of blast waves generates higher overpressure than a single traveling wave, ev cases where it is the Mach stem that generated the overpressure peak at the corner pro the frontal blast. This highlights the importance of understanding the complexities of b waves and their interactions, which can have significant implications for safety and des considerations. It has been found that in the case of the mosque front explosion, the overpressure adjacent to the middle of the sidewall (probe E) surpasses probe B in the c of the mosque, even though probe E is nearly 8 meters further away from the center o explosion than probe B. These findings are applicable to all blast intensities. A critical fac to consider is that placing the probe close to the sidewall exposes it to the high-pressure of the moving Mach stem [5].

In conclusion, this subsection presents trends in peak overpressure and positive phase duration across multiple probe locations for varying blast intensities. The results show that peak overpressure increases with proximity to the blast epicenter and intensity of the explosion, but the duration of the positive phase varies with location and reflection dynamics. For frontal explosions, probes near corners (e.g., D and F) experienced high overpressure due to wave reflections, whereas central explosions exhibited a more uniform distribution of overpressure across the mosque. These trends are crucial for predicting injury severity, as areas with prolonged positive phases or amplified overpressure are associated with higher risks of injuries.

PRIMARY BLAST INJURIES (PBIs)

Denny and his colleagues [11] created a graphical tool to estimate the likelihood of PBIs. tool is visualized in Fig. 5 and displays the various zones of relevant blast loading conditi through solid and dashed lines. The graphical presentation provides a clear and compre way to analyze and predict the risk of such injuries. The graph shows the threshold for blast injury for a 70 kg person standing close to a solid wall. It also displays the probabili death for 1%, 50%, and 99% based on previous studies by Bowen [23] and van der Voor *al*. [25]. It has been shown that the severity of lung (pulmonary) injuries depends on the overpressure and the duration of the positive phase caused by an explosion [23, 25]. dependency of lung injury risk on the duration of a blast decreases, as depicted in Fig Conversely, the occurrence of eardrum rupture [21, 22] and 50% mild brain hemorrhage remains unaffected by the duration of the positive phase of the blast, as presented in F Notably, overpressure thresholds of 144 kPa can result in a 50% risk of mild brain hemo [26].

The graphical representation provides a comprehensive and visually intuitive representation to assess the initial PBIs [11]. The graphical representation of predicted overpressures for different blast intensities within the mosque building is critical in asse the risk of PBIs. The markers on the graph shown in Fig. 5 indicate the expected PBI risk the predicted peak overpressure at each gauge location, which is calculated based o simulations conducted in this study. Fig. 5 illustrates these results, providing a clear concise visual representation of the data of probes A, B, C, D, E, and F. These findings w undoubtedly contribute to the development of effective measures that can help redu chances of PBIs and improve the safety of prayers in similar structures. The safety of pra present in the mosque is of utmost importance. To ensure that, predicted risks of PBI carefully considered at two explosion locations, the first row of prayer and the center o mosque. It is important to note that the peak overpressures for the front and center exp are represented on the chart in Fig. 5 by the use of hollow and filled markers, respectiv This visual aid provides a quick and easy way to understand the data presented. Blast overpressure can have a severe impact on the human body.

It has been observed that the auditory system is susceptible to damage from blast overpressure, regardless of the duration of the positive phase. This is demonstrated by the eardrum rupture threshold of 35 kPa [21, 22]. This highlights the importance of protecting the auditory system during high-pressure situations. The onset of complete eardrum rupture occurs at approximately 205 kPa [23, 25]. The literature has not yet specified the blast overpressure threshold for brain hemorrhage. However, it is indicated a 50% risk of mild brain hemorrhage at approximately 145 kPa, as depicted in Fig. 5 [29].

To shed light on the PBIs resulting from a frontal explosion, it is alarming to note that ev
a less severe explosion of 1.5 kg could lead to certain death for those located near prob
and F, as shown in Fig. 5. The risk is higher for probe F, which is 7 meters away from t
epicenter as compared to probe D. This is because of its location at the corner of the mo
which makes it vulnerable to the interaction of two reflected shocks.

These reflected shocks increase the peak overpressure and pose a significant threat to h
life. There are concerns about the safety of those who pray near probes A and E due to s
PBIs, as displayed in Fig. 5. Several potential injuries include total eardrum rupture, 50
lethality from lung injury, and a 50% chance of mild brain hemorrhage for all blast intens
It has been observed that probe E, located at a distance of 18.03 meters from the center
explosion, experiences the same level of injuries as probe A, which is only 1.25 meters a
from the center of the explosion. This can be attributed to the fact that probe E was subj
to a longer duration of the positive phase, which is more than 6 times longer than that a
A, despite the peak overpressure at probe A being twice that of probe E, as presented in
5. Probes B and C indicate that the PBI risk is the lowest for explosives that weigh betwe
2.5 kg and 5.0 kg placed at the front of the mosque. Prayers, in this case, have a 50% ris
eardrum rupture and a 1% risk of death from lung injury. Fig. 5 illustrates that a low-inte
explosion weighing 1.5kg poses the same 50% risk of eardrum rupture as more intense
explosions. However, in comparison, it poses less than 1% risk of death due to lung injur
depicted in Fig. 5.

The blast at the center of the mosque results in the detection of primary blast injuries
(PBIs). It is crucial to note that those who are praying at the location where probe B is sit
are exposed to a deadly peak overpressure, regardless of the intensity of the explosion.
Furthermore, individuals who are praying in the locations, where probes C, E, and F a
located, are at serious risk of lung injury and death due to excessive peak overpressure
presented in Fig. 5. The intensity of the blast has a different impact on the prayers at poi
as the explosions of weights 2.5 kg and 5.0 kg at the center of the mosque lead to 10
eardrum rupture, 50% lethality from a lung injury, and 50% mild brain hemorrhage. The
overpressure from a 1.5 kg explosion can cause 50% mild brain damage, 50% ruptu
eardrum, and 1% death due to lung injury, as displayed in Fig. 5.

The data clearly indicate that probe A is the safest location at 11.25 meters from the epicenter of the explosion. Whereas the higher two blasts can cause significant eardrum rupture and lung injuries, the minimum peak pressure of 1.5 kg has only a minor impact on prayers. However, probe C, located at the same distance as A, but near the back wall, suffered more serious injuries. This can be attributed to the location's proximity to the back wall, resulting in a higher peak overpressure. This highlights the importance of location in protecting oneself during such events. Based on the results, it is recommended that one should aim to avoid being close to any walls to minimize the risk of injury.

In conclusion, the subsection assesses the risk of PBIs based on the overpressure data different probe locations for frontal and central explosions. In frontal explosions, probes the epicenter (A) and reflective surfaces (D and F) had the highest injury risks, including l rupture, eardrum rupture, and brain hemorrhage. Conversely, in central explosions, pr at the detonation epicenter showed the most extreme overpressure, resulting in near-c fatality regardless of blast intensity. Peripheral probes like E and C also faced significa injury risks due to prolonged positive phases. These findings stress the importance of identifying high-risk zones within confined spaces to guide safety protocols and evacua planning.

D. *COMPARISON OF BLAST SCENARIOS: FRONTAL VS. CENTRAL EXPLOSIONS*

Two primary blast scenarios are investigated, frontal explosions (detonated in the front of the mosque) and central explosions (detonated in the middle of the mosque). Each sc exhibits distinct blast-wave propagation dynamics and injury risk profiles, influenced by location of the detonation relative to structural boundaries and occupants. This section provides a detailed comparison of frontal and central blast scenarios. It explores the distribution patterns of the overpressure generated by each type of blast, examining ho patterns differ in terms of intensity and area affected. It also analyzes the dynamics of reflection in various environments are analyzed, highlighting how the direction and pow the blast interact with surrounding structures. Furthermore, the risk of PBI associated each scenario is assessed, considering the potential injuries that could result from expos different levels of overpressure. Finally, the implications for safety measures that shoul implemented in response to each type of blast are discussed.

In the frontal explosion scenario, the highest peak overpressure was recorded at probe (1.25 meters from the explosion), with values up to 447 kPa for the 5.0 kg TNT equivale However, these effects were spatially localized due to the short positive phase duration ms). High overpressure levels were also observed at probes D and F near the corners, d by shock-wave reflections from solid walls. In contrast, the central explosion generated a uniform distribution of overpressure across the mosque, with probe B at the epicenter experiencing an extreme overpressure of 6837 kPa (5.0 kg TNT equivalent). Corner prob and F also recorded substantial overpressures (602–604 kPa), reflecting a more widesp impact due to wave interactions and prolonged positive phases.

Frontal explosions primarily endangered individuals close to the detonation and reflective surfaces. For example, probe A experienced the highest risk of PBIs due to the proximity to the explosion, including lung and eardrum injuries, although the short positive phase provided some mitigating effects. Corners D and F saw amplified injury risks due to Mach stem formation and wave reflections. Central explosions posed more widespread threats, with probe B indicating certain fatality risks for individuals at the epicenter, regardless of blast intensity. Peripheral probes such as E and C also showed increased risks due to prolonged wave interactions and higher overpressures compared to their counterparts in the frontal explosion scenario.

The differences in outcomes underscore critical considerations for safety planning. Fron explosions exhibit higher localized risk near the front row and reflective surfaces, necessitating attention to the design of corners and proximity to walls. Central explosi however, result in more extensive overpressure distribution, emphasizing the importar structural reinforcements and protective measures across the entire mosque layout. Em planning should prioritize evacuation routes that avoid high-risk areas like corners and c rows while considering the dynamics of each blast scenario to optimize protective strate

In conclusion, this comparison highlights that while frontal explosions are more predictable in terms of injury localization, central explosions demand broader mitiga efforts due to their extensive impact range. Future architectural designs and safety mea should account for these distinctions to effectively reduce blast-related casualties in con spaces.

5. conclusion

The paper emphasizes the critical need for measures to protect individuals from the harmful effects of blast waves, especially in high-risk environments like mosques. The findings of the study are useful for those interested in assessing and mitigating risks associated with explosions, as well as clinicians who need to determine safe limits for injuries caused by blast loads. The research utilized computational fluid dynamics to investigate explosions that occurred inside a confined mosque. The explosions are caused by the detonation of 1.5, 2.5, and 5.0kg TNT bombs, and they took place in the front and center of the mosque.

The interaction between the blast and the structure of the mosque significantly complicated th evolution of the blast wave. The history of overpressures is recorded at various locations aroun mosque. In fact, the shock focusing on the interaction of two or more waves creates regions of high pressure and temperature which can lead to various issues. As such, it is crucial to be aware phenomenon and take appropriate measures to mitigate its effects. The probe placed close sidewall is undoubtedly exposed to the high-pressure region of the moving Mach stem, which significantly impacts the primary blast injuries (PBIs). The location closest to the explosion cente poses the highest risk of injury or death, even with a TNT package weighing as little as 1.5 kg. No the sidewalls record high overpressure with long wave duration due to reflection. However, the co of the mosque (probes D and F) have the second-highest peak overpressure. Based on the res findings, it can be concluded that those who pray adjacent to the solid walls, especially near the co of the mosque, are at the highest risk of PBIs.

For the frontal explosion, although the peak overpressure is the highest at probe A, the short du of its positive phase makes it uncertain whether prayers located there will survive or not.

Raising awareness among the public, engineers, and healthcare professionals about the potent health impacts of explosions is vital for preventing tragic events and enhancing preparedness. Numerical simulations play a critical role in identifying high-risk buildings and informing safer architectural designs. The study's findings underscore the importance of minimizing reflective sur and sharp corners in mosque designs to reduce pressure amplification and associated risks. Str placement and proper sizing of emergency exits are essential to facilitate efficient evacuations in occupancy spaces. Furthermore, public education initiatives should focus on raising awareness a blast-related risks and protective measures, while emergency response agencies can leverage insights to improve disaster planning and preparedness. By integrating these recommendations, communities can enhance the safety of gathering places like mosques and better protect indivi from the devastating effects of confined explosions. Another important consideration in architec planning is human behavior during emergency evacuations. To ensure an effective evacuation pla large groups, it is important to carefully design the location and size of emergency exits [34, 3 Emergency response agencies should use this data to improve disaster education and response p minimize morbidity and mortality in the event of a terrorist attack.

Future research should explore confined explosions in diverse environments, such as schools, transportation hubs, and public gathering spaces, to generalize findings and refine safety meas Incorporating human response modeling would provide valuable insights into the dynamic beha of individuals during emergency scenarios, enabling the development of more effective evacua plans and injury mitigation strategies. Additional studies could also investigate the effects of va structural designs and materials on blast-wave propagation to propose safer architectural practic

REFERENCES

[1] C. Kingery, and G. Bulmash "Airblast parameters from TNT spherical air burst and hemispheric surface burst," Technical report ARBL-TR-02555, April 1984

[2] START (National consortium for the study of terrorism and responses to terrorism). Global ter database 1970-2020. [Online]. Available: https://www.start.umd.edu/gtd/

[3] Wikipedia, List of terrorist incidents in Saudi Arabia. [Online]. Available: https://en.wikipedia.or wiki/List_of_terrorist_incidents_in_Saudi_Arabia

[4] B. Roggio "Pakistani Taliban kills scores in mosque bombing in Peshawar". FDD's Long War Jou (30 January 2023). [Online]. Available: https://www.longwarjournal.org/archives/2023/01/pakis taliban-kills-scores-in-mosque-bombing-in-peshawar.php

[5] A. Bagabir "Cylindrical blast wave propagation in an enclosure," *Shock Waves*, vol. 22, no. 6, pp. 556, 2012. DOI:10.1007/s00193-012-0406-7

[6] A. Bagabir, and D. Drikakis "Shock wave induced instability in the internal explosion," *The Aeronautical Journal*, vol. 109, no. 1101, pp. 537-556, 2005. DOI:10.1017/S0001924000000890

[7] J. Denny, G. Langdon, S. Rigby, A. Dickinson, and J. Batchelor "A numerical investigation of blas structure interaction effects on primary blast injury risk and the suitability of existing injury pr methods," *Int. J. Prot. Struct*., vol. 15, no. 1, pp. 1-20, 2024. DOI:10.1177/20414196221136157

[8] K. Gault, I. Sochet, L. Hakenholzm, and A. Collignon "Influence of the explosion center on shoc propagation in a confined room," *Shock Waves*, vol. 30, pp. 473-481, 2020. DOI:10.1007/s00193 00946-z

[9] A. Bagabir, A. Abdulrahman, and A. Balabel "Shock-wave diffraction over single and double wedge *Emirates Journal of Engineering*, vol. 12, no. 2, pp. 53-66, 2007.

[10] A. R. Loflin, and C. E. Johnson "A review of current safe distance calculations and the risk of mild traumatic brain injury," *Shock Waves*, vol. 34, no. 4, pp. 303-314, 2024. DOI.10.1007/s00193-024-01197-y

[11] J. Denny, A. Dickinson, and G. Langdon "Defining blast loading 'zones of relevance' for primary blas injury research: a consensus of injury criteria for idealized explosive scenarios," *Medical Engineerin and Physics*, vol. 93, pp. 83-92, 2021. DOI:10.1016/j.medengphy.2021.05.014

[12] I. Kokkinakis, and D. Drikakis "Internal explosions and their effects on humans," *Physics of Fluids*, vol. 35, no. 4, 046101, 2023. DOI: 10.1063/5.0146165

[13] P. Peters "Primary blast injury: An intact tympanic membrane does not indicate the lack of a pulm blast injury," *Mil. Med*., vol. 176, no. 1, pp. 110-114 (2011). DOI:10.7205/milmed-d-10-00300.

[14] M. Westrol, C. Donovan, and R. Kapitanyan "Blast Physics and Pathophysiology of Explosive Injurie DOI:10.1016/ *Annals of Emergency Medicine*, vol. 69, no. 1, pp. S4-S9, 2017. j.annemergmed.2016.09.005

[15] J. Wightman and S. Gladish "Explosions and blast injuries," *Ann. Emerg. Med*., vol. 37, no. 6, pp. 664 678, 2001. DOI:10.1067/mem.2001.114906

[16] T. E. Scott, A. M. Johnston, D. D. Keene, M. Rana, and P. F. Mahoney "Primary blast lung injury: The 2020. military experience," *Military Medicine*, vol. 185, no. 5/6, pp. 568, DOI:10.1093/milmed/usz453 J. Bukowski, C. Nowadly, S. Schauer, A. Koyfman, and B. Long

[17] "High risk and low prevalence diseases: Blast injuries," *American Journal of Emergency Medicine*., vol. 70, pp. 46-56, 2023. DOI:10.1016/j.ajem.2023.05.003 W. C. Moss, M. J. King, and E.G. Blackman "Skull flexure from blast waves: a mechanism for brain injury with

[18] implications for helmet design," *Physical Review Letters*, vol. 103, no. 10, 108702. DOI:10.1103/PhysRevLett.103.108702 A. Matthew, B. Tovar, A. Rebecca, B. Pilkington, M. Tress Goodwin, M. Jeremy and M. Root "Pediatric blast trauma: a systematic review and

[19] meta-analysis of factors associated with mortality and description of injury profiles," *Prehosp Disaster Med*., vol. 37, no .4, pp. 492-501, 2022. DOI: 10.1017/S1049023X22000747. J. Denny, A. Dickinson, and G. Langdon "Guidelines to inform the generation of clinically relevant and realistic blast loading conditions for primary blast injury research," *BMJ Military*

[20] *Health*, vol. 169, no. 4, pp. 364-369, 2023. DOI:10.1136/bmjmilitary-2021-001796 P. Acosta "Overview of UFC 3-340-02 structures to resist the effects of accidental explosions," *In Structures Congress 2011*, American Society of Civil Engineers, pp.1454-1469, 2011. J. Jensen,

[21] and P. Bonding "Experimental pressure induced rupture of the tympanic membrane in man," *Acta Otolaryngol*, vol. 113, no. 1-2, pp. 62-67, 1993. I. Bowen, E. Fletcher, and D.

[22] Richmond "Estimate of man's tolerance to the direct effects of air blast," Lovelace Foundation for Medical Education and Research, Albuquerque, NM, USA, 1968.

[23] DOI:10.21236/ad0693105 G. van Haesendonck, V. van Rompaey, A. Gilles, V. Topsakal, and P. van de Heyning "Otologic outcomes after blast injury: The Brussels bombing experience," *Otol. Neurotol*, vol. 39, no. 10, pp. 1250-1255, 2018. DOI:10.1097/MAO.0000000000002012

[24] M. van der Voort, K. Holm, P. Kummer, J. Teland, J. van Doormaal, and H. Dijkers "A new standard for predicting lung injury inflicted by Friedlander blast waves," *Journal of Loss Prevention in the Process Industries*, vol. 40, pp. 396-405, 2016. DOI:10.1016/j.jlp.2016.01.014

[25] H. Huang, B. Xia, L. Chang, Z. Liao, H. Zhao, L. Zhang, and Z. Cai "Experimental study on intracranial pressure and biomechanical response in rats under the blast wave," *Journal of Neurotrauma*, vol. 41, no. 5-6, pp. 671-684, 2024. DOI:10.1089/neu.2022.0229.

[26]

[27] R. Guy, and N. Cripps “Abdominal trauma in primary blast injury,” *Br. J. Surg*., vol. 98, no. 2, 1033-1033, 2011). DOI:10.1002/bjs.7268 Y. Zhang, X. Kang, Q. Wu, Z. Zheng, J. Ying and M-N.
[28] Zhang “Explosive eye injuries: characteristics, traumatic mechanisms, and prognostic factors for poor visual outcomes,” *Military Medical Research*, vol. 10, no. 3, 2023. DOI:10.1186/s40779-022-00438-4 K. Rafaels *et al*. “Brain injury risk from primary blast,”
[29] *Journal of Trauma Acute Care Surgeon*, vol. 73, no. 4, pp. 895-901, 2012. DOI:10.1097/TA.0b013e31825a760e FEMA 425 “Risk assessment - A How-To Guide to
[30] mitigate potential terrorist attacks against buildings,” Risk Management Series, FEMA, Department of Veterans Affairs, USA, 2005. Wikipedia, Explosive belt. [Online]. Available:
[31] https://en.wikipedia.org/wiki/Explosive_belt M. Stewart “Simplified calculation of airblast
[32] variability and reliability-based design load factors for spherical air burst and hemispherical surface burst explosions,” *International Journal of Protective Structures*, vol. 13, no. 4, 2021. DOI: 10.1177/20414196211043537 A. Bagabir “Comparison of compression and blast
[33] waves diffraction over 90° sharp corner,” *Aljouf University Science and Engineering Journal*, vol. 3, no. 2, pp. 10-20, 2016.
[34] M. Barth, K. Palm, H. Andersson, T. Granberg, A. Gullhav, and A. Kruger “Emergency exit layout planning using optimization and agent-based simulation,” *Computational Management Science*, vol. 21, no. 1, 2024. DOI:10.1007/s10287-023-00482-y H. Kurdi, Sh.
[35] Al-Megren, R. Althunyan, and A. Almulifi “Effect of exit placement on evacuation plans,” *European Journal of Operational Research*, vol. 269, pp. 749-759, 2018.

Table 1: Peak overpressure (P) and positive-phase duration (D) at probes for the frontal and ce explosions.

Explosion	Probe	Distance (m)	1.5 kg		2.5 kg		5.0 kg	
			P (kPa) 365	D (ms) 2.9	P (kPa) 423	D (ms) 2.4	P (kPa) 447	D (ms) 2.6
Frontal	A	1.25	112	7.3	143	12.5	149	12.7
	B	8.75	114	19.2	127	24	132	17.5
Frontal	C	18.75	326	10.3	383	12.2	399	10.9
	D	15.05	199	13.2	234	13.4	249	13.5
Frontal	E	17.37	295	18.6	323	20	333	20
	F	24.01	94	10	106	20.7	112	21.6
Frontal	A	10.0	5407	0.6	6837	0.6	5891	0.6
	B	0.0	255	20.1	300	13	325	11.6
Frontal	C	10.0	458	13.5	563	13	602	13.9
	D	18.3	176	11.4	210	11.5	236	10.7
Frontal	E	15.0	459	13.5	563	13	604	13.9
	F	18.3						
Central								
Central								
Central								
Central								
Central								
Central								

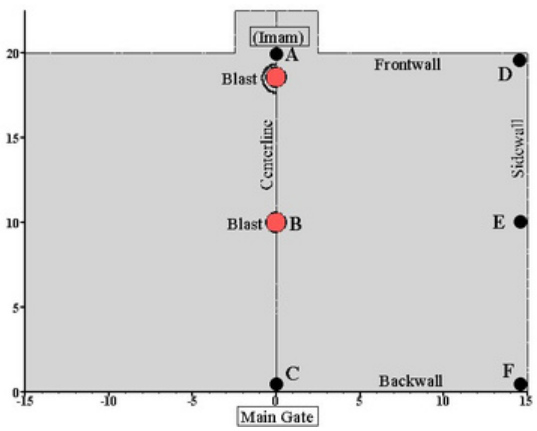

Fig. 1: Layout of the mosque showing the boundary conditions and assigned probe locations.

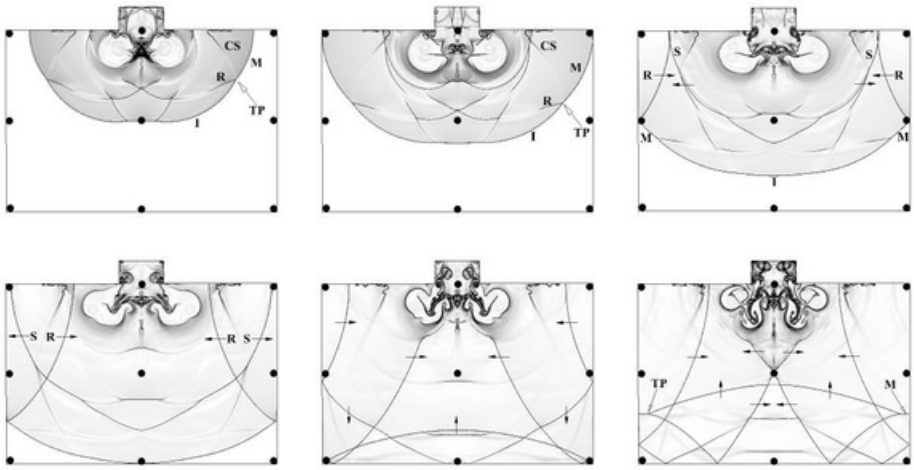

Fig. 2: Schlieren patterns for the propagation of the frontal-mosque explosion; black dots indica
probes. Incident wave, I; reflected wave, R; contact surface, CS; Mach stem, M; triple point, TP;
secondary wave, S.

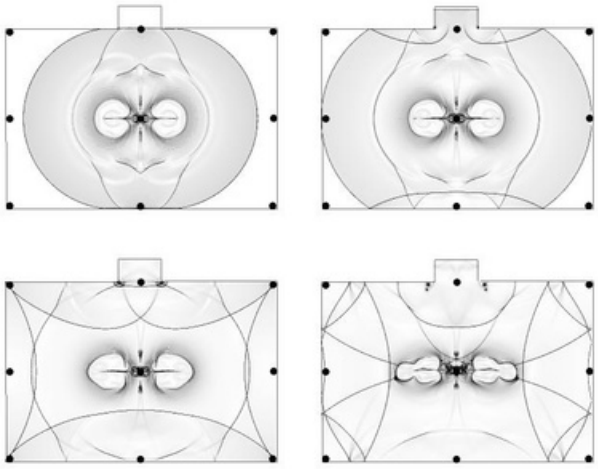

Fig. 3: Schlieren patterns for the propagation of central-mosque explosion; black dots indicate pr

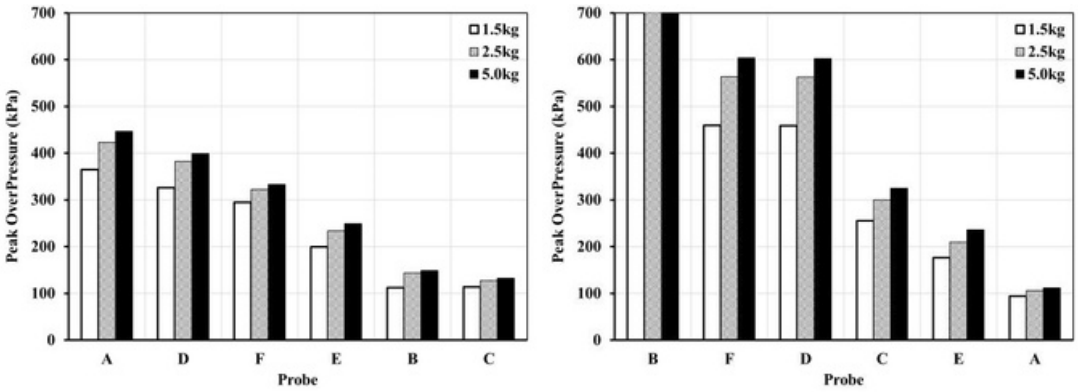

Fig. 4: Peak overpressure (arranged highest to lowest) at the probes for the frontal (left) and cen
(right) explosions.

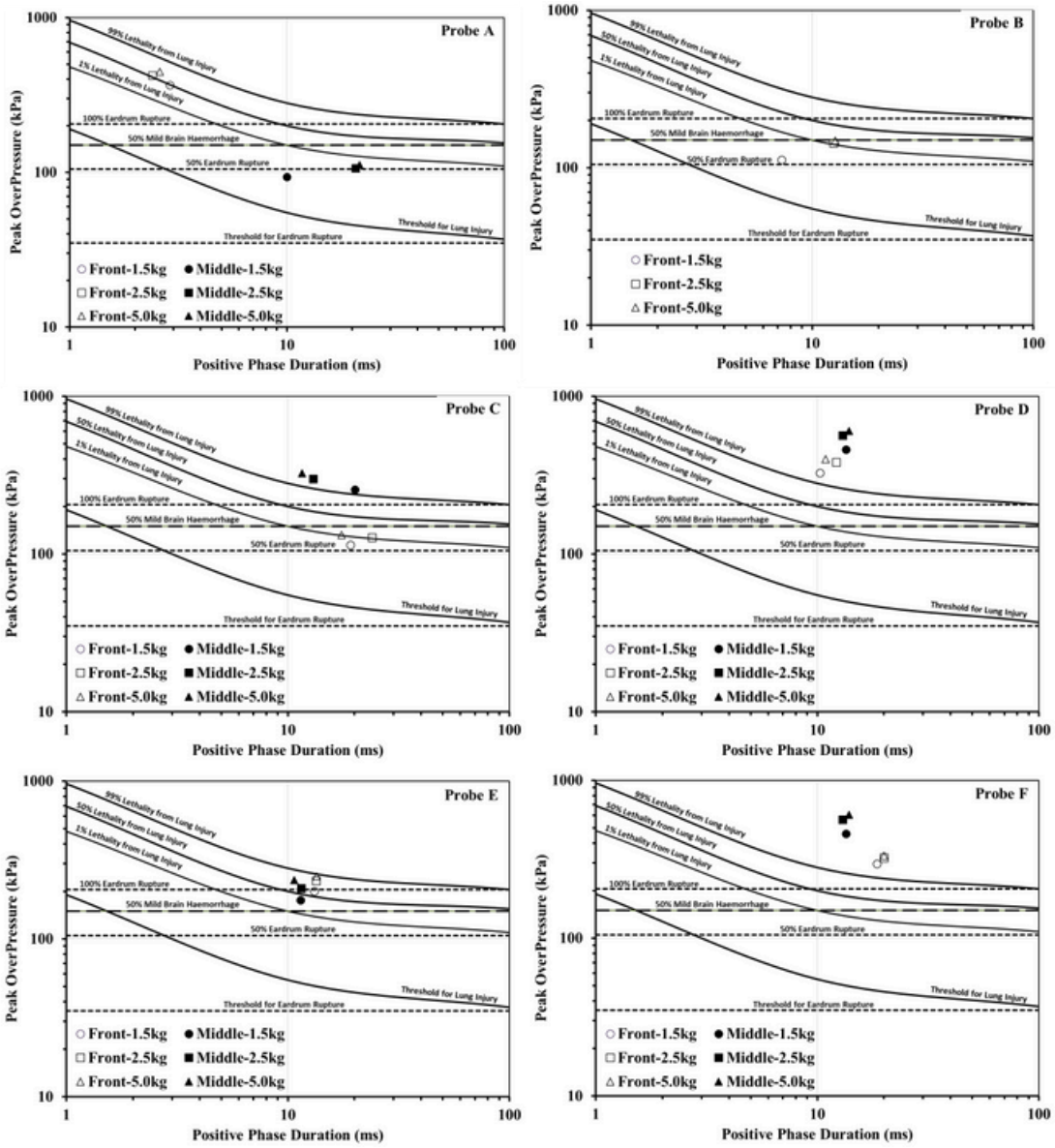

Fig. 5: Primary blast injury (PBI) risk at probes (denoted by markers) for different blast intensity plotted against the PBI criteria represented by Denny *et al*. [11] (denoted by lines).

Influence of Red Bricks Infill Walls on Seismic Response of a Regular RC Framed Building by (SBC-CR-18) Code

A.E. Hassaballa
Assistant Prof., Civil and Architectural Engineering Department, College of Engineering and Computer Science, Jazan University, Jazan 45142, KSA.
Email: ahassaballa@jazanu.edu.sa

Abstract: This paper aims to investigate the impact of red brick infill walls on seismic response of a RC framed building using the Saudi Building Code 301-2018 (SBC301-18). The Equivalent Latera Force Procedure was utilized to conduct a seismic analysis of a ten-story office reinforced concr building in Jizan city, both with and without infill walls. The Ordinary Reinforced Concrete Mome Resisting Frame (ORCMRF) building has been studied in accordance with SBC-301-2018's requirements. The frame under analysis used infill walls at ratios of 0% (bare frame), 20%, 40%, 80%, and 100% (fully infilled frame with walls). Dead load, live load, and seismic loads were the main factors influencing this frame's analysis. The maximum seismic ground motion of 0.2 seco Spectral Response Acceleration (Ss in %g) and 1.0 second Spectral Response Acceleration (S1 in in the Kingdom of Saudi Arabia were used to calculate seismic loads. The findings of this investi showed that the infill walls significantly impact the investigated frame's seismic response. By m the building parts stiffer, these walls have the impact of increasing base shear, seismic lateral fo storey shear forces, and overturning moments, which in turn reduces the building's lateral displacements.

Keywords: Infill walls, Seismic response, base shear, lateral force, storey shear force, overturni

moment.

تأثير جدران الحشو من الطوب الألأحمر على الاستجابة الزلز
لمبنى من الخرسانة المسلحة العادية حسب SBC
18)

الملخص: تهدف هذه الورقة إلى دراسة تأثير جدران الحشو من الطوب الألأحمر على الاستجابة الزلزا
من الخرسانة المسلحة العادية باستخدام الكود السعودي للبناء 2018-301 .(SBC301-18) تم استخد
القوة الجانبية المكافئة لإجراء تحليل زلزالي لمبنى مكاتب مكون من عشرة طوابق من الخرسانة المس
مدينة جازان، مع أو بدون جدران الحشو. تمت دراسة مبنى الإطار الخرساني المسلح العادي المقاوم
(ORCMRF)وفقًا لمتطلبات الكود السعودي للبناء 301-2018. استخدم الإطار قيد التحليل جدران ح
إطار عارٍ(، 20%، 40%، 60%، 80%، و100%)إطار حشو بالكامل مع جدران(. كانت الألأحمال(0%
المُيَّتة والحيوية والألأحمال الزلزالية هي العوامل الرئيسية الثلاثة التي أثرت على تحليل هذا الإطار.
ة تسارع الاستجابة g%) في (Ss أقصى حركة أرضية زلزالية تبلغ 0.2 ثانية تسارع الاستجابة الطيفية
كة العربية السعودية لحساب الألأحمال الزلزالية. أظهرت نتائج هذا البحث أن g%) ف ي (S1 الطيفية
جدران الحشو تؤثر بشكل كبير على الاستجابة الزلزالية للإطار قيد البحث. من خلال جعل أجزاء ال
صلابة، فإن هذه الجدران لها تأثير زيادة قص القاعدة و القوى الجانبية الزلزالية وقوى قص الطابق وعز
الانقلاب، مما يقلل بدوره من النزوح الجانبي للمبنى.

1. Introduction

Because of their strength and rigidity, infill walls, which are enclosed in steel and concrete frames, can withstand part of the force generated by an earthquake. The mechanism of Infill walls to withstand forces is that they act as diagonal struts between the columns and beams that surround them when subjected to seismic forces. By carrying compressive forces, these struts can help the main structure bear some of the earthquake loads. By serving as a supplementary load path and sharing the load with the main structural system (beams, columns, or shear walls), it also adds lateral stiffness to the structure. A schematic of infill walls is shown in Figure 1. Although infill walls are usually not structural—that is, they do not support the weight of the building—they are nevertheless important for aesthetics, partitioning, and insulation. When designed and built correctly, infill walls can significantly contribute to a building's ability to withstand seismic forces. They can improve a structure's strength and stiffness, which can improve the building's performance in the case of an earthquake, despite most people considering them to be non-structural. Infill walls can aid in earthquake resistance by increasing lateral stiffness, redundancy, absorbing and dispersing seismic energy, reducing frame collapse, preventing pounding between structures, and improving structural ductility. In their work, Alessandra De Angelis et al. [1] examined the function of infill walls in the seismic upgrading and dynamic behavior of a reinforced concrete framed building. The study only looked at the life and death loads of an infilled RC frame structure that was built in a higher seismic zone in Southern Italy in the 1960s. A 4-RC building in Benevento, Campania, Southern Italy, with an acceleration of 0.26 g, is one example. Because it is based on the ratio of the in-stiffness to the plane stiffness of the floor of the vertical resisting components, this study discovered that the flexibility of the floor may be altered by the connection between the masonry panels and the frame. The FRCM approach, which increases the resistance of the masonry walls that are cut away from the RC columns, can also be used to improve the filler walls. The interference may be helpful when the increase in resistance is small compared to the difference in building rigidity. The study by Abdelkader Nour et al. focused on the role that masonry walls play in improving the seismic resilience of reinforced concrete buildings [2]. Several models of multi-story frame buildings with double-leaf hollow brick masonry, one of the most popular infill materials in Algeria, located in high seismic zones were analyzed in compliance with the country's seismic regulations.

This analysis was carried out using the finite element program ETABS and was based on the response spectrum technique. The investigation's conclusions suggest that masonry infill walls may have a major impact on the seismic behavior of reinforced concrete. In a study by shendkar mangeshkumar R. et al [3], a four-story structure was studied by modeling the case study using a double strut nonlinear cyclic model. The study’s findings showed the factor of response reduction for the frames reduces in tandem with the hardened strength of the masonry infill furthermore the R values for the bare frames are less than that the BIS regulation recommends. The effect of the apertures on the seismic response of an infilled RC building was investigated by Andre furtado et al [4]. According to this study, the natural frequencies were reduced by roughly 20% as a result of the openings compared to the full infill (which decreased the without openings). Also, as comparison to the model without openings, the openings

This study concludes that the stiffness of a building is significantly increased when infill is present. The stiffness of the structure is decreased with a larger opening percentage. A variety of modeling techniques have been used to assess how infill walls affect the seismic response of RC buildings with vertical irregularity and dual frames [10, 11, 12].

For deterministic and probabilistic analysis employing infill walls, Laura Liberatore et al. [13] developed a comprehensive equivalent strut model built on experiments. Several models based on the equivalent strut approach were evaluated in this work using a data set of 162 experimental tests, taking uncertainty into consideration. Apart from the masonry's mechanical characteristics, the model also considers other factors, such as whether the units have vertical or horizontal hollows. Finally, a sample of how the suggested model is put to use is given. The comparison between the experimental and expected values, the paper concluded, demonstrated that while some of these models may predict the strength to some extent, none of them can satisfactorily represent the actual stiffness. The inclusion of masonry infill action considerably alters the building model's dynamic response behavior when compared to the bare frame model, according to Ram Krishna Shrestha et al. [14].
The study revealed that, in comparison to the model with an infill wall on all levels, the natural period of the infilled models with a soft story rose. In a research published by Abdelghaffar Messaoudi et al., [15], the impact of openings and changes to the arrangement of masonry panels on the overall performance of buildings was investigated. The study's conclusions demonstrate how the distribution and openings of the brick panels changed the overall behavior of the structures, improving their strength and ability to absorb energy. Salah Guettala et al.'s research [16] showed how infill walls significantly improved lateral stiffness, which resulted in an important increase in structural rigidity. Additionally, the research demonstrated that the addition of infill walls causes a displacement decrease, which occurs more strongly in models with lower shear wall ratios but becomes less significant at higher ratios. The combined effect of shear and infill walls is extremely critical and complex in order to achieve the maximum possible structural performance. Although a lot of research has been done, there is still debate on whether infill walls make a structure more or less vulnerable [17]. The seismic performance of a structure can be enhanced by infill walls, as several studies have shown (Murty and Jain 2000).
Furthermore, infill walls increase a building's susceptibility to earthquakes, according to other researchers. The lateral load transmission process is altered by masonry infill walls, which in fact greatly increase the frame's initial stiffness [18] [19]. The variation related with the uncertain

Civil engineers typically overlook the influence of brick walls in the structural analysis throughout building design techniques, according to Hossein Mostafaei et al. [25]. Only their masses as non-structural elements and their analysis of structures as bare frames are provided by filling walls. Th results of this study and the creation of analytical models with and without openings showed that walls significantly impacted the structural response of the building. Mouzzoun Mouloud et al. [26] presented a paper investigating infill walls on seismic behavior framed buildings adopting Morocc earthquake code RPS2000.

The earthquake response was assessed adopting pushover analysis. The results of this investig

demonstrate that these walls show an impact on the frame resistance. Many analytical and experi investigations have demonstrated that the inclusion of these panels considerably affects the stiffn RC frame buildings, adding structural stiffness and strength while simultaneously introducing br failure mechanisms such as short columns and soft stories [27, 28]. A. Fiore et al.'s study [29] investigated the impact of infill panel uncertainty on the rigidity of current RC buildings. The objec of the study is to identify the factors that affect the building's overall response. Following the determination of important factors, the variation in the building's safety verification findings quantified. Then, using a range of allowable values, the characteristic points (maximum point and strength) of the cyclic non-linear law were modified for two existing structures of varying heights. study's final recommendations established a foundation for more investigation into modeling uncertainty concerns and the development of simpler models for evaluating existing structures b support just vertical loads. There exist various approaches for the modeling of the infill walls. In o to investigate the impact of masonry infill wall configuration and modeling approach on the beha of RC frame structures, Kamaran et al. [30] employed the equivalent diagonal strut model. Usin nonlinear pushover analysis, they evaluated 36 distinct RC frame models and found significant cap loss, particularly in the case of infills that were terminated at the ground level.

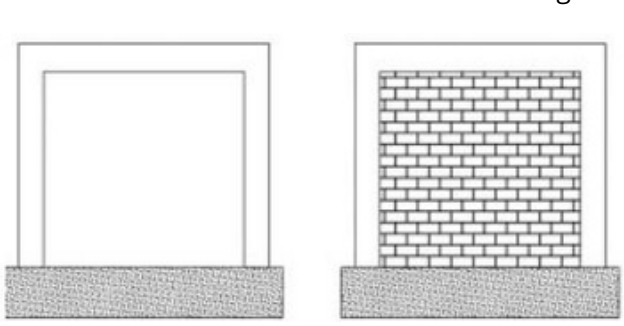

a. Frame without infill wall (bare frame) b. frame with infill wall

Figure 1. Schematic of infill walls

2. Description of the studied building

As illustrated in Figure 3, a ten-storey Ordinary Reinforced Concrete Moment Resisting Frame (ORCMRF) office building in Jazan City with a 16 m x 20 m design and a normal floor height of 3 m was examined to determine how seismically sound it was. Gravitational forces are resisted by a structure of solid slabs held up by beams and columns. Three primary elements influenced the analysis of this frame: dead load, live load, and seismic loads. Table 1 shows the sections of the beams and columns.

According to SBC301-2018, the frame under study was analyzed using the following particular lo
combinations (see Eqs. (1 to 3):
Load Case 1:

1.4 DL + 1.7 LL (1)

Load Case 2 (L/C2):

1.2 DL + 1.0 E + LL (2)

Load Case 3 (L/C3):

0.9 DL + 1.0 E (3)

Where:
DL is dead load
LL is live load
E is earthquake load
In this analysis live load is taken as follows:

On floor 2.5 kN/ m2.
On roof 1.0 kN/ m2.

For comparison purposes, equation 2 has only been adopted in this analysis.
Jazan region is located on the southwest corner of Saudi Arabia on the coast of the Red Sea and d
north of the border with Yemen. Jazan City lies in an active zone of earthquakes classified as zone
with maximum applied horizontal acceleration of 0.2g.
In this study, walls in the frame under study were filled with red bricks. Often used as building ma
red bricks are formed from natural clay and have a number of structural and physical qualities tha
them perfect for building. Depending on the quality, red bricks can have a compressive strength o
to 35 MPa and a density of 1600–2000 kg/m³. Water absorption rates for red bricks range from 1
20%, depending on the material and the production procedure. Because red bricks are made of
they can tolerate high temperatures without suffering major damage, making them extremely
resistant. In certain cases, they can tolerate temperatures as high as 1,000°C. Red bricks are a po
choice in many construction applications because of their strength, durability, thermal qualities
aesthetic appeal. This is especially true in areas that experience seismic activity, as their bulk a
structural qualities help improve stability. Red bricks vary widely in size from one country to anot
In this analysis, 200 mm x 100 mm x 70 mm red bricks were used (Figure 2).

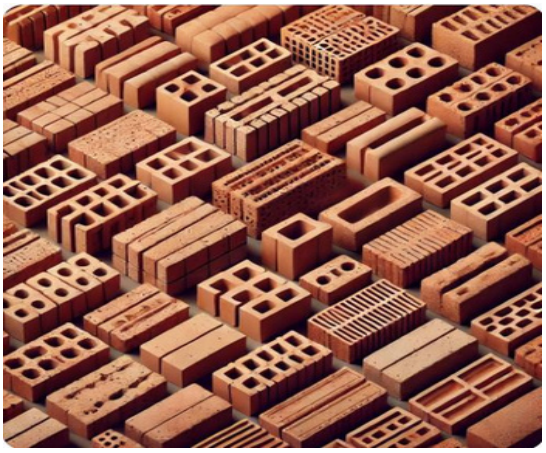

Figure 2. Variety of red clay bricks

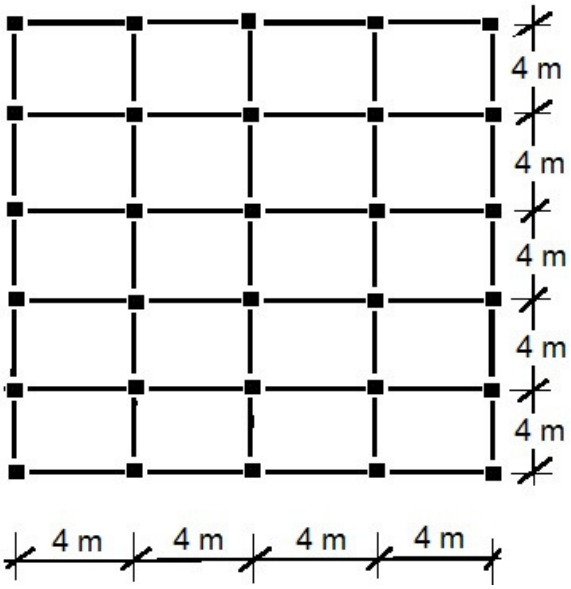

a. Plan

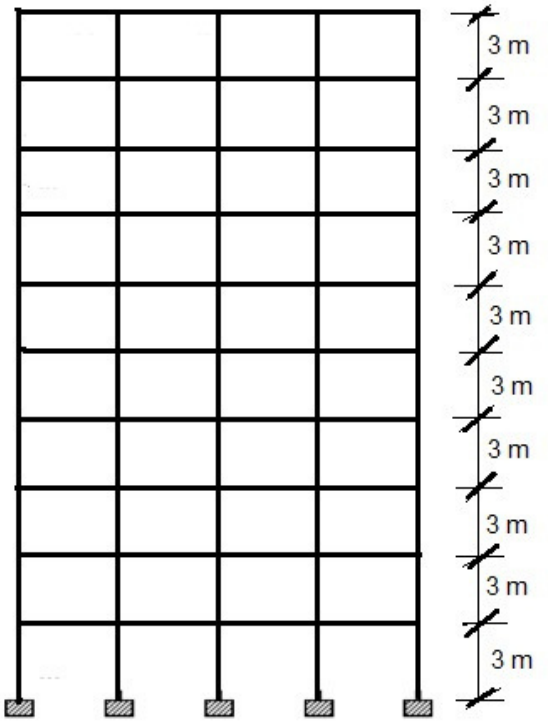

b. Elevation

Figure 3. Building configuration (plan and elevation)

Table 1. Sections of columns and beams

Building	Floor Level	Typical beams sections (mm)	Column sections (mm)
10-Storey office	Ground – 4th Floor	500 x 300	600 x 300
	5th – 7th Floor		500 x 300
	8th - Roof		400 x 300

Typical slabs' thicknesses = 150 mm

3. Results and discussion

3.1 Calculations of design acceleration for Jizan city using the Saudi Building Code (SBC301-18) [31]

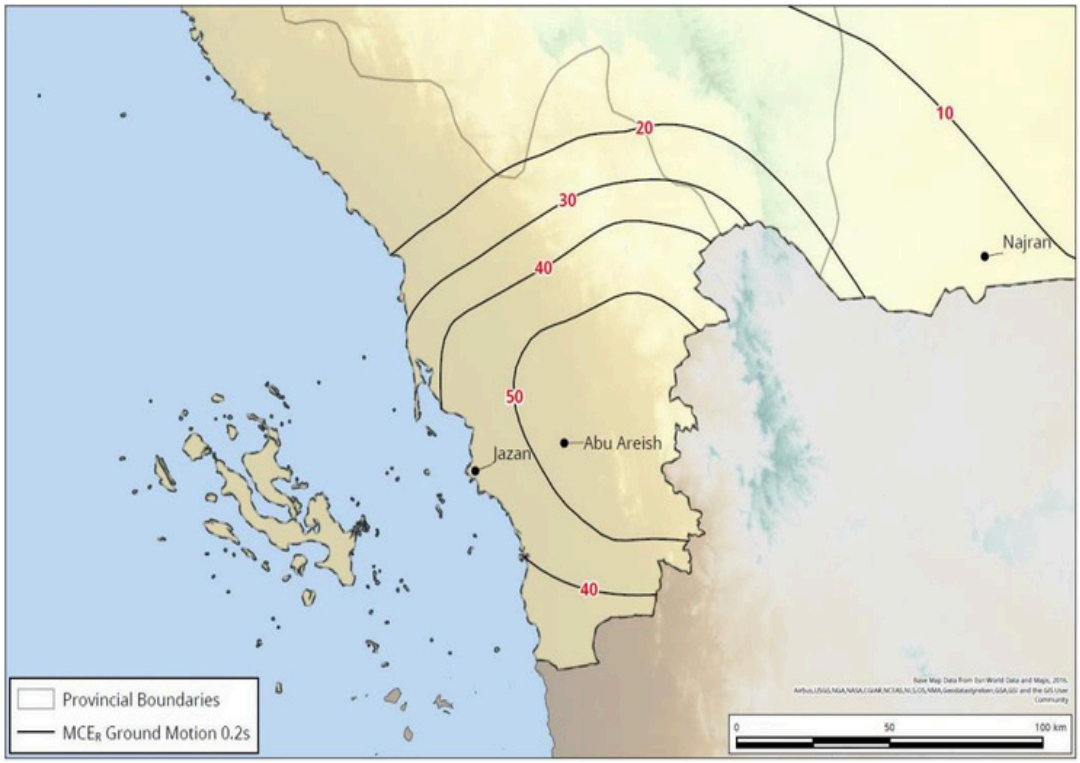

Figure 4. The ground motion for the SS Risk Targeted Maximum Considered Earthquake (MCER) a site class B in Southern Saudi Arabia for a 0.2 sec spectral response acceleration (5% of critical damping) [31].

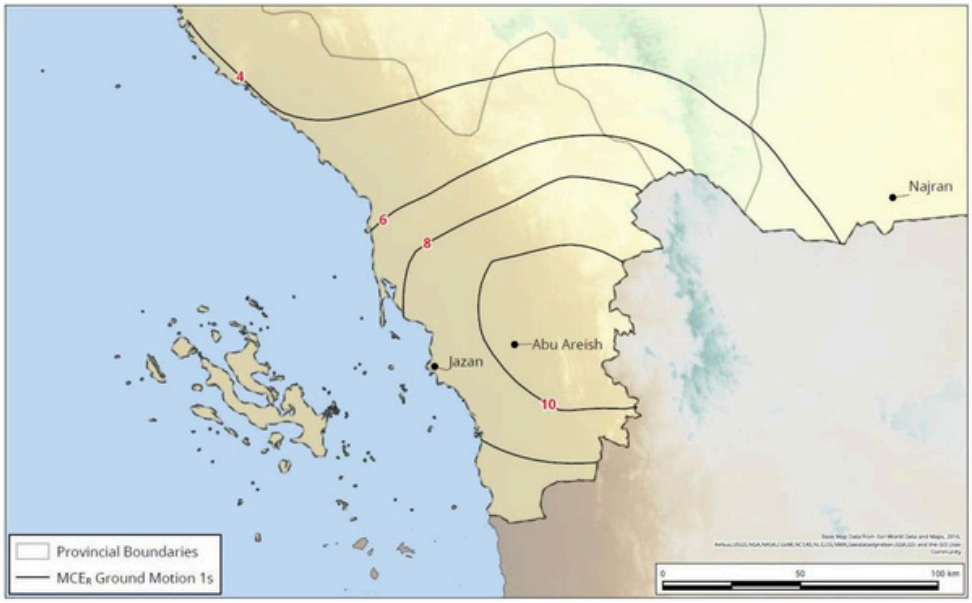

Figure 5. The ground motion parameter for the S1 Risk-Targeted Maximum Considered Earthqual (MCER) at site class B in Southern Saudi Arabia for a 1 sec spectral response acceleration (5% of critical damping) [31].

The designed response coefficients SS,, S1, SMS, SM1, Fa and Fv are calculated using SBC 301-18 follows:

SS = 0.4 g (From Figure 4)
S1 = 0.08 g (From Figure 5)

Fa and Fv = site coefficients

SMS = The Maximum considered earthquake spectral acceleration for short periods, adjusted fo class effects

$S_{MS} = Fa \; Ss = 1.2 \; x \; 0.4 = 0.48 \; m/sec2$

SM1 = The Maximum earthquake spectral acceleration for at 1-sec periods, adjusted for site class

$S_{M1} = Fv \; S1 = 1.7 \; x \; 0.08 = 0.136 \; m/sec2$

R = the structural system factor (SBC-301-2018):

R = 2.5 (Ordinary Reinforced Concrete Moment Resisting Frame)

I = importance factor determined from (SBC-301-2018):

I = 1 (for occupancy category I and II)

SDS = the design spectral response acceleration at short periods.

$S_{DS} = \frac{2}{3} S_{MS} = \frac{2}{3} x \; 0.48 = 0.32 \; m/sec$

SD1 = the design acceleration at 1-sec periods.

$S_{D1} = \frac{2}{3} S_{M1} = \frac{2}{3} x \; 0.136 = 0.09 \; m/sec$

Calculation of time perid, T0, Ts, T and TL:

$T_0 = 0.2 \times \frac{S_{D1}}{S_{DS}} = 0.2 \times \frac{0.09}{0.32} = 0.056 \; sec$

$T_s = \frac{S_{D1}}{S_{DS}} = \frac{0.09}{0.32} = 0.28 \; sec$

T = 0.1 N = 0.1 x 10 = 1 sec

T_L=4 sec (for Jazan region- SBC-301-2018)

the design acceleration, S_a, can be calculated as following:

- For periods less than T_0 (Eq. 4):

$$S_a = S_{DS}\left(0.4 + 0.6\frac{T}{T_0}\right) \quad (4)$$

For periods greater than or equal to $T_0$and less than or equal to T_s (Eq. 5):

$$S_a = S_{DS} \quad (5)$$

For periods greater than T_s , and less than or equal to T_L (Eq. 6):

$$S_a = \frac{S_{D1}}{T} \quad (6)$$

Using the calculated accel vs time period the design curve for jizan city is constructed as shown Table 2 and Figure 6.

Table 2. Design response spectrum for Jizan city

Coordinates of Design Response Spectrum Curve	
Time Period	Spectrum Response Acceleration
0.000	0.128
0.056	0.320
0.280	0.320
0.400	0.225
0.600	0.150
0.800	0.113
1.000	0.090
1.200	0.075
1.400	0.064
1.600	0.056
1.800	0.050
2.000	0.045
2.200	0.041
2.400	0.038
2.600	0.035
2.800	0.032
3.000	0.030
3.200	0.028
3.400	0.026
3.600	0.025
3.800	0.024
4.000	0.023
4.200	0.021

The design response spectrum curve shown in Figure 6 is used to determine the design spectral r accelerations for a given structure in a specific site.

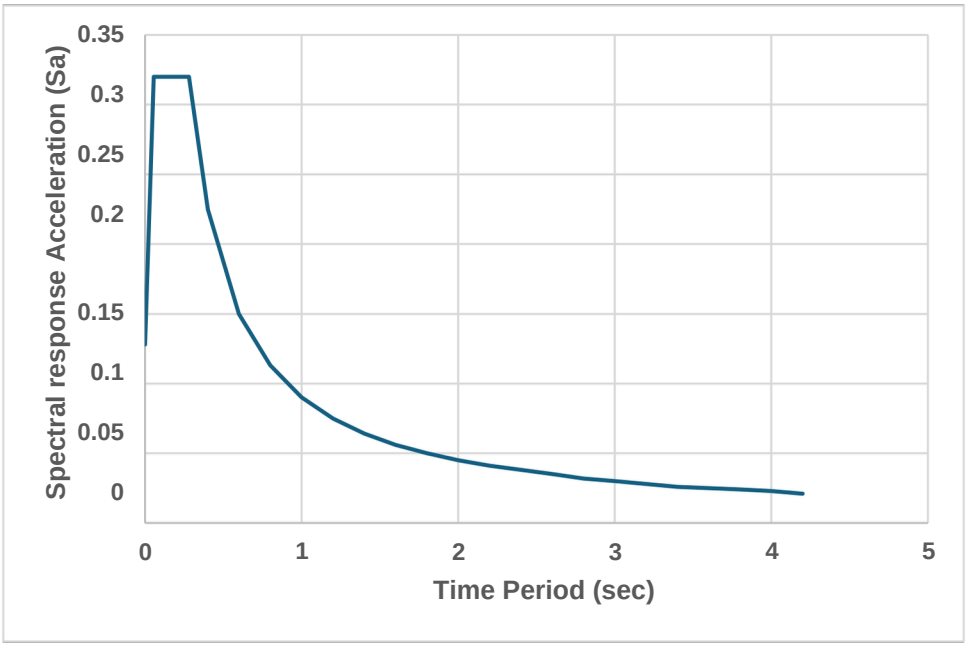

Figure 6. Design Response Spectrum for Jizan city

3.2 Seismic Base Shear (V)
Seismic base shearcan be calculated using the equivalent static lateral force procedure as given in 7:

$$V = Cs\ W \quad (7)$$

Where W is the effective seismic total weight of building

Cs = The seismic response coefficient determined in accordance with SBC301-CR-18), as defined Eq. 8:

$$Cs = SDS\ /(R/I) \quad (8)$$

SDS = The design spectral acceleration parameter in the short period range

R = The response modification factor.

I= The importance factor.

$Cs = (0.32 / (2.5 / 1)) = 0.128$

$V = 0.128 \times 30718 = 3931.9\ kN$

Fx can be obtained using Eq. 9:

$$F_x = C_{vx}\ V \quad (9)$$

$$C_{vx} = \frac{w_x h_x^k}{\sum_{i=1}^{n} w_i h_i^k} h_n \quad (10)$$

Where:

Cvx = vertical distribution factor, calculated using Eq. 10.

V = total design lateral force or shear at the base of the structure (kN).

wi and wx = the portion of the total effective seismic weight of the structure (W) located or assigne
Level i or x.

hi and hx = the height (m) from the base to Level i or x.

k = an exponent related to the structure period as follows:

For structures having a period of 0.5 s or less, k = 1.

For structures having a period of 2.5 s or more, k = 2.

For structures having a period between 0.5 and 2.5 s, k shall be 2 or shall be determined by li
interpolation between 1 and 2.

Horizontal Distribution of Forces.

Any story's seismic design story shear (Vx in kN) can be calculated using Eq. 11 as follows:

$$V x = \sum n\ i = x\ F\ i \quad (11)$$

where, Fi = the portion of the seismic base shear (V in kN) induced at Level i.

Overturning Moment

The overturning moments at level x (Mx) (kN.m) shall be determined from the Eq. 12:

$$M x = \sum_{i=x}^{n} (F_i (h\ i - h) \quad (12)$$

Where:

Fi= the portion of the seismic base shear (V) induced at level i.

hi and hx= the height "m" from the base to level i or x.

The following Tables and Figure show the results of the seismic analysis of the studied frame

Table 3. influence of infill walls on base shear of the frame

Infill walls (%)	Base shear (kN)	% Difference in base shear
100%	6601.6256	
80%	5998.0736	10.05
60%	5274.5216	11.17
40%	4610.9696	12.58
20%	3947.4176	14.39
0%	3288.8656	16.81

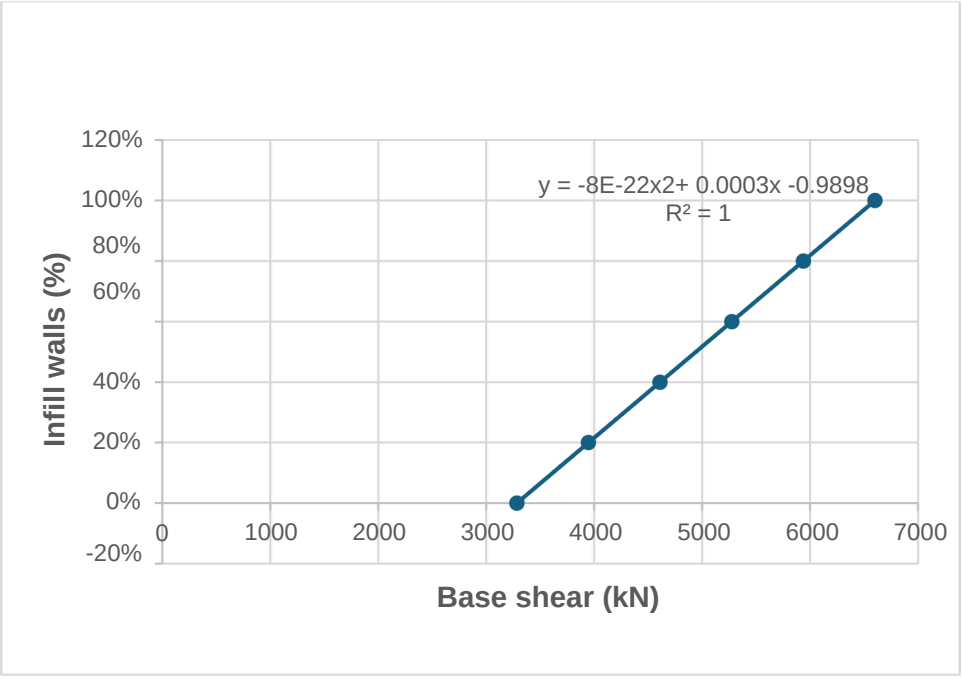

Figure 7. Effect of infill walls on base shear in the frame

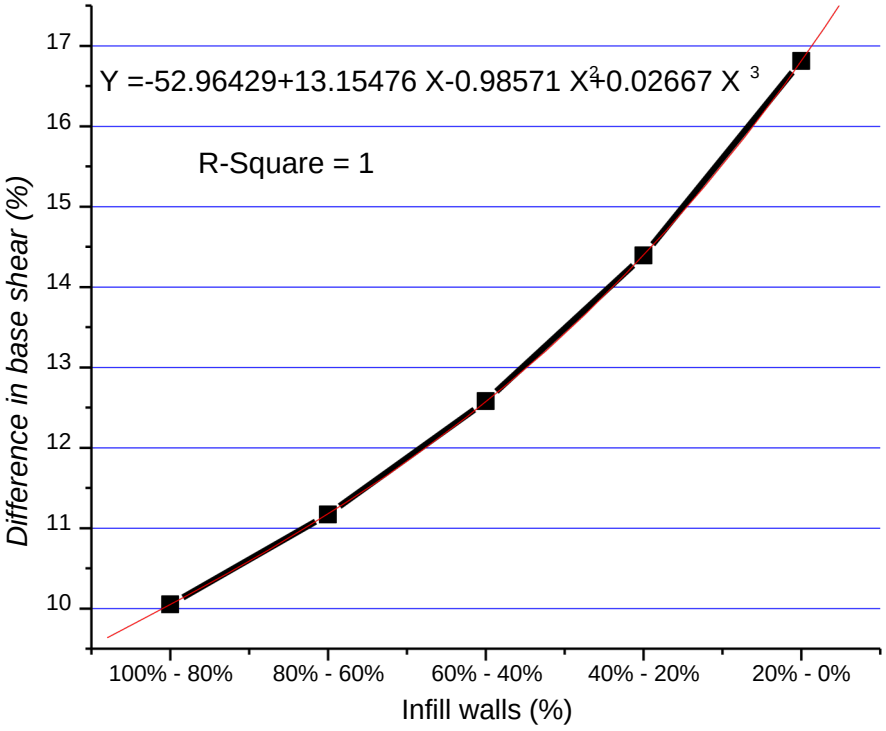

Figure 8. Relation between infill walls and % difference in base shear

Table 3 and Figures 7 and 8 demonstrate that the base shear reported for frames with heavier infill wall weights is higher, and the percentage difference in base shear increases as the percentage of infill walls decreases. This indicates that the seismic response of buildings is certainly influenced by infill walls carrying significant loads. For example, base shear is increased by 50.3% higher by a fully infill wall than by a bare frame. In comparison to the bare frame, the fully infilled frame's base shear is amplified by 2.0.

Table 4. Influence of infill walls on the seismic lateral forces

Floor level	Infill walls (%)						% Difference
	0%	20%	40%	60%	80%	100%	
Roof	597.066472	717.712290	838.358109	959.003927	1079.6497	1200.29556	0
8th	537.359825	645.941061	754.522298	863.103534	971.684770	1080.26600	10
7th	477.653178	574.169832	670.686487	767.203141	863.719796	960.236450	11.1
6th	417.946530	502.398603	586.850676	671.302749	755.754821	840.206894	12.5
5th	358.239883	430.627374	503.014865	575.402356	647.789847	720.177338	14.3
4th	298.533236	358.856145	419.179054	479.501963	539.824872	600.14778	16.7
3rd	238.826589	287.084916	335.343243	383.601570	431.859898	480.118225	20.0
2nd	179.119941	215.313687	251.507432	287.701178	323.894923	360.088669	25.0
1st	119.413294	143.542458	167.671621	191.800785	215.929949	240.059112	33.3
Ground	59.7066472	71.7712209	83.83581091	95.90039273	107.96497	120.02955	50.0

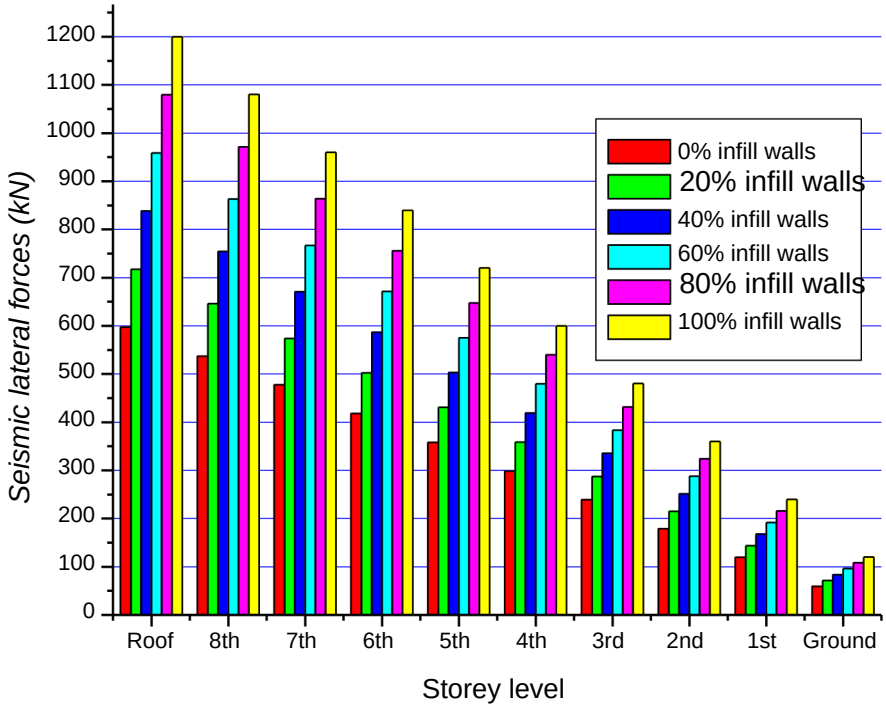

Figure 9. Influence of infill walls on the seismic lateral forces

Despite the fact that infill walls are often considered as non-structural elements, Table 4 and Figu demonstrate how much of an impact they have on the distribution and magnitude of seismic late forces in buildings. On the other hand, it is evident that the lateral forces increased as building he increased maximum at the roof. This is due to the fact that the base shear distributes laterally along the floor levels based on how high each floor is raised above the ground.

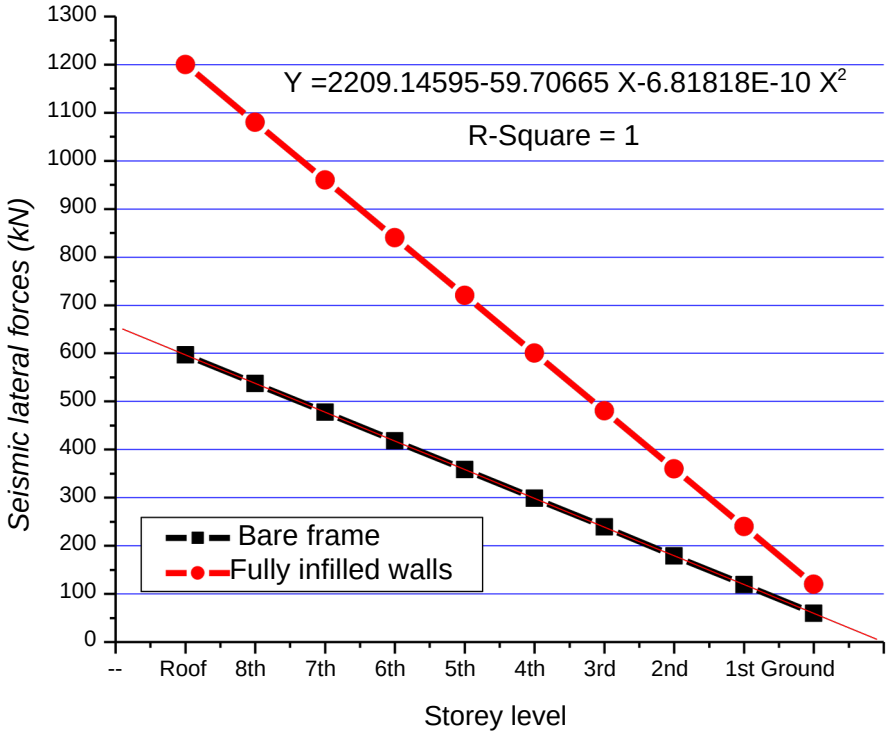

Figure 10. Seismic lateral force of the analysed frame

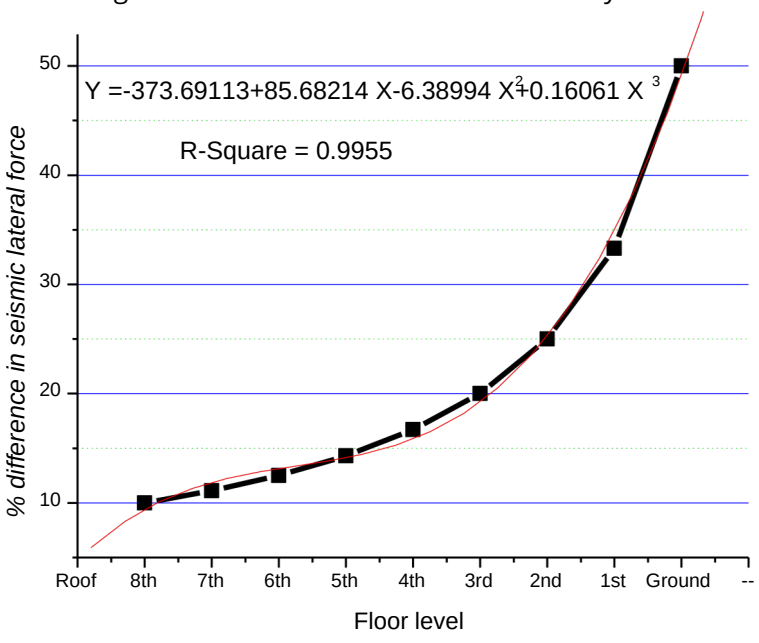

Figure 11. % difference of lateral forces with floor level

Figure 10 illustrates the seismic lateral force relationship between bare frame and completely infilled structures. At each story, the lateral pressures in the frame with infill walls were found to be 50% more than those in the bare frame due to the fact that infill walls improve a building's overall stiffness. This is because the walls serve as braces, fortifying the structure and minimizing lateral displacements inside the frame. Stiffer constructions tend to be more susceptible to seismic forces. According to seismic principles, there is a proportionate link between structural stiffness and lateral seismic force. In the lower floors, the difference between the ground floor and the first floor rises considerably to 50%, whereas in the upper floors, the percentage difference in lateral forces grows little. Figure 11 illustrates the fluctuations in the percentage difference, which indicate a non-linear connection for the weight of the infill walls employed in this study.

Table 5. Influence of infill walls on the lateral displacements of the frame (mm)

Storey level	Infill walls (%)						% Difference
	0%	20%	40%	60%	80%	100%	
Roof	240	199.7	170.9	149.4	132.7	119.4	0
8th	216	179.7	153.8	134.5	119.5	107.5	9.97
7th	192	159.7	136.8	119.5	106.2	95.5	11.16
6th	168	139.7	119.6	104.6	92.9	83.6	12.46
5th	144	119.8	102.5	89.6	79.6	71.6	14.35
4th	120	99.8	85.4	74.7	66.4	59.7	16.62
3rd	96	79.8	68.4	59.8	53.1	47.7	20.10
2nd	72	59.9	51.3	44.8	39.8	35.8	24.95
1st	48	39.9	34.2	29.9	26.5	23.9	33.24
Ground	24	20	17.1	14.9	13.3	11.9	50.21

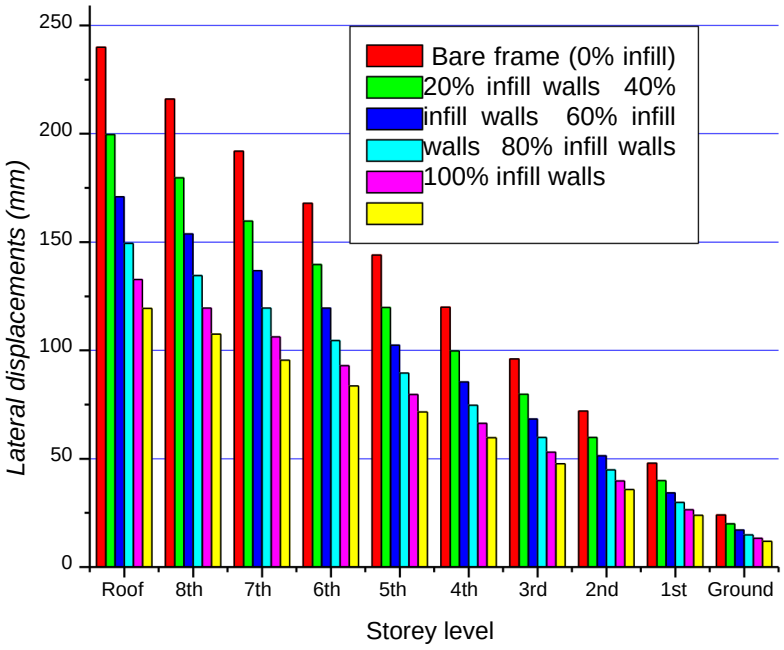

Figure 12. Seismic lateral displacements of the analysed frame

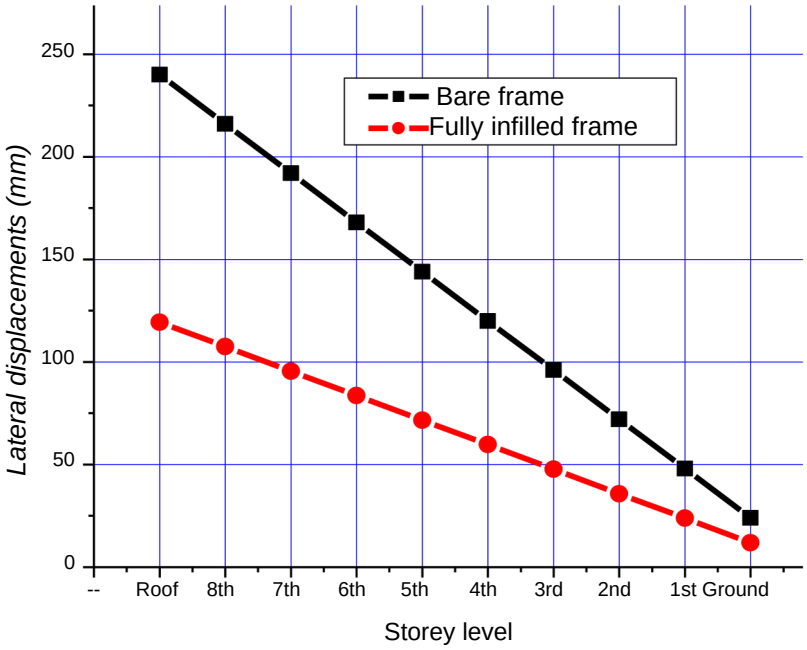

Figure 13. % difference of lateral displacements with floor level

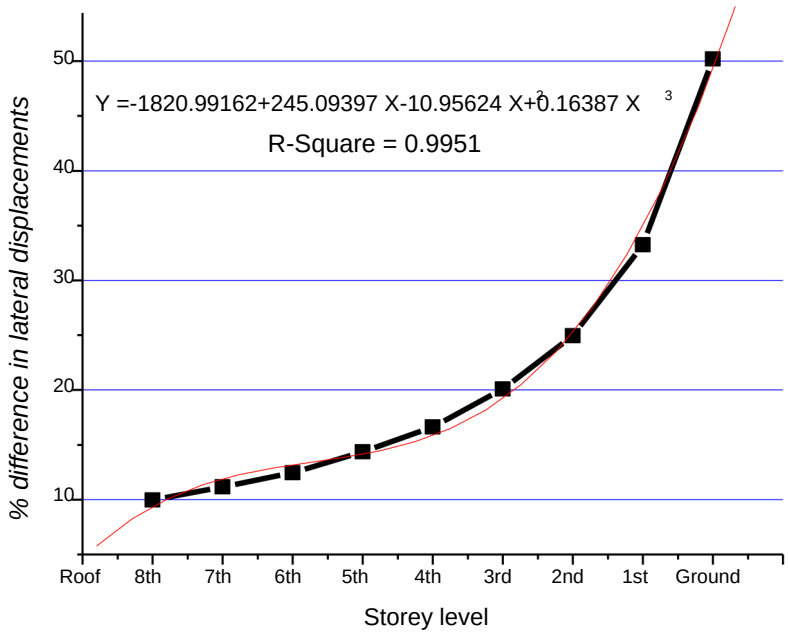

Figure 14. % Difference of lateral displacements with floor level

Table 5 shows that Infill walls have a clear impact on the lateral displacements of building by redu
the displacement capacity of the studied frame by a value of 50.0 % comparing to the bare fra
Reducing displacements and drift, by providing significant initial stiffness and strength, may decre
after cracking. Similar to the behavior of seismic lateral forces, the percentage difference in lat
forces increases little in the upper floors; however, in the lower floors, the difference increases
significantly, reaching up to 50% between the ground floor and the first floor as illustrated in Figu
12 to 14.

Table 6. Influence of infill walls on the storey shear forces.

Floor level	Infill walls (%)					
	0%	20%	40%	60%	80%	100%
Roof	597.066472	717.712290	838.358109	959.003927	1079.65	1200.29556
8th	1134.42629	1363.65335	1592.88040	1822.10746	2051.33451	2280.56157
7th	1612.07947	1937.82318	2263.56689	2589.31060	2915.05431	3240.79802
6th	2030.02600	2440.22178	2850.41757	3260.61335	3670.80913	4081.00491
5th	2388.26589	2870.84916	3353.43243	3836.01570	4318.59898	4801.18225
4th	2686.79912	3229.70530	3772.61149	4315.51767	4858.42385	5401.33003
3rd	2925.62571	3516.79022	4107.95473	4699.11924	5290.28375	5881.44826
2nd	3104.74565	3732.10391	4359.46216	4986.82042	5614.17867	6241.53693
1st	3224.15895	3875.646371	4527.133789	5178.621207	5830.10862	6481.5960
Ground	3283.8656	3947.4176	4610.9696	5274.5216	5938.07	6601.625

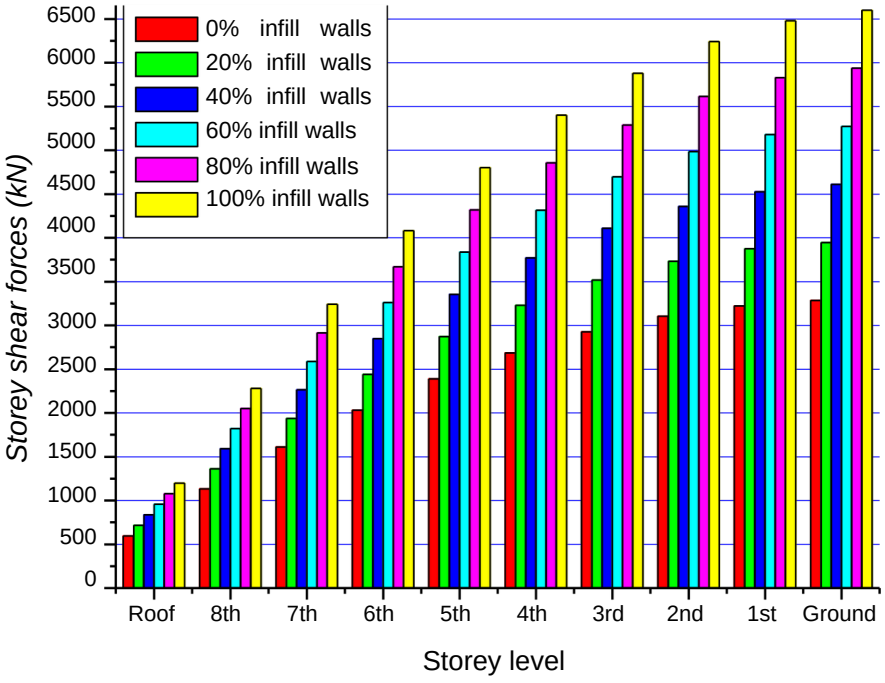

Figure 15. Influence of infill walls on the storey shear forces

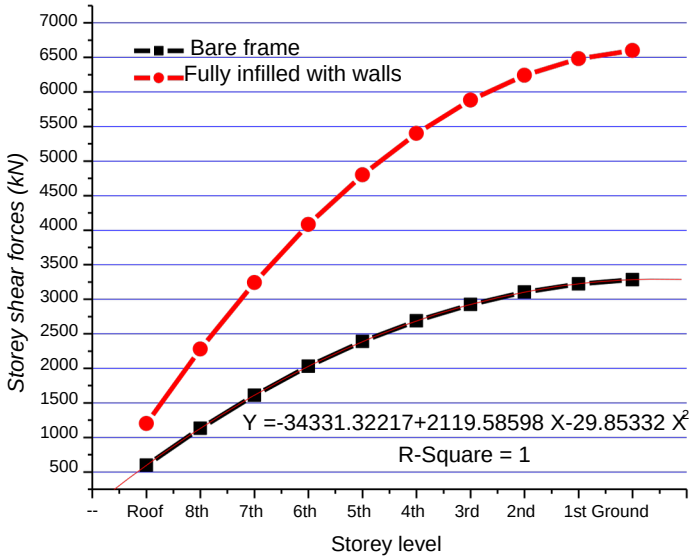

Figure 16. Influence of infill walls on the storey shear forces for fully infilled and bare frames

Referring to Table 5 and Figures 12 and 13 infill walls show a significant impact on the seismic sto
shear forces in buildings by modifying the building's dynamic behavior during an earthquake.

There is a large difference in storey shear forces in the upper three stories. The shear force in 9th
is less than that in 8th floor by an amount of 47 % and 30 % between 8th and 7th floor for (fully in
frame). Then the difference becomes very slight in the lower stories; between ground and first sto
was found to be 1.8%. in this case, higher seismic storey shear forces in the lower stories result f
the increased stiffness due to the presence of infill walls. Finally, the value of storey shear for
increased by 50.3% in fully infill walls compared to bare frame in all levels.

Table 7. Influence of infill walls on the overturning bending moments

Floor level	Infill walls (%)					
	0%	20%	40%	60%	80%	100%
Roof	0	0	0	0	0	0
8th	1791.19941	2153.13687	2515.07432	2877.01178	3238.94 92	3600.88669
7th	6985.67773	8397.23380	9808.78987	11220.3459	12631.9020	14043.4580
6th	17016.3944	20454.8002	23893.2061	27331.6119	30770.017	34208.4235
5th	33137.1892	39833.0321	46528.8750	53224.7179	59920.56	66616.4037
4th	56422.7816	67823.8114	79224.8413	90625.8711	102026.9	113427.930
3rd	87768.7714	105503.706	123238.642	140973.577	158708.5	176443.447
2nd	127891.638	153733.972	179576.307	205418.641	231261	257103.309
1st	177328.742	213160.550	248992.358	284824.166	320656	356487.782
Ground	236438.323	284214.0672	331989.8112	379765.555	427541.29	475317.04

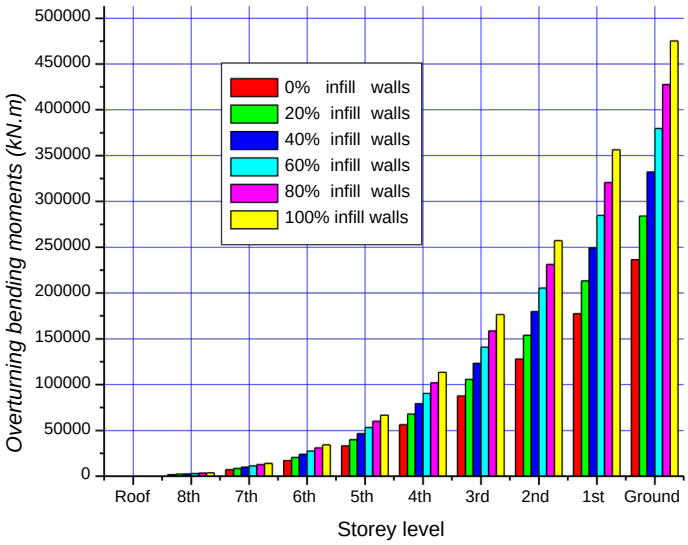

Figure 17. Influence of infill walls on the overturning bending moments

As seen in Figure 14, Table 6 demonstrates that the Infill walls significantly impact the seismic overturning moments in the buildings under study. The building becomes stiffer in the lower sto which causes the moments to steadily increase from the top to the base of the frame. This relatio is in good agreement with the findings of I. K. Ejiogu et. al. [4].

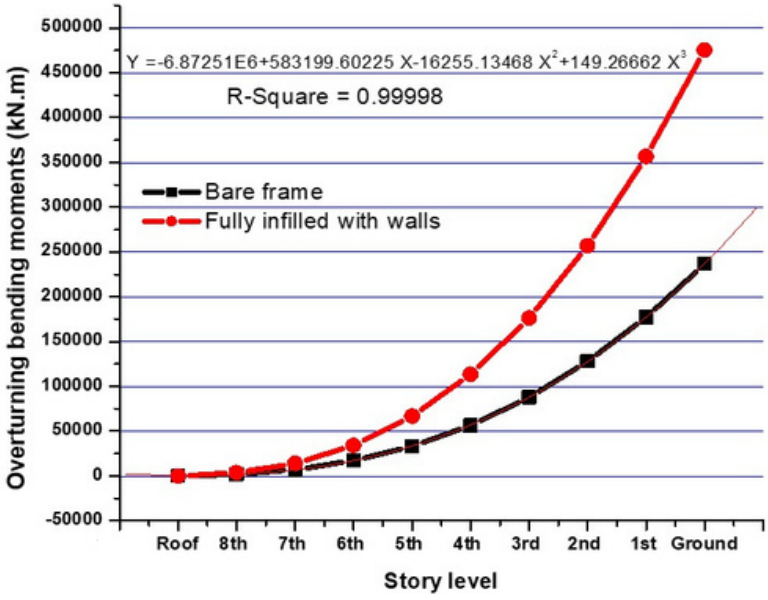

Figure 18. Overturning moments for bare and fully infilled frame

Table 8. % Difference in overturning moments with floor levels

Floor Level	% difference in overturning moment
Roof	0
8th	100
7th	74.4
6th	58.9
5th	48.6
4th	41.3
3rd	35.7
2nd	31.4
1st	27.8
Ground	25.0

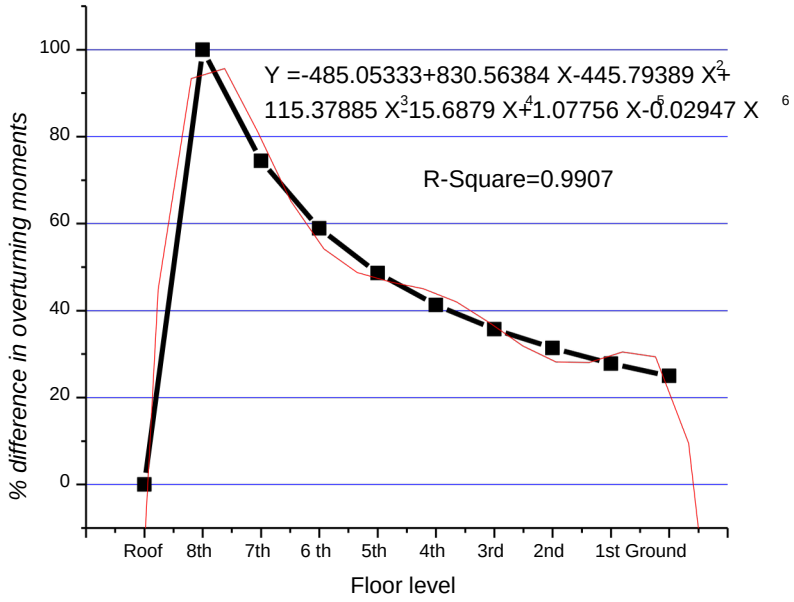

Figure 19. % difference in overturning moments with floor heights

For this polynomial formula, the coefficient of determination (R2) is R2 = 0.9907 as shown in Table and illustrated in Figure 15. Because the overturning moment at the roof is zero, the differenc moments increases by 100% at the eighth floor, and then there is a gradual decrease until the g floor, which gave the lowest value, this relationship could not have been achieved without the us the highest power of polynomial (exponent = 6).

The findings of this study closely align and bear similarities to those of Abdelkader Nour (2022), Ayman (2015), Waleed Abo El-Wafa (2012), Ram Krisna (2024), Abdelghffar (2022), and Robin (2004) as a sample of results' agreement.

This paper investigates into how infill walls influenced an ordinary RC moment-resisting frame (ORCMRF) in Jizan city, Saudi Arabia. A 10-storey moment-resisting frame with and without infill walls was analyzed for purposes of comparison. Investigations were conducted on the effects of infill walls on seismic base shear, lateral forces, storey shear forces, and overturning moments. The study's findings demonstrated that the inclusion of infill walls significantly increased the building's base shear when compared to a building without infill walls; in fact, this increase was 100%. This indicates the infill walls' weights have noticeable effects on the building's seismic response.

Even though infill walls are sometimes regarded as non-structural elements, they have signific

effects on how much and where seismic lateral forces are distributed throughout buildings. On th hand, it is evident that the lateral forces and displacements increased as building height incre peaking at the roof. This is due to the fact that the base shear distributes laterally within the floor based on how high each floor is raised above the ground. The weight of the infill walls used in investigation has a non-linear relationship to the variation in the percentage difference between values. In the upper floors, the percentage difference in lateral forces increases little; however, i lower floors, the difference increases significantly, reaching 50% between the ground floor and th floor. A non-linear relationship between the height of floors and the ratios of infill walls utilized in study can be found by observing variations in the percentage difference in lateral forces across successive floors. Additionally, when the weight of the infill walls increases from top to bottom of investigated frame, the storey shear forces increase significantly. It was found that, for all floor lev the value of shear forces is increased by 50.3% more than that of the bare frame. Additionally, bec the building becomes stiffer in the lower stories, it has been noticed that adding infill walls to the f increased the overturning moment from the top to the base of the structure. Moreover, the overt moments increased by 50.3% in the fully filled frame compared to the bare frame. Because infill w improve a building's total stiffness, they usually increase base shear, lateral force, shear force, bending moments. This decreases lateral displacements, or drifts, during seismic events. In gene is found that, compared to the bare frame model, the dynamic response behavior of the building is considerably changed by the inclusion of masonry infill action.

4. Conclusion

The impact of wall filling on an ordinary RC frame in jizan city, Saudi Arabia was checked in this trial. Investigation was performed into how filling with walls affected base shear, lateral forces, shear forces and overturning moments.

From the results obtained, it can be concluded that:

1. The addition of infill walls significantly increased base shear by 100 % when compared to a bare frame. The lateral forces and displacements increased as building height increased
2. peaking at the roof, due to the fact that the base shear distributes laterally within the floor
3. levels based on how high each floor is raised above the ground. In the upper floors, the percentage difference in lateral forces increases little; however, in the lower floors, the difference increases significantly, reaching 50% between the ground floor and the first
4. floor. It was found that, for all floor levels, the value of shear forces increased by 50.3% more than that of the bare frame. It was noticed that the overturning moments increased by 50.3% in the fully filled frame compared to the bare frame. In general, it was found that, compared to the bare frame model, the dynamic response behavior of the building model is considerably changed by the inclusion of masonry infill action.

Author Contributions:

5.

6.

The author confirms sole responsibility for the following: study conception and design, data collec
analysis and interpretation of results, and manuscript preparation.

Funding:

This research received no external funding.

Institutional Review Board Statement:

No applicable.

Informed Consent Statement:

Not applicable.

Data Availability Statement:

All data used in this work are incorporated into the article and its online supplementary material.

Conflicts of Interest:

The author declares no conflicts of interest.

REFERENCES

[1] Alessandra De Angelis and Maria Rosaria Pecce, The Role of Infill Walls in the Dynamic Behavio and Seismic Upgrade of a Reinforced Concrete Framed Building. Frontiers in built environment, published: 03 December 2020. doi: 10.3389/fbuil.2020.590114. www.frontiersin.org. (2020).

[2] Abdelkader Nour a, Abdelkader Benanane a, Humberto Varum, Importance of Infill Masonry W in Improving the Seismic Response of Reinforced Concrete Buildings, International Journal on Advanced Science Engineering and Information Technology,Vol.12 (2022) No. 2. ISSN: 2088-5334. DOI: 10.18517/ijaseit.12.2.14040. https://www.researchgate.net/publication/360050781, (2022).

[3] Shendkar, M. R., Kontoni, D. P. N., Işık, E., Mandal, S., Maiti, P. R., & Harirchian, E. Influence of masonry infill on seismic design factors of reinforced-concrete buildings. Shock and Vibration, 202

[4] André Furtado, Hugo Rodrigues and António Arêde, Effect of the Openings on the Seismic 2020
Response of an Infilled Reinforced Concrete Structure, Buildings 2022, 12, https://doi.org/10.3390/buildings12112020. https://www.mdpi.com/journal/buildings. (2022).

[5] Ali Zine, Abdelkrim Kadid, Abdallah Zatar, Effect of Masonry Infill Panels on the Seismic Response of Reinforced Concrete Frame Structures,
Civil Engineering Journal (E-ISSN: 2476-3055; ISSN: 2676-6957). Vol. 7, No. 11. http://dx.doi.org/10.28991/cej-2021-03091764. www.CivileJournal.org. (2021).

[6] Hussam Oreiby, Mahmoud El-Kateb, Ayman Hussein, The effect of infill walls of infill walls on
the seismic response of irregular R.C. frames, International Journal of Creative Research Thoughts
(IJCRT). Volume 10, Issue 10 October 2022 | ISSN: 2320-2882. www.ijcrt.org. (2022).

[7] Ayman Abd-Elhamed, Sayed Mahmoud, Effect of Infill Walls on Response of Multi Storey Reinforced Concrete Structure, World Academy of Science, Engineering and Technology International Journal of Civil, Environmental, Structural, Construction and Architectural Engineering. Vol:9, No:5. (2015). [8] Mrs. Sanaa Elmalyh , Mr. Azzeddine Bouyahyaoui and Mr. Taoufik Cherradi, Seismic behaviour of reinforced concrete frame with infill panels, MATEC Web of Conferences 149, 02064 (2018). https://doi.org/10.1051/matecconf/201814902064.

(2018).

[9] A. K. Mapari, Prof. Y. M. Ghugal, SEISMIC RESPONSE OF RC FRAMES CONSIDERING EFFECT OF INFILL WALLS, International journal of Advanced Research in Science and Enginee Vol. 6, issue 3. ISSN (O) 2319-8354, ISSN (P) 2319-8346. www.ijarse.com, (2017).
[10] V.H. Akansel, A. Yakut, J. P. Moehle, EFFECT OF INFILL WALLS ON STRUCTURAL BEHAVIOR OF RC BUILDINGS WITH VERTICAL IRREGULARITIES, 16th World Conference on Earthquake Engineering, 16WCEE 2017 Santiago Chile, January 9th to 13th 2017. Paper N° 163 (Abstract ID). Registration Code: S-T1464744697.
[11] M. S. Razzaghi, M. Javidnia, Evaluation of the effect of infill walls on seismic performance of RC dual frames, Int J Adv Struct Eng (2015) 7:49–54. DOI 10.1007/s40091-015-0081-x.
[12] Waleed Abo El-Wafa Mohamed, PARAMETRIC STUDY ON THE EFFECT OF MASONRY INFILLWALLS ON THE SEISMIC RESISTANCE OF RC BUILDINGS, Journal of Engineering Sciences, Assiut University, Vol. 40, No. 3, (2012), pp.701 -721.
[13] Laura Liberatore, Fabrizio Noto, Fabrizio Mollaioli, Paolo Franchin, In-plane response of maso infill walls: Comprehensive experimentally based equivalent strut model for deterministic and probabilistic analysis, Engineering Structures 167 (2018) 533–54. Journal homepage: www.elsevier.com/locate/engstruct.
[14[Ram Krishna Shrestha, Mukil Alagirisamy, Purushottam Dangol, Binod Pradhananga, Om Prak Giri, Impact of irregular masonry infill walls on the seismic response of reinforced concrete frame buildings using linear dynamic analysis, International Journal of Advanced and Applied Sciences, 1 2024, Pages: 98-110.
[15] Abdelghaffar Messaoudi, Rachid Chebili, Hossameldeen Mohamed and Hugo Rodrigues, Influence of Masonry Infill Wall Position and Openings in the Seismic Response of Reinforced Concrete Frames. Appl. Sci. 2022, 12, 9477. https://doi.org/10.3390/app12199477. https://www.mdpi.com/journal/applsci. (2022).
[16] Salah Guettala1, Akram Khelaifia, Rachid Chebili, Salim Guettala, Effect of infill walls on seismic performance of multi-story buildings with shear walls, Asian Journal of Civil Engineering. 25:3989–3999. https://doi.org/10.1007/s42107-024-01025-9. (2024).
[17] Pujol S, Fick D (2010), The test of a full-scale three-story RC structure with masonry infill walls, Eng Struct 32(10): (2010), 3112–3121. [18] Murty CVR, Jain SK, Beneficial influence of masonry infill walls on seismic performance of RC frame buildings, In: 12th World Conference on Earthquake Engineering, Auckland, (2000). [19] Kaushik HB, Rai DC, Jain SK, Code approaches to seismic design of masonry-infilled reinforced concrete frames: a state-of the-art review. Earthq Spectra 22(4):961–983. Earthquake Spectra, Volume 22, No. 4, (2006), pages 961—983, Earthquake Engineering Research Institute. [20] Taher, S.E.-D.F. and H.M.E.-D. Afefy, Role of masonry infill in seismic resistance of RC structures. The Arabian Journal for Science and Engineering, 33: (2008), pp. 291-306. [21] Saatcioglu, M., et al., The August 17, 1999, Kocaeli (Turkey) earthquake — damage to structures, Canadian Journal of Civil Engineering, 2001. 28(4): p. 715-737. [22] Ayman Abd-Elhamed, Sayed Mahmoud, Effect of Infill Walls on Response of Multi Storey Reinforced Concrete Structure, World Academy of Science, Engineering and Technology International Journal of Civil, Environmental, Structural, Construction and Architectural Engineering Vol:9, No:5, 2015. scholar.waset.org/1999.3/10001324. (2015).
[23] Nisar Ali Khan, Giorgio Monti, Camillo Nuti and Marco Vailati, Effects of Infills in the Seismic Performance of an RC Factory Building in Pakistan, Buildings 2021, 11, 276. https://doi.org/10.3390/buildings11070276. https://www.mdpi.com/journal/buildings. (2021).
[24] Waleed Abo El-Wafa Mohamed, PARAMETRIC STUDY ON THE EFFECT OF MASONRY INFILL WALLS ON THE SEISMIC RESISTANCE OF RC BUILDINGS, Journal of Engineering Sciences, Assiut University, Vol. 40, No. 3, (2012), pp.701 -721, May 2012.

[25] Hossein Mostafaei and Toshimi Kabeyasawa, Effect of Infill Masonry Walls on the Seismic Response of Reinforced Concrete Buildings Subjected to the 2003- Bam Earthquake Strong M A Case Study of Bam Telephone Center, Bull. Earthq. Res. Inst. Univ. Tokyo. Vol. 13. (2004), pp 133- 156. Kojiok@hiroshima-u.ac.jp. https://www.researchgate.net/publication/29770061.
[26] Mouzzoun Mouloud and Cherrabi Abdelkader, SEISMIC BEHAVIOUR OF REINFORCED CONCRETE FRAME BUILDINGS WITH MASONRY INFILL, International Journal of GEOMATE, Nov., 2019 Vol.17, Issue 63, (2019), pp. 203 - 209 ISSN: 2186-2982 (P), 2186-2990 (O), Japan, DOI: https://doi.org/10.21660/2019.63.72884 Special Issue on Science, Engineering & Environment.
[27] Abla. Chertout Pr. Nabil. Djebbar, Influence of Masonry Panels on Seismic Performance of Reinforced Concrete Buildings, International Journal of Innovative Studies in Sociology and Humanities. ISSN 2456-4931 | Open Access | Volume 8, Issue 1. DOI: https://doi.org/10.20431/2456-4931.080148. www.ijissh.org. (2023).
[28] G.Uva, D.Raffaele, F.Porco, A.Fiore, On the role of equivalent strut models in the seismic assessment on infilled RC buildings, Engineering structures. vol. 42, (2012), pp 83-94. https://doi.org/10.1016/j.engstrct.2012.04.005.
[29] A. Fiore, F. Porco, G. Uva & M. Sangirardi, The influence of uncertainties of infill panels relative to the seismic response of RC existing buildings, WIT Transactions on The Built Environment, Vol 141, © 2014 WIT Press. www.witpress.com, ISSN 1743-3509 (on-line). doi:10.2495/SUSI140411, (2014). [30] Kamaran Mohammed Kareem and Esra Mete, Effect of Masonry Infill Wall Configuration and Modelling Approach on the Behaviour of RC Frame Structures, Arabian Journal for Science and Engineering, Volume 44, pages 4309–4324, (2019). https://link.springer.com/.
[31] Saudi Building Code (SBC301-CR-2018). Saudi Loading Code. (Printed: May-2019).
[32] Robin DAVIS, Praseetha KRISHNAN, Devdas MENON, A. Meher PRASAD, EFFECT OF INFILL STIFFNESS ON SEISMIC PERFORMANCE OF MULTI-STOREY RC FRAMED BUILDINGS IN INDIA, 13th World Conference on Earthquake Engineering, Vancouver, B.C., Canada, August 1-6, 2004, Paper No. 1198.

Optimizing Performance and Exhaust Emission of a Direct Injection Diesel Engine Running on Fuel Additives with Variable Loads: An Experimental Investigation

Faisal Mahroogi, Mahmoud Bady

Mechanical Engineering Department, Islamic University of Madinah, Saudi Arabia

Abstract: Saudi Arabia is dedicated to sustainable development and clean energy. It uses cutting-edge approaches to address energy-related issues, including the circular carbon economy and a more varied energy mix. For Saudi Arabia to achieve its Vision 2030 goal of having a net zero future by 2060, sustainability is essential. By addressing the energy and climate issues of the modern world with responsibility and innovation, Vision 2030 is turning into a global role model for the transition to a sustainable future. The current study, which presents an experimental analysis of a diesel engine's performance and exhaust emissions mainly running on waste cooking oil (WCO), plays a crucial role in this transition. The engine type utilized is a single-cylinder direct injection diesel engine with constant speed and natural aspiration. The research was done on the engine's performance and emission parameters when fueled with two blends. The first is a mixture of 10% butanol, 70% diesel, 10% WCO, and 10% diethyl ether (D85B5W5DD5), while the second is a mixture of 5% butanol, 85% diesel, 5% WCO, and 5% diethyl ether (D85B5W5DD5). The study's findings demonstrated that engine emissions of nitrogen oxides (NOX) and carbon monoxide (CO) varied significantly depending on the applied load. The brake thermal efficiency and cylinder pressure were all impacted by load change. Also, the engine emissions change considerably with the engine load.

تحسين الأداء وانبعاثات العادم لمحرك ديزل يعمل بالحقن ا
على إضافات الوقود بأحمال متغيرة: دراسة تجريبية

الملخص:تلتزم المملكة العربية السعودية بالتنمية المستدامة والطاقة النظيفة. وهي تستخدم مناهج مت
القضايا المتعلقة بالطاقة، بما في ذلك اقتصاد الكربون الدائري ومزيج الطاقة الأكثر تنوعًا. ولكي تحق
العربية السعودية هدف رؤيتها 2030المتمثل في مستقبل خالٍ من الانبعاثات بحلول عام 2060، فإن الاستدامة
ضرورية. ومن خلال معالجة قضايا الطاقة والمناخ في العالم الحديث بالمسؤولية والابتكار، تتحول ر
إلى نموذج عالمي يحتذى به للانتقال إلى مستقبل مستدام. تلعب الدراسة الحالية، التي تقدم تحليلاً
محرك ديزل وانبعاثات العادم التي تعمل بشكل أساسي على زيت الطهي المستعمل (WCO) حاسمًا في
هذا التحول. نوع المحرك المستخدم هو محرك ديزل أحادي الأسطوانة يعمل بالحقن المباشر بسرعة
طبيعي. تم إجراء البحث على أداء المحرك ومعايير الانبعاثات عند تشغيله بمزيجين. الأول عبارة عن
بيوتانول و 70٪ ديزل و 10٪ ثنائي إيثيل الأثير(D85B5W5DD5)، بينما الثاني عبارة
عن مزيج من 5٪ بيوتانول و 85٪ ديزل و 5٪ ثنائي إيثيل الأثير(D85B5W5DD5) أظهرت .
نتائج الدراسة أن انبعاثات المحرك من أكاسيد النيتروجين (NOx) بشكل)CO(وأول أكسيد الكربون)
كبير اعتمادًا على الحمل المطبق. تأثرت الكفاءة الحرارية للفرامل وضغط الأسطوانة بتغير الحمل. أيضً
انبعاثات المحرك بشكل كبير مع حمل المحرك.

1. Introduction

The growing global concern over air pollution and depleting fossil fuel resources has driven extensive research in improving the efficiency and emission profiles of internal combustion engines, particularly diesel engines. Diesel engines, widely used in transportation, agriculture, and power generation, are known for their high thermal efficiency but also their significant contribution to harmful emissions such as nitrogen oxides (NOx), particulate matter (PM), and hydrocarbons (HC) [1]. The current study, which explores alternative fuels and fuel additives, significantly contributes to this area, offering potential solutions to mitigate these environmental impacts and instilling hope for a cleaner and sustainable future.

Fuel additives, particularly in biodiesel-diesel blends, have shown promise in enhancing combustion efficiency and reducing emissions in diesel engines [2]. These additives can alter the physical and chemical properties of the fuel, influencing key factors such as combustion temperature, fuel atomization, and soot formation [3]. However, the performance and emission characteristics of engines running on fuel additives vary significantly with engine load, making it crucial to evaluate their behavior under different operational conditions [4].

Several renewable resources can be used to produce biodiesel, which is recyclable, toxic-free, and pleasant to our planet. In gas turbines, Habib et al. [5] investigated blended biodiesel made of soybean, canola, recycled rapeseed, and hog fat against Jet A1. They observed a decrease in HC, CO, NOx, and static thrust compared to Jet A-1. Moreover, waste cooking oil (WCO) can be utilized to make biodiesel, which helps lessen the worldwide food shortage brought on by foreign conflicts, particularly the war between Russia and Ukraine [6].

Waste cooking oil has been put to the test by certain scholars as an additive to fuel for diesel-powered engines [7]. Waste cooking oil is classified as a third-generation substrate, along with fat chicken oil, fish oil, and microalgae, by Radwan et al. [8]. These substrates are frequently utilized to produce biodiesel [9]. Thus, waste cooking oil is explored experimentally in this work as a potential substitute fuel supplement for compression ignition engines [10]. The regular usage of CI engines in all arenas releases toxic gases like NOx, CO, and HC, triggering significant environmental emissions, ozone layer depletion, and bronchial diseases [11].

2. Experimental setup

A four-stroke, single-cylinder, water-cooled diesel engine was operated as an experimental bed exclusively designed for research in the field of automotive engineering, as illustrated in Fig. 1. The setup encompasses a single-cylinder, four-stroke diesel engine fixed to an eddy current dynamometer that regulates engine loading. The engine's bore is 87.5 mm, its stroke length is 110 mm, and the total swept volume is 661.5 cm3. The trials were carried out at a compression ratio of 17.9 with a steady speed of 1630 rpm. The paraphernalia essential for measuring in-cylinder pressure and crank angle was installed in the engine. In addition, interfaces for load measurement, temperature, airflow, and fuel flow were all installed. For determining the P0-PV diagrams, these engine signals are interfaced to a computer via a data logger device. The configuration facilitates the analysis of engine performance for the following parameters: mechanical efficiency (ME), volumetric efficiency (VE), specific fuel consumption (SFC), air-fuel (A/F) ratio, heat balance, brake mean effective pressure (BMEP), brake power (BP), frictional power (FP), brake thermal efficiency (BTE), indicated thermal efficiency (ITE), and brake mean effective pressure (IMEP). The setup consists of an isolated panel box with an air box, a fuel tank, and transmitters that monitor air and fuel flow. "ICEngine _ SoftL V9 .1" is the application program for engine recital assessment. A model of the software interface is shown in Fig. 2.

A flue gas analyzer is installed on the engine exhaust pipe to measure and record the exhaust gas components and their concentrations. To ensure precise and high-performing procedures, ea sample is dried and cleaned using specialized gas specimen conditioner equipment. Via an inlet a particulate filter, an inner pump sucks a gas stream into the sensor's chamber. The device was de to detect the concentration of 6 species: CO, CO2, CxHy, NOx, O2, and SOx.

Fig. 1 The test engine used in the experimental investigation

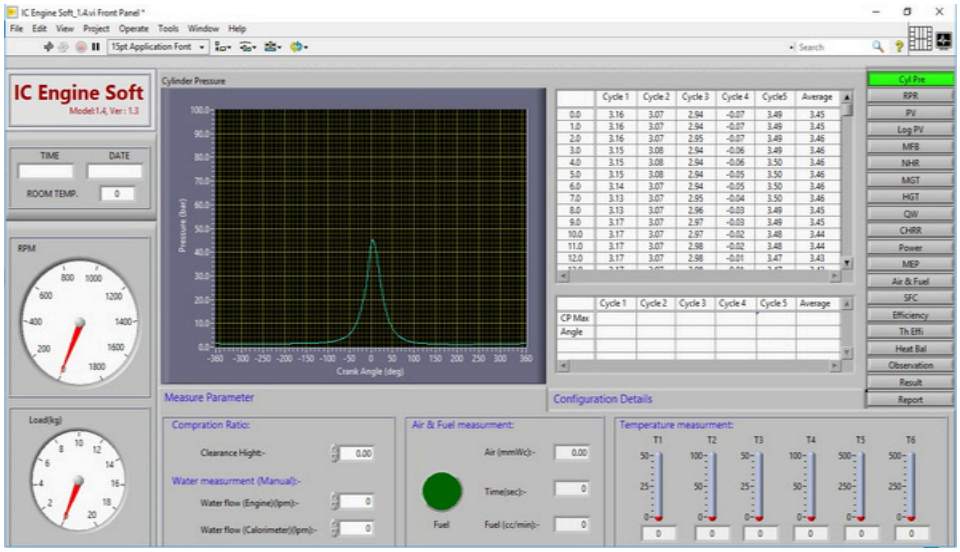

Fig. 2 Front panel of the engine performance software.

Table 1 presents the properties of pure diesel and the two blends. Blend 1 (D70B10W10DD10) has highest viscosity, which could affect fuel injection and flow characteristics compared to pure die Blend 2 (D85B5W5DD5) has a lower viscosity than Blend 1 but is still higher than pure diesel. Als the table shows that all blends have lower heating values than pure diesel, with Blend 1 being the This indicates that the blends may produce less energy upon combustion than pure diesel. At the time, the densities of both blends are slightly lower than that of pure diesel, reflecting the influen the lighter components (butanol and diethyl ether) in the blends.

Table 1: Physical and chemical properties of the fuels used in the investigation

	Diesel	Blend 1	Blend 2
Composition	Pure diesel fuel	D70B10W10DD10	D85B5W5DD5
Viscosity	3.0 cSt at 40°C.	5.9 cSt at 40°C.	4.4 cSt at 40°C
LHV	42.5 MJ/kg.	40.5 MJ/kg	41.8 MJ/kg
Density	0.850 g/cm³	0.831 g/cm³	0.836 g/cm³

3. Results and discussions

3.1. Performance parameters

Figure 3 presents the p-theta diagram of the engine for the three fuels at zero load and 75% load. The peak pressure is around 50 bar and occurs slightly after the top dead center (TDC, at 0° crank angle), typical in diesel engines. The pressure for pure diesel rises gradually as the crank angle approaches TDC. It reaches a peak pressure of just over 50 bar around TDC and gradually drops afterward. Blend 1 exhibits a slightly higher peak pressure than pure diesel, peaking at around 50-52 bar. The pressure rise begins earlier than pure diesel, indicating faster combustion or better ignition characteristics. Blend 2 shows the highest peak pressure of the three, peaking just above 52 bar. Like Blend 1, it has an earlier pressure rise than pure diesel, suggesting more rapid combustion.

Blends 1 and 2 produce higher peak pressures than pure diesel, indicating more efficient combustion at zero load. This could be attributed to the improved ignition or combustion characteristics of the additives in the blends. Blend 2, in particular, shows the highest pressure, implying it has the most enhanced combustion behavior. The earlier pressure rise in Blends 1 and 2 suggests better fuel atomization, quicker ignition, and possibly oxygenated additives, which promote faster combustion. Pure diesel has a slightly delayed pressure build-up, which might indicate a less aggressive combustion at zero load. After the pressure peaks, all curves follow a similar pattern, gradually dropping in pressure. However, the blends maintain higher pressure values for slightly longer after TDC, suggesting a more sustained combustion phase than pure diesel.

Both blends perform better in peak pressure and faster combustion, indicating improved engine performance and potentially lower fuel consumption or fewer unburnt hydrocarbons. Blend 2 shows the highest pressure and fastest combustion among the blends. This could indicate that blend 2 might provide better energy output performance, but the increased peak pressure might also lead to higher NOx emissions.

The pressure history at 75% load has the same trend as the zero load. However, the greater the load, the greater the peak pressure inside the cylinder. In both figures, blend 2 exhibits the maximum pressure among the three fuels. At zero load, the maximum pressure is 53 bar, while at 75%, the peak pressure is 74 bar.

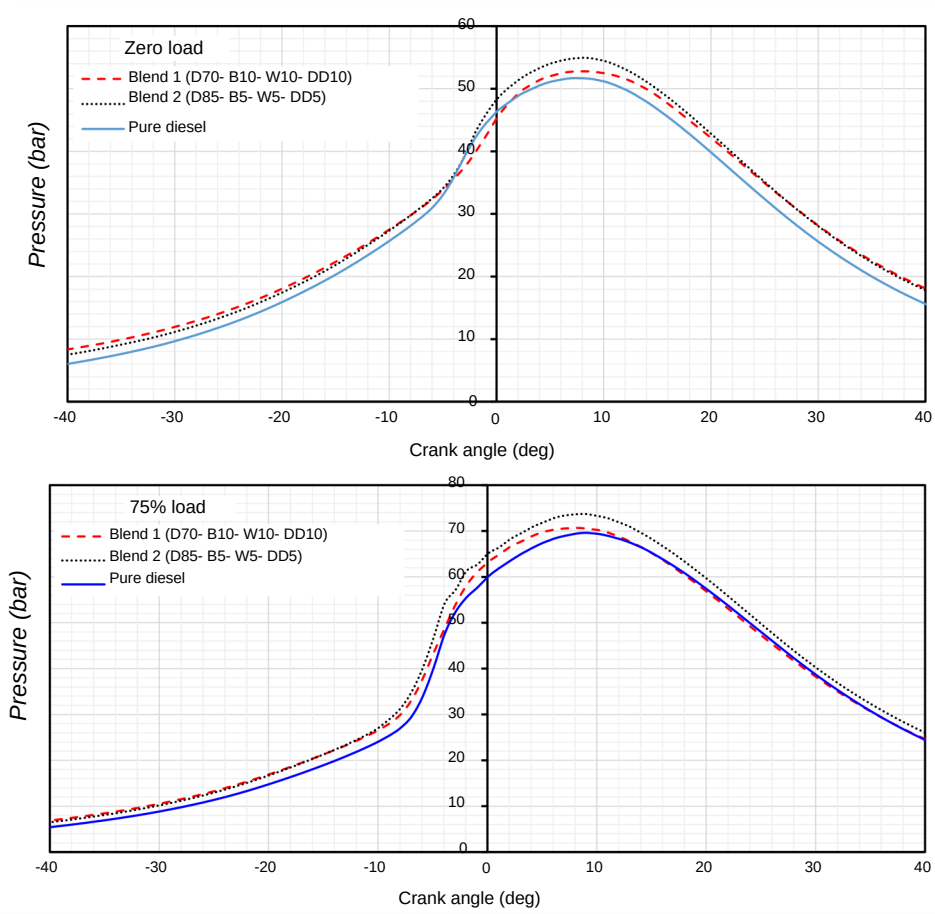

Fig. 3 The p-theta diagram for the three fuels: at zero load and 75% load.

Figure 4 shows the p-v indicator diagram of the three fuels at no load and 75% load. This type of diagram helps evaluate the efficiency and combustion characteristics of different fuel blends, whi essential when assessing alternatives to pure diesel for improved performance and reduced emis For the zero load case, pure diesel shows the pressure rise and fall during the engine cycle for diesel fuel. Peak pressure occurs early, around 50 bar, then rapidly drops as the volume increases 1 results in a slightly higher peak pressure than pure diesel, with a peak around 53 bar. The curve closely follows the diesel curve but suggests a marginally more powerful combustion phase. Ble shows a peak pressure similar to Blend 1, around 53 bar, with a slightly faster pressure drop-off the other curves, indicating a quicker release of energy during combustion. Blends 1 and 2 demor slightly higher peak pressures than pure diesel, which could improve engine performance.

The differences in pressure distribution and drop-off rates suggest slight variations in how each blend combusts within the engine. Blend 2 may release energy more quickly, leading to quicker combustion phases. No significant difference is noted for the 75% load case, which has almost the same trend but with higher peak pressure than the no-load case.

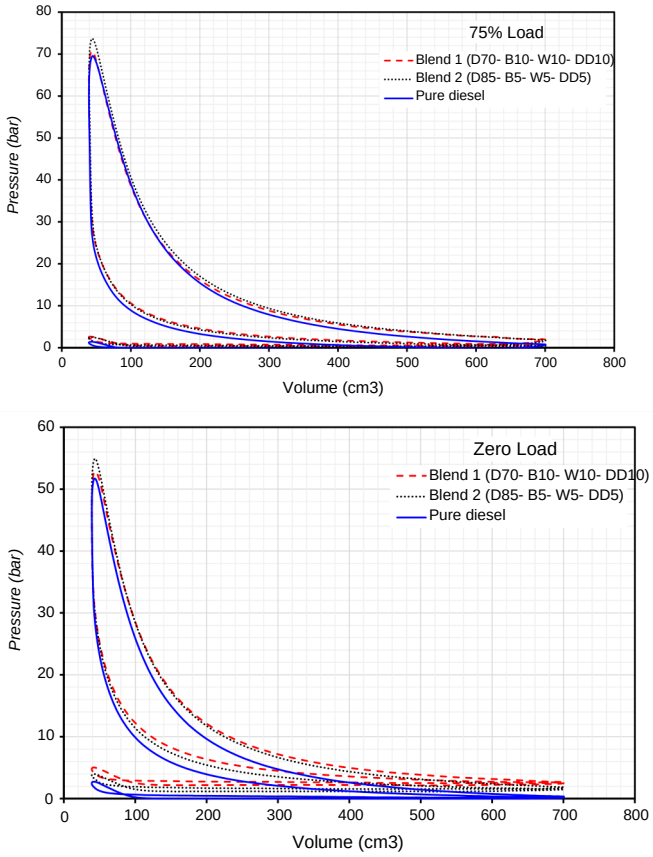

Fig. 4 The indicator diagram for the three fuels at zero load and 75% load.

Figure 5 illustrates the brake thermal efficiency (BTE) of two fuel blends compared to conventiona diesel at varying engine loads. Blend 1 shows an increase in brake thermal efficiency from 0% to 5 load, peaking around 50%, then gradually decreasing beyond that point. Blend 2 shows a much h peak brake thermal efficiency at around 75% load, surpassing Blend 1 and Diesel at mid to high conditions, but drops quickly afterward. Pure diesel shows a relatively stable and moderate increa efficiency, peaking at around 75% load, but it doesn't reach the levels of the other two blends. Ble offers the highest efficiency at higher loads (around 75%), outperforming Blend 1 and diesel.

Also, Blend 1 has a strong performance at mid loads (50%) but falls off more sharply beyond th compared to diesel. Diesel maintains a more consistent performance across various loads but d excel at any particular point compared to the blends.

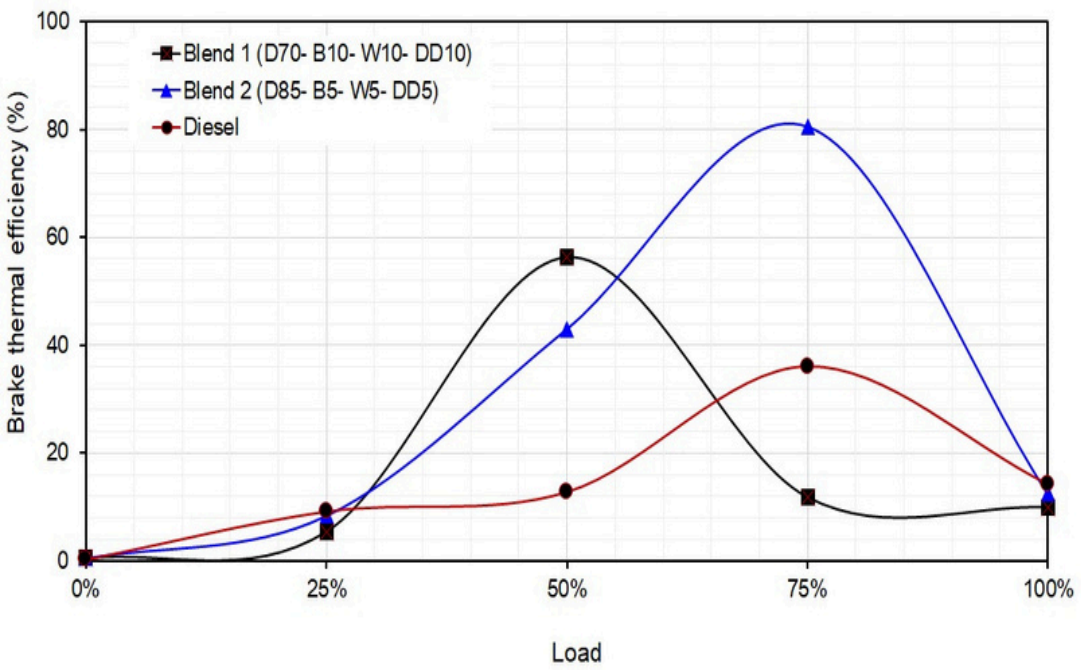

Fig. 5 Variation of the brake thermal efficiency with the applied load for the different fuels.

3.2. Engine emissions

Figure 6 compares three fuel blends' nitrogen oxide emissions under varying load conditi
The fuels compared are Blend 1 (D70-B10-W10-DD10), represented by black squares; Blend 2 (D85- B5-W5-DD5), represented by blue triangles; and Diesel, represented by orange circles. Blend 1 starts at approximately 50 ppm NO_x at 0% load and increases steadily, peaking around 150 ppm at 75%. At 100% load, it decreases slightly. Blend 2 starts at around 100 ppm NO_x at 0% load, rises sharply to about 200 ppm at 50% load, then stabilizes and slightly decreases as the load increases to 100%. Diesel exhibits much lower NO_x emissions than both blends, starting around 50 ppm at 0% load, maintaining a relatively stable level until around 50% load. Afterward, it begins to rise but remains significantly lower than the two blends, even at full load. The important note is that higher NO_x emissions from Blends 1 and 2, where both blends produce significantly higher NO_x emissions than conventional diesel, particularly at higher loads.

Blend 2 exhibits a steeper increase in NO_x emissions as the load increases, peaking earlier at around
50% load. Diesel fuel shows more consistent NO_x emissions across the load spectrum, comparatively low, though it does begin to rise at higher loads.

The components of Blend 1 and Blend 2 might contribute to different combustion characteristics, leading to variations in NO_x emissions. Also, adding waste cooking oil to fuel ble
remaining
reduces combustion temperatures, which can sometimes lower NO_x emissions.

However, the specific amounts in these blends may not be sufficient to achieve this effect, especially as the load increases. While butanol and other alcoholic fuels can offer renewable or lower-carbon advantages, they may also lead to higher NO_x emissions due to their combustion properties.
DEE is oxygenated like butanol and can increase combustion efficiency, possibly producing higher local temperatures and NOx emissions. Both butanol and DEE introduce more oxygen int combustion process, which can enhance combustion and pose a risk of increased NOx due to h local combustion temperatures.

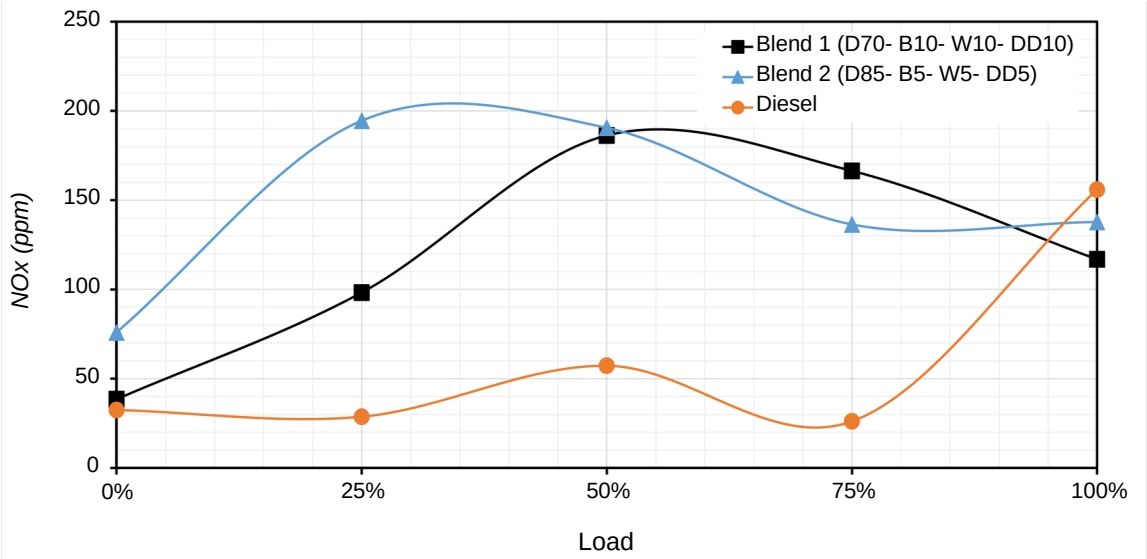

Fig. 6 Variation of the NOx emissions with load for the different blends.

Figure 7 presents the carbon monoxide emissions as a percentage (%) for three different fuel blends under varying load conditions. Diesel fuel starts at around 0.03% CO at 0% load, decreasing slightly at 25%, then rises steeply after 50%, peaking around 0.17% at 100% load. Blend 1 begins slightly above 0.03% CO at 0% load. It shows a mild decrease as load increases, staying relatively stable up to 75% load, then increasing slightly to around 0.05% at 100% load. Blend 2 shows a slight increase in CO emissions as load increases, starting at around 0.03% at 0% load, peaking just above 0.06% at 75% load, and then slightly decreasing at 100% compared to pure diesel.
Diesel shows the steepest increase in CO emissions at higher loads, indicating that its combustion efficiency significantly decreases as the load increases. This trend suggests that diese not burn as cleanly at higher loads, leading to incomplete combustion and higher CO production. 1 demonstrates more stability across the load spectrum, with lower overall CO emissions than d especially at higher loads. This could indicate better combustion characteristics under high-load conditions. Blend 2 shows a moderate rise in CO emissions, peaking at around 75% load, then dec slightly by 100%. This suggests that its combustion process might stabilize or become more effic at full load than diesel.

The CO emissions are typically a sign of incomplete combustion. Diesel emits more CO at higher loads, suggesting that its combustion efficiency declines as the load increases. On the other hand, both blends seem to maintain more stable or improved combustion at higher loads, likely due to the butanol or waste cooking oil components improving fuel combustion characteristics.
Both blends' waste cooking oil and diesel-diluted components (W and DD) could contribute to complete combustion and lower CO emissions, particularly in Blend 1. The waste cooking oil in blends often leads to more complete combustion by reducing combustion temperatures, while ac may enhance combustion efficiency.

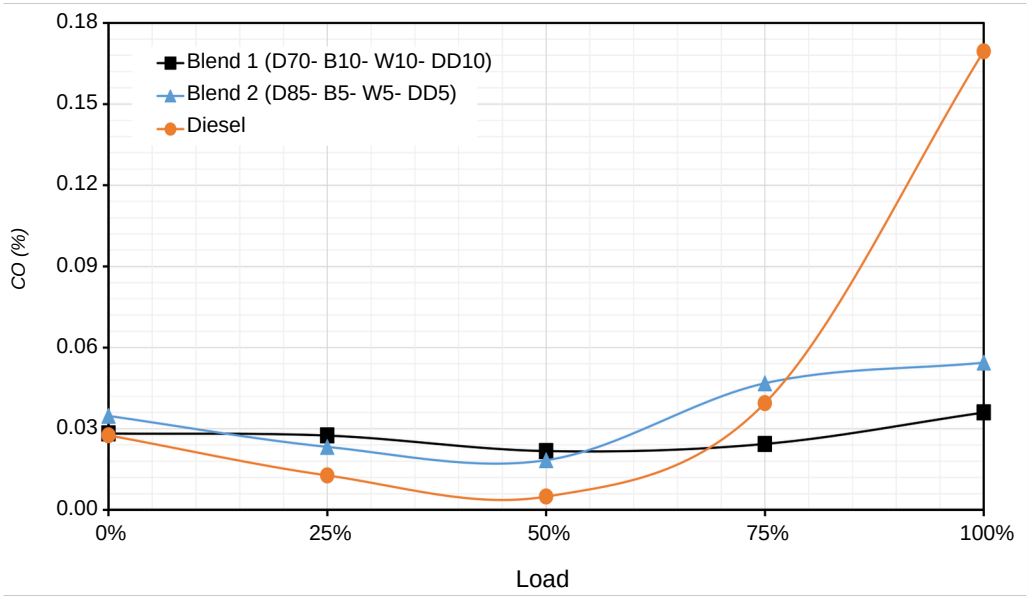

Fig. 7 Variation of the CO emissions with load for the different blends.

Figure 8 shows the variation of the emitted hydrocarbons with the engine load for the three studi fuels. At low loads (0% to 25%), diesel has the lowest HC emissions, with values under 50 ppm. T HC emissions increase significantly at higher loads (75% to 100%), peaking around 200 ppm at 7 load before dropping slightly at 100%. Diesel's HC emissions sharply increase with load, significan beyond 50%, suggesting it produces more hydrocarbons at high engine loads.

For Blend 1, this fuel blend maintains a reasonably consistent HC emission level across the load range. The highest emissions are observed at 25% and 100% load, but emissions remain below 100 ppm even at their peak. It shows the most stable behavior regarding HC emissions across different loads.Blend 2's HC starts moderately low and increases to 50% load, where emissions peak near 100 ppm. After 50% load, the emissions drop significantly, making it the lowest emitting blend at high loads (75% to 100%). Such a blend emits more HC at lower to mid loads (25% to 50%) but performs better at high loads, reducing emissions significantly after 50%.

Fig. 8 Variation of the HC emissions with load for the different blends

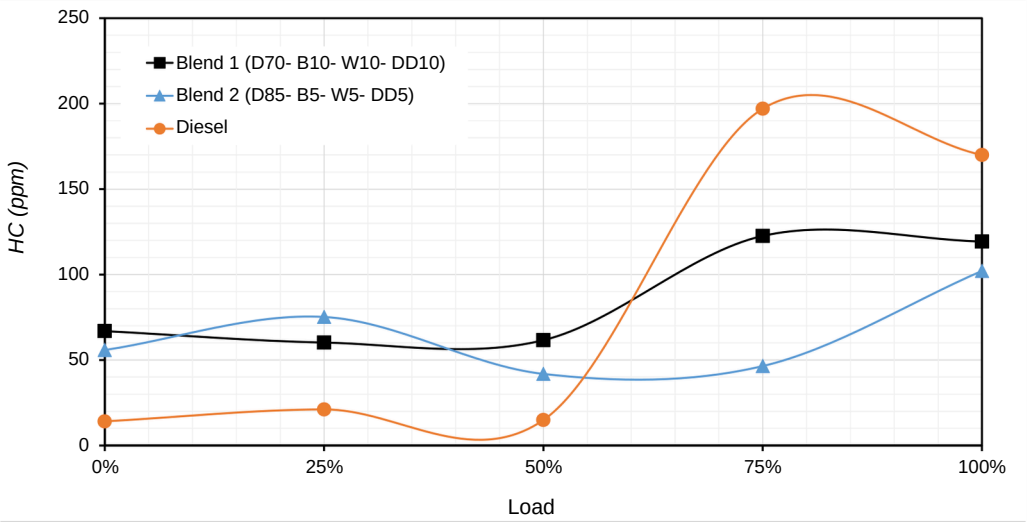

4. Conclusions

The current study presents an experimental analysis of a diesel engine's performance and exhaust emissions mainly running on waste cooking oil (WCO). The engine type utilized is a single-cylinder direct injection diesel engine with constant speed and natural aspiration. The research was done on the engine's performance and emission parameters when fueled with a mixture of 5% butanol, 85% diesel, 5% WCO, and 5% diethyl ether (D85B5W5DD5). The study's findings demonstrated that engine emissions of nitrogen oxides (NOX) and carbon monoxide (CO) varied significantly depending on the
applied load. The brake thermal efficiency and cylinder pressure were all impacted by load change.

Also, the engine emissions change considerably with the engine load. Based on the study

1. findings, the
following points arise:
2. Blends 1 and 2 perform better in peak pressure and faster combustion, indicating improved engine
performance and potentially lower fuel consumption or fewer unburnt hydrocarbons. Blend 2 shows the highest pressure and fastest combustion among the blends. This reflects that blend 2 provides better

3. Blend 2 shows a much higher peak brake thermal efficiency at around 75% load, surpassing Blend 1 and Diesel at mid to high load conditions, but drops quickly afterward. Diesel exhibits much lower NO_x emissions than both blends, starting around 50 ppm at 0% load, maintaining a relatively stable level until around 50% load. Afterward, it begins to rise but remains significantly lower than the two blends, even at full load. The studied blends can interact in intricate ways. For example, the oxygen concentration of butanol and waste cooking oil can boost combustion efficiency, while DEE's high cetane number can increase ignition quality. These factors can all contribute to increases in NOx emissions, although the overall effect depends on the blend ratios and engine operating circumstances. Blend 2 shows a slight increase in CO emissions as load increases, starting at around 0.03% at zero- load, peaking just above 0.06% at 75% load, and then slightly decreasing at 100% compared to pure diesel. Blend 2's HC starts moderately low and increases to 50% load, where emissions peak near 100 ppm. After 50% load, the emissions drop significantly, making it the lowest emitting blend at high loads (75% to 100%). Such a blend emits more HC at lower to mid loads (25% to 50%) but performs better at high loads, reducing emissions significantly after 50%. There will be many challenges faced when implementing biodiesel-diesel blends because the complexity of the fuel and the additives in the combustion process where high temperature existed, and no one can predict the products of the combustion unless the experimental testing is done to find the final percentage of the gas results for each new blend.

4. 5. 6. 7.

In conclusion, research involving experimentation and mathematical modeling is necessary to accurately assess the effect of different fuel blends on NOx, CO, and HC emission levels. Blend 2 reduces overall emission levels compared to pure diesel fuel. Still, more investigations will be done to understand the emission behavior in the experimental work by adding different additives like nano particles or improving the biodiesel mixture characteristics.

References

[1] Agarwal AK, Krishnamoorthi M. Review of morphological and chemical characteristics of particulates from compression ignition engines. International Journal of Engine Research. 2023;24(7):2807-2865. https://doi:10.1177/14680874221114532.
[2] Lv, J.; Wang, S.; Meng, B. The Effects of Nano-Additives Added to Diesel-Biodiesel Fuel Blends on Combustion and Emission Characteristics of Diesel Engine: A Review. *Energies* 2022, *15*, 1032. https://doi.org/10.3390/en15031032.
[3] Musculus, Mark P, and Dietz, Jeff. Effects of diesel fuel combustion-modifier additives on In-cylinder soot formation in a heavy-duty Dl diesel engine. United States: N. p., 2005. Web. https://doi:10.2172/876311.
[4] Modi, A., Gosai, D., Gillawat, A. (2024). 'Impact of nano-fuel additives and nano-lubricant oil additives on diesel engine performance and emission characteristics', Journal of Heat and Mass Transfer Research, https://doi: 10.22075/jhmtr.2024.33460.1531
[5] Habib Z, Parthasarathy R, and Gollahalli S. Performance and emission characteristics of biofuel in a small-scale gas turbine engine. Applied Energy 87 (2010).
[6] Esfandabadi ZS, Ranjbari M, Scagnelli SD. The imbalance of food and biofuel markets amid Ukraine-Russia crisis: a systems thinking perspective. Biofuel Resources Journal 9 (2022).
[7] EL-Seesy A., Waly M., Zhixia H., El-Batsh H., Nasser A., and Radwan M., Influence of quaternary combinations of biodiesel/methanol/n-octanol/ diethyl ether from waste cooking oil on combustion, emission, and stability aspects of a diesel engine. Energy Conversion and Management 240 (2021).
[8] Radwan M., Ahmed S., Huzayyin A.S., and EL-Seesy A., Effect of diethyl ether addition to waste cooking oil biodiesel on the combustion and emission characteristics of a swirl-stabilized premixed flame. Energy Conversion and Management 286 (2023).
[9] Sandouqa A, and Al-Hamamre Z. Energy analysis of biodiesel production from jojoba seed oil. Renewable Energy 130 (2019).
[10] El-Seesy A., Hamdy H., Latif I., Zhixia H. and Manzoore E., Combustion, emission, and phase stability features of a diesel engine fueled by Jatropha/ ethanol blends and n-butanol as co-solvent. International Journal of Green Energy 17:12, 793-804, DOI: 10.1080/15435075.2020.1798770
[11] Venkatesan P. E., B Dinesh., Samuel O.D., Kaisan M.U., Murugesan P. (2021) Effect of Hybrid Nanoparticle on DI Diesel Engine Performance, Combustion, and Emission Studies. In: Singh A.P., Agarwal A.K. (eds) Novel Internal Combustion Engine Technologies for Performance Improvement and Emission Reduction. Energy, Environment, and Sustainability. Springer, Singapore. https://doi.org/10.1007/978-981-16-1582-5_10.

Machine Learning Pipeline: Feature Selection and Adaptive Training for DDoS Detection to Improve Cloud Security

Yazed Alsaawy

0000-0001-5031-3388

Department of Computer Science

Faculty of Computer and Information Systems

Islamic University of Madinah

yalsaawy@iu.edu.sa

Madinah 42351, SAUDI ARABIA

Abstract: DDoS attacks are a concern in most distributed and cloud environments, and they can be a threat to any multi-cloud system. This research offers an innovative method to detect DDoS using adaptive machine learning techniques. The proposed methodology deploys a combination of algorithms, such as LightGBM, CatBoost, and XGBoost, with an overall accuracy of 99.32%, 99% specificity, and 99% sensitivity for most attack classes. In addition, the methodology addressed the challenges of the minority classes, where CatBoost had a recall of 85% for previously marginalized attacks. The results indicate the effectiveness of the proposed system across different DDoS attack types and traffic patterns, making it viable and effective for the protection of cyber security structures that operate in a multi-cloud system.

Keywords: Distributed Denial-of-Service, Machine Learning, LightGBM, CatBoost, XGBoost, Adaptive Detection, Cloud Security, Cybersecurity, Minority Class Handling, Scalable Solutions.

خط أنابي ب التعلم الآلي: اختيار الميزا ت والتدري س التكيفي للاكتشا ف هجمات الحرمان من الخدم ة الموز لتحسين أمان السحابة

الملخص: تشكل هجمات الحرمان من الخدمة الموزعة مصدر قلق في معظم البيئات الموزعة والسحابية، ويمكن أن تشكل تهديدًا لأي نظام متعدد السحابة. يقدم هذا البحث طريقة مبتكرة للكشف عن هجمات الحرمان من الخدمة الموزعة باستخدام تقنيات التعلم الآلي. تم تطوير [illegible] المقترحة، مجموعة من الخوارزميات مثل LightGBM و CatBoost و XGBoost، بدقة إجمالية تبلغ 99.32% وحساسية 99% لمعظم فئات الهجوم. بالإضافة إلى ذلك، تناولت المنهجية تحديات الفئات الأقلية، حيث كان لدى CatBoost قدرة تذكر تبلغ 85% للهجمات المهمشة سابقًا. تشير النتائج إلى فعالية النظا م المقترح عبر أنواع مختلفة من هجمات DDoS وأنماط حركة المرور، مما يجعله قابلً للتطبيق وفعالًا لحماية هياكل الأمن السيبراني التي تعمل في نظام متعدد السحابة.

1. Introduction

The cloud computing paradigm can be defined as on-demand computing services, such as the availability of servers, storage, network management, databases, software, platforms, and applications via the Internet [1]. Cloud resources are distributed over multiple cloud centers across continents. Today, the top listed cloud computing service providers are Google Cloud Platform, Amazon Web Services (AWS), and Microsoft Azure. The Cloud computing paradigm is no longer a buzzword; it has matured today. However, with the advent of online and ubiquitous services, human interaction, businesses, healthcare, and education have renewed perspectives. Individuals, businesses, and governments have a massive demand for the adoption of cloud computing services in the recent past [2]. As per a Statista report [3], cloud computing generated an enormous revenue in 2021 of $400 billion, worldwide.

Classically, cloud service is divided into three services, which are Software as a Service (SaaS Infrastructure as a Service (IaaS), and Platform as a Service (PaaS). SaaS allows users to use clou based software connecting to the Internet, such as email, Microsoft Office 365, and Zoom. In cont IaaS provides computing resources that are part of the cloud over the Internet. Users get the impr that they own powerful computing resources, but not in reality. The user handles the cloud infrast by using the concept of cloud virtualization.

Further, PaaS is the fusion of infrastructures like servers, storage, and network hardware and a platform where users can code, test, and deploy the application—for example, Azure and Google Engine. The three cloud service models and their applications are depicted in Figure 1.

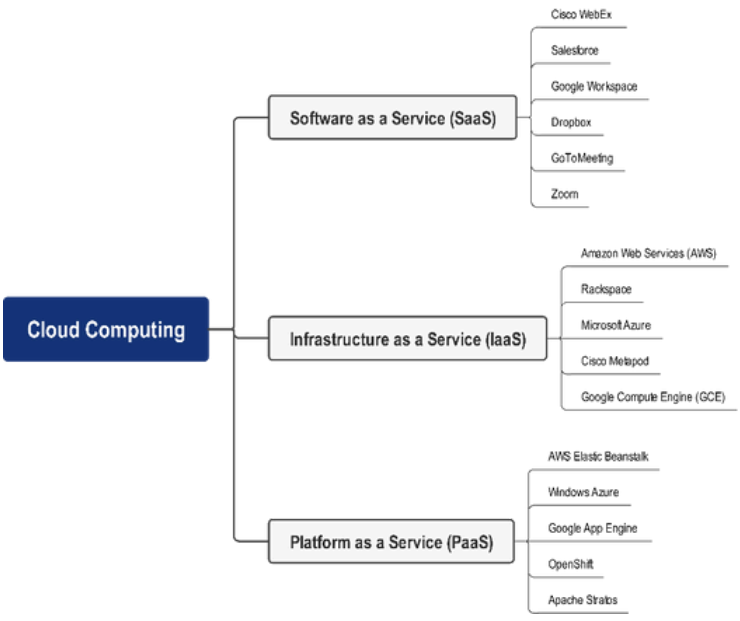

Figure 1. Cloud computing services.

The cloud computing demand is growing. At the same time, there is incremental growth in serious threats from hackers, malicious users, and cyber criminals who need to be countered with effective measures [4], [5]. The security concerns are complex and diverse, including data privacy concerns, denial-of-service (DoS) attacks, and minimal transparency about intrusions from cloud service providers. A DoS attack sends bulk traffic to the cloud server from a single IP or a computer. Distributed denial-of-service (DDoS) is a DoS attack that uses multiple IPs or computers sendin requests to a cloud server. Due to this sudden traffic flooding, a website or cloud resource crashes or is unavailable for processing users' requests [6]. The most significant DDoS attack ever recorded against a European customer on the Prolexic platform was detected and mitigated by Akamai on Thursday, July 21, 2022 [7]. Here are a few recent examples of DDoS attacks:

- GitHub DDoS attack in February 2022.
- Akamai DDoS attack in June 2021.
- Amazon Web Services (AWS) DDoS attack in May 2021.
- T-Mobile DDoS attack in August 2020.
- University of California San Francisco DDoS attack in June 2020.

This paper addresses a frequent and practical problem cloud services face today: DDoS attacks. U conventional machine learning approaches that rely heavily on static datasets, this study introc adaptive methods to address the dynamic and evolving nature of modern DDoS attacks. This s leverages advanced machine learning algorithms, including LightGBM, CatBoost, and XGBoost, which provide scalable and high-performance solutions for DDoS detection. Unlike binary classification methods that classify traffic as either normal or attack, this study addresses a multi problem, identifying both normal requests and multiple types of attacks. By incorporating fea selection techniques, this approach enhances computational efficiency while improving detection accuracy across diverse traffic types. This categorization aids in designing better cybersecurity solutions by enabling attack-specific mitigation strategies.

1.1 Research Contributions

The contributions of the proposed study are in two folds, which are:

- Propose an adaptive machine learning-based approach to detect DDoS attacks, integratin advanced algorithms such as LightGBM, CatBoost, and XGBoost. This approach is capabl of managing the dynamic and evolving nature of modern-day DDoS attacks.
- Develop a multiclass prediction method for DDoS attack detection that not only classifies regular requests but also identifies specific types of attacks. This advancement enables creation of more targeted and powerful attack-specific defense technologies.
- Design a scalable and lightweight DDoS detection method that achieves high accuracy and sensitivity while requiring less computational and data resources, making it suitable for dynamic cloud environments.

1.2 Paper Structure

The paper is divided into five sections. Section 2 discusses literature related to research and development concerning methods used to detect DDoS attacks. Section 3 comprehensively explai proposed machine learning-based DDoS attack detection method, integrating advanced algorithm as LightGBM, CatBoost, and XGBoost, whereas section 4 critically discusses the results. Finally, th study is concluded in Section 5, highlighting key contributions and potential directions for fut research.

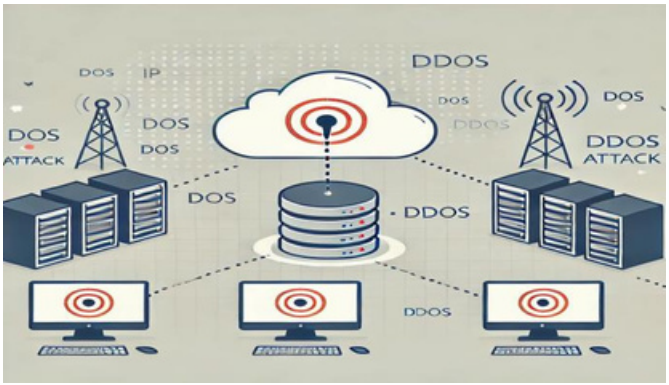

Figure 2. Block diagram of DoS and DDoS attacks on a cloud server.

2. Literature Review

For a seamless operating cloud computing application, it is imperative to detect threats to the before they cause any server crash or resource unavailability. The most common and critical threa are DDoS attacks [8]. DoS attacks are easy to identify as they come from a single machine. Howev DDoS attacks are not easily detectable as these attacks pretend to originate from different machi as depicted in Figure 2. Thus, it is hard for security devices to distinguish between regular user requests and DDoS attacks [6], [9]. Machine learning started to play an essential role in identifying DoS and DDoS attacks in the last decade because rather than just focusing on malicious IP addres these algorithms tried to understand the pattern and behaviors of DDoS attacks [1] [10]. The proceeding subsections discuss machine learning and deep learning-based methods for detecting DDoS attacks on cloud servers.

2.1 Machine Learning

Machine learning helps to understand an environment and its processes comprehensively. Machine learning algorithms learn from examples and acquire the ability to perceive unseen scen for the given task.

Machine learning is widely used to defend cloud servers from DoS and DDoS attacks. Some o the popular choices of algorithms are Decision trees, Support Vector Machines (SVM), Random Forests, and Ensembles.

Decision tree classifiers are robust and quite popular in detecting DDoS attacks. Lakshminarasimman et al. [19] used a classical J48 decision tree classifier on the KDDCup'99 datas to predict attacks. One major issue with decision tree classifiers is that they get slower and resour exhausted with increasing feature space, tree, and depth. There are multiple studies performed t address this issue. Latif et al. [20], [21] proposed a fast decision tree classifier and analyzed it for DDoS attacks on cloud-based wireless body area networks (WBAN). Further, to address the resou exhausted issues, Kareem et al. [22] proposed a lightweight partial decision tree classifier for DDo attack prediction.

SVM is a powerful classifier, particularly for binary classification problems. SVM aims to find an optimal decision boundary, a hyperplane, which can differentiate among classes for DDoS atta detection. Such as Ye et al. [23] proposed a method that used the fusion of an SVM classifier with feature extraction to predict DDoS attacks. In [21], Tang et al. [22] also used feature extraction to power the SVM classifier. Further, Abusitta et al. [24] proposed an SVM-based method that monit in an adaptive manner where it updates its knowledgebase as per the real-time state of the cloud which helped the method improve DDoS attack detection accuracy. A modified version of SVM is proposed by Oo et al. [25], which has better execution times and improved accuracy in predicting DDoS attacks. One disadvantage of SVM is that its performance is not good when there are overlapping classes that the author in [25] tried to address.

Ensemble learning classifiers try to mitigate the weaknesses of various classifiers and fuse th to strengthen the classification process. A recent study by Alduailij et al. [26] used feature selectio and ensemble learning fusion. First, they used Mutual Information (MI) and Random Forest for feature selection. Then, the authors applied Random Forest (RF), Weighted Voting, and Gradient Boosting. Similarly, in another study, Thanh and Lang [27] used the UNSW-NB15 dataset to critically analyze the performances of Bagging, Random Forest, AdaBoost, Stacking, and Voting classifiers. The study showed that the Stacking classifier produced the best results.

In contrast, Jia et al. [28] proposed hybrid and heterogeneous ensemble classifiers that conta classifiers from different algorithmic families to detect DDoS attacks. Another ensemble classifier was proposed by Firdaus et al. [29] as a fusion of Random Forest and K-means++ classifiers for DDoS attack detection, producing enhanced prediction accuracy. Ensemble learning is a prevalent choice in DDoS attack detection. However, it has a computation tradeoff as it needs a powerful system and more processing time.

2.2 Deep Learning

Deep learning methods mimic the learning process of humans. Neural network-based algorit are solving some of the most complex problems today. They can learn from nonlinear data, maki them perfect from images to the natural language processing domain [30], [31]. Several deep lea architectures are proposed, and the six widely used ones are given in Table 2. Slowly, these deep learning methods are making inroads in detecting DDoS attacks. In this quest, Yuan et al. [32] proposed DeepDefense, a deep learning-based approach for classifying DDoS attacks. The results were compared with classical machine learning methods, and there was a 5.4% decrease in the e rate, proving the usefulness of DeepDefense. Another deep learning method proposed by Lopes

[33], known as CyDD, is the fusion of feature engineering and deep learning. CyDDoS was tested o the CICDDoS2019 dataset. Furthermore, [33] focused on reducing the processing overheads as m deep learning-based methods are resource-exhaustive. More recently, Xinlong and Zhibin [34] proposed a hybrid deep learning method using Hierarchical Temporal Memory to detect DDoS attacks.

From the above-mentioned literature, it is evident that for DDoS attack detection, the researc community is putting deep learning methods into practice. In the proceeding section, a deep lear based method powered by an adaptive mechanism is proposed to detect DDoS attacks. As per th above literature, no prior study is adaptive and capable of handling newer DDoS attacks.

Table 1 highlights the diverse approaches to machine learning and deep learning for DDoS th detection and categorization. From traditional methods like KNN and SVM to more complex syste such as DCNN and NDAE, each study focuses on different aspects of DDoS detection, employing a variety of techniques to improve accuracy, reduce resource consumption, or enhance the ability t distinguish between benign and malicious traffic. The table underscores the advancements in AI-driven cybersecurity measures, displaying the potential of both machine learning and deep learni combating DDoS attacks effectively.

Table 1. Tabular Representation of the Literature Review

Study & Reference	Technique Used	Detailed Approach Description	Dataset Used	Outcome / Performance
Wang et al. [12]	Dynamic MLP (SBSMLP classifier)	31 optimized sequence features, feedback mechanism	NSL-KDD	High accuracy with a specific feature set and classifier
Can et al. [13]	DDoSNet (fully-connected MLP)	24 selected features for a fully-connected MLP classifier	CICDDoS2019	High accuracy in binary classification using a neural network approach
Samom & Taggo [14]	ML models (LR, RF, MLP, etc.)	20 selected features for classifying four different attack types	CICDDoS2019	Random Forest showed the best performance; lower performance with the entire feature set

Wei et al. [15]	Hybrid AE-MLP	Autoencoder for feature extraction (5 optimal features)	CICDDoS2019	Effective for multi-class classification of various attack types
Kalutharage et al. [16]	Autoencoder, Kernel SHAP	Detecting DDoS anomalies with instance-by-instance explanations and feature correlations.	USBIDS	Static dataset limits the generalizability
Antwarg et al. [17]	Kernel SHAP	Explaining the impact of reconstruction error features to experts.	NSL-KDD	-
Šarčević et al. [18]	SHAP, If-then decision tree	Comparison of SHAP and If-then decision tree rules for transparency and comprehensiveness.	CICIDS2017	If-then rules increase tree depth, SHAP is less comprehensive.
Lakshmi-narasimman et al. [19] [20]	Decision Tree (J48)	Employed a classical J48 decision tree classifier to predict DDoS attacks, highlighting its robustness in detection despite issues with scalability and resource exhaustion.	KDD Cup'99	Predictive success in DDoS attack detection, with scalability concerns.
Latif et al. [21]	Fast Decision Tree	Developed a fast decision tree classifier to efficiently address DDoS attacks, specifically tailored for cloud-based wireless body area networks (WBAN).	Cloud-based WBAN	Improved speed and efficiency in detecting DDoS attacks on WBAN.
Kareem et al. [22]	Lightweight Partial Decision Tree	Proposed a partial decision tree classifier designed to be resource-efficient for DDoS attack prediction, addressing traditional decision tree limitations.	Not specified	Enhanced DDoS attack prediction with reduced resource consumption.
Ye et al. [23]	SVM with Feature Extraction	Combined SVM classifier with feature extraction techniques to predict DDoS attacks, aiming to improve classification accuracy through optimal decision boundary identification.	Not specified	Improved DDoS attack detection accuracy with the fusion of SVM and feature extraction.

Abusitta et al. [24]	Adaptive SVM	Introduced an adaptive SVM-based method for real-time DDoS detection that updates its knowledge base according to the cloud's state, addressing overlapping class issues.	Cloud environments	Improved real-time DDoS attack detection with adaptive learning capabilities.
Oo et al. [25]	Modified SVM	Proposed a modified version of SVM with better execution times and accuracy for predicting DDoS attacks, specifically addressing the challenge of overlapping classes.	Not specified	Enhanced prediction accuracy and efficiency in DDoS attack detection.
Alduailij et al. [26]	Ensemble Learning	Applied feature selection via Mutual Information (MI) and Random Forest, followed by an ensemble of RF, Weighted Voting, and Gradient Boosting for DDoS detection.	Not specified	Enhanced accuracy in DDoS attack prediction, with computational tradeoffs.
Thanh and Lang [27]	Ensemble Classifiers	Critically analyzed performances of various ensemble methods (Bagging, RF, AdaBoost, Stacking, Voting) on the UNSW-NB15 dataset, finding the Stacking classifier to be superior.	UNSW-NB15	The stacking classifier produced the best results in DDoS attack detection.
Jia et al. [28]	Hybrid Ensemble Classifiers	Proposed hybrid and heterogeneous ensemble classifiers from different algorithmic families to detect DDoS attacks, aiming for diversified detection strategies.	Not specified	Highlighted the strength of algorithmic diversity in enhancing DDoS attack detection.
Yuan et al. [32]	DeepDefense	Deep learning-based approach for classifying DDoS attacks, emphasizing improvement over classical ML methods.	Not specified	Achieved a 5.4% decrease in error rate compared to classical ML methods.
Lopes et al. [33]	CyDD	Fusion of feature engineering and deep learning for DDoS detection, aiming to reduce processing overheads.	CICDDoS2019	Demonstrated effectiveness in DDoS detection with reduced resource consumption.

Xinlong and Zhibin [34]	Hybrid Deep Learning	Utilizes Hierarchical Temporal Memory for DDoS attack detection, highlighting a novel approach in deep learning.	Not specified	The proposed method highlights the potential for detecting DDoS attacks with a hybrid deep learning model.
Tabassum et al. [35]	SHAP, LIME, ELI5	Explaining binary classification of IoT network attacks, highlighting decision-making.	IoT network attacks	-
Houda et al. [36]	SHAP, LIME, RuleFit	Enhancing interpretability of deep learning decisions through global and local explanations.	IoT-related IDSs	-
Wei et al. [37]	Autoencoder-MLP (AE-MLP)	Hybrid deep learning for DDoS detection and classification, extracting optimal features for MLP classification.	CICDDoS2019	Specific focus on multi-class classification, challenges not detailed.
N.H. Vu [38]	K-Nearest Neighbor (KNN)	Utilizes the KNN algorithm to identify the k-closest training examples in the feature space, employing a voting mechanism for test data categorization based on the most common class among the k-nearest neighbors.	Not specified	Excellent results in categorizing network DDoS assaults.
Cheng et al. [39]	Support Vector Machine (SVM)	Employs SVM to construct a hyperplane or set of hyperplanes in a high-dimensional space, which can be used for classification, regression, or other tasks. The method is particularly useful for distinguishing between benign and malicious traffic by analyzing labeled training data and applying it to classify unseen data.	Not specified	Effective in differentiating between malicious and benign traffic.
Wang et al. [40]	Random Forest (RF)	Implements Random Forest, an ensemble of decision trees for classification tasks. The method relies on the majority vote from numerous decision trees constructed during the training process to make the	Not specified	Acceptable performance in classifying DDoS attacks with a properly

		final decision, offering robustness against overfitting by considering various subsets of features and training examples.		selected feature set.
Fadlil et al. [41]	Naive Bayes (NB)	Applies Naive Bayes classification, leveraging statistical techniques based on Bayes' theorem with an assumption of independence among predictors. The model is particularly noted for its simplicity and effectiveness in cases where the features are independent of each other, utilizing mean difference and standard deviation for attack detection.	Not specified	Achieved good results in identifying DDoS attacks, highlighting the utility of the Naive Bayes approach.
Dincalp [42]	DBSCAN Clustering	Uses Density-Based Spatial Clustering of Applications with Noise (DBSCAN) to identify clusters of high-density data points, effectively grouping similar data points while identifying outliers. This approach is adept at managing various attack vectors by recognizing clusters of attack patterns within network traffic.	Not specified	Demonstrated effectiveness in handling a variety of attack vectors through clustering.
Ahanger [43]	Artificial Neural Network (ANN)	Develop an ANN model for DDoS attack detection, leveraging the back-propagation algorithm for learning. This approach mimics the way biological neural networks operate, adjusting weights and biases within the network based on the error rate of outputs compared to expected results, thereby improving the model's ability to detect attacks.	Not specified	Successfully developed ANN for the detection of DDoS attacks, displaying the potential of neural networks in cybersecurity.
Hasan et al. [44]	Deep Convolution Neural Network (DCNN)	Implements a DCNN model to analyze network traffic, taking advantage of convolutional layers for feature extraction and classification. This method is	Not specified	Outperformed shallow machine learning algorithms in terms of

		well-suited for situations with fewer data points, offering superior accuracy by extracting and learning complex features from the input data.		accuracy, demonstrating the efficacy of deep learning models in DDoS detection.
Krishnan et al. [45]	Non-symmetric Deep Autoencoder (NDAE)	Introduces a deep learning model based on a non-symmetric deep autoencoder that lacks a decoder phase, focusing solely on the encoding process to learn a representation of the input data. This model is combined with Random Forest for an attack detection system in SDN security, aiming to reduce training duration, memory, and processing requirements while maintaining high accuracy.	NSL-KDD, CIC-IDS2017	Achieved high accuracy rates on both datasets, underscoring the efficiency and resource-effectiveness of the NDAE model in detecting DDoS attacks.
Zhu et al. [46]	FNN and CNN	Explores the use of Feedforward Neural Networks (FNN) and Convolutional Neural Networks (CNN) for the analysis of network traffic to detect DDoS intrusions. These deep learning models offer sophisticated mechanisms for identifying patterns and anomalies in data, outperforming traditional machine learning techniques in distinguishing different types of network anomalies.	NSL-KDD	Demonstrated superior accuracy in identifying anomaly types and network intrusion detection, highlighting the advantages of deep learning in cybersecurity.
Alzahrani and Hong [47]	Artificial Neural Network (ANN)	Advocates for the use of ANN models to analyze network data for the detection of DDoS attacks, emphasizing the model's ability to process complex datasets and extract meaningful patterns for classification tasks. The study highlights the potential of ANN in providing accurate and reliable detection	Not specified	Found high success rates in detecting DDoS attacks, suggesting that deep learning models are highly effective at

	mechanisms in the context of increasing cyber threats.	analyzing network data and identifying cybersecurity threats.

3. Methodology

The existing literature presents various machine learning-based techniques for detecting DDo attacks, but these methods often need help in real-world dynamic situations. Our proposed method, using Feedforward deep neural networks (FDNN), adaptively adjusts to evolving threats. While most research focuses on binary classification, our approach delves into classifying attacks into specific types, a more complex multiclass problem. By accurately identifying and categorizing attacks, targeted defense strategies can be substantially improved, enhancing their effectiveness.

3.1 Experimental Setup

All the experiments are performed on a system equipped with an Intel Core i7 processor (16 cores, 32 GB RAM). Python programming language is utilized, incorporating Jupyter Notebook as the integrated development environment (IDE) [6]. The main libraries are pandas for data manipulation [48], LightGBM [49], CatBoost [50], and XGBoost [51] to implement machine learning, while imbalanced-learn has been used to balance classes with the SMOTE algorithm [52]. Feature selection is performed with SHAP (SHapley Additive exPlanations) [53] and recursive feature elimination (RFE) [54] techniques. This process enhances computational efficiency and ensures interpretability, critical for adaptive learning in cybersecurity applications. The models are trained using multi-class classification strategies and evaluated with metrics such as accuracy, recall, specificity, and F1-score [55]. Data processing pipelines and results are stored in Excel files using the openpyxl library [56].

3.2 Data Preparation

In this study, the DDoS Evaluation Dataset (CIC-DDoS2019) from the Canadian Institute of Cybersecurity is used [57]. This dataset has modern reflective DDoS attacks. For training, 18 DDoS attack classes were conducted using the following targets: UDP, MSSQL, Benign, Portmap, Syn, NetBIOS, UDPLag, LDAP, DrDoS_DNS, UDPLag, WebDDoS, TFTP, DrDoS_UDP, DrDoS_SNMP, DrDoS_NetBIOS, DrDoS_LDAP, DrDoS_MSSQL, and DrDoS_NTP. For testing, seven attack types were conducted, targeting protocols such as PortScan, NetBIOS, LDAP, MSSQL, UDP, UDPLag, and SYN. The diversity of attack types ensures a comprehensive evaluation of the adaptive model's performance.

The dataset [57] is split based on two types of attack classes: (1) Exploitation-based and (2) Reflection-based attacks. Further, these are subdivided into additional categories, as depicted in T 2. Our dataset consists of 431,371 data instances with 77 features. This dataset reflects the divers modern DDoS attack patterns, ensuring robust training and evaluation for adaptive learning algorithms.

The dataset was split into training (50%) and testing (50%) ratios. The training and testing datasets comprise 215,685 and 215,686 data instances, respectively. There are 18 classes, where 1 represent attack classes and one represents normal requests. Further, in Table 2, all training and data details are given. The test data was divided into five equally-sized test datasets, and another synthetic datasets were generated. Ten test datasets are used, each consisting of approximately 4 rows. This rigorous division helps evaluate the adaptability and robustness of the proposed meth against diverse and evolving data scenarios.

Label	UDP	MSSQL	Benign	Portmap	Syn	NetBIOS	UDPLag	LDAP	DrDoS_DNS
total	18090	8525	97831	685	49373	644	55	1906	3669
training	90445	4262	48916	343 34	24687	322	27.5	953	1835
test	90445	4261	48915		24686	322	27.5	953	1834

Label	UDP-lag	WebDDoS	TFTP	DrDoS_UDP	DrDoS_SNMP	DrDoS_NetBIOS	DrDoS_LDAP	DrDoS_MSSQL	DrDoS_NTP
total	8872	51	98917		2717	598	1440	6212	
training	4436	25.5	49459	10420	1359	299	720	3106	121368
	4436	25.5		5210	1358	299	720	3106	60684
test			49458	5210					60684

Table 2. Whole dataset, training, and testing datasets attack-wise details.

3.3 Adaptive Model Phases

The principle behind the proposed method is tackling the dynamic nature of DDoS attacks, which more practical than the conventional machine learning approaches, which are trained on historica data for DDoS attack detection. The proposed Adaptive Machine Learning-Based DDoS Detection method works in two phases: (1) the conventional phase and (2) the adaptive phase. The convent phase has two key functions: feature selection and training using advanced algorithms such as LightGBM, CatBoost, and XGBoost.

In the adaptive phase, the method adjusts itself to the latest nature of DDoS attacks. It is achieved employing checkpoint mechanisms and incremental learning. In real-world scenarios, attackers a intelligent and adjust their methods over time. One approach is to train the machine learning clas classically and use it without updates. A more effective strategy, as employed in this method, is to train a machine learning classifier and update it incrementally with new data, avoiding the need to retrain from scratch. The proposed method improves this by incrementally updating the trained m with new data, avoiding the need for retraining from scratch. This approach is highly effective for handling evolving attack patterns, saving time and computational resources, and ensuring the me remains lightweight and efficient.

3.3.1 Integrated Feature Selection Using Random Forest, SHAP, and Mutual Information

To enhance the robustness and accuracy of DDoS attack detection, we propose an integrated feature selection workflow that combines multiple advanced techniques. This approach leverages strengths of Random Forest for feature ranking, SHAP (SHapley Additive exPlanations) for interpretability, and Mutual Information for statistical dependency analysis. The selected features then used to train a classifier, optimizing model performance while reducing computational complexity.

Feature Importance Calculation

The overall importance score for each feature f_i is defined as a weighted sum of its importance from the three methods:

$$S(f_i) = w_1 \cdot RF(f_i) + w_2 \cdot SHAP(f_i) + w_3 \cdot RMI(f_i)$$

Where:

$RRF(fi)$: Importance score of feature (fi) derived from Random Forest.

$RSHAP(fi)$: SHAP value indicating the impact of (fi) on predictions.

$RMI(fi)$: Mutual Information score quantifying the dependency of (fi) with the target variable.

$w1, w2, w3$: Weights assigned to each method (default to equal weighting if no prior knowledge is available).

Algorithm

The workflow for feature selection and model training is summarized in Algorithm 1.

Algorithm 1: Feature Selection and Model Training Workflow

Input: Dataset D with features F and target labels Y

Output: Trained XGBoost model M and evaluation metrics E

1. Data Preprocessing

1.1 Handle missing values in D

1.2 Normalize all numeric features in F

2. Feature Selection

2.1 Apply Random Forest to rank feature importance

2.2 Compute SHAP values to interpret feature influence

2.3 Calculate Mutual Information to measure feature dependency with Y

2.4 Combine rankings from 2.1, 2.2, and 2.3

2.5 Select the top N features (e.g., N = 20)

3. Data Balancing

3.1 Apply SMOTE to oversample minority classes in Y

3.2 Generate a balanced dataset D_balanced with F_balanced and Y_balanced

4. Model Training

4.1 Initialize the XGBoost model with default parameters

4.2 Optimize hyperparameters using GridSearchCV:

4.2.1 Search over combinations of max_depth, learning_rate, n_estimators, and scale_pos_weight

4.2.2 Use 3-fold cross-validation and F1-weighted scoring

4.3 Train the XGBoost model M on F_balanced and Y_balanced using optimal parameters

5. Model Evaluation

5.1 Use M to predict on test dataset F_test

5.2 Compute evaluation metrics:

5.2.1 Accuracy

5.2.2 Precision, Recall, and F1-Score for each class

5.2.3 Confusion Matrix

5.3 Analyze feature importance using SHAP and XGBoost feature weights

6. Continuous Improvement

6.1 Incorporate new data and repeat Steps 1–5 as necessary

6.2 Adapt hyperparameters and feature selection thresholds based on evolving datasets

End

Impact of the Integrated Workflow

This integrated workflow addresses key challenges in DDoS detection:

1. Class Imbalance: SMOTE ensures adequate representation of minority classes, improving recall underrepresented attack types.
2. Feature Relevance: Combining Random Forest, SHAP, and Mutual Information highlights the mo predictive and interpretable features, reducing complexity while maintaining accuracy.
3. Model Robustness: XGBoost's optimized hyperparameters enable high accuracy (99%) and significantly improved performance for minority classes, as seen in recall metrics.

This methodology provides a scalable, interpretable, and efficient solution for multiclass DDo detection.

To visualize the results of the integrated feature selection methodology, two figures are presente

1. Figure 3: Cumulative Feature Importance - Random Forest

Figure 4 illustrates the cumulative contribution of features ranked by their importance scores as d from the Random Forest model. This visualization highlights:

- The rapid growth in cumulative importance at the beginning of the curve, indicates that a small su of features captures the majority of predictive power.
- The flat section of the curve, where additional features contribute minimally, suggesting diminish returns.

This information supports the decision-making process for selecting a subset of features based chosen importance threshold (e.g., 90% cumulative importance).

2. Figure 4: Cumulative Feature Importance with Maximum Marker - SHAP

Figure 4 complements the insights from Figure 3 by presenting feature contributions using SH (SHapley Additive exPlanations) values. Unlike Random Forest, SHAP provides an interpretable game-theoretic perspective on feature importance.

Key highlights from the figure include:

- The red marker denotes the maximum cumulative importance achieved by SHAP values, offerin data-driven reference point for feature selection thresholds.
- The interpretability of SHAP values ensures that even subtle but impactful feature contributions accounted for in the selection process.

This visualization underscores the fairness and robustness of the integrated feature selection methodology. These charts demonstrate the effectiveness of the combined approach, which bala feature efficiency (Random Forest) with interpretability (SHAP), ensuring an optimized and explainable feature subset for subsequent modeling.

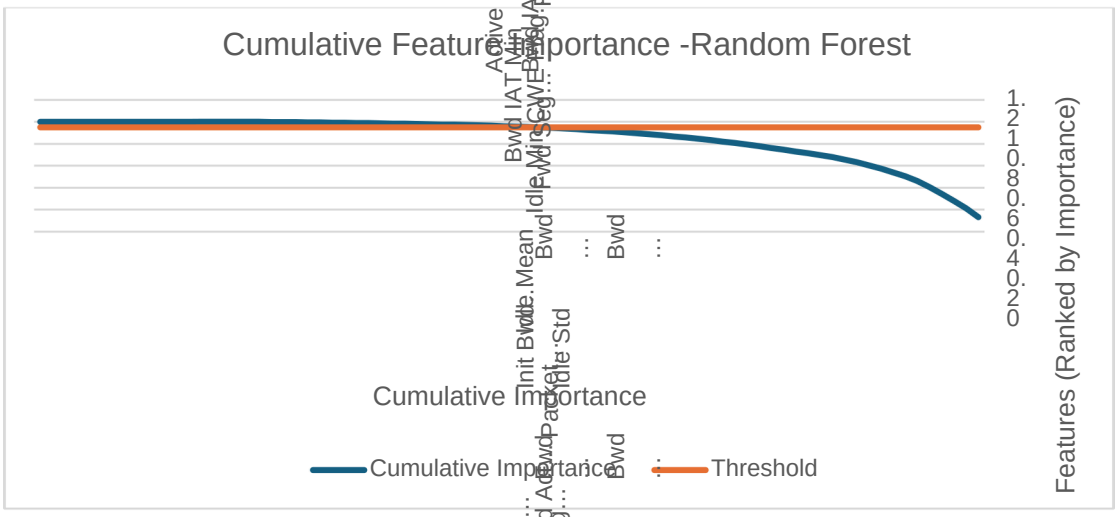

Figure 3 Cumulative Feature Importance - Random Forest

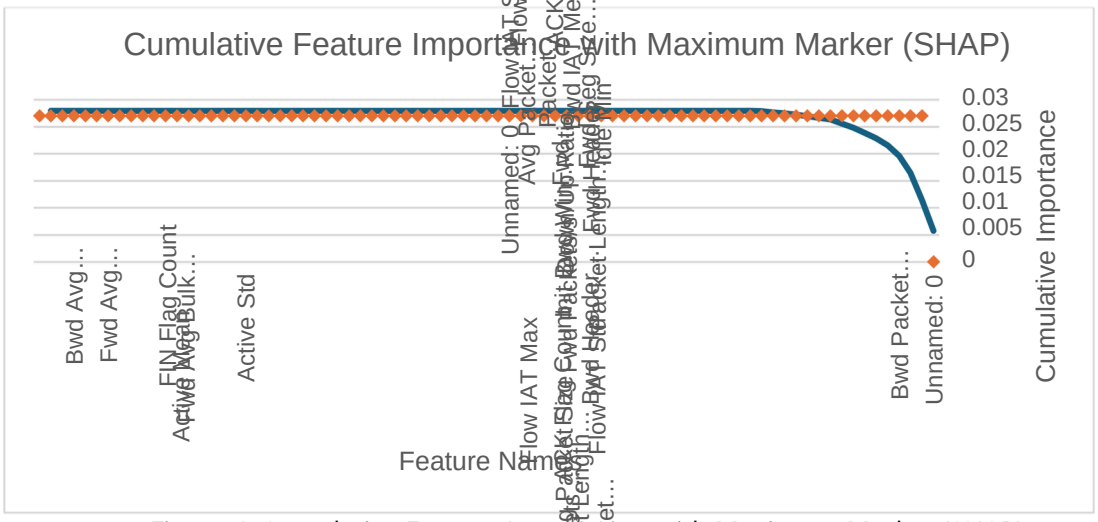

Figure 4: Cumulative Feature Importance with Maximum Marker (SHAP)

3.3.2 Model Training and Optimization

After using the two algorithms (mentioned in the previous section) to select features, we now wor building and training a model for effective DDoS detection. We use XGBoost (Extreme Gradient Boosting) algorithms, which are powerful and efficient algorithms known for their scalability and high performance in classification operations. The set of features extracted (20 features) were use train the XGBoost model.

To deal with the imbalance in classes present in the CIC-DDoS2019 dataset, the SMOTE (Synthetic Minority Oversampling Technique) technique was applied. This ensured a balanced distribution o classes, allowing the model to achieve better generalization and higher recall for minority classes. conduct a Grid search in order to optimize the key hyperparameters, including learning rate, maximum tree depth, and the number of estimators, ensuring optimal performance for the detec task.

Our model achieved 99% accuracy, demonstrating its effectiveness in distinguishing between ben and malicious traffic. Table 3 provides a detailed analysis of precision, recall, and F1 scores for all classes, and these significant improvements in the performance of the minority class are due to SMOTE. These results verify the effectiveness of the selected features and the XGBoost model in detecting various types of DDoS attacks.

For instance:

- Majority classes, such as benign traffic (Class 0) and certain attack types (Class 4), achieved perfe precision, recall, and F1-scores.
- Minority classes, such as Class 16 and Class 17, showed notable improvement in recall due to SMO though their precision remained relatively low.

This evaluation underscores the efficacy of combining Random Forest and SHAP for feature selection, demonstrating improvements in both efficiency and explainability.

3.3.2 Evaluation of Selected Features

The evaluation of selected features plays a critical role in optimizing the machine learning model's performance while maintaining computational efficiency. In this study, an integrated methodolog combining Random Forest, SHAP (SHapley Additive exPlanations), and cumulative feature importance analysis were employed to select the most relevant features. This approach ensures t the selected features not only improve prediction accuracy but also provide insights into feature importance and interpretability, a crucial aspect in cybersecurity applications like DDoS detection

The CIC-DDoS2019 dataset, with its high dimensionality, originally contained 78 features. Using th integrated methodology, we reduced the feature set to 20, which accounted for approximately 95 the cumulative importance. This significant reduction in feature count contributed to lower computational requirements and enhanced model interpretability without sacrificing classificatio performance.

Table 3 presents the classification report for the XGBoost model trained with the selected feature The model achieved an overall accuracy of 99.35%, demonstrating its ability to distinguish betwee benign and malicious traffic effectively. Class-specific metrics such as precision, recall, and F1-scor highlight the robustness of the feature selection methodology. For instance:

- Majority classes, such as benign traffic (Class 0) and certain attack types (Class 4), achieved ne perfect precision, recall, and F1-scores.
- Minority classes, such as Class 16 and Class 17, showed notable improvements in recall, with sc of 0.65 and 0.79, respectively, due to the application of SMOTE.

These results underscore the efficacy of combining Random Forest and SHAP for feature selectio demonstrating improvements in both efficiency and explainability.

After feature selection, the next step involved training and optimizing the model for effective DDo detection. This study utilized three advanced machine learning models: XGBoost (Extreme Gradie Boosting), LightGBM, and CatBoost, each known for its scalability and performance in classificatio tasks. The selected feature set, reduced to 20 features, was used to train all three models for comparative analysis.

Key Findings:

- XGBoost achieved an overall accuracy of 99.32%, with class-specific F1-scores exceeding 0.98 fo most classes. It showed robustness in handling imbalanced data, with macro-averaged F1-scor 0.93.
- LightGBM demonstrated competitive performance with an accuracy of 99.35%. It achieved high recall for some minority classes, such as Class 16 (0.65), and performed efficiently in terms of computational speed.
- CatBoost achieved slightly lower performance compared to LightGBM, with an accuracy of 99.31% However, it demonstrated strong interpretability and precision metrics for the majority of classes

Metric	*XGBoost*	*LightGBM*	*CatBoost*
Accuracy	99.32%	99.35%	99.31%
Macro F1-Score	0.935	0.938	0.933
Weighted F1-Score	0.993	0.994	0.993

Table 3: Classification Metrics for the Models

Grid search was conducted to optimize key hyperparameters, including learning rate, maximum t depth, and the number of estimators, ensuring optimal performance for the detection task. The r validate the efficiency of the selected features and the three models in detecting diverse types of DDoS attacks.

Equations for Evaluation Metrics

The performance of the proposed Adaptive Machine Learning-Based DDoS detection is estimated a set of indicators. This includes the accuracy, the recall, the specificity, and F1-score metrics. Thes have been chosen to provide a comprehensive picture of the model's effectiveness in a multiclass classification problem.

1. Accuracy: it measures the proportion of correctly classified instances out of the total instance reflects the overall correctness of the model but can be insufficient when dealing with imbalan datasets.

$$Accuracy = \frac{(TP + TN)}{(TP + TN + FP + FN)} \quad ...(1)$$

2. Recall (Sensitivity): it calculates the proportion of actual positive cases (e.g., attacks) that are correc identified by the model. It is particularly critical for evaluating the model's ability to detect mino attack classes, a key focus of this study.

$$Recall = \frac{TP}{(TP + FN)} \quad .....(2)$$

3. Specificity: it is the proportion of true negative cases correctly identified. This assesses the mod ability to minimize false positives, which is crucial for maintaining the reliability of normal traff classification.

$$Specificity = \frac{TN}{(TN + FP)} \quad .....(3)$$

4. F1-Score: Combines precision and recall into a single metric, offering a balanced measure of the model's performance. The F1-score is especially relevant in multiclass classification, where trade-offs between precision and recall can vary across classes.

$$F1 - Score = 2 \times \frac{Precision \times Recall}{Precision + Recall} \quad .....(4)$$

5. Precision: Evaluates the proportion of true positive predictions among all instances predicted as positive. This metric is critical for assessing the model's ability to minimize false positives, particula for attack classes that could otherwise cause false alarms.

$$Precision = \frac{TP}{TP + FP} \quad .....(5)$$

This study prioritizes metrics such as recall, precision, and F1-score for minority classes, ensuring that the proposed method effectively handles imbalanced data and evolving attack patterns.

These metrics are calculated and analyzed for all 18 classes, with additional focus on the adaptabi and robustness of the model under diverse testing conditions.

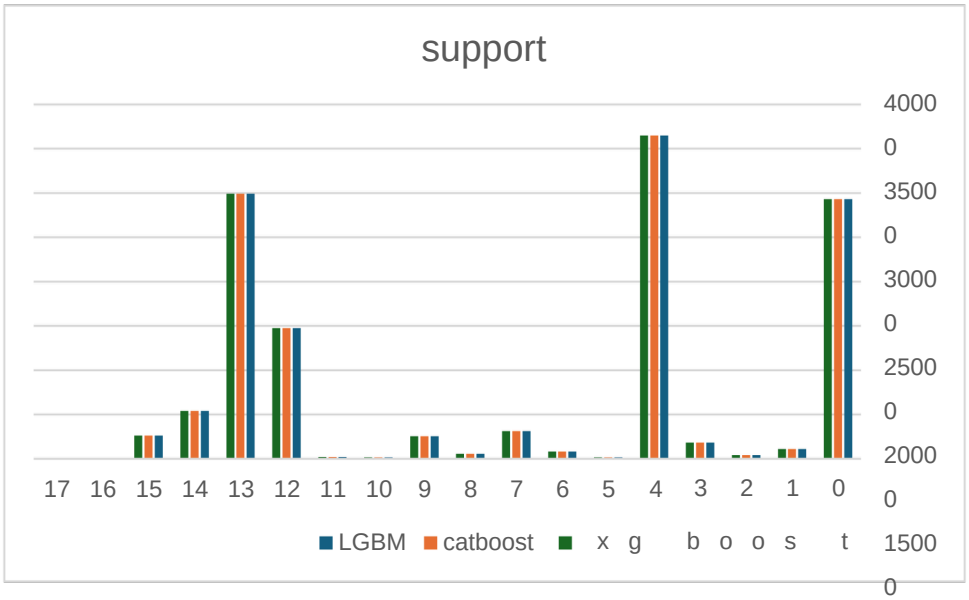

Figure 5: Support Distribution

Distribution of class instances in the dataset is sown in Figure 5. Classes 5 and 0 dominate in frequency, emphasizing the need for balancing techniques like SMOTE for fair model training.

3.4 Impact of Feature Selection and Oversampling on Model Performance

The integration of feature selection and oversampling techniques had a profound impact on the performance of the models. By reducing the feature set from 78 to 20 using the combined methodology of Random Forest and SHAP, the training time decreased significantly without compromising accuracy.

Summary of Key Metrics:

- Macro-averaged precision, recall, and F1-scores exceeded 0.93 for all models.
- Weighted averages of these metrics were all above 0.99, reflecting the models' robustness acros classes.
- Minority classes, such as Class 16 and Class 17, showed notable improvement in recall scores, rea 0.65 and 0.79, respectively, when using LightGBM.

4. Results and Analysis

For the performance evaluation of the XGBoost, LightGBM, and CatBoost models, the following performance evaluation benchmarks are used: (1) prediction accuracy percentage, (2) sensitivity, a (3) specificity. The prediction accuracy percentage, sensitivity, and specificity are computed using a confusion matrix.

4.1 Prediction Accuracy

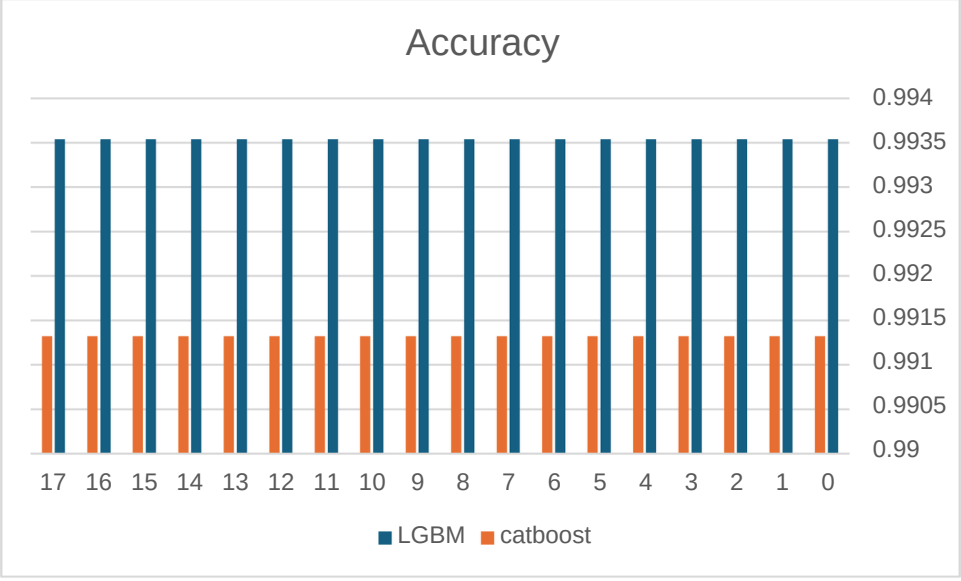

Figure 6: Accuracy Comparison

Figure 6 shows the prediction accuracy in percentage for the CatBoost and LightGBM methods in performing classification tasks. In all test cases, the accuracy for LightGBM stood at 99.35%, wh that of CatBoost was 99.13% across all classes.

These results reveal the stability and effectiveness of both CatBoost and LightGBM in DDoS detection tasks. Both algorithms performed well, although LightGBM showed slightly better predic accuracy in general. The consistency across classes underlines their reliability and applicability cybersecurity applications such as DDoS detection.

Recall or true positive rate-TPR, informs about the classifier's capability to rightly identify true positive cases among all actual positive cases. Recall can be applied to sensitivity assessment as True Positive / (True Positive + False Negatives). Sensitivity trends of performance, as depicted in Figure 7, indicate that across most of the classes, LightGBM and CatBoost, along with XGBoost, perform admirably and have stable metrics of performance.

4.2 Recall

Interestingly, for minority classes such as UDPLag (Class 16), CatBoost produced the highest recall 0.85, whereas LightGBM and XGBoost both achieved 0.65. This demonstrates CatBoost's super ability to handle imbalanced data effectively. Furthermore, for most attack classes, such as Class 3 Class 4, all three algorithms achieved near-perfect recall values, signifying their strong sensitivity detecting diverse network traffic types.

For normal traffic (Class 0), LightGBM and XGBoost slightly outperformed CatBoost with recall values of 0.9987 and 0.9986, respectively, while CatBoost achieved 0.9956. These results highlight the slight variability in performance across different algorithms but underscore their overall robustness in sensitivity metrics.

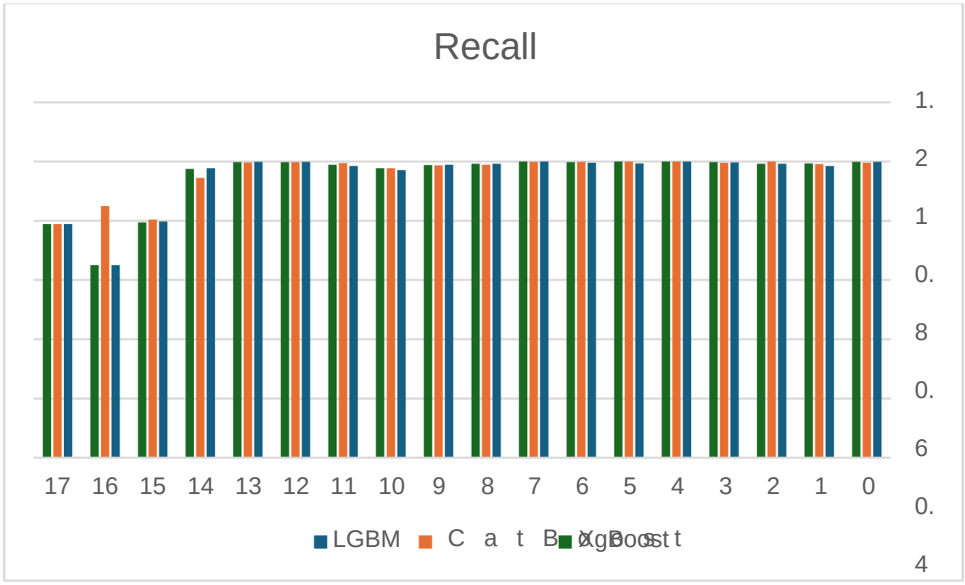

Figure 7: This comparison confirms that CatBoost, LightGBM, and XGBoost exhibit strong recall across normal and attack classes, with CatBoost demonstrating a notable edge in detecting min classes effectively.

4.3 Specificity

The prediction accuracy for the 10 test cases of CatBoost, LightGBM, and XGBoost methods is shown in Figure 8. LightGBM maintained a consistent accuracy of 99.35%, slightly higher than CatBoost's 99.13% across all classes.

Both CatBoost and LightGBM showed stable and effective performance in DDoS detection tasks, with LightGBM slightly outperforming CatBoost. This consistency highlights their reliability in cybersecurity applications.

Specificity, or true negative rate, measures the ability of a classifier to correctly identify negative data instances. It is calculated using equation (3) Figure 8 depicts the specificity trends for LightGBM, CatBoost, and XGBoost.

LightGBM achieved the highest specificity values across most classes, with scores close to 1. CatBoost and XGBoost also performed very well, with minimal differences. All three algorithms achieved perfect specificity for Class 4. LightGBM slightly outperformed the other algorithms f Classes 15 and 16, with values of 0.999999802 and 0.999997708, respectively.

Overall, the results show that all three algorithms effectively minimize false positives and are hi reliable for handling negative classifications in DDoS detection.

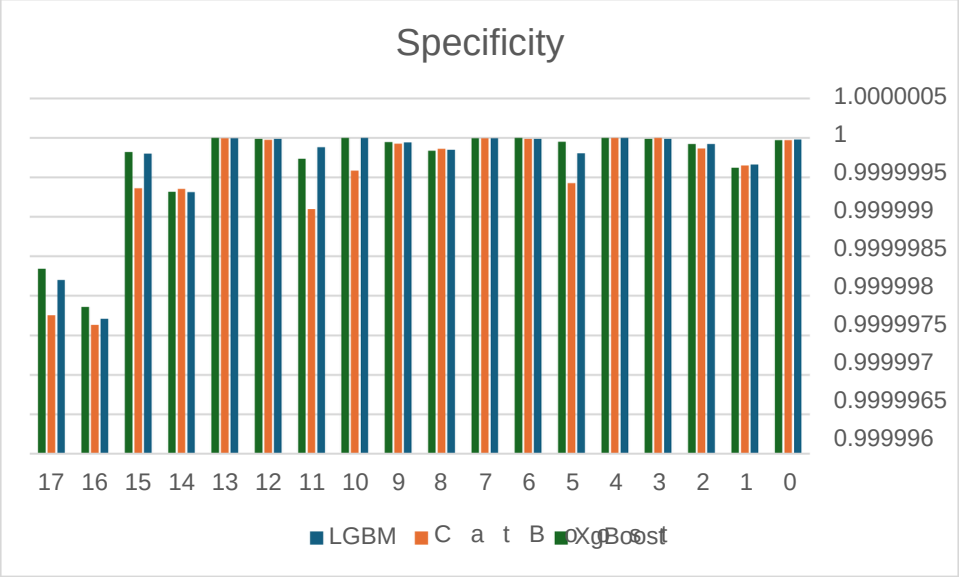

Figure 8:*Specificity comparison*

4.4 F1-Score

The F1-score is a harmonic mean of precision and recall, providing a balanced measure that accounts for both false positives and false negatives. Figure 9 presents the F1-scores for LightGBM, CatBoost, and XGBoost across all classes.

LightGBM consistently achieved high F1-scores across most classes, often outperforming CatBoost and XGBoost. For normal traffic (Class 0), LightGBM achieved an F1-score of 0.9981, marginally higher than CatBoost (0.9960) and XGBoost (0.9975). Similarly, for Class 4, all three algorithms achieved near-perfect F1-scores of 0.9999 or higher, demonstrating their ability to handle this class effectively.

In contrast, for minority classes such as Class 16 and Class 17, there was a noticeable drop in performance. CatBoost achieved an F1-score of 0.430 for Class 16, while LightGBM and XGBoost had lower scores of 0.464 and 0.377, respectively. For Class 17, XGBoost slightly outperformed LightGBM and CatBoost with an F1-score of 0.750, while CatBoost lagged at 0.295.

These results highlight that while all three algorithms perform exceptionally well for majority classes, their performance decreases for minority classes, with LightGBM showing slightly better overall consistency.

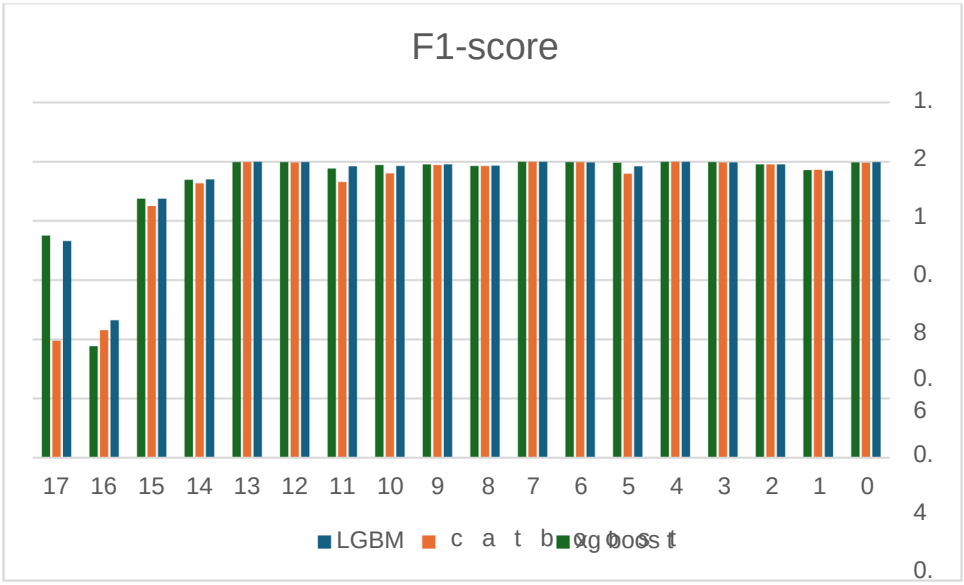

Figure 9: F1-score trends across various classes, providing a comprehensive view of the balance between precision and recall achieved by the three models.

5. Conclusion

Recently, cloud computing has facilitated versatile communication between students, teacher and professionals to collaborate and share knowledge seamlessly on an international scale. Howe a significant threat to the seamless availability of cloud computing services is distributed denial-of service attacks. Over time, DDoS attacks have become more sophisticated and dynamic, making detection methods more challenging.

Advanced machine learning methods such as LightGBM, CatBoost, and XGBoost in DDoS attack detection have been proposed in this study. These methods are effectively addressing mod day DDoS attacks and are adaptable to future challenges. The proposed approach not only classif normal and abnormal traffic but also sub-classifies various attack types, which can be used in the development of more powerful attack-specific defense technologies.

The results demonstrated exceptionally good accuracy, sensitivity, and specificity for the class and test cases involved, proving the solidity of the investigated approaches. Among these, LightGB performed slightly better regarding overall accuracy and specificity, while CatBoost demonstrated stronger performance in cases with minority attack classes.

Future work can be done regarding the feature aspects of these attacks in order to understand ho features develop over time. This knowledge will further enhance the detection methods with bett adaptability and efficiency against ever-evolving DDoS threats.

REFERENCES

[1] M. Jangjou and M. K. Sohrabi, "A Comprehensive Survey on Security Challenges in Different Network Layers in Cloud Computing," Archives of Computational Methods in Engineerin 2022, pp. 1–22, Jan. 2022, doi: 10.1007/S11831-022-09708-9.
[2] Gaurav Aggarwal, "How the Pandemic Has Accelerated Cloud Adoption," Forbes. Accessed: Aug. 14, 2022. [Online]. Available: https://www.forbes.com/sites/forbestechcouncil/2021/01/15/how-the-pandemic-has-accelerated- cloud-adoption/?sh=463f9b836621
[3] Lionel Sujay Vailshery, "Cloud computing - Statistics & Facts," Statista. Accessed: Aug. 14, 2022. [Online]. Available: https://www.statista.com/topics/1695/cloud-computing/#dossierKeyfigu
[4] E. Abdurachman, F. Lumban Gaol, and B. Soewito, "ScienceDirect ScienceDirect Survey on Threats and Risks in the Cloud Computing Environment," Procedia Comput Sci, vol. 161, pp. 1325- 1332, 2019, doi: 10.1016/j.procs.2019.11.248.
[5] Bob Violino, "Google, Microsoft ramp up cloud security as cyberattacks increase," CNBC. Accessed: Aug. 14, 2022. [Online]. Available: https://www.cnbc.com/2022/03/29/google-microsoft- ramp-up-cloud-security-as-cyberattacks-increase.html
[6] M. Masdari and M. Jalali, "A survey and taxonomy of DoS attacks in cloud computing," Security and Communication Networks, vol. 9, no. 16, pp. 3724–3751, Nov. 2016, doi: 10.1002/SEC.1539.
[7] Craig Sparling and Max Gebhardt, "Largest European DDoS Attack on Record," Akamai Blog. Accessed: Mar. 29, 2023. [Online]. Available: https://www.akamai.com/blog/security/largest- european-ddos-attack-ever
[8] Z. Liu, B. Xu, B. Cheng, X. Hu, and M. Darbandi, "Intrusion detection systems in the cloud computing: A comprehensive and deep literature review," Concurr Comput, vol. 34, no. 4, p. e6646 Feb. 2022, doi: 10.1002/CPE.6646.
[9] M. Darwish, A. Ouda, and L. Fernando Capretz, "Cloud-based DDoS Attacks and Defenses".
[10] V. Chang et al., "A Survey on Intrusion Detection Systems for Fog and Cloud Computing," Future Internet 2022, Vol. 14, Page 89, vol. 14, no. 3, p. 89, Mar. 2022, doi: 10.3390/FI14030089.
[11] Stephenson et al., "Survey of Machine Learning Techniques in Drug Discovery," Curr Drug Metab, vol. 20, no. 3, pp. 185–193, Aug. 2019, doi: 10.2174/1389200219666180820112457.
[12] M. Wang, Y. Lu, and J. Qin, "A dynamic mlp-based ddos attack detection method using feature selection and feedback," Computers & Security, Vol. 88, p. 101645, 2020.
[13] D.-C. Can, H.-Q. Le, and Q.-T. Ha, "Detection of distributed denial of service attacks using automatic feature selection with enhancement for imbalance dataset," in Intelligent Information a Database Systems: 13th Asian Conference, ACIIDS 2021, Phuket, Thailand, April 7–10, 2021, Proceedings 13. Springer, 2021, pp. 386–398.
[14] P. Singh Samom and A. Taggu, "Distributed denial of service (ddos) attacks detection: A machine learning approach," in Applied Soft Computing and Communication Networks: Proceedir of ACN 2020. Springer, 2021, pp. 75–87.

[15] Y. Wei, J. Jang-Jaccard, F. Sabrina, A. Singh, W. Xu, and S. Camtepe, “Ae-mlp: A hybrid deep learning approach for ddos detection and classification,” IEEE Access, vol. 9, pp. 146 810–146 821, 2021.
[16] C. S. Kalutharage, X. Liu, C. Chrysoulas, N. Pitropakis, and P. Papadopoulos, “Explainable ai-based ddos attack identification method for iot networks,” Computers, vol. 12, no. 2, p. 32, 2023
[17] L. Antwarg, R. M. Miller, B. Shapira, and L. Rokach, “Explaining anomalies detected by autoencoders using Shapley additive explanations,” Expert Systems with Applications, vol. 186, p. 115736, 2021.
[18] A. ˇ Sarˇcevi´c, D. Pintar, M. Vrani´c, and A. Krajna, “Cybersecurity knowledge extraction using XAI,” Applied Sciences, vol. 12, no. 17, p. 8669, 2022.
[19] S. Lakshminarasimman, S. Ruswin, and K. Sundarakantham, “Detecting DDoS attacks using decision tree algorithm,” 2017 4th International Conference on Signal Processing, Communication and Networking, ICSCN 2017, Oct. 2017, doi: 10.1109/ICSCN.2017.8085703.
[20] R. Latif, H. Abbas, S. Latif, and A. Masood, “EVFDT: An Enhanced Very Fast Decision Tree Algorithm for Detecting Distributed Denial of Service Attack in Cloud-Assisted Wireless Body Area Network,” Mobile Information Systems, vol. 2015, Jan. 2015, doi: 10.1155/2015/260594.
[21] R. Latif, H. Abbas, S. Assar, and S. Latif, “Analyzing feasibility for deploying very fast decision tree for DDoS attack detection in cloud-assisted WBAN,” Lecture Notes in Computer Science (including subseries Lecture Notes in Artificial Intelligence and Lecture Notes in Bioinformatics), vol. 8588 LNCS, pp. 507–519, 2014, doi: 10.1007/978-3-319-09333-8_57/COVER.
[22] M. I. Kareem and M. N. Jasim, “DDOS Attack Detection Using Lightweight Partial Decision Tree algorithm,” Proceedings of the 2nd 2022 International Conference on Computer Science and Software Engineering, CSASE 2022, pp. 362–367, 2022, doi: 10.1109/CSASE51777.2022.9759824.
[23] J. Ye, X. Cheng, J. Zhu, L. Feng, and L. Song, “A DDoS Attack Detection Method Based on SVM in Software Defined Network,” Security and Communication Networks, vol. 2018, Apr. 2018, doi: 10.1155/2018/9804061.
[24] A. Abusitta, M. Bellaiche, and M. Dagenais, “An SVM-based framework for detecting DoS attacks in virtualized clouds under changing environment,” vol. 7, p. 9, 2018, doi: 10.1186/s13677-018-0109-4.
[25] M. Myint Oo, S. Kamolphiwong, T. Kamolphiwong, and S. Vasupongayya, “Advanced Support Vector Machine-(ASVM-) based detection for Distributed Denial of Service (DDoS) attack on Software Defined Networking (SDN),” Journal of Computer Networks and Communications, vol 2019, 2019, doi: 10.1155/2019/8012568.
[26] M. Alduailij, Q. Waqas Khan, M. Tahir, M. Sardaraz, M. Alduailij, and F. Malik, “Machine-Learning-Based DDoS Attack Detection Using Mutual Information and Random Forest Feature Importance Method,” Symmetry 2022, Vol. 14, Page 1095, vol. 14, no. 6, p. 1095, May 2022, doi: 10.3390/SYM14061095.
[27] H. N. Thanh and T. Van Lang, “Use the ensemble methods when detecting DoS attacks in Network Intrusion Detection Systems,” EAI Endorsed Transactions on Context-aware Systems and Applications, vol. “6,” no. 19, p. 163484, Nov. 2019, doi: 10.4108/EAI.29-11-2019.163484.
[28] Bin Jia, Xiaohong Huang, Rujun Liu, and Yan Ma, “A DDoS Attack Detection Method Based on Hybrid Heterogeneous Multiclassifier Ensemble Learning,” Journal of Electrical and Computer Engineering. Accessed: Aug. 17, 2022. [Online]. Available: https://www.hindawi.com/journals/jece/2017/4975343/

[29] D. Firdaus, R. Munadi, and Y. Purwanto, "DDoS Attack Detection in Software Defined Network using Ensemble K-means++ and Random Forest," 2020 3rd International Seminar on Research of Information Technology and Intelligent Systems, ISRITI 2020, pp. 164–169, Dec. 2020, doi: 10.1109/ISRITI51436.2020.9315521.
[30] L. Alzubaidi et al., "Review of deep learning: concepts, CNN architectures, challenges, applications, future directions," Journal of Big Data 2021 8:1, vol. 8, no. 1, pp. 1–74, Mar. 2021, doi 10.1186/S40537-021-00444-8.
[31] S. Dong, P. Wang, and K. Abbas, "A survey on deep learning and its applications," Comput Sci Rev, vol. 40, p. 100379, May 2021, doi: 10.1016/J.COSREV.2021.100379.
[32] X. Yuan, C. Li, and X. Li, "DeepDefense: Identifying DDoS Attack via Deep Learning," 2017 IEEE International Conference on Smart Computing, SMARTCOMP 2017, Jun. 2017, doi: 10.1109/SMARTCOMP.2017.7946998.
[33] I. Ortet Lopes, D. Zou, F. A. Ruambo, S. Akbar, and B. Yuan, "Towards Effective Detection of Recent DDoS Attacks: A Deep Learning Approach," Security and Communication Networks, vol. 2021, 2021, doi: 10.1155/2021/5710028.
[34] L. Xinlong and C. Zhibin, "DDoS Attack Detection by Hybrid Deep Learning Methodologies," Security and Communication Networks, vol. 2022, pp. 1–7, May 2022, doi: 10.1155/2022/7866096.
[35] S. Tabassum, N. Parvin, N. Hossain, A. Tasnim, R. Rahman, and M. I. Hossain, "Iot network attack detection using xai and reliability analysis, "in 2022 25th International Conference on Computer and Information Technology (ICCIT). IEEE, 2022, pp. 176–181.
[36] Z. Abou El Houda, B. Brik, and L. Khoukhi, "why should I trust your ids?": An explainable deep learning framework for intrusion detection systems in internet of things networks," IEEE Ope Journal of the Communications Society, vol. 3, pp. 1164–1176, 2022.
[37] Y. Wei, J. Jang-Jaccard, F. Sabrina, A. Singh, W. Xu, and S. Camtepe, "Ae-mlp: A hybrid deep learning approach for ddos detection and classification," IEEE Access, vol. 9, pp. 146 810–146 821, 2021
[38] Vu, N.H. DDoS attack detection using K-Nearest Neighbor classifier method. In Proceeding of the International Conference on Telehealth/Assistive Technologies, Baltimore, Maryland, USA, 16–18 April 2008; IEEE: Piscataway Township, NJ, USA, 2008; pp. 248–253.
[39] Cheng, J.; Yin, J.; Liu, Y.; Cai, Z.; Wu, C. DDoS attack detection using IP address feature interaction. In Proceedings of the IEEE International Conference on Intelligent Networking and Collaborative Systems, Thessalonika, Greece, 24–26 November 2010; IEEE: Piscataway Township, NJ, USA, 2009; pp. 113–118.
[40] Wang, C.; Zheng, J.; Li, X. Research on DDoS attacks detection based on RDF-SVM. In Proceedings of the 10th International Conference on Intelligent Computation Technology and Automation, Changsha, China, 9–12 October 2017.
[41] Fadlil, A.; Riadi, I.; Aji, S. Review of detection DDoS attack detection using Naïve Bayes classifier for network forensics. Bull. Electr. Eng. Inform. 2017, 6, 140–148.
[42] Dincalp, U. Anomaly based distributed denial of service attack detection and prevention w machine learning. In Proceedings of the 2nd International Symposium on Multidisciplinary Studies and Innovative Technologies, Ankara, Turkey, 19–21 October 2018.
[43] Ahanger, T.A. An effective approach of detecting DDoS using artificial neural networks. In Proceedings of the 2017 International Conference on Wireless Communications, Signal Processing and Networking, Chennai, India, 22–24 March 2017; IEEE: Piscataway Township, NJ, USA, 2017; pp. 707–711.

[44] Hasan, Md., Zubair Hasan, K. M., & Sattar, Abdus (2018). Burst header packet flood detection in optical burst switching network using deep learning model. Procedia Computer Science, 143, 970–977.

[45] Krishnan, Prabhakar, Duttagupta, Subhasri, & Achuthan, Krishnashree (2019). VARMAN: Multi-plane security framework for software defined networks. Computer Communications, 148, 215–239.

[46] Li, M., Ye, K., & Xu, C. Z. (2018). Network anomaly detection and identification based on deep learning methods. In M. Luo, & L. J. Zhang (Eds.), Cloud Computing – CLOUD 2018. CLOUD 2018. Lecture Notes in Computer Science. Cham: Springer.

[47] Alzahrani, S., & Hong, L. (2018). Detection of distributed denial of service (DDoS) attacks using artificial intelligence on cloud. In 2018 IEEE World Congress on Services (SERVICES), San Francisco, CA (pp. 35–36). [48]McKinney, W. (2010). Data Structures for Statistical Computing in Python. Proceedings of the 9th Python in Science Conference. [49] Ke, G., Meng, Q., Finley, T., Wang, T., Chen, W., Ma, W., … & Liu, T. Y. (2017). LightGBM: A highly efficient gradient boosting decision tree. Advances in Neural Information Processing Systems [50] Prokhorenkova, L., Gusev, G., Vorobev, A., Dorogush, A. V., & Gulin, A. (2018). CatBoost: unbiased boosting with categorical features. Advances in Neural Information Processing Systems. [51] Chen, T., & Guestrin, C. (2016). XGBoost: A scalable tree boosting system. Proceedings of the 22nd ACM SIGKDD International Conference on Knowledge Discovery and Data Mining [52] Chawla, N. V., Bowyer, K. W., Hall, L. O., & Kegelmeyer, W. P. (2002). SMOTE: Synthetic Minority Over-sampling Technique. Journal of Artificial Intelligence Research [53] Kluyver, T., Ragan-Kelley, B., Pérez, F., Granger, B., Bussonnier, M., Frederic, J., … & Willing, C. (2016). Jupyter Notebooks - A publishing format for reproducible computational workflows. Proceedings of the 20th International Conference on Electronic Publishing [54] Lundberg, S. M., & Lee, S. I. (2017). A Unified Approach to Interpretable Model Predictions. Advances in Neural Information Processing Systems [55] Guyon, I., Weston, J., Barnhill, S., & Vapnik, V. (2002). Gene Selection for Cancer Classification using Support Vector Machines. Machine Learning [56] Powers, D. M. W. (2011). Evaluation: From Precision, Recall, and F-Measure to ROC, Informedness, Markedness & Correlation. Journal of Machine Learning Technologies. [10] Python Software Foundation. (2023). Openpyxl: A Python library to read/write Excel 2010 xlsx/xlsm files. Available at https://openpyxl.readthedocs.io/.

[57] I. Sharafaldin, A. H. Lashkari, S. Hakak, and A. A. Ghorbani, “Developing realistic distributed denial of service (DDoS) attack dataset and taxonomy,” Proceedings - International Carnahan Conference on Security Technology, vol. 2019-October, Oct. 2019, doi: 10.1109/CCST.2019.8888419.

هيئة التحرير

الهيئة الاستشارية

قواعد النشر في المجلة

- أن يكون البحث جديدا، ولم يسبق نشره
- أن يتسم بالأصالة والجدة والابتكار والاضافة للمعرفة
- أن لا يكون مستلا من بحوث سبق نشرها للباحث/للباحثين
- أن تراعى فيه قواعد البحث العلمي الاصيل، ومنهجيته.
- أن يشتمل البحث على:
  - صفحة عنوان البحث باللغة الانجليزية.
  - مستخلص البحث باللغة الانجليزية.
  - صفحة عنوان البحث باللغة الانجليزية.
  - مستخلص البحث باللغة العربية.
  - مقدمة.
  - صلب البحث.
  - خاتمة تتضمن نتائج وتوصيات.
  - ثبت الملمصادر والملمراجع.
  - الململاحق الململازمة(إن وجدت.)
- في حال (نشر البحث ورقا)يمنح الباحث نفسه نسخة من عدد
الذ ي نشر بحثه بها و10 نسخ من بحثة بشكل مستقل
- في حال اعتماد نشر البحث تؤول حقوق نشره كافة للمجلة، ول
تعيد نشره ورقيا أو إلكترونيا، ويحق لها

- إدراجه في قواعد البيانات الملمحلية والعالملمية- بمقابل أو بدو
  وذلك دون حاجة للإإذن الباحث.
- لالا يحق للباحث إعادة نشر بحثه الملمقبول للنشر في الملمجلة
  من أوعية النشر -إلالا بعد إذن
- كتابي من رئيس هيئة تحرير الملمجلة
- نمط التوثيق الملمعتمد في الملمجلة هو نمط IEEE

معلومات الإيداع

النسخة الورقية :

تم الإيداع في مكتبة الملمك فهد الوطنية برقم 1439/8742 وتاريخ 1439/09/17 ه

الرقم التسلسلي الدولي للدوريات (ردمد) 1658-7936

النسخة الإلكترونية:

تم الإيداع في مكتبة الملمك فهد الوطنية برقم 14394287 تاريخ 1439/09/17 هـ

الرقم التسلسلي الدولي للدوريات (ردمد) 1658-7944

الملموقع الإلكتروني للمجلة:

https://jesc.iu.edu.sa

ترسل البحوث باسم رئيس تحرير الملمجلة إلى ال
الإلكتروني

jesc@iu.edu.sa

الآراء الواردة في البحوث الملمنشورة تعرب ع
الباحث فقط، ولاتعرب بالضرورة عن الملمج

مجلة الجامعة الإسلالامية للعلوم التطبيقية

مجلة علمية دورية محكمة

العدد: السادس الجزء الثاني السنة :1446هـ